Title 40 CFR Part 191
Subparts B and C
Compliance Recertification Application 2019
for the
Waste Isolation Pilot Plant

Appendix SOTERM-2019
Actinide Chemistry Source Term

United States Department of Energy
Waste Isolation Pilot Plant

Carlsbad Field Office
Carlsbad, New Mexico

Compliance Recertification Application 2019
Appendix SOTERM-2019
Actinide Chemistry Source Term

Table of Contents

List of Figures

List of Tables

Acronyms and Abbreviations

%	percent
α	alpha particle
A_γ	Debye-Hückel parameter
a_i	activity of a chemical species
μs	microsecond
am	amorphous
aq	aqueous
ASTP	Actinide Source Term Program
atm	atmosphere
β	(apparent) stability constant, or beta particle
BNL	Brookhaven National Laboratory
Bq	becquerel
℃	Celsius; centigrade;
C	concentration
CAPHUM	maximum (cap) actinide concentration associated with mobile humic colloids
CAPMIC	maximum actinide concentration that could be associated with microbes
CCA	Compliance Certification Application
CDP	cellulose degradation products
CE-ICP-SF-MS	capillary electrophoresis mated to inductively coupled plasma sector field mass spectrometry
CFR	Code of Federal Regulations
Ci	Curie
CN	coordination number
coll	colloid
CONCINT	actinide concentration associated with mobile actinide intrinsic colloids
CONCMIN	actinide concentration associated with mobile mineral fragment colloids
CPR	cellulosic, plastic, and rubber materials
cr	crystalline phase
CRA	Compliance Recertification Application
D-H	Debye-Hückel theory or approach
DBR	direct brine release
DMSO	dimethyl sulfoxide

DNA	deoxyribonucleic acid
DOE	U.S. Department of Energy
DRZ	disturbed rock zone
E°	standard potential
E_h	oxidation/reduction (redox) potential
EDTA	ethylenediaminetetraacetic acid
EPA	U.S. Environmental Protection Agency
ERDA	Energy Research and Development Administration
EQ3/6	software program for geochemical modeling of aqueous systems
eV	electron volt
EXAFS	Extended X-Ray Absorption Fine Structure
F	Fahrenheit
f_{CO_2}	fugacity of carbon dioxide
FMT	Fracture-Matrix Transport
γ	gamma radiation or activity coefficient
g	gaseous, or gram, or gravity of Earth
G	molecular yield in molecules/100 eV of absorbed ionizing radiation
GBq	giga becquerel
GWB	Generic Weep Brine
Gy	Gray (absorbed dose unit equivalent to 1 Joule/Kg of absorbing material)
h	hours
I	ionic strength
ISA	isosaccharinic acid
K	degree Kelvin or stability constant
kg	kilogram
K_d	dissociation constant
K_s	solubility constant
K_{sp}	solubility product
λ_{ij}	second-order interaction coefficient
L	liter, or Ligand
LANL	Los Alamos National Laboratory
LET	Linear Energy Transfer

log	logarithm
$\log_{10}$	logarithm base 10
μ_{ijk}	third-order interaction coefficient
m	meter, molal (moles/Kg solvent)
M	mole per liter
m^3	cubic meter
mM	millimole per liter
mol	mole
molec	molecule
MPa	megapascal
mV	millivolt
n	neutron, or number
N	degree of polymerization number
NEA	Nuclear Energy Agency
nm	nanometer
PA	performance assessment
PABC	Performance Assessment Baseline Calculation
pC_{H+} or pcH	Negative logarithm of H^+ concentration in moles per liter
pCO_2	Partial pressure of carbon dioxide
pH	negative logarithm of H^+ activity
PHUMCIM	Proportionality constant for the actinide concentration associated with mobile humic colloids, in Castile brine
PHUMSIM	Proportionality constant for the actinide concentration associated with mobile humic colloids, in Salado brine
pm	picometer
PROPMIC	proportionality constant describing the bioassociation of actinides with mobile microorganisms
RH	relative humidity
s	solid or second
SEM	scanning electron microscope
SIMS	Secondary ion mass spectrometry
SIT	Specific Ion Interaction theory
SNL	Sandia National Laboratories

SOTERM	Actinide Chemistry Source Term (WIPP)
SRB	sulfate-reducing bacteria
T	temperature
$t_{½}$	half-life
TG/DTA	thermogravimetry/differential thermal analyzer
TIC	total inorganic carbon
TMAO	trimethylamine oxide
TRLFS	Time-resolved laser fluorescence spectroscopy
TRU	transuranic
V	volt, or vanadium
w	with
WDS	Waste Data System
WIPP	Waste Isolation Pilot Plant
XAFS	X-ray Absorption Fine Structure
XANES	X-Ray Absorption Near Edge Structure
XPS	X-ray photoelectron spectroscopy
XRD	X-Ray Diffraction
yr	year

Elements and Chemical Compounds

Am	Americium
Am(II)	Americium in the +2 oxidation state
Am(III)	Americium in the +3 oxidation state
Am(IV)	Americium in the +4 oxidation state
Am(V)	Americium in the +5 oxidation state
Am(VI)	Americium in the +6 oxidation state
Am^{2+}	Americium cation - Aqueous form of the americium in the +2 oxidation state that only exists as a transient
Am^{3+}	Americium cation - Aqueous form of the americium in the +3 oxidation state
Am^{4+}	Americium cation - Aqueous form of the americium in the +4 oxidation state
$AmAc^{2+}$	Americium-acetate complex with a +2 charge
$AmAc_2^{+}$	Americium-di-acetate complex with a +1 charge
$Am(Cl)_n^{(3-n)}$	Americium (III) chloride complex with n = 1 or 2
$Am(CO_3)_n^{(3-2n)}$	Americium (III) carbonate complex with n=1, 2, 3 or 4
Am OH CO_3	Americium (III) carbonato hydroxide
AmO_2^{+}	Americium oxo-cation – Aqueous form of the americium in the +5 oxidation state
AmO_2^{2+}	Americium oxo-cation – Aqueous form of the americium in the +6 oxidation state
AmO_2OH	Americium (V) oxide hydroxide
$AmOH^{2+}$	Americium (III) hydroxide cation – (1:1) complex
$Am(OH)_2^{+}$	Americium (III) hydroxide cation – (1:2) complex
$Am(OH)_3$	Americium hydroxide
$Am(OH)_4^{-}$	Americium (III) hydroxide anion – (1:4) complex
$Am(OH)_n^{(3-n)}$	Americium (III) hydroxide ion – (n:3-n) complex
$AmPO_4$	Americium (III) phosphate
$Am(SO_4)_n^{(3-2n)}$	Americium (III) sulfate complex with n = 1 or 2
$[An]_p$	Concentration of an adsorbed actinide element (mol/particle)
An	Actinide
An(III)	General actinide in the +3 oxidation state
An(IV)	General actinide in the +4 oxidation state
An(V)	General actinide in the +5 oxidation state
An(VI)	General actinide in the +6 oxidation state
An^{3+}	Aqueous form of the actinide in the +3 oxidation state

An^{4+}	Aqueous form of the actinide in the +4 oxidation state
An^{n+}	Aqueous form of the actinide in the +n oxidation state
$An_2(CO_3)_3$	Actinide (III) carbonate – (2:3) complex
$An_2(CO_3)_2^{2+}$	Actinide (III) carbonate ion – (2:2) complex
$AnB_4O_7^{+}$	Actinide (III) tetraborate ion – (1:1) complex
$AnCl^{2+}$	Actinide (III) chloride ion – (1:1) complex
$An(CO_3)^{+}$	Actinide (III) carbonate ion – (1:1) complex
$An(CO_3)_2^{-}$	Actinide (III) carbonate ion – (1:2) complex
$An(CO_3)_3^{3-}$	Actinide (III) carbonate ion – (1:3) complex
$AnCO_3OH$	Actinide (III) carbonate hydroxide
$AnL^{(n+m)}$	Complex of an actinide with a charge n and an organic ligand L with a charge m
$An(V)O_2^{+}$ or AnO_2^{+}	Aqueous form of the actinide in the +5 oxidation state
$An(VI)O_2^{2+}$ or AnO_2^{2+}	Aqueous form of the actinide in the +6 oxidation state
$AnOH^{2+}$	Actinide (III) hydroxide cation – (1:1) complex
$An(OH)_3$	Hydroxide of the actinide (III)
$AnPO_4$	Actinide (III) phosphate
$AnSO_4^{+}$	Actinide (III) sulfate ion – (1:1) complex
$B_3O_3(OH)_4^{-}$	Hydroxy polynuclear form of boric acid
$B_4O_7^{2-}$	Tetraborate anion
$B(OH)_x^{3-x}$	Hydroxyborate ions
Br^{-}	Bromide anion
[C]	Concentration of species *C* in solution
$[C_\theta]$	Concentration of a chosen standard state
C	Carbon or concentration
$C_6H_{10}O_5$	Cellulose
CH_4	Methane
$CH_3CO_2^{-}$	Acetate anion
$(CH_2CO_2)_2C(OH)(CO_2)^{3-}$	Citrate anion
$(CH_2CO_2)_2N(CH_2)_2N(CH_2CO_2)_2^{4-}$	Ethylenediaminetetraacetate (EDTA) anion
$C_2O_4^{2-}$	Oxalate anion
Ca	Calcium
Ca^{2+}	Calcium cation
$CaCl_2$	Calcium chloride

$CaCO_3$	Calcium carbonate
$CaMg(CO_3)_2$	Dolomite, calcium magnesium carbonate
$Ca[M(OH)_3]^{2+}$	Calcium metal (III) hydroxide cation – (1:1:3) complex
$Ca_2[M(OH)_4]^{3+}$	Calcium metal (III) hydroxide cation – (2:1:4) complex
$Ca_3[M(OH)_6]^{3+}$	Calcium metal (III) hydroxide cation – (3:1:6) complex
$Ca(OH)_2$	Calcium hydroxide
$Ca_p[Cm(OH)_n]^{3+2p-n}$	Calcium curium (III) hydroxide ion – (p:n:3+2p-n) complex
$Ca_4[Pu(OH)_8]^{4+}$	Calcium plutonium (IV) hydroxide cation complex
$CaSO_4$	Anhydrite, calcium sulfate
$CaSO_4 \cdot 2H_2O$	Gypsum, hydrated calcium sulfate
$Ca_4[Th(OH)_8]^{4+}$	Calcium thorium (IV) hydroxide cation complex
Cl	Chlorine
Cl^-	Chloride ion
Cl_2	Chlorine
Cl_2^-	Chlorine free radical
Cl_3^-	Chlorine anion
$ClBr^-$	Chloride bromide radical
ClO^-	Hypochlorite anion
ClO_2^-	Chlorite anion
ClO_3^-	Chlorate anion
ClO_4^-	Perchlorate anion
Cm	Curium
Cm(III)	Curium in the +3 oxidation state
Cm(IV)	Curium in the +4 oxidation state
Cm^{3+}	Curium cation – Aqueous form of the curium at the +3 oxidation state
$Cm_m(OH)_{3m}$	Curium hydroxide polymer
$Cm(OH)_3$	Curium hydroxide
$Cm(OH)_4^-$	Curium (III) hydroxide anion – (1:4) complex
CO_2	Carbon dioxide
CO_3^{2-}	Carbonate anion
Cr	Chromium
Cs	Cesium

F^-	Fluoride
Fe	Iron
Fe(0), Fe^0	Zero-valent iron, metallic iron
$FeCO_3$	Iron (II) carbonate, ferrous carbonate
$Fe_2(OH)_3Cl$	Iron-hibbingite, ferrous chloride trihydroxide
Fe_3O_4	Magnetite, iron (II,III) oxide
Fe^{2+}	Aqueous form of the iron in the +2 oxidation state, ferrous cation
Fe^{3+}	Aqueous form of the iron in the +3 oxidation state, ferric cation
Fe(II)	Iron in the +2 oxidation state
$Fe(II)(OH)_2$	Ferrous hydroxide
Fe(III)	Iron in the +3 oxidation state
$Fe(III)_2Fe(II)_4(OH)_{12}CO_3•2H_2O$	Green rust
$Fe(OH)_3$	Ferric hydroxide
$Fe(OH)_2·(x-2)H_2O$	Hydrated ferrous hydroxide
FeOOH	Goethite, iron oxide hydroxide
FeS	Iron (II) sulfide
H	Hydrogen (atomic)
H^+	Hydrogen cation
H_2	Hydrogen (molecular)
HPO_4^{2-}	Hydrogenphosphate anion
HCO_3^-	Bicarbonate anion, hydrogen carbonate anion
H_2O	Water
H_2O_2	Hydrogen peroxide
HOBr	Hypobromous acid
HOCl	Hypochlorous acid
$H_2PO_4^-$	Dihydrogen phosphate anion
H_2S	Hydrogen sulfide
K	Potassium
K^+	Potassium cation
KCl	Potassium chloride
$K_2MgCa_2(SO_4)_4·2H_2O$	Polyhalite
$KNpO_2CO_3·2H_2O$	Hydrated potassium neptunium (V) carbonate – (1:1:1) complex

$K_3NpO_2(CO_3)_2 \cdot 0.5H_2O$	Hydrated potassium neptunium (V) carbonate – (3:1:2) complex
KOH	Potassium hydroxide
K_2SO_4	Potassium sulfate
$K_2U_2O_7$	Potassium diuranate
Li^+	Lithium ion
M(III)	Metal in the +3 oxidation state
Mg	Magnesium
Mg^{2+}	Magnesium cation
$MgCl_2$	Magnesium chloride
$Mg_3(OH)_5Cl \cdot 4H_2O$	Magnesium chloride hydroxide hydrate
$MgCO_3$	Magnesite, magnesium carbonate
$Mg_5(CO_3)_4(OH)_2 \cdot 4H_2O$	Hydromagnesite
$Mg_2(OH)_3Cl \cdot 4H_2O$	Magnesium chloride hydroxide hydrate, magnesium oxychloride
MgO	Periclase, magnesium oxide
$Mg(OH)_2$	Brucite, magnesium hydroxide
Mn	Manganese
N_2	Nitrogen
Na	Sodium
Na^+	Sodium cation
NaBr	Sodium bromide
NaCl	Sodium chloride, Halite
$NaClO_4$	Sodium perchlorate
NaOH	Sodium hydroxide
Na_2SO_4	Sodium sulfate
$Na_2S_2O_4$	Sodium hydrosulfite
$NaAm(CO_3)_2$	Sodium americium (III) carbonate
$NaHCO_3$	Sodium bicarbonate
$NaNpO_2CO_3 \cdot 3.5H_2O$	Hydrated sodium neptunium (V) carbonate – (1:1:1) complex
$Na_3NpO_2(CO_3)_2$	Sodium neptunium (V) carbonate – (3:1:2) complex
NaOH	Sodium hydroxide
$Na_2U_2O_7 \cdot xH_2O$	Sodium diuranate hydrate
Nd	Neodymium

Nd(III)	Neodymium in the +3 oxidation state
$Nd(OH)_3$	Neodymium (III) hydroxide
Ni	Nickel
Ni^{2+}	Nickel (II) cation
NO_3^-	Nitrate anion
Np	Neptunium
Np(IV)	Neptunium in the +4 oxidation state
Np(V)	Neptunium in the +5 oxidation state
Np(VI)	Neptunium in the +6 oxidation state
Np^{4+}	Neptunium cation – Aqueous form of the neptunium at the +4 oxidation state
NpO_2	Neptunium (IV) oxide
NpO_2^+ or $Np(V)O_2^+$	Neptunyl cation – Aqueous form of the neptunium at the +5 oxidation state
NpO_2^{2+} or $Np(VI)O_2^{2+}$	Neptunyl cation – Aqueous form of the neptunium at the +6 oxidation state
NpO_5^{3-}	Neptunyl anion – Aqueous form of the neptunium at the +7 oxidation stateNp$O_2CO_3^-$ Neptunium (V) carbonate ion – (1:1) complex
$NpO_2(CO_3)_2^{3-}$	Neptunium (V) carbonate ion – (1:2) complex
$NpO_2(CO_3)_3^{5-}$	Neptunium (V) carbonate ion – (1:3) complex
$Np(OH)_3$	Neptunium (III) hydroxide
$Np(OH)_4$	Neptunium (IV) hydroxide
$Np(OH)_5^-$	Neptunium (IV) hydroxide ion – (1:5) complex
NpO_2OH	Neptunium (V) hydroxide
$NpO_2(OH)_2$	Neptunium (VI) hydroxide
$NpO_2(OH)_2^-$	Neptunium (V) hydroxide ion – (1:2) complex
O	Oxygen
O_2	Molecular oxygen
OBr^-	Hypobromite anion
OCl^-	Hypochlorite anion
OH	Hydroxide
OH^-	Hydroxide anion
$OH\cdot$	Hydroxyl radical
Pb	Lead

Pb^{2+}	Lead cation – Aqueous form of the lead at the +2 oxidation state
Pb^{4+}	Lead cation – Aqueous form of the lead at the +4 oxidation state
$PbCl_2$	Lead (II) chloride
$PbCO_3$	Lead (II) carbonate
$[Pb_6O(OH)_6]^{4+}$	Lead (II) polyoxyhydroxide cation
PbO	Lead (II) oxide
PO_4^{3-}	Phosphate anion
$(PbOH)_2CO_3$	Lead (II) hydroxide carbonate
PbS	Lead (II) sulfide
$PbSO_4$	Lead (II) sulfate
Pu	Plutonium
Pu(III)	Plutonium in the +3 oxidation state
Pu(IV)	Plutonium in the +4 oxidation state
Pu(V)	Plutonium in the +5 oxidation state
Pu(VI)	Plutonium in the +6 oxidation state
Pu(VII)	Plutonium in the +7 oxidation state
Pu^{3+}	Plutonium cation – Aqueous form of the plutonium at the +3 oxidation state
Pu^{4+}	Plutonium cation – Aqueous form of the plutonium at the +4 oxidation state
$Pu(CO_3)^+$	Plutonium (III) carbonate ion – (1:1) complex
$Pu(CO_3)_2^-$	Plutonium (III) carbonate ion – (1:2) complex
$Pu(CO_3)_3^{3-}$	Plutonium (III) carbonate ion – (1:3) complex
PuF_2^{2+}	Plutonium (IV) fluoride cation
PuO_2	Plutonium (IV) dioxide
PuO_{2+x}	Oxidized plutonium (IV) dioxide
PuO_2CO_3	Plutonium (VI) carbonate
$PuO_2CO_3^-$	Plutonium (V) carbonate ion – (1:1) complex
$PuO_2(CO_3)_2^{3-}$	Plutonium (V) carbonate ion – (1:2) complex
$PuO_2(CO_3)_2^{2-}$	Plutonium (VI) carbonate ion – (1:2) complex
$PuO_2(CO_3)_3^{4-}$	Plutonium (VI) carbonate ion – (1:3) complex
PuO_2F^+	Plutonium (VI) oxofluoride cation
PuO_2^+ or $Pu(V)O_2^+$	Plutonyl cation – Aqueous form of the plutonium at the +5 oxidation state
PuO_2^{2+} or $Pu(VI)O_2^{2+}$	Plutonyl cation – Aqueous form of the plutonium at the +6 oxidation state
$PuO_2(OH)_2$	Plutonium (VI) hydroxide

$PuO_3 \cdot xH_2O$	Plutonium (VI) trioxide-hydrate
$Pu(OH)_3$	Plutonium (III) hydroxide
$Pu(OH)_3^+$	Plutonium (IV) hydroxide cation – (1:3) complex
$Pu(OH)_4$	Plutonium (IV) hydroxide
$[Pu(H_2O)_m]^{n+}$	Hydrolysis complex of plutonium
$[Pu(O)Pu(O)Pu(O)...]_n$	Plutonium polymer
S^{2-}	Sulfide anion
SO_4^{2-}	Sulfate anion
Sr	Strontium
Th	Thorium
Th(IV)	Thorium in the +4 oxidation state
Th^{3+}	Thorium cation – Aqueous form of the thorium at the +3 oxidation state
Th^{4+}	Thorium cation – Aqueous form of the thorium at the +4 oxidation state
$Th(CO_3)_5^{6-}$	Thorium (IV) pentacarbonyl ion complex
$ThISA_2^{2+}$	Thorium (IV) isosaccharinic acid ion – (1:2) complex
ThO_2	Thorium dioxide
$Th(OH)^{3+}$	Thorium (IV) hydroxide ion – (1:1) complex
$Th(OH)_2^{2+}$	Thorium (IV) hydroxide ion – (1:2) complex
$Th(OH)_3^+$	Thorium (IV) hydroxide ion – (1:3) complex
$Th_4(OH)_{12}^{4+}$	Thorium (IV) hydroxide ion – (4:12) complex
$Th_6(OH)_{15}^{9+}$	Thorium (IV) hydroxide ion – (6:9) complex
$Th(OH)_4$	Thorium hydroxide
$Th(OH)(CO_3)_4^{5-}$	Thorium (IV) hydroxide carbonate ion – (1:1:4) complex
$Th(OH)_2(CO_3)_2^{2-}$	Thorium (IV) hydroxide carbonate ion – (1:2:2) complex
$Th(OH)_3CO_3^-$	Thorium (IV) hydroxide carbonate ion – (1:3:1) complex
$Th(OH)_2SO_4$	Thorium (IV) hydroxide sulfate ion – (1:2:1) complex
$Th(OH)_4ISA_2^{2-}$	Thorium (IV) hydroxide isosaccharinic acid ion – (1:4:2) complex
$Th(SO_4)_3^{2-}$	Thorium (IV) sulfate ion – (1:3) complex
$Th(SO_4)_2$	Thorium (IV) sulfate
$Th(SO_4)_2 \cdot K_2SO_4 \cdot 4H_2O$, $Th(SO_4)_2 \cdot 2K_2SO_4 \cdot 2H_2O$, $Th(SO_4)_2 \cdot 3.5K_2SO_4$	Hydrated potassium thorium (IV) sulfate complex
$Th(SO_4)_2 \cdot Na_2SO_4 \cdot 6H_2O$	Hydrated sodium thorium (IV) sulfate complex
U	Uranium

U(III)	Uranium in the +3 oxidation state
U(IV)	Uranium in the +4 oxidation state
U(V)	Uranium in the +5 oxidation state
U(VI)	Uranium in the +6 oxidation state
U^{3+}	Uranium cation – Aqueous form of the uranium at the +3 oxidation state
U^{4+}	Uranium cation – Aqueous form of the uranium at the +4 oxidation state
UO_2	Uraninite, uranium (IV) dioxide
UO_2^{2+} or $U(VI)O_2^{2+}$	Uranyl cation – Aqueous form of the uranium at the +6 oxidation state
UO_2CO_3	Rutherfordine, uranium (VI) carbonate
$UO_2(CO_3)_2^{2-}$	Uranium (VI) carbonate ion – (1:2) complex
$UO_2(CO_3)_3^{4-}$	Uranium (VI) carbonate ion – (1:3) complex or triscarbonato complex
$(UO_2)_3(CO_3)_6^{6-}$	Uranium (VI) carbonate ion – (3:6) complex
$(UO_2)_2(CO_3)(OH)_3^-$	Uranium (VI) carbonate hydroxide ion – (2:1:3) complex
$(UO_2)_{11}(CO_3)_6(OH)_{12}^{2-}$	Uranium (VI) carbonate hydroxide ion – (11:6:12) complex
$UO_2(OH)_3^-$	Uranium (VI) hydroxide ion – (1:3) complex
$UO_2(OH)_4^{2-}$	Uranium (VI) hydroxide ion – (1:4) complex
$U(OH)_4$	Uranium (IV) hydroxide
$UO_2.xH_2O$	Hydrous uranium (IV) dioxide
$(UO_2)(OH)_2 \cdot xH_2O$ or $UO_3 \cdot xH_2O$	Schoepite, hydrated uranium trioxide
V	Vanadium
ZrO_2	Zirconium dioxide

This page intentionally left blank.

SOTERM-1.0 Introduction

Appendix SOTERM-2019 (Actinide Chemistry Source Term) is a summary of the U.S. Department of Energy's (DOE's) understanding of the Waste Isolation Pilot Plant (WIPP) chemical conditions, processes and underlying actinide chemistry; and the resulting actinide concentrations that were calculated based on this repository chemistry.

The information in this Appendix supports the Compliance Recertification Application (U.S. DOE 2019) deferred performance assessment (PA) (U.S. DOE 2019, Appendix PA-2019). The updated inventory (Van Soest 2018) is presented and discussed in the context of how this impacts the actinide source term. New literature and project data since the CRA-2014 data cutoff (December 31, 2012) are summarized and their impact on the actinide source term is assessed. Lastly, the contributions to the actinide source term, calculated as part of the CRA-2019 PA process, are summarized and compared with past mobile actinide source terms.

Actinide release from the WIPP is a critical performance measure for the WIPP as a transuranic (TRU) waste repository. There are a number of potential pathways for actinide release considered by WIPP PA; these are discussed in detail in Appendix PA-2019 (U.S. DOE 2019, Appendix PA Section 2.1). Quantifying the impact of these releases contributes directly to assessing compliance with 40 Code of Regulations (CFR) Part 191 (U.S. EPA 1993).

In the undisturbed scenario for PA, actinide release up the shafts or laterally through the marker beds are insignificant in all realizations and have no impact on compliance (U.S. DOE 2019, Appendix PA Section 7.2). The self-sealing of the salt and the reducing anoxic environment in the repository provide the primary mechanisms for geologic isolation of the TRU waste in the undisturbed scenario. For the disturbed scenarios, actinide releases can occur as a result of inadvertent human intrusions (i.e., boreholes drilled into or through the repository). For example, direct brine release (DBR) to the accessible environment may occur during a drilling intrusion, or actinides may be transported up a borehole to the Culebra Dolomite Member of the Rustler Formation and then move laterally through the Culebra to the Land Withdrawal Boundary. The potential for human intrusions makes it important to assess the range of possible repository conditions and actinide concentrations associated with the disturbed scenarios.

This appendix focuses on the mobile actinide source term used in the calculation of actinide release from the WIPP for DBR and transport through the Salado Formation and Culebra. This actinide source term is the sum of the soluble and colloidal species in brine. Direct release of actinide particulates to the surface resulting from cuttings, cavings, and spallings is not considered part of the actinide source term because these particulate releases do not depend on the mobilized actinide concentrations in brine.

The relative importance of radioelements (U.S. DOE 2019, Appendix PA Section 4.4) that significantly contribute to the actinide source term and consequently impact the long-term performance of the WIPP is:

$$\text{Pu} \approx \text{Am} \gg \text{U} > \text{Th} \gg \text{Np, Cm, Ac, and fission products} \qquad \text{(SOTERM.1)}$$

The TRU components for this list of radionuclides are the alpha (α)-emitting isotopes of plutonium (Pu), americium (Am), neptunium (Np), curium (Cm), and californium (Cf) with half-lives greater than 20 years. These TRU actinides make up the waste unit factor used to calculate the normalized release from the WIPP in U.S. Environmental Protection Agency (EPA) units, as required by 40 CFR Part 191(U.S. EPA 1993). In SOTERM, the chemistry of actinium (Ac), thorium (Th), and uranium (U) is also discussed, since these actinides are present in the WIPP waste and their chemistry is analogous to the TRU components.

This appendix has the following overall organization:

- A short summary of key near-field conditions is presented in SOTERM Section 2.0.
- An overview of post-emplacement factors that impact the actinide source term is presented in SOTERM Section 3.0.
- Microbial processes are updated and their effects on the biogeochemistry of the actinides in the source term are discussed in SOTERM Section 4.0.
- An updated environmental chemistry overview, a summary of new literature, and a summary of WIPP-relevant results (if available) for the key actinides is given in SOTERM Section 5.0.
- A summary of the WIPP actinide PA approach and assumptions in the current PA baseline, along with the calculated actinide solution concentrations, is provided in SOTERM Section 6.0.

Each of these sections identifies important new information (if present) since the CRA-2014 (U.S. DOE 2014).

SOTERM-2.0 Ambient Geochemical Conditions, Repository Conditions and Emplacement Chemistry in the WIPP

The near-field conditions that could affect actinide concentrations in the WIPP are briefly summarized in this section. This section is now accompanied by Appendix GEOCHEM where the discussion of the models that describe this chemistry and new geochemical data for CRA-2019 are found. Overall, there are no significant changes in the WIPP repository conditions and pre-emplacement chemistry since the CRA-2014. The main changes are in updates of some of the post-emplacement chemistry processes (Appendix GEOCHEM).

SOTERM-2.1 Ambient Geochemical Conditions

Geochemical conditions that could potentially affect the mobile actinide source term are briefly summarized in this section. These include repository pressure, repository temperature, water content and relative humidity, the minimum free volume for DBR release, and the extent of the disturbed rock zone (DRZ). A summary of the current WIPP chemistry model assumptions and conditions is given in Table SOTERM-1, along with cross-references to a more detailed discussion in CRA-2014, as well as the relevant sections in CRA-2019 Appendix GEOCHEM.

The ambient geochemical conditions are discussed in detail in the Compliance Certification Application (CCA) (U.S. DOE 1996) and the CRA-2004, Chapter 2 and Chapter 6, Section 6.4.3 (U.S. DOE 2004). The Salado, which is the host formation, is predominantly pure halite (NaCl), with clay interbeds (marker beds) consisting mainly of anhydrite ($CaSO_4$). The nearly pure halite contains accessory evaporite minerals such as anhydrite ($CaSO_4$), gypsum ($CaSO_4{\cdot}2H_2O$), polyhalite ($K_2MgCa_2(SO_4)_4{\cdot}2H_2O$), magnesite ($MgCO_3$), and clays. Small quantities of intergranular (grain-boundary) brines and intragranular brines (fluid inclusions) are associated with the salt at the repository horizon. These brines are highly concentrated solutions (ionic strength up to 8 moles per liter [M]) of predominantly sodium (Na^+), magnesium (Mg^{2+}), potassium (K^+), chloride (Cl^-), and sulfate (SO_4^{2-}), with smaller amounts of calcium (Ca^{2+}), carbonate (CO_3^{2-}), and borate ($B(OH)_4^-$ and/or $B_4O_7^{2-}$). These brines have been in contact with the Salado evaporite minerals since their deposition (estimated to be 250 million years) and are saturated with respect to these minerals.

Underlying the Salado is the Castile Formation, composed of alternating units of interlaminated carbonate, anhydrite, and nearly pure halite. The Castile in the vicinity of the WIPP site is known to contain localized brine reservoirs with sufficient pressure to force brine to the surface if penetrated by a borehole. Castile brines are predominantly saturated NaCl solutions containing Ca^{2+} and SO_4^{2-}, as well as small concentrations of other elements, and are about eight times more concentrated than seawater. Overlying the Salado in the vicinity of the WIPP site is the Culebra Dolomite Member of the Rustler Formation, a fractured dolomite ($CaMg(CO_3)_2$) layer. The Culebra is significant because it is expected to be the most transmissive geologic pathway to the accessible environment. Culebra brines are generally more dilute than the Salado and Castile brines, and are predominantly NaCl with the following cations/anions: K^+, Mg^{2+}, Ca^{2+}, SO_4^{2-}, and CO_3^{2-}.

Table SOTERM-1. Summary of Current WIPP Chemistry Model Assumptions and Conditions

Repository Condition or Parameter	CRA-2019 PA Assumptions	SOTERM-2014 Section	CRA-2019 Appendix GEOCHEM	Changes since CRA-2014
Ambient Geochemistry	Predominantly halite of the Salado Formation, with anhydrite interbeds and inclusions.	2.1	1.2.1 and 1.2.2	None
Temperature	Ambient temperature is 27 °C (80 °F). A transient, short–lived, increase of up to 12 oC (21.6 °F) is possible as a result of the emplacement of TRU waste.	2.2.2	1.2.5.2	None
Humidity	~73 percent (%) relative humidity (RH) at the repository temperature.	2.2.3	1.2.5.3	None
Water Content	Host rock is groundwater-saturated with inclusions in the salt that range from 0.057% to 3% by mass. Repository is initially unsaturated until a borehole intrusion occurs. An intrusion cannot occur until 100 years after closure.	2.2.3	1.2.5.3	None
Pressure	A maximum pressure in the repository of about 15 megapascals (MPa) (148 atmospheres [atm]), equivalent to the lithostatic stress at the repository level; a hydrostatic pressure of about 8 MPa (79.0 atm) at the bottom of an intrusion borehole at repository depth.	2.2.1	1.2.5.1	None
Gas Phase	Initially air/oxic at repository closure, but rapidly transitions to an anoxic atmosphere dominated by hydrogen with smaller amounts of methane and nitrogen. Trace amounts of carbon dioxide, hydrogen sulfide, and other microbial gases may be present.	2.2.3 2.4.1	2.1.1	None
Disturbed Rock Zone (DRZ)	Upper bound of 12 meters (m) above the repository and 2 m below the repository horizon.	2.2.5	N/A	None
Minimum Brine Volume for DBR	The calculated minimum volume of brine from any source needed for DBR release is 17,400 cubic meters (m^3). This volume is the basis of the variable brine volume approach now used in PA.	2.2.4	1.2.5.4	None
WIPP Brine	High-ionic-strength brine that varies with pH and reaction with magnesium oxide (MgO) but is bracketed by generic weep brine (GWB) and Energy Research and Development Administration (ERDA)-6 brine formulations used in the WIPP project.	2.3.1	3.2.1 and 3.2.3	See additional discussion in SOTERM-3.1

Table SOTERM-1. Summary of Current WIPP Chemistry Model Assumptions and Conditions (Continued)

Repository Condition or Parameter	CRA-2019 PA Assumptions	SOTERM-2014 Section	CRA-2019 Appendix GEOCHEM	Changes since CRA-2014
pH	The expected pH is about 9 (ionic-strength-corrected measured pH (pCH+) of 9.5) and controlled by MgO. The borate and carbonate present add to the brine buffer capacity.	2.3.2	3.2.1	None

SOTERM-2.2 Repository Conditions: Assumptions and Role of the Engineered Barrier and Key WIPP Processes

A summary of the assumptions/role of the engineered barrier and key WIPP-relevant processes is given in Table SOTERM-2. This information is also cross-referenced to relevant and more detailed discussions in CRA-2014 Appendix SOTERM (U. S. DOE 2014) and the CRA-2019 Appendix GEOCHEM. Radiolysis and microbial effects are discussed further in Sections SOTERM 3.4 and SOTERM 4 respectively.

Table SOTERM-2. Assumptions/Role of the Engineered Barrier, Emplaced Waste, and Key WIPP Subsurface Processes

Barrier or Process	CRA-2019 Assumptions and Role in PA	SOTERM-2014 Section	CRA-2019 Appendix GEOCHEM	Changes since CRA-2014
MgO	Engineered barrier for the WIPP that will sequester carbon dioxide (CO_2) and control increases and decreases in pH by the precipitation of brucite $Mg(OH)_2$, hydromagnesite $Mg_5(CO_3)_4(OH)_2.4H_2O$, and magnesite.	2.3.3	2.2.3 and 3.2.4	See updated information in Appendix MgO
Corrosion	Container steel and metals in WIPP waste will react to remove oxygen and produce hydrogen. These produce Fe(II) phases and magnetite.	2.3.4	2.2.1, 3.2.8 and 3.3.8	Sulfidation was removed. See discussion in Appendix GEOCHEM
Iron(Fe) and Lead(Pb) Chemistry	The chemistry of iron and lead, which are added to the repository, contributes to our overall understanding of the chemistry of actinides in brine, but this chemistry is selectively implemented in PA.	2.3.4 and 2.3.5	3.2.7 and 3.2.8	See updated discussion of new data in Appendix GEOCHEM, Also new speciation models were added.

Table SOTERM-2. Assumptions/Role of the Engineered Barrier, Emplaced Waste, and Key WIPP Subsurface Processes (Continued)

Barrier or Process	CRA-2019 Assumptions and Role in PA	SOTERM-2014 Section	CRA-2019 Appendix GEOCHEM	Changes since CRA-2014
Organic Chelating Agents	The four organic chelating agents addressed by PA are acetate, oxalate, citrate and ethylenediaminetetraacetic acid (EDTA). These are assumed to not degrade under the expected WIPP conditions; their concentration is defined by their inventory (except for oxalate, which is solubility limited); these complexing agents form actinide complexes that increase their solubility in the source term.	2.3.6	3.2.5	Solubility controlling phases for EDTA and citrate have been added. See GEOCHEM Section 3.2.5
Cellulosic, Plastic and Rubber materials (CPR)	These materials are introduced to the WIPP as waste, packaging material and emplacement material. Their biodegradation leads to the formation of carbon dioxide that dissolves in brine to form bicarbonate/carbonate species that impact pH and complex actinides.	2.3.7	2.2.2	See updated inventory data in SOTERM Section 3.1
Microbial Effects	Gas generation, primarily carbon dioxide and hydrogen sulfide, resulting from the biodegradation of CPR materials and creation of reducing conditions, including bioreduction of actinide elements from higher oxidation states. Microbial processes are assumed to occur in all PA realizations.	2.4.1, also see section 3.1 in this appendix	Microbial gas generation is addressed in Section 2.2.2	See updated discussion of new data in SOTERM Section 4
Radiolysis	Localized oxidizing effects possible near high-activity actinides, but overall radiolytic processes are largely controlled by the in-room chemistry. Radiolytic contribution to gas generation is a more significant contributor to overall gas generation due to the significant increase of plutonium in the WIPP inventory and changes in the screening argument.	2.4.2, also see section 3.2 in this appendix	2.1.7	See updated discussion in SOTERM Section 3.4

SOTERM-3.0 Post-emplacement Inventory, Chemical, and Radiolytic Processes

There are a number of important post-emplacement processes that take place in the WIPP after repository closure. In the salt repository concept, the post-emplacement chemistry is defined by the reaction of high ionic-strength brines and the emplaced waste and materials. In this view, many of the key chemical parameters, although altered by the host geology, are mostly defined by what is emplaced (e.g., pH, redox potential (E_h), solubility and colloidal tendencies). Defining the post emplacement chemistry, for this reason, starts with an update of the key waste constituents based on the Performance Assessment Inventory Report (Van Soest 2018) for CRA-2019. These inventory data are compared to the CRA-2014 inventory reported to provide insight to the overall trends. Corrosion, MgO reactivity, iron chemistry, and lead chemistry, are discussed in Appendix GEOCHEM (see Table SOTERM-2). The brine chemistry used to support the actinide solubility studies, potential concentration of key organic complexants, and radiolytic effects are discussed in this section.

SOTERM-3.1 Inventory of Emplaced Materials in the WIPP

The total PAIR 2018 waste (non-radioactive), packaging and cement materials used in the deferred CRA-2019 PA are summarized in Tables SOTERM-3 (inorganic) and SOTERM-4 (organic). These are also compared to the inventory data used in CRA-2014 to establish trends. A full reporting and updating of these inventory data can be found in CRA-2019 PAIR-2018 (Van Soest 2018).

The CRA-2019 inorganic inventory data show significant, but not impactive (i.e., less than a factor of two), changes when compared to CRA-2014. The projected iron content is ~ 25% higher, the projected aluminum-based alloys are ~ 22% higher and there is an increase of ~43% in the category of “other” inorganic materials. The categories of cement (down ~18%) and soils (down ~ 16%) show decreases. The one large and significant change is in the projected lead inventory which shows a ~1700-fold planned increase from CRA-2014 due to the increased use of shielded containers.

The CRA-2019 organic emplacement inventory also shows significant but not impactive changes. Total CPR (up ~15%), cellulosics (up ~28%), plastics (up ~ 11%) all show significant increases. Rubber shows a very slight decrease. Organic chelating agents are mostly unchanged, with small decreases in oxalate (down ~4%) and citrate (down ~1%) and a slight increase in EDTA (up ~7%). Only acetate shows a significant change and is up ~ 23%.

The impacts of this updated total (projected and emplaced) inventory on the approach to defining the mobile actinide source term are:

- Iron, as zero valent and Fe(II) phases, remains in great excess and will continue to define reducing/anoxic conditions for the actinides should brine inundation occur.
- Lead is now a very significant part of the repository chemistry and model updates that reflect the potential impacts of this on the actinide chemistry are now increased in importance. A lead model has been added in CRA-2019. The presence of lead, due to

competition with organic ligands and the expectation that it will contribute to the establishment of reducing conditions, will help immobilize actinides and the absence of a model that takes credit for this chemistry is one of many conservatisms in the actinide model.

- Cement content is not increasing and remains a non-factor in the WIPP chemistry due to the high magnesium (added MgO) in the WIPP repository concept.
- The increase in CPR will correspondingly increase the MgO content (this is implemented operationally to meet the 1.2 safety factor requirement). This engineered barrier will continue to define the low carbonate concentrations and moderately high pH in our current conceptual model.
- Organic chelating agents, although they remain a dominant factor in defining the mobile actinide source term, did not change significantly. Calcium and magnesium competition was added to the model implementation. More specifically, only small changes to EDTA and citrate inventories, which are the key complexants relative to the An(III) actinides, were observed. The significant increase in acetate is a non-factor from the point of view of source term definition. The acetate should be readily biodegraded in the WIPP although it is assumed to be nondegradable.

Table SOTERM-3. Total PAIR 2018 Inorganic Waste, Packaging and Emplacement Materials in the WIPP Repository (PAIR 2012 and PAIR 2018)

Material	Source/Type	[1]CRA-2014 (Data Cutoff: December 31, 2011)		[2]CRA-2019 (Data Cutoff: December 31, 2017)	
		Amount by component or source (kg)	Total (kg)	Amount by component or source (kg)	Total (kg)
Aluminum-based metals/alloys	CH and RH Waste	N/A	4.57×10^5	N/A	5.56×10^5
Lead	Packaging	N/A	8.28×10^3	N/A	1.38×10^7
Iron-based metals/alloys	CH and RH Waste	N/A	1.22×10^7	N/A	1.54×10^7
Other Inorganic Materials	CH and RH Waste	N/A	7.37×10^6	N/A	1.05×10^7
Other Metal/Alloys	CH and RH Waste	N/A	1.23×10^6	N/A	9.83×10^5
Cement[3]	Reacted	4.22×10^6	1.08×10^7	2.33×10^6	8.88×10^6
	Unreacted	0		3.20×10^3	
	Combination	6.55×10^6		6.55×10^6	
Soils	CH and RH Waste	N/A	5.94×10^6	N/A	5.01×10^6
MgO	Emplacement	N/A	51,430[4] tons	N/A	33,400[5] tons as of 8/13/19 (Offner 2019)

[1] PAIR-2012 (Van Soest 2012)
[2] PAIR-2018 (Van Soest 2018)
[3] Contains only site reported data since not specifically tracked in the Waste Data System (WDS) – reacted means already fully hydrated, combination means that a combination of reacted and unreacted cement was reported.
[4] 2014 amount included projected.
[5] 2019 amount included emplaced only.
N/A – Not Applicable

Table SOTERM-4. Total PAIR 2018 Organic Waste, Packaging and Emplacement Materials in the WIPP Repository (PAIR 2012 and 2018)

Material	[1]Source/Type	[2]CRA-2014 (Data Cutoff: December 31, 2011)		[3]CRA-2019 (Data Cutoff: December 31, 2017)	
		Amount (kg)	Total (kg)	Amount (kg)	Total (kg)
CPR total	Waste	1.03×10^{7}	1.54×10^{7}	1.11×10^{7}	1.78×10^{7}
	Packaging	3.57×10^{6}		4.85×10^{6}	
	Emplacement	1.51×10^{6}		1.77×10^{6}	
	Operational	NA		9.72×10^{3}	
Cellulosics	Waste	3.66×10^{6}	4.65×10^{6}	4.27×10^{6}	5.97×10^{6}
	Packaging	7.23×10^{5}		1.47×10^{6}	
	Emplacement	2.6×10^{5}		2.24×10^{5}	
	Operational	NA		4.50×10^{1}	
Plastics	Waste	5.50×10^{6}	9.51×10^{6}	5.73×10^{6}	1.06×10^{7}
	Packaging	2.77×10^{6}		3.30×10^{6}	
	Emplacement	1.25×10^{6}		1.54×10^{6}	
	Operational	NA		4.89×10^{3}	
Rubber	Waste	1.18×10^{6}	1.25×10^{6}	1.14×10^{6}	1.22×10^{6}
	Packaging	7.33×10^{4}		7.85×10^{4}	
	Emplacement	0		0	
	Operational	NA		4.79×10^{3}	
Organic Ligands (total)	All	N/A	5.07×10^{4}	N/A	5.54×10^{4}
[4]Organic Ligands	Acetate	9.96×10^{3}	2.41×10^{4}	1.37×10^{4}	2.96×10^{4}
	Acetic Acid	1.41×10^{4}		1.59×10^{4}	
	Oxalate	6.50×10^{2}	1.85×10^{4}	7.00×10^{2}	1.77×10^{4}
	Oxalic Acid	1.78×10^{4}		1.70×10^{4}	
	Citrate	2.55×10^{3}	7.78×10^{3}	2.63×10^{3}	7.70×10^{3}
	Citric Acid	5.23×10^{3}		5.08×10^{3}	
	EDTA	3.76×10^{2}	3.76×10^{2}	4.03×10^{2}	4.03×10^{2}

[1]Emplacement materials are non-containerized CPR material used in emplacement; Operations materials are CPR materials used in the operation of emplacing waste or MgO.

[2]PAIR-2012 (Van Soest 2012)

[3] PAIR-2018 (Van Soest 2018)

[4] Contains only site reported data since not specifically tracked in the WDS – reacted means already fully hydrated, combination means that a combination of reacted and unreacted cement was reported.

NA – Not Available

SOTERM-3.2 WIPP-Relevant Brine Chemistry

The range in brine composition expected in the WIPP is based on sampling within and around the WIPP horizon and is discussed extensively elsewhere (Lucchini et al. 2013c; Appendix GEOCHEM, Section 3.1.6). The modeling approach and associated mineral and chemical equilibrium reactions are described in Appendix GEOCHEM Section 3.2. The end-member brines GWB (high magnesium representing seep brine) and ERDA-6 (higher pH, low Mg, representing the underlying Castile Formation brine) bracket the range of brine composition expected. These brines essentially transition into one another upon pH titration and were shown to be stable over the multi-year timeframes toward precipitation (see Table SOTERM-5).

Although some early studies within the WIPP project utilized real-system brines, simulated brines have always been used throughout the WIPP project to assure experimental consistency. The formulation of these simulated brines has evolved somewhat with time (see Lucchini et al. [2013c] and Appendix GEOCHEM for this historical context) but the GWB to ERDA-6 bracketing and/or transitional brines have been used in most recent WIPP-relevant laboratory studies (Borkowski et al. 2009; Lucchini et al. 2010a, 2013a, 2013c; Reed et al. 2006; Reed et al. 2010). These are typically diluted by 5 or 10% to permit the sampling of long-term experiments (otherwise salt precipitation could occur) and minimize mineral colloid and pseudo-colloid formation. This dilution is a necessary step, in particular, for anoxic experiments that must be done in a glovebox that is typically very dry.

Table SOTERM-5. WIPP-relevant Brine Compositions as a Function of pC_{H+}. Data are Based on the Experimental GWB (100% Saturated Formulation) pH Titration Experiments. Composition of Full-strength GWB and ERDA-6 Brines (100% Saturated Formulation) is Also Given (Lucchini et al. 2013c, Table 11).

pC_{H+} or Brine	[1]Element/Species - Measured Concentrations (M)								
	Na^+	K^+	Mg^{2+}	Ca^{2+}	Li^+	$B_4O_7^{2-}$	Cl^-	SO_4^{2-}	Br^-
GWB	3.53	0.467	1.02	1.38×10^{-2}	4.48×10^{-3}	3.95×10^{-2}	5.6	0.177	2.66×10^{-2}
9	3.50	0.458	1.03	1.35×10^{-2}	3.75×10^{-3}	3.89×10^{-2}	5.43	0.176	2.35×10^{-2}
9.5	3.72	0.459	0.850	1.31×10^{-2}	3.70×10^{-3}	1.64×10^{-2}	5.55	0.176	2.42×10^{-2}
10	4.59	0.450	0.117	1.34×10^{-2}	3.57×10^{-3}	2.77×10^{-3}	5.35	0.169	2.34×10^{-2}
10.5	4.91	0.454	2.86×10^{-2}	1.24×10^{-2}	3.54×10^{-3}	1.66×10^{-2}	5.39	0.169	2.32×10^{-2}
ERDA-6	4.87	9.70×10^{-2}	1.90×10^{-2}	1.20×10^{-2}	N/A	1.58×10^{-2}	4.80	0.170	1.10×10^{-2}
11	4.96	0.449	1.11×10^{-2}	1.09×10^{-2}	3.54×10^{-3}	3.05×10^{-2}	5.31	0.168	2.30×10^{-2}
12	5.02	0.454	1.05×10^{-2}	6.97×10^{-3}	3.46×10^{-3}	3.29×10^{-2}	5.31	0.169	2.32×10^{-2}
13	5.11	0.452	9.74×10^{-3}	2.14×10^{-3}	3.55×10^{-3}	2.99×10^{-2}	5.32	0.167	2.35×10^{-2}

[1]Uncertainties in the analytical data are ± 10%

These simulated brine compositions, however, cannot be used for the collection of thermodynamic data due to their inherent complexity and more simplified binary brines are used

for this purpose (e.g., sodium chloride (NaCl), magnesium chloride ($MgCl_2$), and calcium chloride ($CaCl_2$)). The range in pH, E_h, total inorganic carbon (TIC), and ionic strength (I) are summarized in Table GEOCHEM-38 and help define the range in parameters for experimental studies.

All these brine studies are site-specific and relevant to the WIPP project. They, as augmented by their reactivity with key waste constituents (e.g., Pb, Fe and MgO), define the scope of constituents and brine components that are needed to define the WIPP relevant chemistry. These site-specific studies challenge the model predictions and have been instrumental in identifying key interactions and impacts of the lesser components (e.g., bromine (Br), sulfate (SO_4^{2-}), and borate (BO_3^{3-})/tetraborate ($B_4O_7^{2-}$) that would be missed in simplified brine studies.

SOTERM-3.3 Complexation of Actinides by Organic Chelating Agents

The complexation of chelating agents with actinides has a significant impact on the concentrations of actinides in brine. At the pH of interest to the WIPP PA, only EDTA and citrate complex strongly enough to impact observed concentrations and this impact is mostly centered on the An(III) oxidation state although there are also significant effects on the An(IV) oxidation state as well. Organic complexes also dominate the speciation of An(V).

SOTERM-3.3.1 Projected Concentration of Organic Chelating Agents under WIPP-relevant Conditions

The concentrations of the four organic chelating agents used for CRA-2019, based on the data summarized in the PAIR-2018 report, are shown in Table SOTERM-6. These, in PA, are assumed to persist for the regulatory lifetime of the WIPP repository (10,000 years) and the EDTA and citrate complexes continue to be key contributors to the actinide solubilities calculated.

Table SOTERM-6. Concentration Range of Acetate, Oxalate, Citrate and EDTA in the WIPP Repository Should Brine Inundation Occur (Domski and Sisk-Scott, 2019). These are Calculated Based on the Inventory and the Minimum Brine Volume (17,400 m^3) for DBR.

Organic Complexant	*Concentration at 1X dilution (M)	*Concentration at 5 X dilution (M)	Potential Impact on Actinide Solubility
Acetate	2.83×10^{-2}	5.67×10^{-3}	Relatively low. Weak complexant and highly biodegradable.
Oxalate	1.13×10^{-2}	2.26×10^{-3}	Relatively low. Weak complexant and biodegradable
Citrate	2.30×10^{-3}	4.61×10^{-4}	Moderate. Strong complexant, but likely degraded under WIPP conditions.
EDTA	7.92×10^{-5}	1.58×10^{-5}	High. Very strong complexation. Likely recalcitrant to degradation under WIPP conditions.

*1X and 5X refer to the dilution factor relative to the minimum brine volume needed for DBR.

SOTERM-3.3.2 Stability Constants for Organic Complexation with Actinides

The stability constants for organic ligand-actinide complexation were determined as part of the WIPP Actinide Source-term Test Program (ASTP) at Florida State University (Choppin et al. 1999). These data are summarized in Table SOTERM-7 and demonstrate some key trends in actinide complexation. For acetate, oxalate, and citrate, the strength of the complex formed is in the same order: IV > VI > III > V. For EDTA, the VI and III are switched. For the most part, the III and IV actinides, which are the two most important oxidation states in the WIPP, are strongly affected by organic complexation and thus can out-compete carbonate and hydrolysis if the organic concentrations are high enough. Of the four organic chelating agents considered, based on the formation constants in Table SOTERM-7 and WIPP-specific data in Figure SOTERM-1, only citrate and EDTA are expected to form strong enough complexes to influence the speciation of actinides and potentially increase actinide concentrations under the expected conditions in the WIPP.

Table SOTERM-7. Apparent Stability Constants for the Complexation of Organic Ligands with Actinides in NaCl Media (Choppin et al. 1999)

Organic Ligand	Actinide Ion	NaCl (molality)	log10 β1
Acetate	Am^{3+}	0.3 to 5	1.44 - 2.2
	Th^{4+}	0.3 to 5	3.68 - 4.18
	NpO_2^{+}	0.3 to 5	1.05 - 1.8
	UO_2^{2+}	0.3 to 4	2.23 - 3.09
Oxalate	Am^{3+}	0.3 to 5	4.17 - 4.63
	Th^{4+}	0.3 to 5	7.04 - 7.47
	NpO_2^{+}	1.0 to 5.0	3.62 - 4.63
	UO_2^{2+}	0.3 to 5	5.82 - 6.7
Citrate	Am^{3+}	0.3 to 5	4.84 - 5.9
	Th^{4+}	0.1 to 5	9.31 - 10.18
	NpO_2^{+}	0.1 to 5	2.39 - 2.56
	UO_2^{2+}	0.3 to 5	7.07 - 7.32
EDTA	Am^{3+}	0.3 to 5	13.76 - 15.1
	Th^{4+}	0.3 to 5	15.56 - 16.94
	NpO_2^{+}	0.3 to 5	5.45 - 6.7
	UO_2^{2+}	0.3 to 4	10.75 - 12.16

SOTERM-3.3.3 WIPP-Relevant Organic Complexation Studies

The effect of organic complexation on the concentration of neodymium, as the An(III) analog, was also evaluated for each key chelating agent (U.S. DOE 2014, Appendix SOTERM Figure SOTERM-21). These data are shown in Figure SOTERM-1. They show a strong effect of citrate and EDTA where a 1:1 complex with the neodymium is being formed and the concentration of

the neodymium is approximately the concentration of EDTA in ERDA-6 brine and approximately 50% of the concentration of EDTA in GWB brine. These data also illustrate the important effect that competition has on the observed effects on solubility.

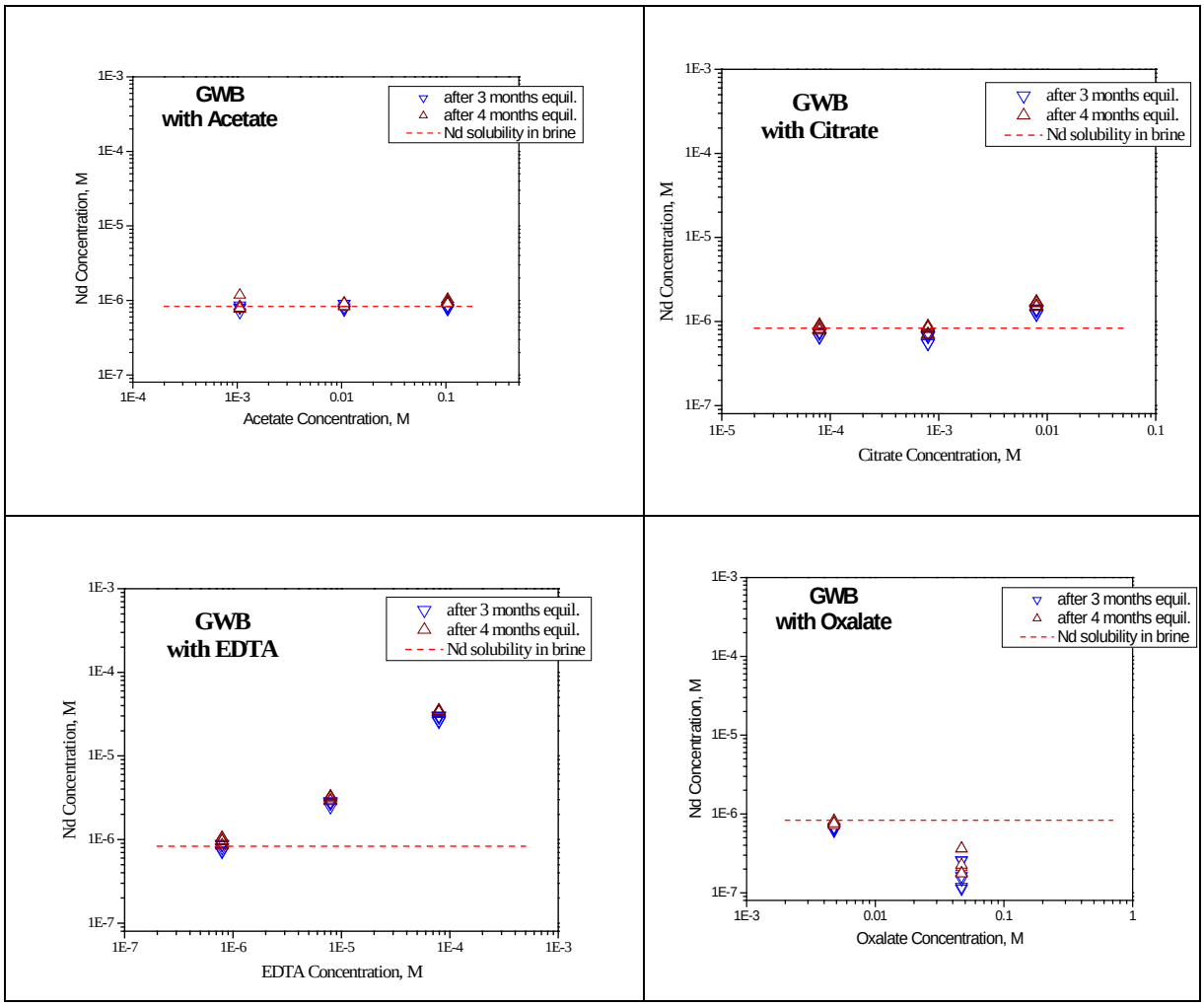

Figure SOTERM-1. Effect of EDTA, Citrate, Oxalate and Acetate on the Solubility of Nd^{3+} in GWB Brine.

The effect of organic complexation on the solubility of Th(IV), as the An(IV) actinide analog, was evaluated in GWB brine in the presence of inventory-predicted organic concentration and reported in the CRA-2014 SOTERM. The simultaneous presence of four organic chelating agents (2.42×10^{-3} M acetate, 3.02×10^{-2} M oxalate, 3.62×10^{-3} M citrate and 9.28×10^{-5} M EDTA) led to a measured thorium solubility of 7.34×10^{-7} M in GWB brine at $pC_{H+} = 9.3$. Although these data agree somewhat with model predictions, this has been shown to be an artifact of using thorium as an analog. Recent developmental studies (Yalcintas et al. 2019) show that the speciation above pH ~ 6 is the hydrolyzed EDTA complex rather than the 1:1 complex initially formed. This leads to an enhanced solubility of the An(IV) actinides that has also been observed for Pu(IV) under similar high pH conditions (Boukhalfa et al. 2004). The uranium (IV) data are shown in Figure SOTERM-2.

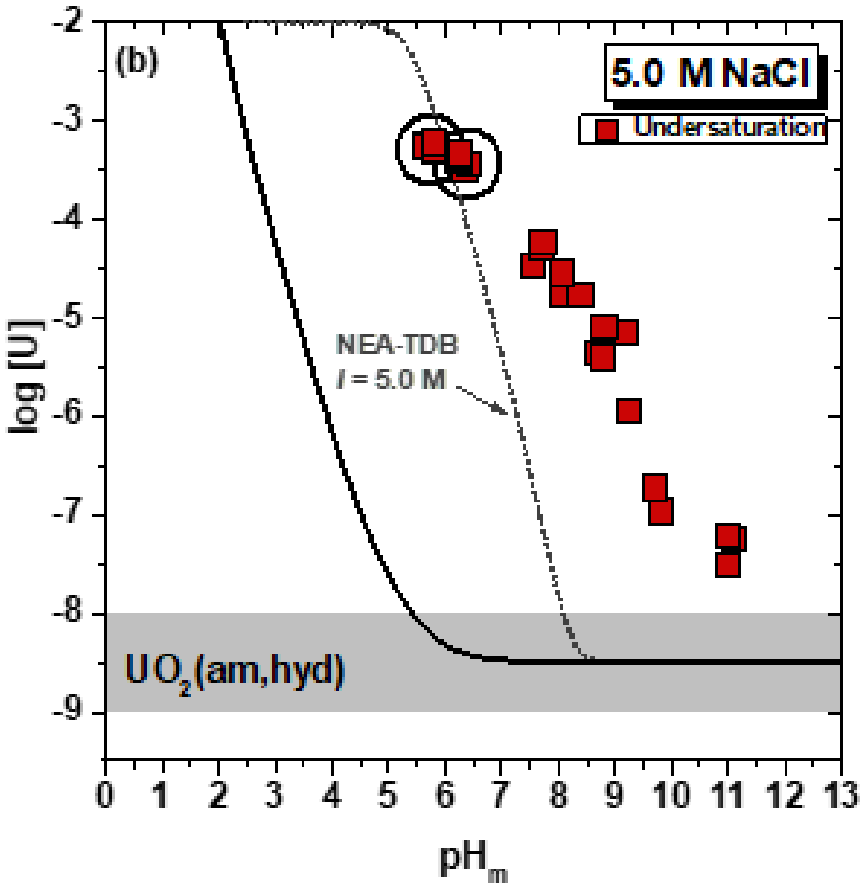

Figure SOTERM-2. Solubility of UO_2(s) in the Presence of 0.01 M EDTA in 5.0 M NaCl Brine. The Solid Line (to the left) Represents the Solubility of UO_2(am, hyd) in the EDTA–free 5.0 M NaCl System Calculated Based on the Data in Neck and Kim (2001). Circles Indicate the Undersaturation Samples Investigated by UV–Vis–NIR After Attaining Equilibrium and Confirmed to be the U(IV)-EDTA Hydrolyzed Complex. The dotted line is what is predicted using the speciation currently in the NEA-TDB database.

Lastly, the possible impact of isosaccharinic acid (ISA) on actinide species was evaluated. ISA is a chemical breakdown product of cellulosic material that has been shown to occur at pH>12. The two diastereoisomers, α- and β-isosaccharinic acids, are the products of chemical degradation of cellulosic materials in alkaline solutions. The alkaline degradation of different cellulosic materials was studied for the alkaline conditions that may exist in the initial stages of a cementitious repository (pH ~ 13.3). ISA is expected to be present in cement pore water, but it is strongly adsorbed to the cement surface. In the pore water, the concentration of ISA is expected to reach 10^{-4} M (Van Loon et al. 1997). Rai et al (2000) developed a model for Th(IV) complexation with ISA. The major feature of their model is the predominance of thorium ternary complexes, e.g., $Th(OH)_4ISA_2^{2-}$, not $ThISA_2^{2+}$ complexes, as was proposed by Allard and Ekberg (2006a and 2006b). According to Rai's model, millimoles per liter (mM) ISA concentrations will not affect solubility of thorium. Data for higher ISA concentrations might be questionable, because Rai's model is based on 15 and 69 days equilibration times for ~10^{-6} M thorium concentrations. On the basis of our experiments (Borkowski et al. 2012) and those published by German researchers (Altmaier et al. 2004), μM thorium concentrations can persist

for years as a metastable state without ISA present. Complexes with a similar stoichiometry were also observed for uranium (VI) and the authors did not observe any enhanced solubility caused by ISA for pH in the range of 9.0 to 13.5 (Warwick et al. 2006).

For WIPP-relevant conditions, the occurrence of cellulosic chemical degradation pathways have a very low probability and, even if degradation occurs, the ISA formed will likely have a negligible effect on An(IV) solubility due to its relatively low concentrations and the presence of strong chelators such as EDTA and citrate.

SOTERM-3.3.4 New Literature Organic Interaction Results Since CRA-2014

Since CRA-2014, six studies focusing on An-organic complexation were published. Brown et al. 2014 investigated the complexation behavior of Nd(III) and Am(III) with citrate up to pH 6.2 by potentiometry, absorption spectrophotometry, micro-calorimetry, and X-ray absorption fine structure (XAFS). The authors reported the formation of NdHL, NdL, $NdHL_2$, and NdL_2 complexes based on potentiometry experiments and thermodynamic data for NdHL, NdL is complemented and confirmed with spectroscopy. The complexation of acetate with Am(III) was studied as a function of the pH (1–6) by extended X-ray absorption fine-structure (EXAFS) spectroscopy (Froehlich et al. 2015). The molecular structure of the Am(III)–acetate complexes determined from Am L_{III}-edge EXAFS spectra are in very good agreement with the thermodynamic model calculations based on the Am^{3+}, $AmAc^{2+}$ and $AmAc_2^{+}$ species from pH 1 to 6. The formation of the 1:1, 1:2 and 1:3 oxalate complexes with U(VI) and Am(III); the formation of the 1:1 and 1:2 oxalate complexes with Np(V) and the formation of only one complex for Pu(V) are reported by capillary electrophoresis (Brunel et al. 2015). Skerencak-Frech et al. 2015 investigated the complexation of Cm(III) with oxalate as a function of the ligand concentration, the ionic strength (NaCl), and the temperature (T = 20−90 °C) by time-resolved laser fluorescence spectroscopy (TRLFS) and quantum chemical calculations. The formation of the complex species ($[Cm(Ox)_n]^{3-2n}$, n = 1, 2, 3, 4) are identified at 20 °C, while $[Cm(Ox)_4]^{5-}$ complex forms only at high temperatures. Precipitation of oxalate Pu(IV) and Am(III) solid phases are investigated under very acidic conditions (Noronha et al. 2017). For all of these new data, the reported species, solid phases, and associated thermodynamic data are only valid up to pH 6.

Recent studies were published on Th(IV), U(IV) and U(VI) solubility in 95%-saturated $Ca(OH)_2$ (pH 12.3) in the presence of organic ligands and CDP (cellulose degradation products) (Felipe-Sotelo et al. 2015 and 2017). An increase of Th(IV) solubility was observed in the presence of citrate (4.2×10^{-5} M) and ISA (7.3×10^{-8} M). The model calculations for the citrate system based on the reported thermodynamic data including $Th(OH)_3(citrate)_3^{8-}$ and $Th(OH)_3(citrate)_3^{8-}$ species (Felmy et al. 2006) or $Th(citrate)^{+}$ and $Th(citrate)_2^{2-}$ species (Bonin et al. 2008) underestimated the experimental results. The model calculations for the ISA system based on the data with $CaTh(H_2ISA)_2$ species (Tits et al. 2005) explain the experimental results. U(IV) solubility increased to $1.03 \times 10^{-5} \pm 1.2 \times 10^{-6}$ M in the presence of EDTA, to 2.6×10^{-5} and 8.3×10^{-5} M in the presence of citrate. U(VI) solubility increases up to 3 orders of magnitude in the presence of citrate and an order of magnitude in the presence of CDP. The solid phase characterization showed that the solubility controlling solid phases are not transformed in the presence of organic ligands. Overall, the authors concluded that known chemical and

thermodynamic models in the literature for the complexation of Th(IV), U(IV) and U(VI) with organic ligands underestimated the experimental data obtained at pH 12.3.

SOTERM-3.3.5 WIPP-specific Data on Organic Complexation Effects Since CRA-2014

There are no new WIPP-relevant quality results on actinide complexation with organic ligands since CRA-2014. This was, however, extensively investigated for the U(IV)-EDTA system (Yalcintas et al. 2019) in developmental studies.

SOTERM-3.4 Radiolysis Effects in the WIPP

Radiolysis effects in the WIPP are caused by the interaction of ionizing radiation and particles (neutrons, α, β, and γ) with the gases, brines, and materials present in the repository. These effects have not been extensively studied under WIPP-relevant conditions, but some early work was done on gas generation due to alpha particle interaction in WIPP brine (Reed et al. 1993). There is also a good general understanding of their extent and nature (Spinks and Woods 1990). For many conditions expected in the WIPP (U.S. DOE 1996), radiolytic effects are predicted to be transient and/or low in significance. In this context, there is a recognition that although radiolysis can lead to localized conditions and effects that could oxidize multivalent actinides, the brine chemistry, metal corrosion, and microbiological activity will combine to very rapidly overwhelm these effects. For this reason, radiolytic effects on actinide solubility are not explicitly included in the CRA-2019 WIPP PA to calculate actinide concentrations. This long-held view is changing somewhat as the relative importance of radiolytic gas generation has increased due to higher TRU content in the WIPP and changes in the screening argument and is now addressed in CRA-2019 (Day 2019a).

More specifics on the overall mechanisms, brine radiation chemistry, and potential radiolytic effects on actinide speciation are given in this section.

SOTERM-3.4.1 Radiation Chemistry of Brine Systems

The radiolysis of high-ionic-strength brine systems has not been extensively studied, however, some studies exist (Büppelman, Kim, and Lierse 1988; Kim et al. 1994; Kelm, Pashalidis, and Kim 1999; Ershov et al. 2002). The many components in the brine systems of interest to the WIPP will lead to relatively complex radiation chemistry and the formation of numerous transients and free radicals.

In contrast to this, the radiation chemistry of pure and dilute aqueous systems has been extensively investigated, and detailed reviews of this research have been published (Draganic and Draganic 1971; Spinks and Woods 1990). The irradiation of pure water leads to the formation of molecular hydrogen peroxide (H_2O_2) and hydrogen (H_2). These molecular yields (G) are relatively insensitive to a wide range of conditions in dilute systems for a given type of ionizing radiation. Molecular yields are G_{H2} = 0.45 molecule (molec)/100 electron-volt (eV) and G_{H2O2} = 0.7 molec/100 eV for low Linear Energy Transfer (LET) ionizing radiation (β, and γ) and G_{H2} = 1.6 molec/100 eV and G_{H2O2} = 1.5 molec/100 eV for high LET radiation (α and neutrons). The radiolytic formation of hydrogen in the WIPP brine due to self-irradiation effects

of ^{239}Pu was established and a molecular yield of G_{H2} = 1.4 molec/100 eV was measured (Reed et al. 1993). This yield is consistent with the high LET literature, even though the irradiations were performed in brine.

The high concentrations of electron and free radical scavengers present in the WIPP brine have a pronounced effect on the radiation chemistry. Most importantly, halides react with the hydroxyl radical (OH·) or act as scavengers (such as Cl^- or Br^-) to gradually lower the molecular yield of H_2O_2 as the concentration of the scavengers is increasing (Kelm, Pashalidis, and Kim 1999). In this context, oxidizing transient species are "chemically" stored as oxychlorides and oxybromides, leading to a shift towards more oxidizing conditions. Figure SOTERM-3 gives an overview of the radiolytic pathways and mechanisms that are likely (Büppelmann, Kim, and Lierse 1988). In NaCl brine, the formation of chloride species (ClO^-, HOCl, Cl_2, and Cl_3^-) is favored, instead of H_2O_2.

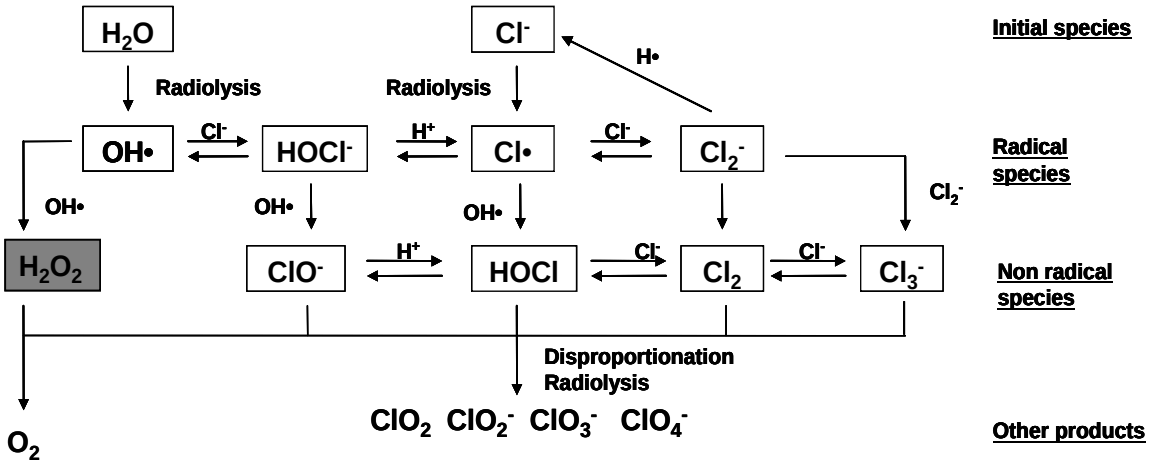

Figure SOTERM-3. NaCl Brine Radiolysis Species and Suggested Mechanism of Production. The Formation of Chloride Species (ClO^-, HOCl, Cl_2, and Cl_3^-) is Favored Instead of H_2O_2 (Based on Data in Büppelmann, Kim, and Lierse 1988).

Kelm, Pashalidis, and Kim (1999) showed that the formation of hypochlorite ion increases with the chloride concentration and the dose (Figure SOTERM-4) in NaCl brine. The authors found that in solutions containing 37 gigabecquerel (GBq)/liter (L) of ^{238}Pu, the hypochlorite concentration increases with time (dose) and appears to approach a steady state (see Figure SOTERM-4). At a constant dose rate, the maximum hypochlorite concentration depends on the chloride concentration. It was also observed that hypochlorite ion generation was negligible when chloride concentrations were smaller than 2 M.

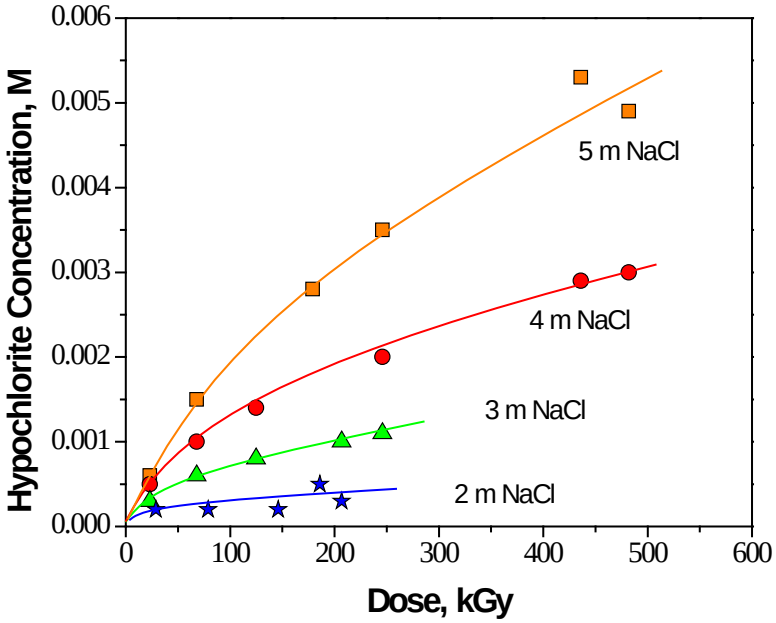

Figure SOTERM-4. Radiolytic Formation of Hypochlorite Ion in Solutions of Various NaCl Concentrations at a Constant Alpha Activity of 37 GBq/L at pH~12 (Based on Data in Kelm, Pashalidis, and Kim 1999).

In the WIPP brine solutes other than chloride may play a role. Ershov et al. (2002) showed that a few mM concentration of bromide in natural brines under radiolysis can give Cl_2^-, $ClBr^-$, and Br^- radical anions at the radical step, and then mixed halogen molecules and trihalide ions by radical recombination at the molecular step (Ershov et al. 2002). The hydrolysis of mixed halogen molecules can then result in the formation of hypobromite (OBr^-) (acidic form: hypobromous acid [HOBr]), a transient species to more stable bromates of higher oxidation state (Ershov et al. 2002).

Some WIPP-specific experiments were performed to establish the key radiolytic product in GWB and ERDA-6 brine (Lucchini et al. 2013b). This study confirms that hydrogen peroxide (H_2O_2) and hypochlorite ion (OCl^-) are unstable in these WIPP brines, due in part to metallic impurities in the brine (e.g., < 0.01% levels of Fe, Pb, Ni and possibly others). There was, however, an accelerated decomposition of these species (by an approximate factor of 2) when bromide (Br^-) was present, which is the case for both ERDA-6 and GWB brines. Here, OCl^- readily and stoichiometricly reacted with Br^- to form hypobromite ion (OBr^-), which appeared to be the most important radiolytic transient observed under these conditions. OBr^-, like OCl^-, is also an oxidizing species (E^o=0.76V), that will likely lead to the oxidation of multivalent actinides in the WIPP, but this reactivity has not been established experimentally under representative WIPP conditions (Lucchini et al. 2010a).

In the WIPP, most of the brine radiolysis is caused by the deposition of alpha particles from the TRU isotopes present in the WIPP waste. The range (distance traveled until the alpha particle's energy is lost) of these alpha particles is very short (<40 microns) and radiolysis of the brine solution will mainly take place at the solid-liquid interface. Locally, the concentration of oxidative radiolytic products of brine, such as hypochlorite, chlorite, chlorate, and products of their reaction with brine components (e.g., hypobromite) may be high, and they may directly

interact with the radioactive surface. These “very-near” radiolytic effects, however, are expected to be quickly mitigated by the bulk brine chemistry and the reaction of reducing agents (e.g., reduced iron) with the oxidizing molecular products formed although a slight elevation in E_h is to be expected.

SOTERM-3.4.2 Potential Radiolytic Effects on Actinide Speciation and Solubility

A buildup of oxidizing radiolytic products in brine may increase the redox potential of the brine (Büppelmann, Kim, and Lierse 1988), and consequently directly generate higher-valent actinide species. Alternatively, these radiolytic products could be inserted into some solid actinide phases. For example, Kim et al. (1994) studied the solubility of schoepite, $(UO_2)(OH)_2 \cdot xH_2O$, with hypochlorite ion in 0.1M NaCl at 25 °C (77 °F), in CO_2-free atmosphere (Kim et al. 1994). Their X-Ray Diffraction (XRD) patterns of the residual precipitates showed the introduction of the hypochlorite ion in precipitates. Kim et al. (1994) observed that the presence of hypochlorite ion in the initial schoepite structure enhanced the solubility of the solid 10 to 100 times in the range of pH 6.0-9.8, compared with its solubility in the absence of hypochlorite ion (Kim et al. 1994). However, this effect was reduced when the molar ratio $[ClO^-]/[UO_2^{2+}]$ increased. This scenario is unlikely to occur in WIPP brines because the potential buildup of oxidizing radiolytic products generated in brine is readily overwhelmed by the overall reducing capacity of the site (reduced metals and microbial processes).

The buildup of oxidizing radiolytic products due to brine radiolysis has also been shown to significantly affect the solution chemistry of Am. For example, Am(III) was oxidized to the more soluble forms of Am, namely AmO_2^+ and AmO_2^{2+} (Magirius, Carnall, and Kim 1985; Katz, Seaborg, and Morss 1986; Stadler and Kim 1988; and Meyer et al. 2002). Magirius, Carnall, and Kim (1985) reported on the radiation effects exerted upon a 5 M NaCl solution at the pH 8 to 9 range using precipitated $Am(OH)_3$ at a concentration of 1.03×10^{-3} M (1.07 curie [Ci]/L). They observed that the precipitate began to show discoloration, changing from pink Am^{3+} to brown AmO_2^+, within 24 hours (h), with quantitative oxidation of all the Am to AmO_2^+ within 1 week. Because Pu is more readily oxidized than Am, the expectation is that Pu could also be oxidized in irradiated brine. The metastability of Pu(VI) in the WIPP brine when no reducing agents were present was established and attributed to self-radiolysis effects of the ^{239}Pu isotope used (Reed, Okajima, and Richmann 1994; Reed et al. 2006).

Stadler and Kim (1988) also report the existence of higher oxidation states of Am, due to self-radiolysis. Solubility experiments on $Am(OH)_3$(solid[s]) in 3 M NaCl resulted in much higher Am concentrations than was calculated from the solubility product. This difference was assigned to the radiolytic oxidation of Am^{3+} to AmO_2^+. Spectrophotometric evidence of AmO_2^+ species in solution was reported. The authors report the value of $\log_{10}K_{S,0} = -9.3 \pm 0.5$ for the reaction:

$$AmO_2OH(s) \leftrightarrows AmO_2^+ + OH^- \qquad \text{(SOTERM.2)}$$

The solubility product of $AmO_2OH(s)$ is in general agreement with other solubility studies on different pentavalent actinides.

These results show there is clearly a potential for oxidized, higher-valent actinides to form in brine when no reducing agents are present. This, however, needs to be interpreted in the context of the strong reducing agents and processes that will predominate in the WIPP, such as bioreduction (SOTERM Section 4.2) in the far field, iron reduction, and reduction by organic complexants. The WIPP-specific data show that the presence of reduced iron (Fe(II/0)) leads to a rapid reduction of Pu(VI) to Pu(IV) species under a wide range of anoxic conditions (Reed et al. 2006 and 2010; and SOTERM Section 5.7). These results are expected to extend to the Am(V) system, since this species is more readily reduced than Pu(V/VI). Reduced iron will also react with radiolytically generated oxidizing species, such as hypochlorite or hypobromite, to prevent their buildup in the brine solution with time. In summary, these WIPP-specific results show that the reductants present in WIPP waste (reduced metals and organics) will overwhelm potential radiolytic effects under the expected conditions in the WIPP, and a significant and sustained radiolytic enhancement of actinide solubilities is not predicted.

SOTERM-3.4.3 WIPP Relevant and Literature Data Since the CRA-2014

There are no new WIPP-relevant or literature data on the radiolysis of brine systems since the CRA-2014. This is also true for autoradiolytic processes of actinide systems although the effects of radiolytic processes are often observed and accounted for in the actinide literature. For this reason there is no basis to change PA implementation and radiolytic effects continue to be low in importance when viewed from the context of direct impacts on how the actinide mobile source term is defined in the WIPP. Although localized effects are recognized (these can be meter-scale due to waste inhomogeneity or micron scale due to alpha particle deposition) and, in part reflected, by redox distribution assumptions data obtained on Pu-Fe systems continue to show that the iron chemistry and expected reducing conditions prevail over radiolytic processes (see more detailed discussion in Section 5.7).

The potential for radiolytic impacts since CRA-2014 is however changing for two reasons: First, the increased plutonium inventory in the WIPP leads to increased radiolytic gas generation and as discussed in Section 3.4.1, predicted microbial gas generation rates are much reduced. So there is a significant increase in the relative importance of radiolytic gas generation as a contributor to the overall rates that will exist in the WIPP. Radiolytic gas generation is now understood to be a significant contributor to gas generation and is now addressed in PA (Day 2019a).

Second, the plutonium oxidation state distribution argument has shifted from Pu (V/VI) vs. Pu(III/IV) to Pu(IV) vs. Pu(III). Here the radiolytic effects, which will always promote higher E_h conditions in a Na/Cl/Br brine system, may have increasing importance. Specifically, the small E_h shifts needed to move between the stability fields of Pu(III) to Pu(IV) are likely significant although not yet evaluated. So there is no question, based on current understanding (see discussion in SOTERM Section 3.4.2) that radiolysis will cause an increase in E_h, but the magnitude of this change in iron dominated systems is not yet defined. This expected effect strengthens the WIPP safety case and continues to support the compliance of the WIPP in CRA-2019.

SOTERM-3.5 Actinide Colloids

The potential for colloidal species to have a role in defining the solution concentration and mobility of actinides in the WIPP was recognized early in the WIPP certification process. This led to the development of a colloid model that accounts for these colloidal species. This model was based on an extensive literature review, some WIPP-specific experimental data, and some conservative simplifications that were peer reviewed prior to the first license application (CCA). In this model, four types of colloids that could contribute to the actinide source term are identified: intrinsic, mineral, microbial and humic. The EPA found this model and approach to be satisfactory in the WIPP certification and subsequently in the CRA-2004, CRA-2009, and CRA-2014 recertifications. There has been essentially no change in this model since its initial certification by the EPA.

Actinide colloids in the WIPP are potentially important since the actinide source term is defined in WIPP PA as the sum of contributions from dissolved actinide species and mobile colloidal actinide species (see U.S. DOE 2004, Appendix SOTERM-2004, Reed et al. 2013, and Appendix GEOCHEM, Section 5 for a more detailed discussion of WIPP-relevant colloids). The importance of colloids in the migration and transport of actinide contaminants, although it continues to receive attention in the literature, remains somewhat controversial and difficult to prove. In this context, the consideration of colloidal enhancement of actinide concentrations by the WIPP PA is, at least in part, a conservatism that is built into the overall PA approach. In this context, the sorption of colloidal actinides onto fixed substrates and their filtration in low-porosity media will also reduce the mobile colloidal actinide source term, but no credit is currently being taken for this potentially significant reduction in colloidal concentrations.

Actinide colloids or pseudocolloids may be generated in the WIPP repository as a result of:

1) Hydrolysis (intrinsic chemistry).
2) The interactions of dissolved actinide species with microbially-derived colloids or colloids formed due to the corrosion of steel and waste constituents.
3) The hydrodynamic entrainment of colloidal-sized mineral fragments, as well as several other mechanisms.

The formation of colloids could enhance actinide release in two ways. First, increased actinide concentration will increase the magnitude of DBR release and the effective actinide source term concentration for transport through the Culebra. Second, colloids have very different transport properties than dissolved species, and are predicted to migrate more rapidly in the subsurface. This transport mechanism could enhance the overall actinide release in the WIPP through migration pathways in the Culebra member and the Salado.

The current WIPP colloidal model defines four potential colloidal contributions to the mobile actinide concentration that comprises the actinide source term (U.S. DOE 1996, Appendix SOTERM):

1. *Mineral fragments are hydrophobic, hard-sphere particles that are kinetically stabilized or destabilized by electrostatic forces, and may consist of crystalline or amorphous*

solids. Mineral fragments may be made kinetically stable by coatings with steric stabilizers that prevent close contact. Mineral fragments may act as substrates for sorption of actinides or they may consist of precipitated or coprecipitated actinide solids.

2. *Actinide intrinsic colloids are macromolecules of actinides that, at least in some cases, may mature into a mineral-fragment-type of colloidal particle. When immature, they are hydrophilic; when mature, they become hydrophobic.*
3. *Humic substances are hydrophilic, soft-sphere particles that are stabilized by solvation forces. They are often powerful substrates for uptake of metal cations and are relatively small (less than 100,000 atomic mass units).*
4. *Microbes are relatively large colloidal particles that are stabilized by hydrophilic coatings on their surfaces, which behave as steric stabilizing compounds. They may act as substrates for extracellular actinide sorption or they may actively bioaccumulate actinides intracellularly.*

It is important to note that the intrinsic colloids formed under WIPP-relevant conditions are nanocluster or nano-filterable species.

In this section, the general environmental aspects of colloid-enhanced transport in the subsurface are discussed, along with an update of relevant WIPP-specific results since the CRA-2014.

SOTERM-3.5.1 Actinide Colloids in the Environment

The extent and potential formation of actinide colloids continues to be debated by researchers in the field. Since the CCA, there have been over 100 publications on actinide colloid chemistry that range in topics from real-system transport studies to the structure and inherent stability of actinide colloids. These remain largely focused on plutonium and its associated and very complex subsurface chemistry, but there are also studies on neptunium, americium, thorium and curium reported in the literature. It is also important to note that relatively few of these studies specifically address ionic-strength effects on colloid formation, stability and mobility. In this context, there are very few studies in high ionic-strength systems (I > 5 M). Additionally, only a small fraction of these studies have direct application to the WIPP repository safety case.

A more extensive literature review is provided elsewhere (Reed et al. 2013) and this is also addressed in CRA-2019 Appendix GEOCHEM, Section 5. Key observations from the literature that impact the WIPP colloid model parameters are:

- A wide variety of actinide colloids are now noted to form in natural systems (see for example Khasanova et al. 2007). This differs somewhat from the conclusion made at the time of the CCA that only Pu colloids could form. This limitation was addressed in CRA-2014 (Reed et al. 2013) by using site-relevant experiments to define colloidal contributions for the key actinides. This more robust approach was continued in CRA-2019 (Reed et al. 2019a).
- Actinide colloids that form in nature tend to be associated with iron colloidal species and tend to help immobilize rather than mobilize actinides. This is consistent with the WIPP model assumptions that only iron mineral colloids seem to form. Colloidal species in the

WIPP conceptualization primarily add to the source term concentration with only a small contribution to transport pathways through the Culebra.

- There are new data showing the existence of nanoclusters as an integral part of the aqueous speciation of some actinides. These are also seen in WIPP-specific brine systems (Reed et al. 2013; CRA-2014, SOTERM Section 3.9.2).
- Bioassociation of actinides is observed in the literature and we have shown that this also extends to halophilic microorganisms (Ams et al. 2013; Reed et al. 2013; CRA-2014, SOTERM Section 3.9.2).

Overall Impact of Literature Publications on the WIPP Colloid Model

There continues to be some progress made in the assessment of the colloidal issue as it applies to the potential subsurface migration of actinide species. The following are the key observations:

- The WIPP model will continue to address the colloid issue. This adds a layer of defensibility to the mobile actinide source term model.
- There is no literature evidence that the current four-colloid type model is inadequate; if anything it continues to be a conservatism built into the model.
- Current literature shows that colloidal species, intrinsic and mineral, of a number of actinides, not just plutonium, are observed – this is a departure from the CCA literature survey that was conducted. These literature data, however, still do not explicitly address high ionic-strength systems.
- The structural data from XRD and synchrotron measurements point towards intrinsic colloids that persist as very small (typically < 10 nanometers [nm]) species.
- Biosorption data show that increased ionic-strength increased the extent of sorption and the overall trend with pH was to go through a maximum at about pH 8 and then decrease with increasing pH.

SOTERM-3.5.2 WIPP-Specific Results since the CRA-2014 PA

The WIPP colloid enhancement parameters used in CRA-2014 PA are given in Table SOTERM-8. These were re-assessed per comments received from the EPA and were converted to element-specific parameters to support WIPP PA. The revised parameters recommended for CRA-2019 are given in Table SOTERM-9 (Reed et al. 2019a). Also see SOTERM Section 4.3.4 for discussion of the biosorption data since CRA-2014. These are element-specific which means that the highest value for the stated oxidation states was used.

Table SOTERM-8. Colloid Enhancement Parameters Used in CRA-2009 and CRA-2014 (Appendix SOTERM-2009; Reed et al. 2013)

Actinide	CONCMIN (Concentration on Mineral Fragments [a])	CONCINT (Concentration as Intrinsic Colloid [b]) (M)		PROPMIC (Proportion Sorbed on Microbes [b])		CAPMIC (Maximum Sorbed on Microbes[c]) (M)		Proportion Sorbed on Humics [b]		CAPHUM[d] (Maximum Sorbed on Humics [a])
								PHUMSIM (Salado) [d]	PHUMCIM (Castile) [d]	
CRA	2009 and 2014	2009	2014	2009	2014	2009	2014	2009 and 2014	2009 and 2014	2009 and 2014
Th(IV)	2.6×10^{-8}	0	2×10^{-8}	3.1	1.76	0.0019	2.3×10^{-6}	6.3	6.3	1.1×10^{-5}
U(IV)	2.6×10^{-8}	0	2×10^{-8}	0.0021	1.76	0.0021	2.3×10^{-6}	6.3	6.3	1.1×10^{-5}
U(VI)	2.6×10^{-8}	0	3×10^{-8}	0.0021	1.76	0.0021	2.3×10^{-6}	0.12	0.51	1.1×10^{-5}
Np(IV)	2.6×10^{-8}	0	2×10^{-8}	12.0	1.76	0.0027	2.3×10^{-6}	6.3	6.3	1.1×10^{-5}
Np(V)	2.6×10^{-8}	0	ND	12.0	1.76	0.0027	2.3×10^{-6}	9.1×10^{-4}	7.4×10^{-3}	1.1×10^{-5}
Pu(III)	2.6×10^{-8}	1×10^{-9}	2×10^{-8}	0.3	1.76	6.8×10^{-5}	2.3×10^{-6}	0.19	1.37	1.1×10^{-5}
Pu(IV)	2.6×10^{-8}	1×10^{-9}	2×10^{-8}	0.3	1.76	6.8×10^{-5}	2.3×10^{-6}	6.3	6.3	1.1×10^{-5}
Am(III)	2.6×10^{-8}	0	4×10^{-9}	3.6	0.32	1.0	3.1×10^{-8}	0.19	1.37	1.1×10^{-5}

a In units of moles colloidal actinide per liter – 2009 and 2014 parameters are the same.

b In units of moles colloidal actinide per mole dissolved actinide. These were implemented as element-specific parameters in PA. When values differed, the higher one was used.

c In units of moles total mobile actinide per liter (CRA-2009) and moles colloidal actinide per liter (CRA-2014).

d Humic colloid parameters for CRA-2009 and CRA-2014 are unchanged.

NOTE: The colloidal source term is added to the dissolved source term to arrive at a total source term. Mineral fragments were provided with distributions, but the maximum was used as described in Appendix PA-2014, Section 8.4.

Table SOTERM-9. Colloid Enhancement Parameters Used in CRA-2019

Actinide	Actinide source Term Colloid Enhancement Parameters						
	Intrinsic	Mineral	Microbial		Humic		
	CONCINT	CONCMIN	CAPMIC	PROPMIC	PHUMCIM	PHUMSIM	CAPHUM
Thorium	4.3×10^{-8} M	2.6×10^{-8} M	3.8×10^{-8} M	0.21	0.01	0.01	1.1×10^{-5} M
Uranium[1]	1.4×10^{-6} M	2.6×10^{-8} M	3.8×10^{-8} M	0.21	0.01 / 0.012	0.01 / 0.51	1.1×10^{-5} M
Neptunium[2]	4.3×10^{-8} M	2.6×10^{-8} M	3.8×10^{-8} M	0.21	0.01 / 9.1×10^{-4}	0.01 / 7.4×10^{-3}	1.1×10^{-5} M
Plutonium[3]	4.3×10^{-8} M	2.6×10^{-8} M	3.8×10^{-8} M	0.21	0.2 / 0.01	0.2 / 0.01	1.1×10^{-5} M
Americium	9.5×10^{-9} M	2.6×10^{-8} M	2.3×10^{-9} M	0.03	0.2	0.2	1.1×10^{-5} M

1 – for uranium, humic colloid parameters are oxidation-state specific. Data are for U(IV) / U(VI)

2- – for neptunium, humic colloid parameters are oxidation-state specific. Data are for Np(IV) / Np(V)

3- – for plutonium, humic colloid parameters are oxidation-state specific. Data are for Pu(III) / Pu(IV)

SOTERM-4.0 Microbial Effects in the WIPP

The potential effects of microbial activity on the fate and transport of actinide metals from deep geological waste repositories have been well described (McCabe 1990; Lloyd and Macaskie 2002; Pedersen 2005; Wang and Francis 2005) and may include 1) gas generation from the degradation of organic waste components, 2) the creation of a reducing environment from the consumption of oxygen, 3) redox reactions with metals and oxyanions, 4) the generation of organic ligands, and 5) the mobilization or immobilization of actinides associated with organisms. The relative importance of each of these effects may vary depending upon site biogeochemistry and is potentially very different for salt-based repository settings (Swanson et al. 2016). The WIPP PA considers gas generation and biocolloid formation to have the largest potential impact on the mobile concentrations of actinides in the source term.

This chapter will review the WIPP conceptual model for microbiology and will discuss how it is affected by the current state of knowledge regarding microbiology in salt-based repositories. This discussion is meant to increase the overall understanding of microbial effects on performance but do not result in a change to the conceptual model.

SOTERM-4.1 Effects of the Biodegradation of CPR

Microbial consumption of CPR materials could affect the actinide source term in three ways:

1. CO2 production could acidify brine, in the absence of an MgO buffer, thereby increasing actinide solubility and could increase levels of the complexant, carbonate, at mildly alkaline pH;
2. Oxygen consumption will lead to a more reducing environment that can affect actinide solubility; and
3. An increase in biomass could lead to an increase in biocolloid potential.

SOTERM-4.1.1 Current WIPP PA Gas Generation Model

The WIPP CPR biodegradation model remains compliant in CRA-2019 in that it continues to overpredict the likely degradation rates in the WIPP. There has been no change in the CPR biodegradation model since the CRA-2009. The implementation and basis for the gas generation rates used in PA have not changed (U.S. DOE 2019, Appendix GEOCHEM Section 2.4). Microbial activity is considered in all PA realizations (vectors). There is a probability of 0.75 that only cellulose is significantly degraded and a probability of 0.25 that all CPR materials are significantly degraded.

The WIPP PA assumes that CPR materials will be consumed through the following sequential reactions, based on energy yield (Brush 1990; Francis and Gillow 1994; Brush 1995; Wang and Brush 1996):

$$C_6H_{10}O_5 + 4.8H^+ + 4.8NO_3^- \rightarrow 7.4H_2O + 6CO_2 + 2.4N_2 \quad \text{(SOTERM.3)}$$

$$C_6H_{10}O_5 + 6H^+ + 3SO_4^{2-} \rightarrow 5H_2O + 6CO_2 + 3H_2S \quad \text{(SOTERM.4)}$$

$$C_6H_{10}O_5 + H_2O \rightarrow 3CH_4 + 3CO_2 \quad \text{(SOTERM.5)}$$

Methanogenesis, as described by reaction SOTERM.5, is no longer included as a degradation pathway because it is assumed that the sulfate present in the host rock is always available and able to sustain bacterial sulfate reduction as the primary mode of microbial respiration and gas generation. Thus, 4% of the gas generation is presumed to occur through denitrification and 96% through sulfate reduction (Nemer and Stein 2005). The omission of methanogenesis, as written in SOTERM.5, is now further supported by the fact that this process is thermodynamically unfavorable at the ionic strengths expected in the WIPP (Oren 2011).

Magnesium oxide is emplaced in the repository to counteract the effects of microbial CO_2 production. It will decrease the dissolved actinide concentration by consuming essentially all of the CO_2, and by buffering and controlling the pH and fugacity of carbon dioxide (f_{CO2}) within ranges that are favorable with respect to actinide speciation and solubility.

SOTERM-4.1.2 Evolution of the WIPP Microbial Gas Generation Model

Early studies on gas generation for the WIPP were carried out as part of the ASTP at Los Alamos National Laboratory (LANL); through collaborations between LANL, the University of New Mexico, and Sandia National Laboratories (SNL); and by SNL in conjunction with Stanford University and contracted to Brookhaven National Laboratory (BNL).

Later, studies conducted at BNL measured gas generation rates from cellulose degradation that were used as the basis for the WIPP PA (Francis and Gillow 1994; Francis et al. 1997; Gillow and Francis 2006). These studies used a mixed inoculum of brine lake sediment and water, underground brine seep, WIPP halite and muck pile salt. Paper products typically found in a laboratory, along with succinate, provided the carbon and energy sources. Potassium nitrate was added to some incubations as a terminal electron acceptor. Other nutrients were present in the form of yeast extract, amino acids, phosphate, and ammonium nitrate.

A recent evaluation of all of these studies drew the following key conclusions and observations (Swanson and Reed 2018a):

- Many of the WIPP-specific results from the pre-CCA and later studies were highly variable, for example:
  - No gas was generated in experiments performed by Grbic-Galic (Brush 1990)
  - 0.14 µmoles CO_2/day/gram cellulose (Barnhart et al. 1980)
  - 0.009 to 0.46 µmoles CO_2/day/gram cellulose (Francis et al. 1997 and 2004)
- Microbial viability and activity was not always tracked in the earliest studies; when tracked, they showed a lack of growth of non-halophiles in brine (Brush et al. 1990);
- Pu inhibited gas generation rates (Caldwell et al. 1987);
- There was only one significant demonstration of the nitrate-reducing capability of extreme halophiles indigenous to the WIPP near-field (Francis and Gillow 1994);

- There was a positive correlation between gas generation and the presence of nutrients (i.e., excess nitrate; Francis and Gillow 1994 and 1997; Gillow and Francis 2006);
- Fermentation by-products were detected (Francis and Gillow 1994 and 1997; Gillow and Francis, 2006); and
- Sulfidogenesis occurred in the presence of bentonite (Gillow and Francis 2006).

The uncertainty surrounding microbial gas generation in the WIPP was recognized very early on (Brush 1994). The main issues attributed to this uncertainty were:

- the survival of microorganisms for the entire lifetime of the repository;
- the presence of sufficient H_2O;
- the presence of sufficient electron acceptors; and
- the presence and availability of sufficient nutrients.

Additionally, this same report raised the issue of hypersalinity and its effects on microbial activity:

> "Although a few halotolerant microbes may survive and a few others may develop halotolerance when exposed to saline conditions, the most potentially significant microbes during most of the 10,000-year period of performance of the repository will be halophilic microbes present in WIPP disposal rooms when they are filled and sealed."

Since the time of the CCA and through the changes made through CRA-2005, it was ultimately decided to use results from the Francis group studies that showed significantly high gas generation rates even though there were some lingering questions (Gillow and Francis 2006). This was thought to be a conservatism in the model and these microbial gas generation rates were not changed in CRA-2019. The issue of hypersalinity constraints, although identified in the pre-CCA documentation, has recently been raised again (Swanson et al. 2013c); SOTERM-2014, Section 2.4.1) and on this basis, the WIPP now believes the actual rates will be much lower.

SOTERM-4.1.3 WIPP-Relevant Gas Generation Results Since CRA-2014

Several attempts have been made over the past few years to measure microbial gas generation under WIPP-relevant conditions. To date, no growth has occurred in anaerobic incubations of WIPP halite, such that no gas has been generated. Indeed, no strictly anaerobic halophiles have been cultivated from any other subterranean halite (Swanson et al. 2016). Although anaerobic respiration under hypersaline conditions does occur, this mode of activity has only been shown in sediments of surficial brine lakes or seas (e.g., Dead Sea, Great Salt Lake), sediments from solar salterns, or using isolates therefrom. The closest evidence for anaerobic respiration in subterranean halite is from Francis and Gillow, who found that organisms in G-seep brine were capable of nitrate reduction (Francis and Gillow 1994).

SOTERM-4.2 Microbial Activity in the WIPP

SOTERM-4.2.1 Constraints on Activity

The microbial ecology of salt-based repositories and WIPP-specific ecology have been discussed elsewhere (Swanson et al. 2013c; SOTERM-2014; Swanson et al. 2016; Swanson and Reed 2018a). This section will review the current state of knowledge, as it pertains to gas generation in the WIPP. Gas generation is a by-product of microbial activity, but activity under WIPP conditions is a large uncertainty because of the severe constraints imposed by both the geochemical conditions of subterranean salt and by the repository itself. These constraints include high ionic strength, low water activity, high chaotropicity, anoxia, radioactivity, alkaline pH, and a lack of suitable substrates. Some of these constraints will be reviewed briefly.

Extremely halophilic archaea (Class *Halobacteria*) and bacteria (Order *Halanaerobiales*) are capable of maintaining osmotic balance with their external environment by "salting in"—i.e., they accumulate high concentrations of ions, such as K^+ and Cl^- intracellularly. All other organisms (most bacteria and all eukaryotes) must either synthesize, or import from their surroundings, small organic compatible solutes to maintain this same balance. The cost of this survival is that only certain modes of metabolism are feasible—i.e., those that generate the most energy or those that are carried out by organisms that "salt in."

In addition to high salt (i.e., NaCl) concentrations, the high ionic strength of WIPP brines and the concentrations of magnesium present lead to low water activities. In the WIPP, water activity is defined as the ratio of the partial vapor pressure of water in the brine to that of pure water and is essentially a measure of available water. Low water activities can effectively eliminate microbial activity (see Figure SOTERM-5). Additionally, high concentrations of chaotropic solutes, such as magnesium or calcium, can also be inhibitory to microbial activity, as they can lead to protein denaturation (Hallsworth et al. 2007).

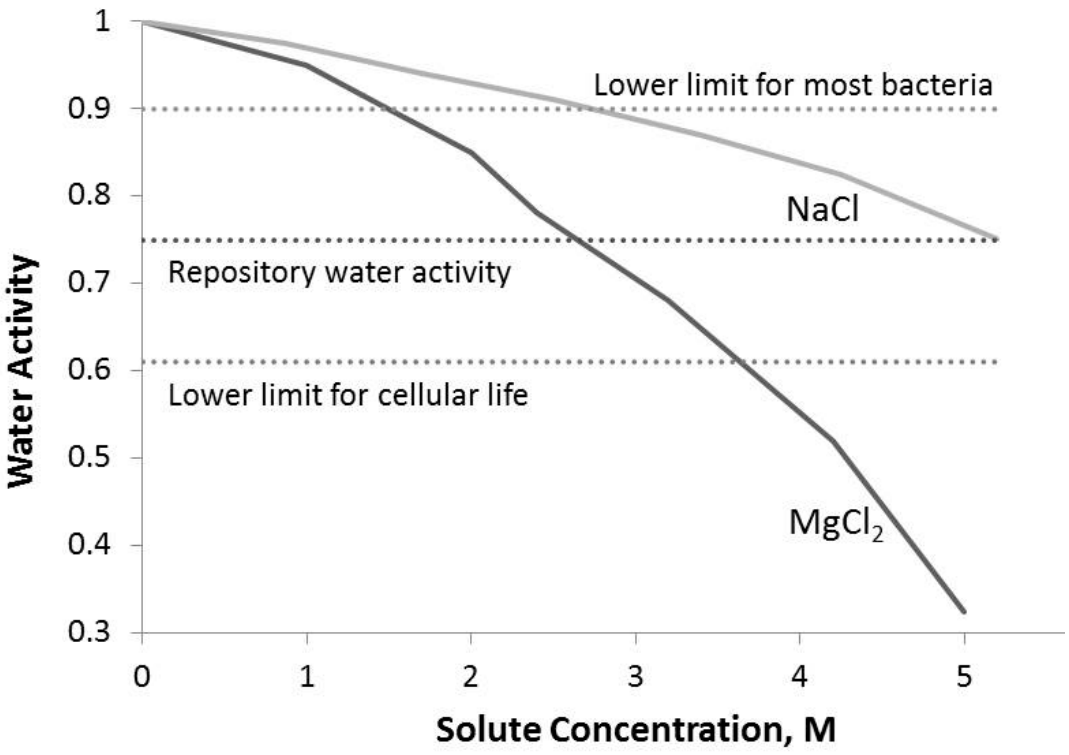

Figure SOTERM-5. Graph Depicting Water Activity in Pure Solutions of NaCl and $MgCl_2$ (Swanson et al. 2016, Modified from Hallsworth et al. 2007).

SOTERM-4.2.2 Modes of Metabolism Among Extreme Halophiles in an Anoxic Environment

As mentioned above, the energy required to maintain osmotic balance in a hypersaline environment limits many modes of metabolism (for excellent reviews, see Oren 1999 and 2011). Thus, the majority of extremely halophilic archaea are obligately aerobic, since this affords them the highest energy yield. Two known haloarchaeal genera (*Haloferax* and *Haloarcula*) are capable of denitrification (Mancinelli and Hochstein 1986; Cabello et al. 2004). These organisms have not been detected in the WIPP near-field and have rarely been detected in other subterranean salt beds. However, the G-seep brine was never fully characterized, and it is possible that these organisms were present in the brine and could have accounted for the denitrification observed by Francis and Gillow (1994).

Only one other mode of anaerobic respiration has been documented among *Halobacteria*—the reduction of sulfur species, such as S^0, $S_2O_3^-$, and dimethyl sulfoxide (DMSO), but not sulfate. These organisms were only recently discovered in incubations of hypersaline sediments using formate, hydrogen or acetate as the electron donors (note: all other organic electron donors yielded negative results; Sorokin et al. 2016 and 2017).

The reductions of fumarate, DMSO, and trimethylamine oxide (TMAO) have also been observed under anaerobic conditions (Oren and Truper 1990; Oren 1991; Müller and DasSarma 2005). Fermentation of arginine has also been observed (Oren 2006).

The extremely halophilic bacteria of the class *Halanaerobiales* are capable of fermenting natural sugars (e.g., glucose, cellobiose, glycerol) and amino acid derivatives used as osmoprotectants by other bacteria and eukaryotes (e.g., glycine betaine; Begemann et al. 2012). They are also capable of sulfidogenesis via the degradation of polymers used in the fracking industry and are the predominant organisms associated with hydraulic fracking operations in hypersaline settings (Liang et al. 2016; Booker et al. 2017; Lipus et al. 2017). *Halanaerobium* spp. have been isolated from anaerobic incubations of Culebra groundwaters (Swanson and Simmons 2013) but to date, none have been isolated from the WIPP near-field or any other subterranean bedded salt formation. However, deoxyribonucleic acid (DNA) sequences related to this class have been detected in the Gorleben salt dome (Swanson et al. 2013c).

In contrast to the above listed modes of metabolism among extreme halophiles in anoxic environments, all repository microbiology concepts are built upon the canonical sequence of terminal electron acceptor usage, based on the decreasing free energy yield of each reaction: O_2 → NO_3^- → Mn(IV)/Fe(III) → SO_4^{2-} → CO_2. For the WIPP, these have been narrowed down to eliminate metals and CO_2/methanogenesis, such that denitrification and sulfate reduction are the only two modes accounted for in the PA. Denitrification can be performed by both haloarchaea (see above) and halophilic bacteria (Gillow and Francis 2006). Sulfate reduction, a process performed only by bacteria, is affected by salt concentration, and rates of reduction decrease with increasing salinity (Brandt et al. 2001; Kjeldsen et al. 2007; Kulp et al. 2007; Porter et al. 2007; Kjeldsen et al. 2010). Methanogenesis, as described by equation SOTERM.5, was ruled out for CRA-2009, based on the excess of sulfate available to sustain the activity of sulfate-reducing bacteria (SRB). However, methanogenesis at high salt concentrations is limited to the use of methylated compounds, and is, therefore, not relevant to the equations deriving methane from cellulosics in the WIPP (reaction SOTERM.5). These organisms will not compete with SRB for H_2, such that both populations can potentially co-exist.

As mentioned earlier (section 4.1.2), it is important to reiterate that no extremely halophilic anaerobes have been either isolated or detected in subterranean halites to date, and all documented hypersaline incubations that have enriched SRB have been inoculated with sediments, their porewaters, or overlying brine. Although sulfidogenesis is now known to occur via the activity of the newly discovered anaerobic haloarchaea and by members of the *Halanaerobiales*, these reactions are not described by reaction SOTERM.4 since they do not use sulfate as the terminal acceptor. Other uncertainties also exist regarding sulfidogenesis at the WIPP: 1) are the sulfur species (e.g., elemental sulfur and thiosulfate) that can be used by haloarchaea or *Halanaerobiales* present in the WIPP?; and 2) are anaerobic haloarchaea present in the WIPP near-field?

SOTERM-4.2.3 Variations in Microbial Communities and Activity with Time and Space

Microbial ecology in the WIPP will vary in both time and space. Variations in time will result from the depletion of terminal electron acceptors (oxygen, nitrate) and nutrients, and from the

generation of inhibitory metabolic by-products. Variations in space will result from the differences in ionic strength and water activity among the inside of the waste drum, the near-field, and the far-field. The WIPP gas generation model does not concern the far-field; however, it should be noted that the generally lower ionic strengths in this space support an entirely different microbial community that is more metabolically diverse (Swanson et al. 2013c).

Impact of introduced microorganisms on gas generation Waste

Recent DNA analysis of two WIPP-bound waste drums resulted in the detection of a low-diversity group of microorganisms (Swanson et al. 2015). The majority (65%) of the population was comprised of known poly-extremotolerant bacteria (phylum *Actinobacteria*). Members of this phylum have also been detected in other radionuclide contaminated environments (Fredrickson et al. 2004). Their primary resistance is to desiccation, but they are also resistant to radiation and extremes of pH and temperature. The second largest contributors (29%) were the *Ascomycota*. This is a fungal phylum containing known cellulose degraders. It is probable that these organisms have transformed waste within the drum while under aerobic conditions. Culture-dependent results were similar in that the two main isolates were from the phylum *Actinobacteria*. In addition, three species of spore-forming bacilli were isolated. These likely survived in spore form and vegetated once transferred to growth media. None of the isolates is halophilic, and none can grow in WIPP brines, suggesting that their biodegradation potential and gas-generating activity will be limited to the period prior to drum breach.

Methane has been detected in some WIPP-bound waste drums, suggesting that microbial activity may have been underway, although the actual source of the methane is unknown. Nevertheless, within-drum waste, degradation and gas generation is not addressed in the gas generation model prior to repository closure. This is the stage where initial breakdown of larger CPR polymers could be taking place, rendering the CPR more degradable to downstream organisms.

Air and mining operations

It has been argued that extreme halophiles, such as anaerobes, could be introduced from area brine lakes into the WIPP via the ventilation system and on mining equipment and personnel. While theoretically possible, anaerobes have yet to be cultivated from WIPP halite or any other subterranean salt bed to date (Swanson et al. 2016). Additionally, air-borne organisms have not been shown to grow on exposed high-salt media at the WIPP, in a British salt mine, or in an Austrian salt mine (Vreeland et al. 1998; McGenity et al. 2000; Swanson and Reed 2018a).

SOTERM-4.2.4 WIPP-relevant Microbial Degradation of CPR

Ideal substrates for haloarchaea include small organics, such as amino acid and nucleic acid derivatives, pyruvate, acetate, and often citrate (Oren 2006). The projected concentrations of introduced organics will overwhelm any naturally occurring organics that might be present. Organic complexing agents—acetate, oxalate, citrate, and EDTA—will be the predominant low-molecular weight carbon substrates at WIPP. WIPP haloarchaea are capable of degrading acetate, citrate, and oxalate in aerobic brines (Swanson et al. 2013b). Of the three higher molecular weight organics—cellulose, plastic, and rubber—only cellulose is projected to be significantly degraded in all PA realizations.

Natural sources of cellulose in hypersaline habitats include dead algal biomass and halophytic debris. Thus, many halophilic microorganisms possessing cellulase activity or capable of growth on cellulosic substrates have been reported. Recently, cellulotrophic haloarchaea was enriched from brine lake sediment that were able to degrade various forms of insoluble cellulose, including Whatman filter papers (Sorokin et al. 2015). Microcolony formation on crystalline fibers was a prerequisite for degradation. One of these isolates was related to *Halosimplex*, a genus first isolated from WIPP halite. In an earlier study, a mixed culture enriched from G-seep brine (presumably archaea) reportedly adhered to and altered Kimwipe® fibers, as observed microscopically (Vreeland et al. 1998). All of these studies were carried out under aerobic conditions. A screening study of 20 haloarchaeal genomes found that 24% contain genes for hypothetical cellulase and/or beta-glucosidase enzymes involved in cellulose breakdown (Sorokin et al. 2015), but only two genera possess functional cellulases.

The PA assumptions, along with our current understanding, regarding microbial activity, the use of sequential terminal electron acceptors, and the degradation of cellulose under WIPP-relevant conditions are (See also Table 4 of Swanson and Reed [2018a]):

- Anaerobic respiration will occur.
  - This is not expected for extreme halophiles (Archaea) since they are typically aerobic heterotrophs.
  - Halophilic anaerobic bacteria exist but are not expected to be active in the high ionic-strength brines in WIPP.
- Sequential use of terminal electron acceptors (TEAs): oxygen → nitrate → iron → sulfate → carbon dioxide.
  - The most likely modes of metabolism will be fermentation rather than anaerobic respiration.
  - Some few archaea will respire nitrate.
- Microorganisms will degrade cellulose
  - Degradation of cellulosics were observed in laboratory WIPP studies but the extent that these extend to the expected WIPP repository conditions is not clear.
  - Cellulose degradation is not a universal capability of bacteria (only 24% of a selection of screened genomes found genes encoding this capability).
  - Many haloarchaea produce cellulases that can degrade oligosaccharides (e.g., cellobiose) but not insoluble cellulose.

SOTERM-4.3 Microbial-Actinide Interactions

Microbial processes can influence actinide speciation and solubility, thereby influencing the source term. In addition, bioassociation of actinides can also affect their mobilization. Actinide-microbial interactions, as illustrated in Figure SOTERM-6 for plutonium, are discussed in this section.

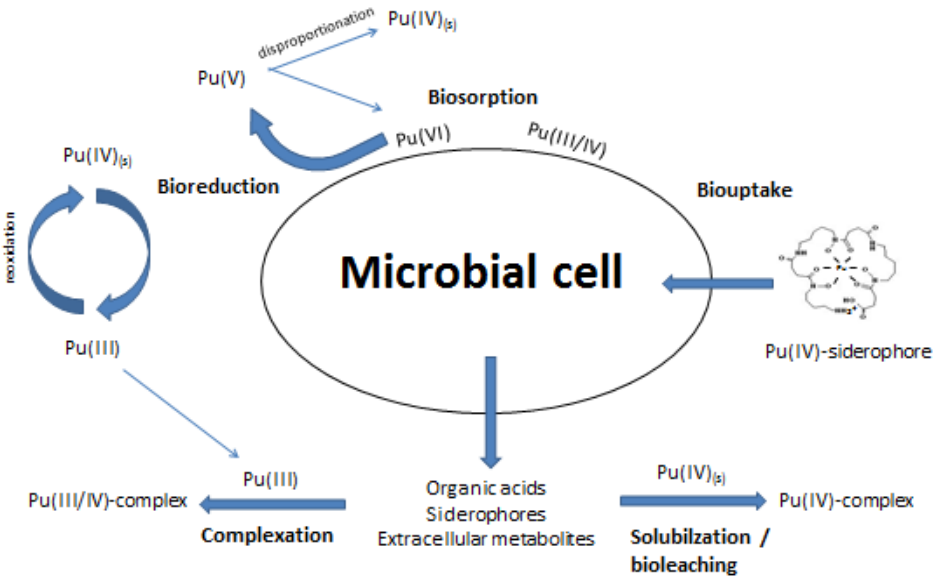

Figure SOTERM-6. Schematic of Plutonium-Microbial Interactions (Reed et al. 2019b)

SOTERM-4.3.1 Actinide Toxicity Towards WIPP-Relevant Microorganisms

The toxicity of actinides towards microorganisms at the WIPP is yet another possible constraint on their activity and potential gas generation. Toxic effects can be either chemically or radiologically induced. Chemical toxicity is presumably similar to heavy metal toxicity and, in general, is a function of the free ion concentration in solution. The metal can bind with essential biomolecules, such as proteins and nucleic acids, and alter their structure and/or inhibit their activity. In contrast, radiological toxicity of actinides is caused by the generation of oxidizing free radicals (e.g., $OH^{\cdot}$, $HO_2^{\cdot}$, and oxychloride radicals), through ionizing radiation, that results in DNA lesions.

Many factors can affect metal/actinide toxicity—such as speciation, oxidation state or isotope, concentration, matrix, ligand presence, and organism (Banaszak et al. 1998a; Banaszak et al. 1998b; Reed et al. 1999; Ruggiero et al. 2005). Microorganisms can combat metal toxicity by using active efflux systems and/or sequestration strategies. Radiation resistance is conferred by nucleic acid repair mechanisms and reactive oxygen species scavenging strategies. Extremely halophilic archaea are known for their resistance to UV and gamma radiation through a number of mechanisms, including pigmentation, polyploidy, high levels of internal salts and high Mn/Fe ratios, among other characteristics and strategies (DeVeaux et al. 2007; Kish et al. 2009; Robinson et al. 2011).

SOTERM-4.3.1.1 WIPP-Specific Toxicity Experiments since CRA-2014

Preliminary toxicity studies have been undertaken for the WIPP in order to gain a better understanding of microbial activity and/or survival in the presence of actinides (Swanson and

Reed 2018a). These studies showed: 1) a loose dose-response relationship in the inhibition of *Halobacterium* sp. growth by plutonium-242 and significant inhibition at ~0.1 mM; 2) significant inhibition of *Halobacterium* sp. growth by neptunium at concentrations of 10^{-6} M; and 3) inhibition of *Arthrobacter* sp. (WIPP waste isolate) growth with uranium-citrate concentrations greater than 0.5 mM.

In contrast, Francis et al. (1998) found that Np-EDTA did not inhibit the growth of a halophile culture until concentrations reached 5×10^{-4} M, whereas Pu-EDTA caused significant growth inhibition to the same culture at ~10^{-5} M. However, results from both earlier and later studies are specific to the conditions tested and highlight the differences in actinide chemistry and speciation under these different conditions.

SOTERM-4.3.2 Bioreduction of Multivalent Actinides

The microbially-induced reduction of higher-valent actinides would be an important beneficial effect for the WIPP, since lower-valent species tend to be less soluble. However, there are few data concerning metal reduction in hypersaline environments, and this mode of metabolism has never been observed in haloarchaea (Sorokin and Muyzer 2010; Oren 2011; Emmerich et al. 2012). While incubations of Culebra groundwaters have resulted in metal reduction, these were at lower ionic strengths than the WIPP near-field and contained organisms other than haloarchaea (Swanson and Simmons 2013). There are no new WIPP-relevant data since CRA-2014.

SOTERM-4.3.3 Biological Influence on Actinide Mobility via Association or Influence on Solubility

The effects of microorganisms on actinide mobility at the WIPP—via bioassociation or inductive precipitation processes—were recently reviewed in detail (Swanson and Reed 2018b; Swanson et al. 2019). Data from associated studies have been used to determine the PROPMIC parameter for the PA colloid model since its inception (for more detail, see SOTERM Section 3.5). These parameters were updated for the CRA-2014, and some have been updated again for CRA-2019 (See Table SOTERM-8 and 9).

Bioassociation of actinides/metals with microorganisms can be internal or external and transient or accumulative. Biosorption is a metabolism-independent process in which metals interact with functional groups at a cell's surface. It can be reversible and can lead to either the mobilization or immobilization of an actinide, depending upon the state and mobility of the biomass. Internal uptake of actinides may result in their efflux (transient) or their sequestration within the cell via complexation and/or compartmentalization (accumulative). In this case, actinide mobility will also depend upon which process is involved. Biomineralization refers to the induction of mineral formation either at a cell's surface via a nucleation site or intracellularly (see above accumulation). In general, mineralization leads to the immobilization of an actinide via precipitation of cells from suspension.

To date, there are still relatively few data on the bioassociation of actinides that are specific to all the unique conditions at the WIPP. The most relevant are those conducted at high ionic strength

with relevant organisms. However, chemical conditions, such as pH, have been controlled in most experiments to better control actinide chemistry and speciation.

SOTERM-4.3.4 WIPP-Specific Results since CRA-2014

A series of experiments was carried out to determine the potential for *Halobacterium* sp. to transport the +3 analog, neodymium, in the WIPP environment (Swanson et al. 2019). Most of this work was conducted in simplified 3.42 M NaCl brine, in order to establish behavior under controlled conditions. These were then extended to simulated WIPP brines at 90% strength. Results of these experiments showed that biological influence on neodymium solubility is a function of biomass concentration, test matrix, and the presence of EDTA. Biological effects were slower than in studies using bacteria (24 hours, as compared to 3 hours, to reach a "sorption" plateau). Neodymium concentration did not affect its loss from solution when an extended exposure period was tested.

The concentration of neodymium in solution was significantly affected by the test matrix (Figures SOTERM-7 and 8), with very little loss from either GWB (3.9%) or pC_{H+} 9.5-specific brine (5.4%) and significant loss from ERDA (up to 78%). The results obtained from these recent studies have contributed to a change in PROPMIC parameter values for the +3 case for CRA-2019 (see SOTERM Section 3.5).

Microbial colloids are one of four types of colloids identified in the model—in addition to intrinsic, mineral, and humic colloids—that can contribute to the mobile actinide source term. The biocolloid contribution is the concentration of actinides that is associated with microorganisms suspended in brine, and hence deemed mobile, under a direct brine release scenario (CCA; Papenguth 1996; CRA-2009; CRA-2014). The biocolloid model defines PROPMIC as a proportionality constant describing the amount of actinide element bound to mobile microbes and is calculated as the ratio between the microbial actinide and the dissolved actinide, as measured by filtration. CAPMIC is defined as the maximum concentration of actinide that can be associated with mobile microbes and was originally measured from toxicity studies as the actinide concentration at which no growth was observed.

The means of calculating CAPMIC was changed for CRA-2014 to a biomass-based approach in order to reflect a better understanding of WIPP microbiology, specifically the geochemical and repository-induced constraints on the possible numbers and types of organisms that could be present (Reed et al. 2013; CRA-2014). These constraints have been discussed in detail elsewhere but are mainly high ionic strength and anoxia (Swanson and Reed 2018b; Swanson et al. 2019; see also Section 4.2.1). Additionally, the new calculations are based on experiments in which actinide speciation and behavior was better defined and which reflected current knowledge about expected WIPP conditions, such as pH and brine composition (Swanson and Reed 2018b). The overall result since CRA-2014 has been a decrease in some parameter values, due to 1) the use of archaeal, rather than bacterial, data; 2) the use of longer-term data; and 3) the use of data derived in the presence of EDTA.

Briefly, the PROPMIC and CAPMIC values for the +3 case have been updated for CRA-2019 (Reed et al. 2019b; also see Tables SOTERM-8 and SOTERM-9 for comparisons of parameter values). These new values were based on studies of the +3 analog, neodymium, with a WIPP-

relevant archaeon in WIPP-simulated brines at WIPP-relevant pH values and in the presence of EDTA over a longer time frame (see section 4.3.4 for further discussion).

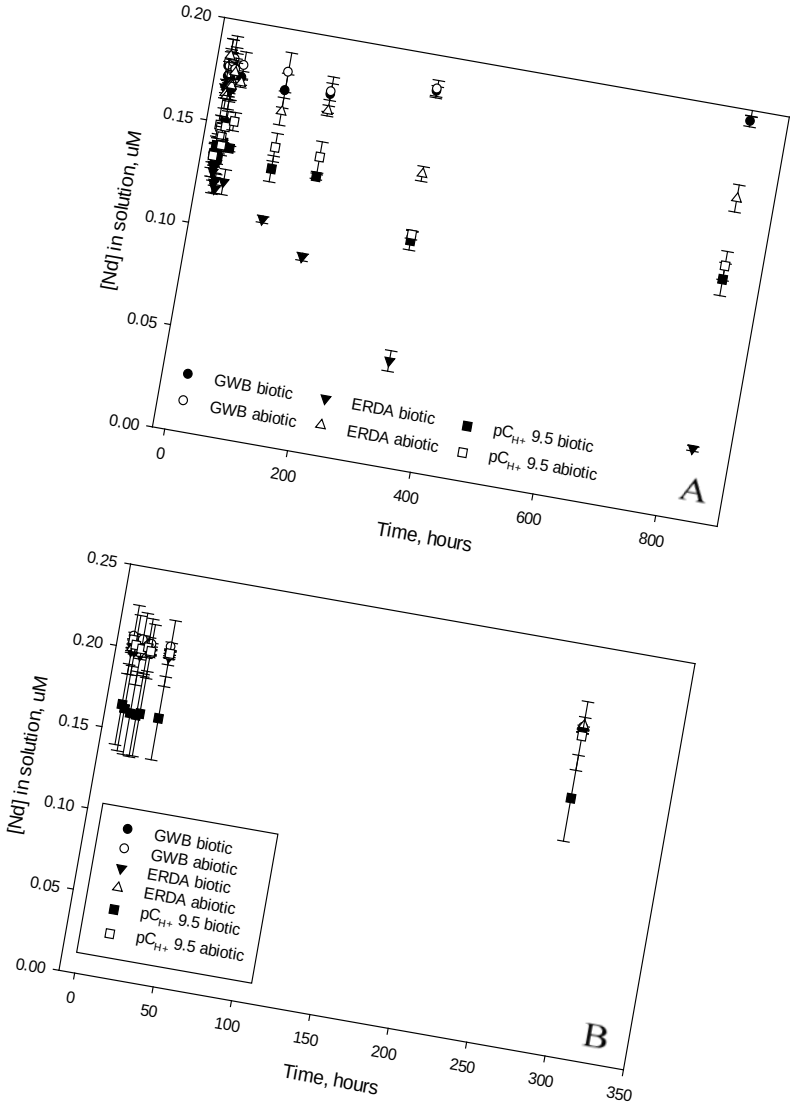

Figure SOTERM-7. A) Neodymium in Solution as a Function of Time in GWB, ERDA, and pC_{H+} 9.5-specific Brines, with and without *Halobacterium* sp. (GWB, 1.75 ± 0.52 x 10^9 cells/ml; ERDA, 1.54 ± 0.23 x 10^9 cells/ml; pC_{H+} 9.5, 1.50 ± 0.20 x 10^9 cells/ml) and B) Neodymium in Solution as a Function of Time in GWB, ERDA, and pC_{H+} 9.5-specific Brines, with and without *Halobacterium* sp. (GWB, 2.06 x 10^9 cells/ml; ERDA, 2.86 x 10^9 cells/ml; pC_{H+} 9.5, 1.70 x 10^9 cells/ml) in the Presence of EDTA.

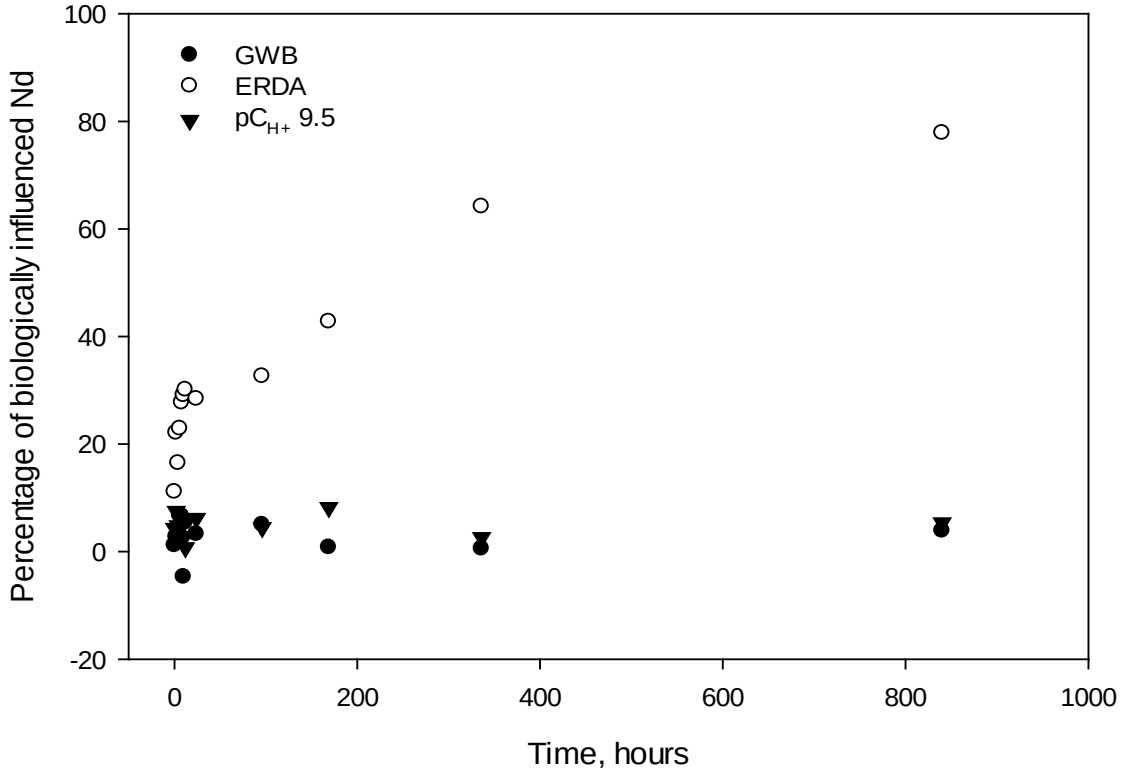

Figure SOTERM-8. Percentage of Biologically Influenced Nd as a Function of Time in GWB, ERDA, and pC$_{H+}$ 9.5-specific Brines.

SOTERM-5.0 WIPP-Relevant Actinide Chemistry

The speciation of actinides under WIPP-relevant conditions defines the source term for actinide release from the WIPP in release scenarios where mobile actinide concentrations are important (e.g., DBR and transport through the Salado or Culebra). The key factors that establish the concentrations of mobile actinides under subsurface conditions are known. The most important of these factors for the WIPP repository are:

1) Actinide redox chemistry is a critical factor in establishing the concentration of actinides in brine. The solubility of reduced lower-valent actinides (III and IV oxidation states) is significantly lower than oxidized forms (V and/or VI). In this context, the iron chemistry and microbial processes that establish and maintain reducing conditions in the WIPP are important.
2) The complexation of each actinide species is a critical factor in defining its solubility. For a given oxidation state, the inorganic and organic complexes present will define the solubility of the actinide. These complexants are in the pre-emplacement environment, are part of the TRU waste that is emplaced, or are produced as a result of subsurface processes, most notably microbial and corrosion processes.
3) Intrinsic and mineral colloid formation is a critical factor in defining the overall mobile concentration of each actinide. The contribution of actinide colloids to the concentration of actinides in WIPP brine is predicted to be significant. Many of the key TRU species in their expected oxidation states tend to form colloids or strongly associate with the non-actinide colloids present (e.g., microbial, humic and mineral).

The WIPP PA approach that was established in the initial WIPP compliance certification application (U.S. DOE 1996), and continued through the CRA-2014 PA calculations (Camphouse et al. 2013), accounts for all three of these key factors. This remains the DOE approach in CRA-2019.

The PA concept of actinide speciation in the WIPP is well grounded in what has been observed for actinide contaminants in near-surface groundwater. In natural systems, the following inorganic ligands are potentially important complexants of radionuclides in solution: CO_3^{2-}/HCO_3^-, OH^-, $C1^-$, SO_4^{2-}/S^{2-}, fluoride (F^-), and phosphate. Additionally, anthropogenic and bioderived chelating agents can strongly bind actinide species and will compete with the inorganic complexants present. Lastly, the tendencies of actinides to form intrinsic colloids and strongly associate or bind with colloidal particles are also well established. The relative importance of these complexants and processes depends on the pH, radionuclide oxidation state present, the presence of other metals, and the relative ligand concentrations. There are a number of general reviews on various aspects of actinide environmental chemistry (Allard 1982; Choppin, Liljenzin, and Rydberg 2004 [pp. 94–112]; Clark, Hobart, and Neu 1995; Banaszak, Rittmann, and Reed 1998b; Runde 2000; Nitsche et al. 1992; Reed, Deo and Rittmann 2010; Runde and Neu 2010).

For the anoxic, reducing, and mildly basic brine systems expected in the WIPP, the most important inorganic complexants are expected to be carbonate/bicarbonate and hydroxide. There are also important organic complexants that coexist in TRU waste with the potential to strongly

influence actinide solubility. In this context, the relative importance of actinides and overall oxidation state with respect to their potential release from the WIPP is:

Actinides: $Pu \approx Am >> U > Th >> Np \approx Cm$ (SOTERM.6)

Actinide Oxidation State: $An(III) > An(IV) >> An(VI) >> An(V)$ (SOTERM.7)

In the CRA-2019 PA (U.S. DOE 2019, Appendix PA Section 4.4), the contribution of Pu, Am, U, Th, Cm, and Np is expressly considered, although only Pu and Am contribute significantly to TRU release from the WIPP. The III oxidation state is the most important oxidation state based on current WIPP PA assumptions that Am always exists in the III state, Pu exists in the III state in ~50% of the vectors, and the III oxidation state is more soluble than the IV (see SOTERM Section 6.4).

In this section, an update of the relevant environmental chemistry and a summary of new literature are provided for each key actinide that defines the WIPP mobile actinide concentration (e.g., Actinide Source Term). A more detailed discussion of the environmental chemistry was given in Appendix SOTERM-2014. SOTERM Section 5.1 gives a summary of changes since the CRA-2014 PA; SOTERM Section 5.2 gives an overview of the projected and current inventory of actinides in the WIPP; SOTERM Section 5.3, SOTERM Section 5.4, SOTERM Section 5.5, SOTERM Section 5.6, SOTERM Section 5.7 and SOTERM Section 5.8 contain an updated overview of the relevant environmental chemistry and WIPP-specific results for Ac, Th, U, Np, Pu, and Am/Cm, respectively. An up-front overview of the current assumptions and understanding of WIPP actinide chemistry is given in Table SOTERM-10.

SOTERM-5.1 Changes/Status in Actinide Chemistry Information since the CRA-2014

Overall, there are no significant developments within or outside the WIPP project since the CRA-2014 that impact overall PA implementation. Some parameter and modeling changes were made and are described in Appendix GEOCHEM. The following key assumptions are continued:

- Oxidation state distributions for the TRU actinides, and correspondingly, assumptions regarding their solubility calculations using redox-invariant analogs, have not changed.
- The approach used to calculate solubilities for Pu and Am oxidation states, which are the key actinides from the perspective of PA have changed somewhat. The geochemical modeling program EQ3/6, rather than Fracture-Matrix Transport (FMT), however, continues to be used to calculate these solubilities with the WIPP actinide database.
    - The Pitzer approach will continue to be used given the high ionic-strengths present in the predicted WIPP brines.
    - Calcium-EDTA competition has been added to the WIPP model – this effectively lowers the concentration of the An(III) actinides significantly and brings the concentration of An(III) and An(IV) within a factor of ~ three.
    - A lead model was added to the WIPP model – this, in its current form, does not however impact the actinide source term because it does not include complexation

with organic chelators (See Appendix GEOCHEM for a more detailed discussion). This model also uses Specific Ion Interaction theory (SIT) rather than Pitzer parameters.

- An iron model was added to the WIPP model. This does not include complexation with organic chelators (See Appendix GEOCHEM for a more detailed discussion).

- Inventory assumptions regarding the amounts of organic chelating agents (See SOTERM Section 3.3) and actinides in TRU waste are being updated annually. A new PAIR was generated and these actinide data are reported in Section 5.2 and compared to the CRA-2014 inventory. The main difference/effect is the significant increase in the plutonium inventory.
- Radiolytic factors have been reconsidered to reflect the increase in plutonium inventory and changes in the screening argument (Day 2019a). This directly leads to a small increase in total gas generation (see Day 2019b for a more detailed discussion). There are also indirect impacts on the net E_h of the actinide-brine system toward a higher E_h and more Pu (IV). The magnitude of this effect under Fe-dominated WIPP-relevant system is the subject of ongoing studies.
- The WIPP colloidal model that accounts for intrinsic, mineral fragment, microbial and humic colloidal enhancements has not changed. The colloidal enhancement parameters were re-evaluated and new parameter recommendations are made as part of the deferred PA strategy for CRA-2019. Experiments specific to intrinsic, microbial, and to a lesser extent mineral fragment colloids are also reported. These data, although still incomplete, provide stronger supporting data for the current WIPP colloid model and the changes initiated in CRA-2014.

There are new data, within and outside the WIPP project, that continue to support and/or expand the robustness of the current PA assumptions. The most important of these are:

- New WIPP-specific data that confirm the predominance of lower-valent plutonium in long-term, iron-dominated brine systems. There are also new data in the literature from outside the WIPP project. These are discussed in SOTERM Section 5.7.
- The effect of the complexation of organic chelating agents on actinide (III/IV) oxidation states continues to be a focus of international and WIPP-specific research. Relatively strong complexation effects that were noted in CRA-2014 with An(III) are being confirmed and this remains consistent with current WIPP modeling. This is being extended to the An(IV) species. These data were discussed in Section 3.3 and in each of the actinide-specific sections (SOTERM 5.3 through 5.8).
- New Pu(III) solubility data and oxidation-state stability data show a lowering of the measured solubility of Pu(III) and that Pu(III) phases are not stable above pH ~ 6. The redox stability of Pu(IV) and Pu(III) continues to be an active area of research that is not definitively resolved. This is discussed in section SOTERM 5.7.

Table SOTERM-10. Overview of the WIPP PA View/Role and Relevant Environmental Chemistry of the Key Actinide Species in the WIPP (References for Each Actinide are Provided in the Following Sections).

Actinide	WIPP PA View/Role	Environmental Chemistry
Actinium	Not a TRU component. Currently shows up in later repository times as a decay product. It adds to the An(III) speciation and release in PA.	Essentially no studies of the environmental chemistry. It follows the same track as the An(III) actinides.
Thorium	Not a TRU component. Currently included in PA calculations, but not a significant contributor to actinide release. Used as an oxidation-state invariant analog for the IV actinides. Th data are used in EQ3/6 to calculate the solubility of Pu(IV), Np(IV), and U(IV).	Exists as Th^{4+} complexes and is sparingly soluble under a wide range of environmental conditions. Th has a high tendency towards intrinsic colloid formation.
Uranium	Not a TRU component. Potentially useful as a VI analog for Pu(VI) species. Currently, U is conservatively assumed to be U(VI) in 50% of the PA vectors (set at a 1 mM solubility) and U(IV) in 50% of the PA vectors. It is not predicted to be a significant contributor to actinide release (based on Ci).	Exists as UO_2^{2+} and U^{4+} species that are strongly correlated with redox conditions. Can form highly insoluble U(VI) and U(IV) phases. Can persist up to mM concentrations in near-surface groundwater.
Neptunium	TRU component. Currently included in the PA calculations, but not a significant contributor to actinide release. Assumed to be IV in 50% of the PA vectors and V in 50% of the PA vectors. Expected to predominate in the IV oxidation state under the conditions expected in the WIPP.	Mobile and relatively soluble as the NpO_2^+ species under oxidizing conditions. Is fairly insoluble and immobile as Np^{4+} under reducing conditions.
Plutonium	TRU component. Major contributor to actinide release calculations. Assumed to be IV in 50% of PA vectors and III in the other 50% of PA vectors.	Relatively immobile and insoluble as a subsurface contaminant. Persists as Pu^{4+} except under bio-mediated, strongly reducing conditions where Pu^{3+} species may be formed. If transported, this will likely be primarily through colloidal mechanisms.
Americium	TRU component. Major contributor to actinide release calculations. Exists in the III oxidation state in all vectors and its thermodynamic data are used by EQ3/6 for all III oxidation state calculations. Significant colloidal contribution due to strong association as a pseudo-colloid.	Relatively immobile and insoluble as a subsurface contaminant. Persists as Am^{3+} complexes under a wide range of environmental conditions.
Curium	Small quantities of ^{243}Cm, ^{245}Cm, and ^{248}Cm are present in the WIPP. ^{244}Cm, although present, is not a TRU waste component due to its <20 year half-life. These are very minor contributors to actinide release. Chemistry is analogous to Am(III).	Not a very significant concern as a subsurface contaminant. Has the same chemistry as Am, so it will persist as a Cm^{3+} species.

SOTERM-5.2 Actinide Inventory in the WIPP

The actinide inventory for the WIPP, based on the Performance Assessment Inventory Report – 2018 (Van Soest 2018), is given in Table SOTERM-11. This is the inventory used in CRA-2019. Also included in this table is the calculated inventory-limited solubility of the various actinides and radionuclides considered by the WIPP PA.

Over long time frames, only Pu and Am are expected to make a significant contribution to releases from the WIPP (see time profile in Table SOTERM-12), although the relative contribution of Am decreases significantly after 1000 years due to its half-life. Curium (Cm), which is predominantly present as ^{244}Cm, is well below the calculated solubility for III actinides when fully dissolved and, with its very short half-life (18.11 years), will not be important beyond the 100-year period of institutional control. Although some cesium (Cs) and strontium (Sr) is initially present in the WIPP, these fission products can only contribute significantly to the overall release from the WIPP for the first 100 years of repository history and are not significant beyond the period of institutional control.

Table SOTERM-11. CRA-2019 WIPP Radionuclide Inventory Decay-Corrected to 2033

Selected Radionuclides	Activity (Ci)	Amount (kg)	Element-Specific Inventory Ci (Kg)	CRA-2014 Reported Amounts	Inventory-Defined Solubility Limit[a] (M)
Actinides					
^{225}Ac	1.25E+00	2.16E-08	27.2 (3.60×10^{-4}-)	N/A	<< Solubility
^{227}Ac	2.59E+01	3.60E-04			
^{229}Th	1.25E+00	5.97E-03	46.3 (1.08×10^{3})	7.04 (1.35×10^{4})	>> Solubility
^{230}Th	2.66E+00	1.27E-01			
^{232}Th	1.19E-01	1.08E+03			
^{234}Th	4.23E+01	1.84E-06			
^{233}U	1.27E+02	1.31E+01	663 (1.28×10^{5})	528 (2.26×10^{5})	>> Solubility
^{234}U	4.86E+02	7.85E+01			
^{235}U	6.41E+00	2.91E+03			
^{236}U	6.77E-01	1.04E+01			
^{238}U	4.23E+01	1.25E+05			
^{237}Np	3.44E+01	4.85E+01	469 (48.5)	23.2 (32.5)	8×10^{-6} M (≥ projected solubility)
^{239}Np	4.35E+02	1.89E-06			
^{238}Pu	9.64E+05	5.67E+01	4.03E6 (1.56×10^{4})	2.02×10^{6} (1.20×10^{4})	>> Solubility
^{239}Pu	8.74E+05	1.41E+04			
^{240}Pu	3.19E+05	1.39E+03			
^{241}Pu	1.87E+06	1.87E+01			
^{242}Pu	1.64E+02	4.20E+01			

Table SOTERM-11. CRA-2019 WIPP Radionuclide Inventory Decay-Corrected to 2033 (Continued)

Selected Radionuclides	Activity (Ci)	Amount (kg)	Element-Specific Inventory Ci (Kg)	CRA-2014 Reported Amounts	Inventory-Defined Solubility Limit[a] (M)
Actinides					
^{244}Pu	3.40E-02	4.79E+00			
^{241}Am	1.14E+06	3.36E+02	1.14×10^{6} (3.38×10^{2})	7.05×10^{5} (203)	5×10^{-5} M (≥ projected solubility)
^{243}Am	4.35E+02	2.17E+00			
^{244}Cm	3.94E+04	4.86E-01	3.99×10^{4} 2.13	9.97×10^{3} (0.122)	~ 3×10^{-8} M
^{246}Cm	5.10E+02	1.64E+00			
^{249}Cf	4.83E+01	1.18E-02			
Fission Products[b]					
^{137}Cs	2.51E+05	2.88E+00	2.51×10^{5} (2.88)	2.35×10^{5} (2.67)	1×10^{-6} M
^{90}Sr	1.97E+05	1.41E+00	1.97×10^{5} (1.41)	2.09×10^{5} (1.51)	1×10^{-6} M

a Moles in the inventory divided by the minimum brine volume (17,400 m3)

b Fission products are not TRU, but are considered in the PA to calculate overall release

Although the comparison in Table SOTERM-12 is qualitative, it provides a sense of the direction of change in the actinide inventory. Neptunium and curium, although a slight increase in inventory may be present remain very low in terms of mass and continue to be discounted in PA based on their low inventory. Uranium inventory is increased, and thorium is decreased, but these remain a relatively small fraction of the mobile actinide source term based on Ci content. Americium has increased slightly and may be insignificant when scaling and corrections are applied. The main increase in overall activity is caused by plutonium which was explained in CRA-2019, Section 194.24 as due to the increased inventory coming from the added surplus plutonium from Savannah River Site. All these new data do not change the core approach used in the CRA-2019 PA.

Table SOTERM-12. Predominance of Actinide Isotopes Over Time in the PAIR 2018 WIPP Inventory. Top 30, By Activity, are Shown in Order of Predominance.

Year 2033	Year 2133	Year 2383	Year 3033	Year 7033	Year 12033
Pu-241	Am-241	Pu-239	Pu-239	Pu-239	Pu-239
Am-241	Pu-239	Am-241	Pu-240	Pu-240	Pu-240
Pu-238	Pu-238	Pu-240	Am-241	U-234	U-234
Pu-239	Pu-240	Pu-238	U-234	Tc-99	Tc-99
Pu-240	Cs-137	U-234	Tc-99	Ni-59	Ni-59
Cs-137	Ba-137m	Tc-99	Ni-59	Am-241	Pa-233
Ba-137m	Y-90	Ni-59	Cm-246	Pa-233	Np-237
Y-90	Sr-90	Cm-246	Np-239	Np-237	Np-239
Sr-90	Pu-241	Np-239	Am-243	Np-239	Am-243
Cm-244	Cm-244	Am-243	Pu-238	Am-243	Pu-242
H-3	U-234	Pu-242	Pa-233	Cm-246	U-233
Eu-154	Tc-99	Np-237	Np-237	Pu-242	Cm-246
Ni-63	Ni-59	Pa-233	Pu-242	U-233	Ra-225
Tc-99	Cm-246	U-233	U-233	At-217	At-217
Kr-85	Ni-63	Ni-63	C-14	Fr-221	Fr-221
Ni-59	Np-239	Cs-137	Th-234	Ac-225	Ac-225
Cm-246	Am-243	Ba-137m	Pa-234m	Ra-225	Th-229
U-234	Po-216	C-14	U-238	Th-229	Bi-213
Pb-212	Pb-212	U-238	Pu-241	Bi-213	Pb-209
Rn-220	Bi-212	Pa-234m	Cm-245	Pb-209	Po-213
Bi-212	Rn-220	Th-234	Ac-227	Po-213	Th-230
Po-216	Ra-224	Y-90	Bi-211	Th-234	U-236
Ra-224	Th-228	Sr-90	Pb-211	U-238	Po-218
Th-228	U-232	Pu-241	Rn-219	Pa-234m	Rn-222
U-232	Pu-242	Cm-245	Ra-223	Th-230	Ra-226
Np-239	H-3	Cf-249	Po-215	U-236	Bi-214
Am-243	U-233	Po-210	Pa-231	C-14	Pb-214
Co-60	Po-212	Bi-210	Tl-207	Po-218	Pb-210
Po-212	Sm-151	Pb-210	Th-227	Rn-222	Po-214
Eu-155	Pa-233	Rn-222	Po-218	Ra-226	Bi-210

Table SOTERM-13. Time Dependence of Radionuclides Discussed in Sections 5.3 to 5.8 (total Ci). Based on Inventory Data in PAIR-2018.

Radionuclide	Repository Time					
	2033	2133	2383	3033	7033	12033
Ac-227	2.59E+01	1.63E+01	1.58E+01	1.57E+01	1.50E+01	1.45E+01
Am-241	1.14E+06	1.03E+06	6.89E+05	2.43E+05	4.18E+02	1.19E+01
Am-243	4.35E+02	4.31E+02	4.21E+02	3.96E+02	2.72E+02	1.70E+02
Cm-244	3.94E+04	8.55E+02	5.94E-02	9.18E-13	--	--
Cm-245	2.44E+01	2.46E+01	2.47E+01	2.42E+01	1.76E+01	1.17E+01
Cs-137	2.51E+05	2.49E+04	7.71E+01	2.31E-05	--	--
Np-237	3.44E+01	7.01E+01	1.39E+02	2.29E+02	2.77E+02	2.77E+02
Pu-238	9.64E+05	4.38E+05	6.07E+04	3.57E+02	4.35E-10	9.06E-21
Pu-239	8.74E+05	8.72E+05	8.65E+05	8.49E+05	7.57E+05	6.56E+05
Pu-240	3.19E+05	3.16E+05	3.08E+05	2.88E+05	1.88E+05	1.11E+05
Pu-244	3.40E-02	3.40E-02	3.40E-02	3.41E-02	3.41E-02	3.42E-02
Th-232	1.19E-01	1.19E-01	1.19E-01	1.19E-01	1.19E-01	1.19E-01
U-235	6.41E+00	6.50E+00	6.71E+00	7.26E+00	1.04E+01	1.39E+01
U-238	4.23E+01	4.23E+01	4.23E+01	4.23E+01	4.23E+01	4.23E+01

SOTERM-5.3 Actinium Chemistry

Actinium is not a TRU component within the WIPP and is currently set to have a relatively low inventory at closure, < 0.5 g in 2033. However, inventory for this species has been increasing greatly (approximately an order of magnitude since the 2012 PAIR) and is set for continued expansion in the coming years. Based on present information and associated half-lives, it is expected that both ^{225}Ac and ^{227}Ac will be amongst the top 20 contributors to radioactivity within the WIPP at various times during the 10,000-year period following closure. The ^{227}Ac isotope ($t_{½}$ = 21.8 yr) is expected to be the predominant actinium species by mass throughout this period, and results from multi-generational radioactive decay of ^{239}Pu as shown in Figure SOTERM-9. By comparison, the ^{225}Ac isotope ($t_{½}$ = 9.92 d) is expected to be less abundant on a mass basis, but a greater contributor to radioactivity by the year 7033; this species results from an extended radioactive decay scheme, starting with ^{241}Pu as illustrated below for comparison.

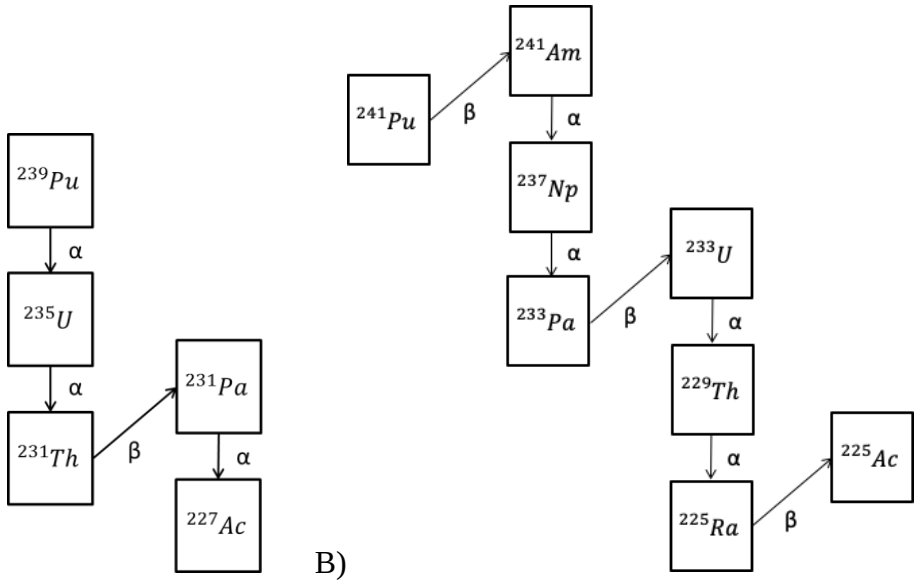

Figure SOTERM-9. Radioactive Decay Chain Yielding A) ^{227}Ac and B) ^{225}Ac

SOTERM-5.3.1 Actinium Environmental Chemistry

Unlike many of the other actinide species of interest, actinium is expected to occur only in a single oxidation state (III) within aqueous media (Altmaier et al. 2013). Generally, actinium chemistry closely follows that of lanthanum, which is considered a near ideal surrogate in many investigations. However, the smaller ionic radius of Ac^{3+} (1.12 Å) is associated with a more basic ionic character that is believed to drive enhanced solubility in some instances (Shannon 1976). For example, previous efforts have supported $Ac(OH)_3$ as having higher solubility relative to all other f-element, trihydroxide species (Barkatt et al. 1983).

Previous efforts at pH 8 support minimal hydrolysis of Ac^{3+}, with an equilibrium constant of 3.5×10^{-9}being measured by Moutte and Guillaumont (1969). Under these conditions, the authors stated that actinium in solution exists as 74% $Ac(OH)^{2+}$ and 26% $Ac(OH)_2^{+}$. Analogous efforts at higher, more WIPP-relevant pH were not identified for comparison.

Unfortunately, as actinium is not a primary concern in most nuclear repository efforts at the present time, significant knowledge gaps exist pertaining to its behavior under WIPP-relevant conditions. For example, in comparison with other species discussed above (e.g., Pu, Np, etc.), analogous thermodynamic/solubility data for WIPP relevant redox, solubility, and reaction chemistries are significantly less available within the literature.

SOTERM-5.3.2 New Literature Results Since the CRA-2014

While several articles related to natural radioisotopes, including actinium species, impacting oil and gas operations like those near the repository were noted, no direct WIPP-relevant literature was found for actinium in the time period since CRA-2014.

SOTERM-5.3.3 WIPP-Specific Results Since the CRA-2014

As actinium is not a key contributor to release from the WIPP at this time, there are no new WIPP-relevant results on the chemistry and speciation of actinium since CRA-2014.

SOTERM-5.4 Thorium Chemistry

Th is not a TRU component, although an estimated 1.08 metric tons of Th will be in the WIPP at closure. The release of Th as the ^{230}Th isotope was calculated in the CRA-2019 PA but does not significantly contribute to the overall release of activity from the WIPP. Th is, however, important for the WIPP in that it is used as a redox-invariant analog for the IV actinides (Pu(IV), Np(IV), and U(IV)), and Th complexation data are used in the EQ3/6 code for the An(IV) solubility calculations (SOTERM Section 6.1).

SOTERM-5.4.1 Thorium Environmental Chemistry

Th, under a wide range of conditions, has one stable oxidation state in aqueous solutions: the Th^{4+} tetravalent ion. For this reason, the environmental chemistry of Th is understood from the perspective of the solubility and complexation of this species, which is also the species expected to be present in the WIPP environment when DBR and transport release scenarios are important.

The hydrolysis of Th^{4+}, as is true for all An(IV) species in the WIPP, is complex and a critically important interaction in defining the overall solubility of Th. This was recently investigated by Ekberg et al. (2000), Rai et al. (2000), Moulin et al. (2001), and Okamoto, Mochizuki, and Tsushim (2003), and was critically reviewed by Neck and Kim (2001) and Moriyama et al. (2005). The authors have proposed a comprehensive set of thermodynamic constants that extends to all tetravalent actinides. The solubility products were determined for amorphous (am) $Th(OH)_4$ (Neck et al. 2002; Altmaier et al. 2005 and 2006) and for crystalline ThO_2 (Neck et al. 2003), as well as for specific ion interaction theory parameters (Neck, Altmaier, and Fanghänel 2006). The thermodynamic stability constants are listed in Table SOTERM-14.

Table SOTERM-14. Thermodynamic Stability Constants for Key Th Hydrolytic Species

Hydrolytic Reaction/Species	Stability Constant
Mononuclear Species	
$Th(OH)_{4,\,am} \leftrightarrows Th^{4+} + 4OH^-$	$\log K_{s,am} = -47.8 \pm 0.3$
$Th(OH)_{4,\,cr} \leftrightarrows Th^{4+} + 4OH^-$	$\log K_{s,cr} = -53.2 \pm 0.4$
$Th^{4+} + OH^- \leftrightarrows Th(OH)^{3+}$	$\log \beta^0_1 = 11.8 \pm 0.2$
$Th^{4+} + 2OH^- \leftrightarrows Th(OH)_2^{2+}$	$\log \beta^0_2 = 22.0 \pm 0.6$
$Th^{4+} + 3OH^- \leftrightarrows Th(OH)_3^{+}$	$\log \beta^0_3 = 31 \pm 1$
$Th^{4+} + 4OH^- \leftrightarrows Th(OH)_{4,aq}$	$\log \beta^0_4 = 38.5 \pm 1$
Polynuclear Species	
$4Th^{4+} + 12OH^- \leftrightarrows Th_4(OH)_{12}^{4+}$	$\log \beta^0_{4,12} = 141$
$6Th^{4+} + 15OH^- \leftrightarrows Th_6(OH)_{15}^{9+}$	$\log \beta^0_{6,15} = 176$

Discrepancies in the crystalline (cr) ThO_2 solubility were studied (Vandenborre et al. 2010) and assigned to the different forms of material present: bulk ThO_2(cr) grains (80%) and $ThO_x(OH)_y(H_2O)_z$(s) grain boundaries (20%). The hydrated material may originate from the initial grain-boundary oxide materials, which are more sensitive to humidity than the bulk materials. The solubilities of these two phases are quite different and together with the "local solubility" (the most active sites) were used to explain the discrepancies noted.

The presence of carbonate in solution greatly increases the solubility of thorium dioxide (ThO_2). An increase by one order of magnitude of the carbonate concentration in the range of 0.1 – 2 M leads to a five-order-of-magnitude increase in the Th(IV) solubility due to the formation of mono- and penta-carbonate complexes. Östhols, Bruno, and Grenthe (1994) proposed the following equilibrium reactions and the corresponding stability constants:

$$ThO_2 + H^+ + H_2O + CO_3^{2-} \leftrightarrows Th(OH)_3CO_3^- \log K_{131} = 6.11 \pm 0.19 \quad \text{(SOTERM.6)}$$

$$ThO_2 + 4H^+ + 5\,CO_3^{2-} \leftrightarrows Th(CO_3)_5^{6-} + 2H_2O \log K_{105} = 42.12 \pm 0.32 \quad \text{(SOTERM.7)}$$

This speciation scheme, however, was criticized in (Altmaier et al. 2005) because it overpredicts the dependency of Th solubility on carbonate and underpredicts the effect of hydrolysis at higher pH. That hydrolysis prevails at pH >10 is supported by detailed experimental results (Figure SOTERM-10). These data are explained by the predominance in this system of $Th(OH)(CO_3)_4^{5-}$ complex rather than $Th(CO_3)_5^{6-}$. A greater role for other ternary complexes of thorium (e.g., $Th(OH)_2(CO_3)_2^{2-}$), which are also likely to be present in the WIPP conditions, is also proposed, and formation constants for these complexation reactions are reported. The use of the pentacarbonate complex for the IV actinides in the WIPP PA, for these reasons, is a conservative assumption that overpredicts the solubility of the IV oxidation state at pH > 10. A correction in the FMT database, now in the EQ3/6 database, to the value of the $Th(OH)_4$(aqueous [aq]) to be consistent with Neck et al. (2002) was incorporated into the CRA-2004 Performance Assessment Baseline Calculation (PABC) and there are no new changes in this speciation scheme in CRA-2019.

The dissolution of crystalline ThO_2 in low ionic strength media and the effect of carbonate and calcium concentration on the solubility of thorium were investigated at alkaline pH (Kim et al. 2010). The observed thorium concentration in the groundwater was greater than predicted. This discrepancy was explained by the authors as the result of colloid formation (based on their sequential filtration data). Carbonate affected the observed thorium solubility as expected. There was no calcium enhancement of the thorium solubility until a calcium concentration of 1.25 mM.

Oxyanions such as phosphate and, to a lesser extent, sulfate, also form Th^{4+} complexes that can precipitate at pH <5. The effect of phosphate on solubility of microcrystalline ThO_2 is very limited. The stability constants for $Th^{4+}/H_2PO_4^-$ and Th^{4+}/HPO_4^{2-} were reported (Langmuir and Herman 1980). Overall, the role of these oxyanions is expected to be unimportant for the mildly basic brines (pH ~8-10) present in the WIPP.

A new perturbation to the understanding of Th speciation, as well as other actinides in the IV oxidation state, is the observation that Ca, and to a lesser extent, magnesium (Mg), enhance Th solubility at pH >10 (see Figure SOTERM-11). The formation of $Ca_4[Th(OH)_8]^{4+}$ and

$Ca_4[Pu(OH)_8]^{4+}$ ion pairs in alkaline $CaCl_2$ solution is reported (Brendebach et al. 2007; Altmaier, Neck, and Fanghänel 2008). These species cause a rapid increase in the solubility of all tetravalent actinides at pH greater than 11. This increased solubility is only observed at $CaCl_2$ concentrations above 0.5 M for Th(IV), and correspondingly above 2 M for Pu(IV) species. This effect can be discounted for the WIPP PA because Ca concentrations in the WIPP are predicted to be approximately 14 mM or less with a pH of approximately 8.7. These are both well below the levels needed to see a significant effect for both Th and Pu.

Actinides in the IV oxidation state, because of the complexity of their solution chemistry and very high tendency towards hydrolysis, form colloidal species in groundwater. The potential effect of colloid formation on solubility of Th(IV) in concentrated NaCl and $MgCl_2$ solution was published by Altmaier, Neck, and Fanghänel (2004) and is shown in Figure SOTERM-12. In neutral-to-alkaline solutions, colloids could be formed as Th oxyhydroxide with log $[Th]_{(colloid\ [coll])} = -6.3 \pm 0.5$, independent of ionic strength. In Mg solutions, the formation of pseudocolloids (i.e., Th(IV)) sorbed onto $Mg_2(OH)_3Cl \cdot 4H_2O$(coll) led to an apparent increase of the total Th concentration up to 10^{-5} M (Walther 2003; Degueldre and Kline 2007; Bundschuh et al. 2000). For these reasons, colloid formation is addressed in the WIPP PA.

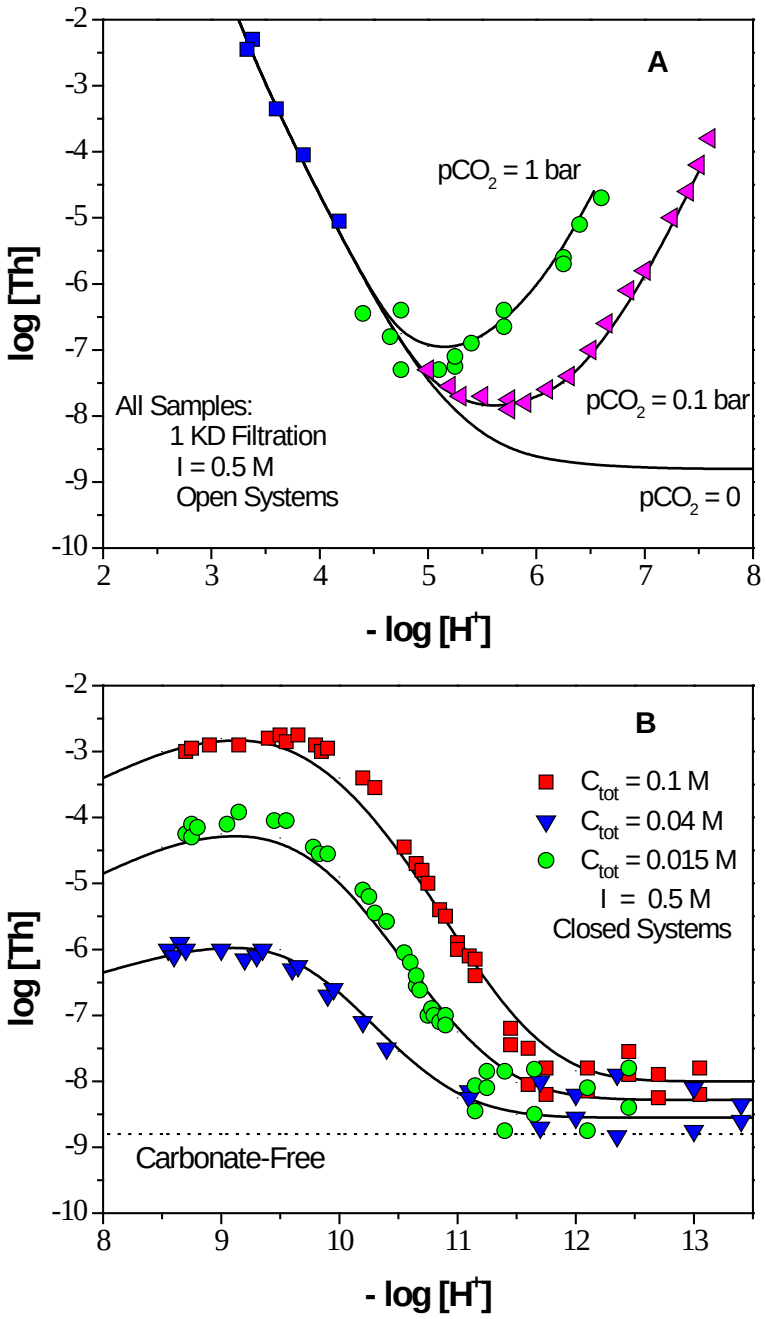

Figure SOTERM-10. Solubility of Amorphous Th(IV) Oxyhydroxide as a Function of Carbonate Concentration in 0.5 M for (A) pH = 2–8 and (B) pH = 8–13.5. The Solid Lines are the Calculated Solubilities (Based on Data in Altmaier et al. 2005).

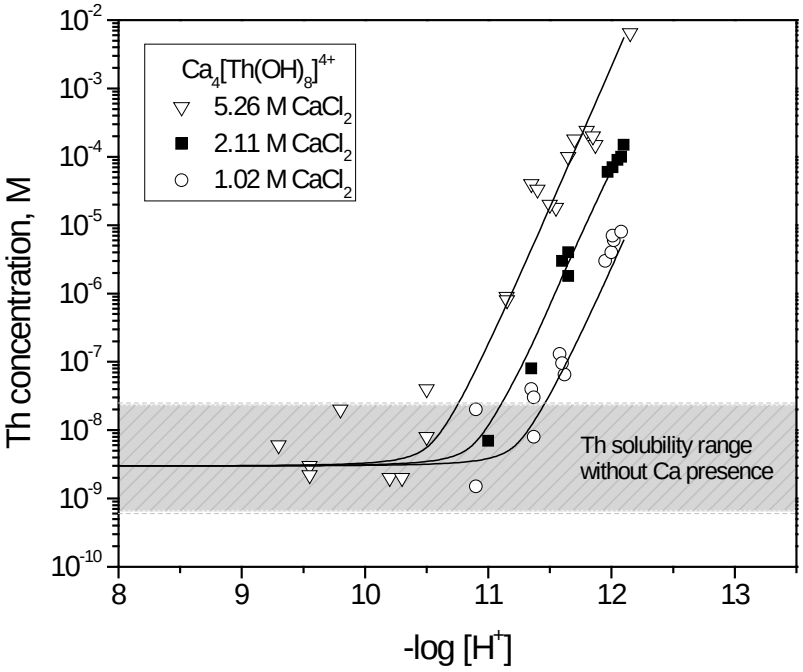

Figure SOTERM-11. Effect of Ternary Ca-Th(IV)-OH Complexes on the Solubility of Th(IV) in Brine (Altmaier et al. 2008).

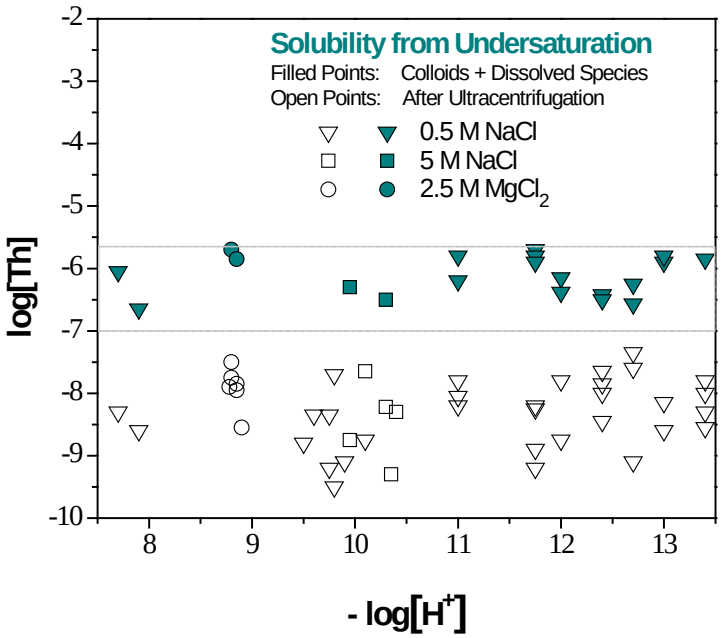

Figure SOTERM-12. Solubility of $Th(OH)_4$(am) Determined from Undersaturation in 0.5 NaCl, 5.0 M NaCl, and 2.5 M $MgCl_2$. Filled Points: Total Th Concentrations (Including Colloids); Open Points: Th Concentrations Measured after Ultracentrifugation at 90,000 Revolutions Per Minute (5×10^5 g) (Based on Data in Altmaier, Neck, and Fanghänel 2004).

A study to establish the solubility of thorium under WIPP-specific conditions was completed between CRA-2009 and CRA-2014. These experiments were performed in carbonate-free and carbonate-containing WIPP simulated brine to establish the effects of carbonate, pC_{H+} and time on thorium (IV) solubility and are published in a report entitled "Solubility of An(IV) in WIPP Brine, Thorium Analog Studies in WIPP Simulated Brine" (Borkowski et al. 2012).

The results obtained are shown in Figure SOTERM-13. After 2 years of equilibration in carbonate-free brine, the measured solubility of thorium was $6\text{-}7\times10^{-7}$ M and was essentially independent of pH and brine composition over the 6.5 to 11.5 pC_{H+} range investigated. Sequential filtration to ~ 10 nm pore size had little effect on the measured concentration. Subsequent ultracentrifugation up to 1,000,000 g resulted in up to a 40% colloidal fraction (but typically 20% or less), indicating that there was much less intrinsic colloid formation than reported in Altmaier, Neck and Fanghänel (2004) (see Figure SOTERM-12). The steady-state thorium concentrations measured, however, are consistent with literature reports for simplified brine systems (Altmaier, Neck and Fanghänel 2004) but show a significantly lower extent of aggregation to form intrinsic colloids.

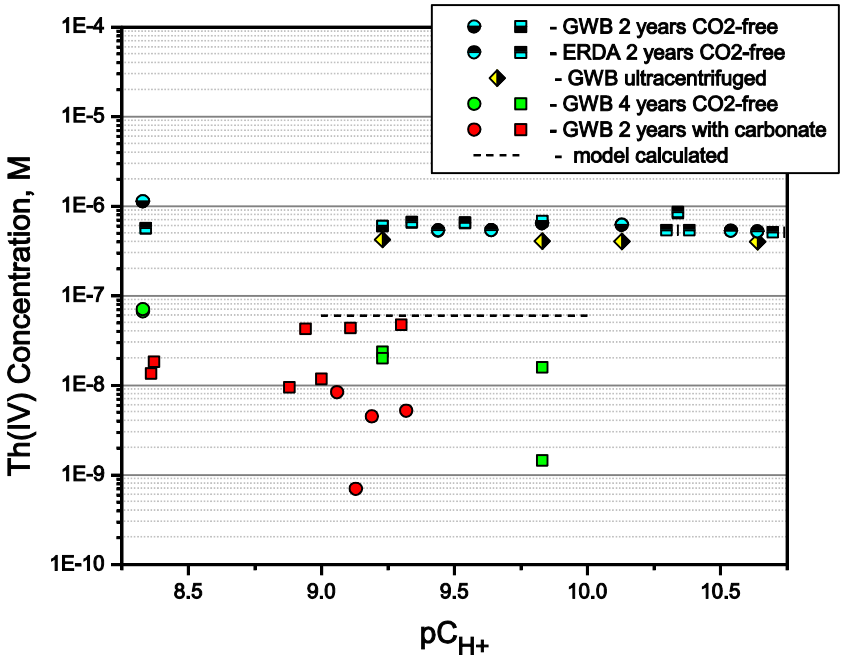

Figure SOTERM-13. The Concentration of Thorium Measured in WIPP Simulated Brine (GWB and ERDA-6) as a Function of Time, Filtration and the Presence of Carbonate. Square Symbols Represent an Undersaturation Approach, Whereas the Circles Represent the Oversaturation Approach. Although High, but Metastable, Concentrations were Initially Present, in Time the Measured Concentrations Decreased and are at or below the WIPP Model-predicted Values (Borkowski et al. 2012).

After an additional 2 years of equilibration, the thorium concentration in carbonate-free GWB significantly decreased (green points in the Figure SOTERM-13). For pC_{H+} in the range of 7.5 to

8.3, some samples did not show a change in the thorium concentration, but others showed a decrease of over one order of magnitude and were similar to the thorium concentrations measured in GWB containing 10^{-2} and 10^{-3} M carbonate.

The presence of carbonate, at a concentration that is ten-fold greater than expected in the WIPP, had little/no effect on the measured thorium concentrations. After two years of equilibration, the thorium concentrations measured from under- and oversaturation in GWB did not depend on carbonate concentration. Concentrations measured from oversaturation were 2.5 orders of magnitude greater than those measured from undersaturation, indicating that metastable states can persist for long periods of time (over 4 years, at least, in WIPP-relevant brine systems). The trend in the oversaturation data (see Figure SOTERM-10) is consistent with the literature data (Altmaier et al. 2005). In the undersaturation experiments, which are more relevant to the WIPP situation, the average thorium concentration was 2×10^{-8} M and continued to decrease at $pC_{H+} > 9$. The oversaturation experiments showed a similar trend and at $pC_{H+} > 9$ the thorium concentrations decreased to below 10^{-8} M. These results reproduce, to some extent, the trends reported in the literature (Altmaier et al. 2005), but the much higher ionic strength solutions used in our experiments shift our pH profile to a lower pC_{H+} value by approximately 1 pH unit.

At the expected WIPP repository pC_{H+}(~ 9.5), in the presence of carbonate, the thorium concentrations in GWB brine were 2×10^{-8} M or lower. This concentration trend suggests that at repository conditions the mixed thorium hydroxy-carbonato complexes do not play any role in the thorium solubility at $pC_{H+} > 9$.

The sequential filtration of thorium (Borkowski et al. 2012, and Reed et al. 2013) in the carbonate system (see Figure SOTERM-13) led to a dissolved thorium concentration of $2\text{-}6\times10^{-8}$ M in GWB. In ERDA-6 brine, however, the dissolved thorium concentration was about ten-fold greater and it is apparent that steady state thorium concentration was not achieved. The colloidal thorium species appear to be very small (see Figure SOTERM-14), less than 10 kDa (~5 nm). Overall, the truly dissolved thorium concentration was $3(\pm2) \times 10^{-8}$ M. The average total thorium concentration consisted of a dissolved fraction of 30 - 60% and a colloidal fraction of 40 - 70%.

The WIPP-specific thorium solubility results just summarized support the ongoing WIPP recertification effort in three important ways: 1) they provide empirical solubilities over a broad range of conditions that improve the robustness of the WIPP PA model, 2) they resolve and address published literature data in simplified brine systems that appeared to disagree with the current WIPP PA approach, and 3) they provide an input that will help establish the intrinsic colloidal enhancement factors for IV actinides. There is general agreement between our data and results reported in the literature for simplified brine systems, although we are seeing a far lower colloidal fraction in the total concentrations measured. After 4 years of equilibration, our measured solubilities are slightly lower (by a factor of ~ 2) than the solubilities calculated in the WIPP PA – this is well within the order of magnitude uncertainty typically observed between the calculated and measured solubilities in complex brine systems.

A key motivation in the WIPP thorium solubility and speciation studies was to explain the reports in the literature that very high colloidal fractions are present in high ionic-strength brine systems (mainly Altmaier et al. 2004). The WIPP-specific data show that there are colloids present in these systems, but these are much less than what was reported. The explanation for

this is a combination of the differences in brine composition (sodium chloride brine vs. GWB/ERDA-6) between the two studies and the presence of MgO colloids in the Altmaier study where mineral fragment colloids were likely formed (which is counted as part of their colloidal fraction). Perhaps a more important result in the WIPP-specific studies is the observation that there is an equilibration between the intrinsic colloidal fraction and the dissolved species. This equilibrium shifts to a lower overall solubility with time that is now consistent with WIPP modeling predictions. This long-term shift defines these higher initial and essentially pH independent values for thorium solubility (Figure SOTERM-13 and SOTERM-12) that were obtained in both the German and WIPP data as metastable concentrations of thorium and explains the apparent discrepancy between model-predictions and experimental results. These solubility data support the current WIPP PA assumptions on An(IV) solubility and extend past project data to a broader range of pH and carbonate levels. These results also note that Ca-enhanced hydroxyl complexation can greatly increase the solubility of actinides (IV), something that has only been understood in the last couple of years; however, this complexation requires relatively high pH in combination with very high Ca levels, something that is not expected in the WIPP. The expected pH and dissolved Ca levels in the WIPP predict no effect on An(IV) dissolved concentration due to formation of this complex.

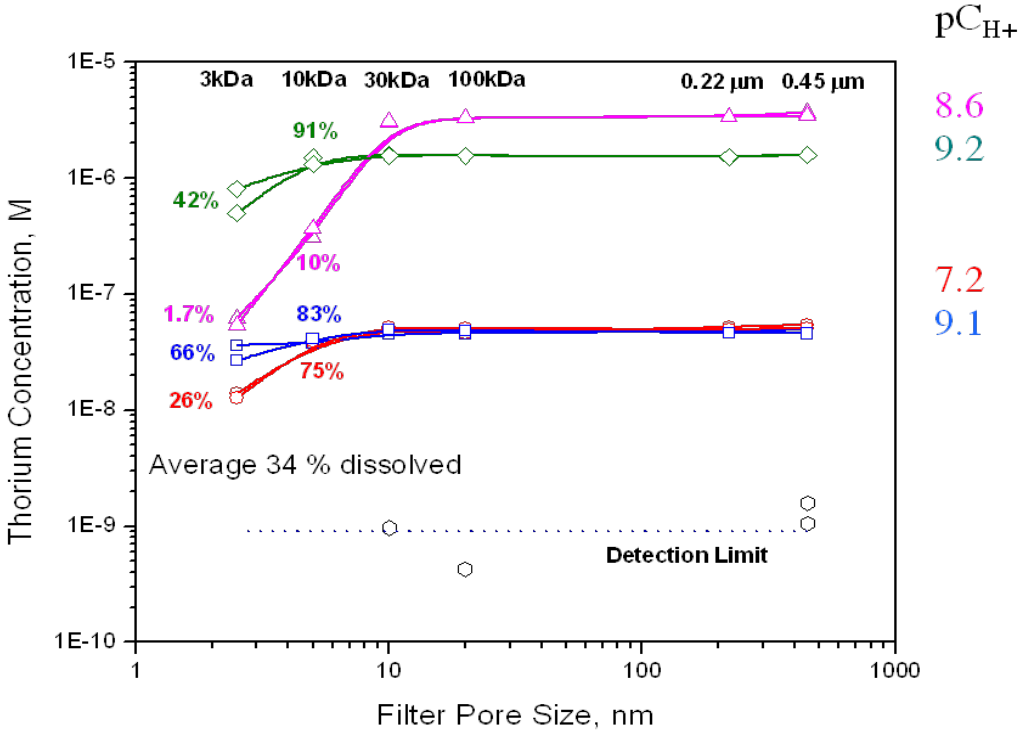

Figure SOTERM-14. Thorium Concentration in Simulated WIPP Brine as a Function of Pore Size. Ultrafilters Used are Given at the Top of the Figure and Correlate with the Filter Pore Size on the X Axis. The % Numbers Shown Correspond to the % of Thorium that Passed Through the Filter for Each Data Point (Reed et al. 2013).

Th(IV) complexes with organic ligands like citrate, acetate, lactate and oxalate reported were investigated in the literature by potentiometric and solvent extraction studies. Moore et al. 1999 performed solvent extraction studies to investigate An-Acetate complexes at pH_c = 2.0-3.0 up to

5.0 m NaCl media. Similar to this study, an extensive report (Choppin et al. 1999) on actinides complexation with organic ligands for WIPP relevant conditions and ionic strength. The Pitzer parameters were derived based on the data collected by potentiometric and solvent extraction experiments in 0.3-5.0 m NaCl. On the other hand, these studies were performed only under the acidic to neutral conditions.

Th(IV) complexes with EDTA were investigated in the literature. Xia et al. 2003 performed solubility experiments with ThO_2(am) as a function of pH (5 to 13), EDTA ($\leq$ 0.01 M) and $NaNO_3$ ($\leq$ 6 M) (Xia et al. 2003). $Th(OH)EDTA^-$ and $Th(OH)_2EDTA^{2-}$ were defined to explain the increase in solubility. In contrast to previous literature data, no formation of dimeric or oligomeric species were found and the absence of these species were confirmed with XAS measurements. The Pitzer parameters were derived based on the solubility data obtained.

SOTERM-5.4.2 Literature review since CRA-2014

The formation of ThO_2(cr) with different crystallinities and their dissolution rates at different temperature and stirring rates were recently investigated (Simonnet et al. 2016). The heat treatment was applied to improve the crystallinity of ThO_2 between 850 and 1500 °C. Dissolution experiments with sulfuric (H_2SO_4) and oxalic ($H_2C_2O_4$) acids did not provide meaningful results, while complete dissolution is observed with increasing HNO_3 concentration in the presence of HF. Although the authors provided extensive solid phase characterization before and after dissolution experiments, neither temperature nor extremely acidic pH were found relevant for WIPP conditions.

Nishikava et al. 2018 investigated Th(IV) solubility at different aging and measurement temperatures including room temperature. The authors performed comprehensive solubility experiments with solid phase characterization. The results showed that $Th(OH)_4$(am) solubility agrees very well with the experimental solubility and the thermodynamic data reported in the literature. The solubility measurements at high temperature (40 and 60 °C) showed lower solubility than the room temperature.

The solubility of ThO_2(am) was recently studied by (Felipe-Sotelo et al. 2015 and 2017) in 95%-saturated $Ca(OH)_2$ (pH 12.3) to simulate a cementitious nuclear waste disposal. The results obtained from oversaturation and under saturation experiments are consistent with the known solubility of ThO_2(am) in equilibrium with $Th(OH)_4$(aq) where Th concentration is about $4 \cdot 10^{-9}$ M.

Recently, there are published studies on Th(IV), U(IV) and U(VI) solubility in 95%-saturated $Ca(OH)_2$ (pH 12.3) in the presence of organic ligands and CDP (cellulose degradation products) (Felipe-Sotelo et al. 2015 and 2017) . An increase of Th(IV) solubility was observed in the presence of citrate (4.2×10^{-5} M) and ISA (7.3×10^{-8} M). The model calculations for the citrate system based on the reported thermodynamic data including $Th(OH)_3(citrate)_2^{5-}$ and $Th(OH)_3(citrate)_3^{8-}$ species (Felmy et al. 2006) or $Th(citrate)^+$ and $Th(citrate)_2^{2-}$ species (Bonin et al. 2008) underestimated the experimental results. The model calculations for the ISA system based on the data with $CaTh(H_2ISA)_2$ species (Tits et al. 2005) explains well the experimental results. Overall, the authors concluded that known chemical and thermodynamic models in the

literature for the complexation of Th(IV), U(IV) and U(VI) with organic ligands underestimated the experimental data obtained at pH 12.3.

SOTERM-5.4.3 WIPP-Specific Results since the CRA-2014 and the CRA-2014 PABC

There are no new WIPP-relevant results on the chemistry and speciation of Th since CRA-2014.

SOTERM-5.5 Uranium Chemistry

Uranium is not a TRU component but is, by mass, the predominant actinide in the WIPP. Current estimates predict that ~128 metric tons will be placed in the repository (Van Soest 2018), but this is believed to be a high estimate since uranium content in waste is often indirectly determined. By mass, approximately 85% of this will be the ^{238}U isotope, with minor amounts of ^{233}U, ^{234}U, ^{235}U, and ^{236}U. Uranium does not contribute significantly to actinide release through cuttings/cavings and spallings because of its low specific activity (3.36×10^{-7} Ci). Uranium release can occur through the Culebra in very small amounts because of its potentially high solubility and low sorption in the VI oxidation state.

Uranium release, as the ^{238}U isotope, was calculated in the CRA-2019 PA. In the WIPP PA, the oxidation state distribution assumption is that U speciates as U(IV) in the reduced PA vectors and as U(VI) in the oxidized vectors (SOTERM Section 6.1). The concentration for U(VI) is currently set at 1 mM (U.S. EPA 2005), since there is no An(VI) model in the WIPP. U(IV) solubility is calculated using the Th(IV) speciation data in the WIPP model.

SOTERM-5.5.1 Uranium Environmental Chemistry

Uranium is by far the most studied of the actinides under environmentally relevant conditions. An extensive review of this chemistry, as it relates to the WIPP case, was completed in 2009 (Lucchini et al 2010a; U.S. DOE 2009), and is updated herein. More general reviews can be found (Morss, Edelstein, and Fuger 2006; Guillaumont et al. 2003; Runde and Neu 2010). An overview of U environmental chemistry is presented in this section.

SOTERM-5.5.1.1 Uranium Subsurface Redox Chemistry

Uranium can theoretically exist in aqueous solution in the III, IV, V, and VI oxidation states (Hobart 1990; Keller 1971 [pp. 195–215]; Clark, Hobart and Neu 1995). In the environment, however, only the IV and VI oxidation states, which exist as U^{4+} and UO_2^{2+} species, are present. U^{3+}, should it be formed, is metastable and readily oxidized in aqueous solution, and U(V) only exists as a very short-lived transient that instantaneously disproportionates to form U(IV) and U(VI) species in the absence of complexing ligands. The corresponding reduction potential diagram for U at pH = 0, 8, and 14 is given in Figure SOTERM-15 (Morss, Edelstein, and Fuger 2006). The oxidation state and the speciation of U in 5.0 M NaCl calculated based on the available thermodynamic data in Table SOTERM-15 are shown in Figure SOTERM-16 with a Pourbaix diagram.

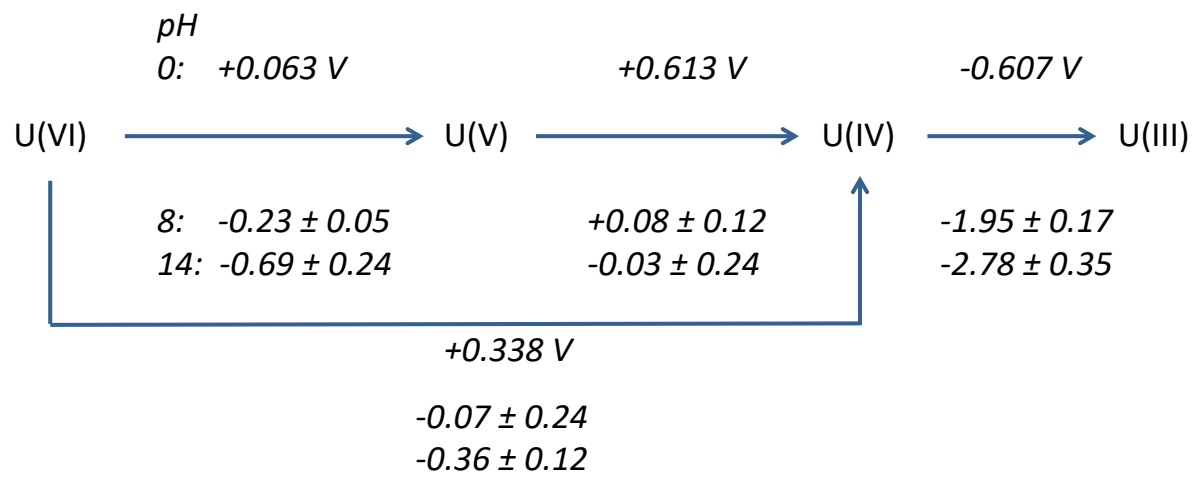

Figure SOTERM-15. Reduction Potential Diagram for U at pH = 0, 8, and 14 (Based on Data in Morss, Edelstein, and Fuger 2006). For the Expected Reducing and Mildly Basic pH Conditions in the WIPP, U(IV) is Predicted to be the Predominant Oxidation State.

Under oxidizing subsurface conditions typical of most near-surface groundwater, U(VI) as UO_2^{2+} uranyl complexes is the predominant oxidation state and is not easily reduced geochemically. Thermodynamically, uranyl species are stable even under mildly reducing conditions and are not reduced by some Fe(II) phases (see Table SOTERM-15). In anoxic WIPP brine experiments with a hydrogen overpressure, uranyl persists as a stable hydrolytic or carbonate complex for over two years (Reed and Wygmans 1997).

In the anoxic and strongly reducing environment expected in the WIPP, however, potential reduction pathways exist. The two most important of these reduction pathways are reaction of uranyl with reduced iron phases (Fe[0/II]), and bioreduction by anaerobic microorganisms (e.g., metal and sulfate reducers). For these reasons, U(IV) is the oxidation state expected to predominate in the WIPP when brine inundation occurs.

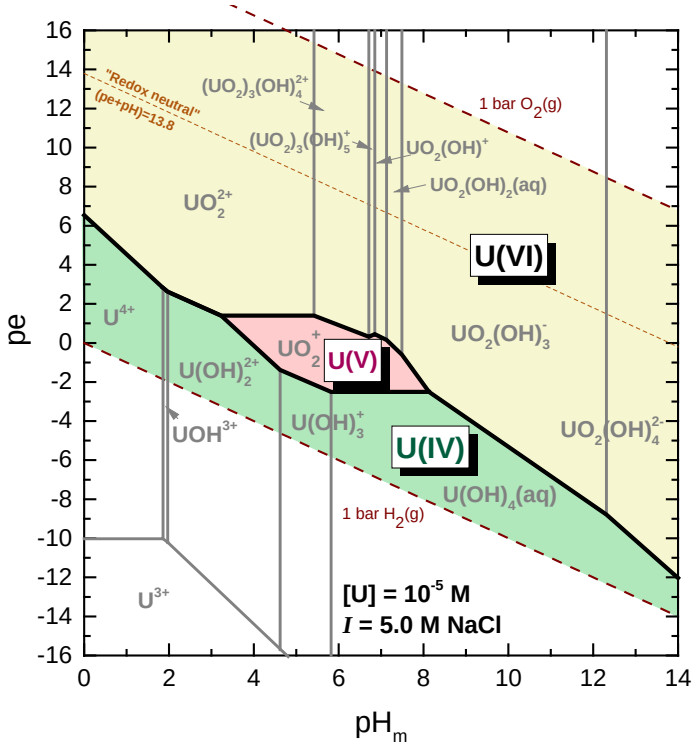

Figure SOTERM-16. Pourbaix Diagram of Uranium Calculated for I = 5.0 M NaCl and $[U]_{tot}= 1 \cdot 10^{-5}$ M Considering Only Aqueous Species of Uranium. Calculations are Performed Using Thermodynamic Data Reported in the Nuclear Energy Agency Thermodynamic Database (NEA-TDB), Neck and Kim (2001) and Altmaier et al. 2017a. Grey Lines Correspond to the 50:50 Distribution Borderlines Between Different Species. The Dashed Lines and Dotted Line Indicate the Borders of Water Stability and Redox Neutral Lines, Respectively.

Table SOTERM-15. Selected Equilibrium Constants for Redox, Solubility and Hydrolysis Reactions of Uranium Considered for Thermodynamic Calculations. Table is taken from Cevirim-Papaioannou et al. 2018.

Reaction	log *K°	Reference
Redox		
$UO_2^{2+} + 4H^+ + 2e^- \leftrightarrow U^{4+} + 2H_2O$	(9.04 ± 0.04)	Guillaumont et al. 2003
$UO_2^{2+} + e^- \leftrightarrow UO2^+$	(1.49 ± 0.02)	Guillaumont et al. 2003
Solubility		
UO_2(am, hyd) + $4H^+ \leftrightarrow U^{4+} + 4H_2O$	(1.50 ± 1.00)	Guillaumont et al. 2003
$UO_3 \cdot 2H_2O$(cr) + $2H^+ \leftrightarrow UO_2^{2+} + 3H_2O$	(5.35 ± 0.13)	Altmaier et al. 2017a
0.5 $Na_2U_2O_7 \cdot H_2O$(cr) + $3H^+ \leftrightarrow$ Na+ + UO_2^{2+} +	(12.20 ± 0.20)	Altmaier et al. 2017a
U(IV) hydrolysis		
$U^{4+} + H_2O(l) \leftrightarrow UOH^{3+} + H^+$	–(0.40 ± 0.20)	Neck and Kim 2001
$U^{4+} + 2H_2O(l) \leftrightarrow U(OH)_2^{2+} + 2H^+$	–(1.10 ± 1.00)	Neck and Kim 2001
$U^{4+} + 3H_2O(l) \leftrightarrow U(OH)^{3+} + 3H^+$	–(4.70 ± 1.00)	Neck and Kim 2001
$U^{4+} + 4H_2O(l) \leftrightarrow U(OH)_4(aq) + 4H^+$	–(10.00 ± 1.40)	Neck and Kim 2001; Guillaumont et al. 2003
U(VI) hydrolysis		
$UO_2^{2+} + H_2O(l) \leftrightarrow UO_2OH^+ + H^+$	–(5.25 ± 0.24)	Guillaumont et al. 2003
$UO_2^{2+} + 2H_2O(l) \leftrightarrow UO_2(OH)_2(aq) + 2H^+$	–(12.15 ±	Guillaumont et al. 2003
$UO_2^{2+} + 3H_2O(l) \leftrightarrow UO_2(OH)^{3-} + 3H^+$	–(20.70 ±	Altmaier et al. 2017a
$UO_2^{2+} + 4H_2O(l) \leftrightarrow UO_2(OH)_4^{2-} + 4H^+$	–(31.90 ±	Altmaier et al. 2017a
$2UO_2^{2+} + H_2O(l) \leftrightarrow (UO_2)_2OH^{3+} + H^+$	–(2.70 ± 1.00)	Guillaumont et al. 2003
$2UO_2^{2+} + 2H_2O(l) \leftrightarrow (UO_2)_2(OH)_2^{2+} + 2H^+$	–(5.62 ± 0.06)	Guillaumont et al. 2003
$3UO_2^{2+} + 4H_2O(l) \leftrightarrow (UO_2)_3(OH)_4^{2+} + 4H^+$	–(11.90 ±	Guillaumont et al. 2003
$3UO_2^{2+} + 5H_2O(l) \leftrightarrow (UO_2)_3(OH)_5^+ + 4H^+$	–(15.55 ±	Guillaumont et al. 2003
$3UO_2^{2+} + 7H_2O(l) \leftrightarrow (UO_2)_3(OH)_7^- + 7H^+$	–(32.20 ±	Guillaumont et al. 2003
$4UO_2^{2+} + 7H_2O(l) \leftrightarrow (UO_2)_4(OH)_7^+ + 7H^+$	–(21.90 ±	Guillaumont et al. 2003

The use of iron barriers in the removal of uranyl from groundwater is well established and has been reported for the removal of U(VI) from groundwater using zero-valent iron barriers (Gu et al. 1998; Fiedor et al. 1998; Farrell et al. 1999) and iron corrosion products formed in saline solution (Grambow et al. 1996). However, in those studies, it was unclear whether the removal of uranyl (UO_2^{2+}) resulted from reductive precipitation or from adsorption onto/incorporation into the iron corrosion products (Gu et al. 1998). In their experiments under saline conditions, Grambow et al. (1996) found that a large percentage of U was rapidly adsorbed onto the iron

corrosion products consisting of over 97% hydrous Fe(II) oxide, and very little U(IV) was found. Myllykylä and Ollila (2011) observed the presence of U(IV) after adding an excess of Fe(II) to 0.01M NaCl and 0.002M $NaHCO_3$ solutions containing U(VI) inside an anaerobic glovebox.

Under anoxic conditions, Trolard et al. (1997) established that the corrosion of steel and iron generates Fe(II)/Fe(III) hydroxide species known as green rusts. Green rusts contain a certain amount of nonhydroxyl anions (carbonate, halides, or sulfate); they have a high specific surface area (Cui and Spahiu 2002) and a high cation sequestration capacity (O'Loughlin et al. 2003). They are considered metastable oxidation products of Fe(II) to magnetite Fe_3O_4 and Fe(III) oxyhydroxides (e.g., goethite α-FeOOH) (O'Loughlin et al. 2003). They could be generated by iron corrosion in the WIPP brines (Wang et al. 2001). A few experimental studies demonstrate that U(VI) is reduced to U(IV) by green rusts (Dodge et al. 2002; O'Loughlin et al. 2003).

The following studies suggest that magnetite can be an effective retention pathway, although retention/reduction mechanisms are mostly depending on the experimental conditions. Scott et al. 2005 showed reduction to U(IV) on the surface of the natural magnetite by (X-ray photoelectron spectroscopy (XPS) and secondary ion mass spectrometry (SIMS). Duro et al. 2008 investigated magnetite as a steel corrosion product in the presence and absence of H_2(g). The authors observed UO_2(am,hyd) only in the presence of H_2(g), U(VI) sorbed on the surface of magnetite in the absence of H_2(g). Latta et al. (2012) demonstrated that stoichiometric and partially oxidized magnetite ($Fe^{2+}/Fe^{3+} \geq 0.38$) reduce U(VI) to U(IV) in UO_2 nanoparticles in 2mM $NaHCO_3$ solution at pH 7.2, whereas with more oxidized magnetite ($Fe^{2+}/Fe^{3+} < 0.38$), possibly sorbed U(VI) is the dominant phase observed. Similar results were observed by Huber et al. 2012, where tetravalent and higher oxidation states of U were found by XPS and EXAFS analysis depending on the Fe(II) content, age of the magnetite and reaction time. Atomistic simulations conducted by Kerisit, Felmy and Ilton (2011), supported by existing EXAFS data provide strong evidence for the structural incorporation of U in Fe (hydro)oxides. The complexity of the U-Fe-H_2O-CO_2 system can explain the lack of a predominant mechanism (reduction-precipitation or adsorption/incorporation) for the removal of U(VI) in the presence of iron phases (Du et al. 2011; Ilton et al. 2012; Singer et al. 2012a and 2012b).

Another iron mineral phase that might form in the WIPP brines is mackinawite (FeS). Gallegos et al. (2013) proposed complete reduction of U(VI) to U(IV) with mackinawite (FeS) in the presence and absence of carbonate. Under anoxic conditions, the authors found that carbonate facilitates the reduction. Under oxic conditions, removal of U(VI) occurred by co-precipitation or sorption onto oxidation products of mackinawite. On the other hand, Lee et al. (2013) reported that U interaction with bio generated mackinawite (FeS) would be different. Even if the reduction of U(VI) to U(IV) was obtained in the experiments, microbial activities did not allow U(IV) to precipitate, U(IV) remains in solutions in colloidal form.

SOTERM-5.5.1.2 Solubility of U(IV)

Tetravalent U is expected to be the dominant oxidation state in the WIPP as a result of the reducing conditions that will prevail. The solubility of U(IV) under these conditions was analogous to that observed for Th (see SOTERM Section 5.4) and is, in fact, calculated in the WIPP PA with the Th(IV) database.

Experimentally, in solution, U^{4+} is readily oxidized to UO_2^{2+}. This occurs even when only trace levels of oxygen exist, often below the limit of detection by most laboratory instrumentation. This explains why there are relatively few studies of U^{4+}. It is also problematic because there are very large discrepancies in the literature as a result of experimental artifact. In particular, there are a number of published results (Rai, Felmy, and Ryan 1990; Gayer and Leider 1957; Ryan and Rai 1983; Tremaine et al. 1981; Casas et al. 1998) that suggest amphotericity for U^{4+} at pH >10. This, however, likely resulted from combined effects of two experimental artifacts: (1) oxidation to UO_2^{2+}, which is much more soluble, and (2) the presence of carbonate, which is a strong complexant of U^{4+}.

The solubility of U(IV) phases were also determined in simplified brines under conditions that relate to the WIPP (Rai et al. 1997 and 1998; Yajima, Kawamura, and Ueta 1995; Torrero et al. 1994). Rai et al. (1997) determined the solubility of freshly precipitated $UO_2 \cdot xH_2O$(am) in NaCl and $MgCl_2$ solutions of various ionic strengths. They estimated the concentration of $U(OH)_4$(aq) in equilibrium with $UO_2 \cdot xH_2O$(am) to be about $10^{-8.0}$ M. A number of data were reported with greater concentrations in the neutral and alkaline range but were ascribed to the presence of U(VI) in solution. This is in fair agreement with the value of $10^{-(8.7 \pm 0.4)}$ M proposed by Yajima, Kawamura, and Ueta (1995). The formation of anionic hydrolysis species $U(OH)_5^-$ and $U(OH)_6^{2-}$ at pH > 11 reported by Fujiwara et al. (2005) were not supported by any other studies or for other tetravalent actinides. It is important to note that U(IV) concentrations at pH >5 show no significant dependence on the initial solid phase; both fresh precipitates in oversaturation experiments or electrodeposited microcrystalline UO_2(s) in undersaturation experiments gave the same results (Torrero et al. 1994).

The most reliable and extensive thermodynamic data for U(IV) solubility and hydrolysis are summarized in Neck and Kim (2001). The authors evaluate the existing solubility data for An(IV) including uranium in terms of crystallinity of the solid phases and the possible oxidation to U(VI). The thermodynamic data are organized to compare the validity of the analogy between the various An(IV) actinides. The NEA-TDB review, by Guillaumont et al. (2003) selects uranium data from Neck and Kim (2001) whenever the experimental data are available and also suggests the estimated formation constants reported in Neck and Kim (2001). Solubility calculations from this study are depicted in Figure SOTER

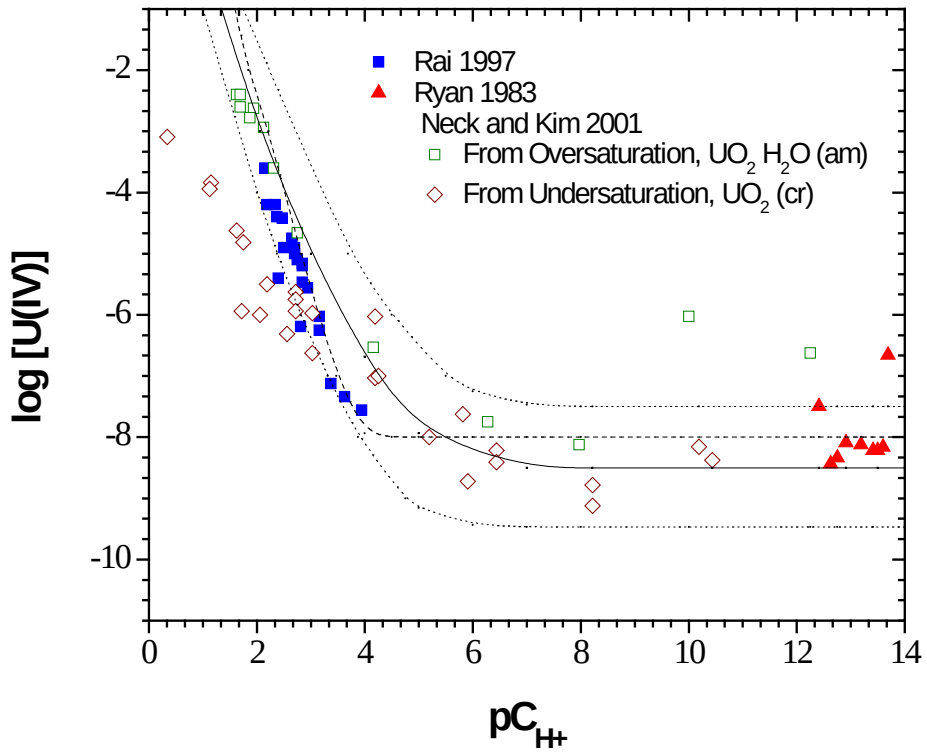

Figure SOTERM-17. Solubility of UO_2(s) as a Function of pH at 20–25 ºC (68–77 °F) in 1M NaCl (Based on Neck and Kim 2001). The Experimental Data are from Ryan and Rai (1983), Rai et al. (1997), and Neck and Kim (2001). The Solid Line is Calculated by Neck with Log K_{sp} = (-54.5 ± 1.0) and the Hydrolysis Constants Selected in Neck and Kim (2001). The Dotted Lines Show the Associated two-sigma Range of Uncertainty in the calculated values. The Dashed Line is Calculated with the Model Proposed by Rai et al. (1997).

SOTERM-5.5.1.3 Speciation and Solubility of U(VI)

U(VI) phases and aqueous species, although not expected to predominate in the WIPP, could be present due to the localized effects of radiolysis (see SOTERM Section 3.4). The WIPP PA currently makes the conservative assumption that U(VI) species predominate in 50% of the PA vectors. The solubility of U(VI) is, however, not explicitly calculated in the WIPP PA, since there is no model for actinides in the VI oxidation state. The potential contribution of U(VI) species to the overall solubility of U in the WIPP is implicitly considered in the WIPP PA by using the 1 mM value for U solubility (U.S. EPA 2005). Prior to this, the solubility of U was defined as 1.2×10^{-5} M based on an assessment of the literature and existing WIPP-relevant experimental data by Hobart and Moore (1996).

The solubility of U(VI) in the WIPP is expected to be defined by the combined contribution of two processes: hydrolysis with oxyhydroxide phase formation, and carbonate complexation with U carbonate phase formation. These are both very complex systems, and there are many proposed speciation schemes. In carbonate-free or low-carbonate solutions, the speciation of U(VI) is dominated by hydrolysis.

Yamazaki et al. (1992) conducted U(VI) solubility experiments from both oversaturation and undersaturation in a synthetic brine at pC_{H+} values ranging from 6.4 to 12.4. The composition of this synthetic brine was close to the composition of the WIPP GWB brine, with higher concentrations of NaCl, NaBr, KCl and $MgCl_2$ and ionic strength ~6 M. This synthetic brine initially contained 0.11 mM of bicarbonate HCO_3^-, but the solution treatment (continuous nitrogen gas flow above the solution) likely removed some of the carbonate from solution before the later uranium additions and prevented any CO_2 uptake during the experiment. The results obtained at the pC_{H+} closest to WIPP repository conditions with no further carbonate additions are listed in Table SOTERM-16. Uranium (VI) concentrations of approximately 10^{-7} M were observed at pC_{H+} = 10.4 and 12.4 when nitrogen gas was continuously passing over the solutions to minimize CO_2 uptake. Despite extensive precipitation of brucite $Mg(OH)_2$ at these high pC_{H+} values, the solubility-controlling phase at $pC_{H+} \geq 9.3$ was found to be potassium di-uranate $K_2U_2O_7$.

Diaz-Arocas and Grambow (1998) investigated uranium (VI) solubility in NaCl solutions up to 5 M at 25 °C and different basic pH values, under an argon atmosphere using an oversaturation approach. Their uranium concentration equilibria in 5 M NaCl are presented in Table SOTERM-16. At pH ≥ 7.5, poorly crystalline sodium-uranates, identified by XRD, were formed in solutions. Diaz-Arocas and Grambow (1998) indicated that the solubility of this phase was about 3×10^{-5} M at pC_{H+} = 8.9 in 5 M sodium chloride in the absence of carbonate.

Carbonate, as CO_3^{2-}, has a significant effect on the solubility of U(VI) (Clark, Hobart and Neu 1995; Guillaumont et al. 2003). In the absence of competing complexing ligands, carbonate complexation will dominate the speciation of the uranyl ion under near-neutral pH conditions as long as there is ample carbonate-bicarbonate available (Clark, Hobart and Neu 1995). Complexation constants for binary U(VI) carbonate complexes at ionic strength (I) = 0 M and 25 ºC (77 °F) are listed in Table SOTERM-17 (Guillaumont et al. 2003).

Table SOTERM-16. Solubility of U(VI) in High-Ionic-Strength Media

U(VI) Concentration (M)	pC_{H+}	Solution	Time (days)	Solid	Reference
$(2.8 \pm 1.8) \times10^{-5}$	8.9	5M NaCl	≈ 50	$Na_{0.68}UO_{3.34}\cdot(2.15\pm0.10)H_2O$	Diaz-Arocas and Grambow 1998
$(8.2 \pm 4.6) \times10^{-5}$	7.6	5M NaCl	≈ 110	$Na_{0.45}UO_{3.23}\cdot(4.5\pm0.1)H_2O$	Diaz-Arocas and Grambow 1998
$(4.2 \pm 1.9) \times10^{-4}$	7.1	5M NaCl	≈ 170	$Na_{0.29}UO_{3.15}\cdot(2.9\pm0.2)H_2O$	Diaz-Arocas and Grambow 1998
$(2.8 \pm 0.9) \times10^{-6}$	6.5	5M NaCl	≈ 170	$Na_{0.14}UO_{3.07}\cdot(2.5\pm0.1)H_2O$	Diaz-Arocas and Grambow 1998
$(1.82 \pm 0.01) \times10^{-3}$	8.4	Brine (air atmosphere)	100	α-schoepite (oversaturation)	Yamazaki et al. 1992
$(1.81 \pm 0.01) \times10^{-3}$	8.4	Brine (air atmosphere)	100	α-schoepite (oversaturation)	Yamazaki et al. 1992
$(1.40 \pm 0.05) \times10^{-3}$	8.4	Brine (air atmosphere)	244	α-schoepite (undersaturation)	Yamazaki et al. 1992

Table SOTERM-16. Solubility of U(VI) in High-Ionic-Strength Media (Continued)

U(VI) Concentration (M)	pC_{H+}	Solution	Time (days)	Solid	Reference
$(1.80 \pm 0.05) \times 10^{-3}$	8.4	Brine (air atmosphere)	244	α-schoepite (undersaturation)	Yamazaki et al. 1992
$(3.8 \pm 0.4) \times 10^{-7}$	10.4	Brine (initial 0.11mM HCO_3^-)	150	$Mg(OH)_2$ and $K_2U_2O_7$ (oversaturation)	Yamazaki et al. 1992
$(3.1 \pm 0.3) \times 10^{-7}$	10.4	Brine (initial 0.11mM HCO_3^-)	150	$Mg(OH)_2$ and $K_2U_2O_7$ (oversaturation)	Yamazaki et al. 1992
$(1.7 \pm 1.4) \times 10^{-7}$	8.1	ERDA-6	705	To be determined (oversaturation)	Lucchini et al. 2013b
$(9.9 \pm 3.0) \times 10^{-8}$	9.6	ERDA-6	705	To be determined (oversaturation)	Lucchini et al. 2013b
$(3.1 \pm 1.3) \times 10^{-8}$	10.5	ERDA-6	705	To be determined (oversaturation)	Lucchini et al. 2013b
$(2.1 \pm 0.6) \times 10^{-6}$	7.4	GWB	705	To be determined (oversaturation)	Lucchini et al. 2013b
$(4.3 \pm 1.3) \times 10^{-6}$	8.2	GWB	705	To be determined (oversaturation)	Lucchini et al. 2013b
$(8.1 \pm 2.4) \times 10^{-7}$	9.2	GWB	705	To be determined (oversaturation)	Lucchini et al. 2013b
$(2.7 \pm 0.5) \times 10^{-7}$	8.0	ERDA-6 (initial 2mM carbonate)	994	To be determined (oversaturation)	Lucchini et al. 2013a
$(3.2 \pm 1.0) \times 10^{-5}$	8.8	ERDA-6 (initial 2mM carbonate)	994	To be determined (oversaturation)	Lucchini et al. 2013a
$(3.5 \pm 2.8) \times 10^{-8}$	12.1	ERDA-6 (initial 2mM carbonate)	994	To be determined (oversaturation)	Lucchini et al. 2013a
$(2.6 \pm 0.8) \times 10^{-6}$	7.6	GWB (initial 2mM carbonate)	994	To be determined (oversaturation)	Lucchini et al. 2013a
$(7.1 \pm 1.4) \times 10^{-7}$	9.0	GWB (initial 2mM carbonate)	994	To be determined (oversaturation)	Lucchini et al. 2013a
$(1.0 \pm 0.2) \times 10^{-7}$	8.9	5.0 M NaCl	200	$Na_2U_2O_7 \cdot H_2O$	Altmaier et al. 2017a
$(1.35 \pm 0.2) \times 10^{-7}$	9.0	5.0 M NaCl	200	$Na_2U_2O_7 \cdot H_2O$	Altmaier et al. 2017a
$(1.74 \pm 0.2) \times 10^{-7}$	9.5	5.0 M NaCl	200	$Na_2U_2O_7 \cdot H_2O$	Altmaier et al. 2017a

Table SOTERM-17. Complexation Constants for Binary U(VI) Carbonate Complexes at I = 0 M and 25 °C (Guillaumont et al. 2003).

Reaction and Solubility Product for UO_2CO_3(cr)	
$UO_2CO_3(cr) \rightleftharpoons UO_2^{2+} + CO_3^{2-}$	Log $K^0_{SP(cr)}$= -14.76 ± 0.02
Reactions and Formation Constants β^0_{nq} for $(UO_2)_n(CO_3)_q^{2n-2q}$	
$UO_2^{2+} + CO_3^{2-} \rightleftharpoons UO_2CO_3(aq)$	Log β^0_{11} = 9.94 ± 0.03
$UO_2^{2+} + 2\ CO_3^{2-} \rightleftharpoons UO_2(CO_3)_2^{2-}$	Log β^0_{12} = 16.61 ± 0.09
$UO_2^{2+} + 3\ CO_3^{2-} \rightleftharpoons UO_2(CO_3)_3^{4-}$	Log β^0_{13} = 21.84 ± 0.04
$3\ UO_2^{2+} + 6\ CO_3^{2-} \rightleftharpoons (UO_2)_3(CO_3)_6^{6-}$	Log β^0_{36} = 55.6 ± 0.5

The three monomeric complexes of general formula $UO_2(CO_3)$, $UO_2(CO_3)_2^{2-}$, and $UO_2(CO_3)_3^{4-}$ are present under the appropriate conditions. There is also evidence from electrochemical, solubility, and spectroscopy data that support the existence of $(UO_2)_3(CO_3)_6^{6-}$, $(UO_2)_2(CO_3)(OH)_3^-$, and $(UO_2)_{11}(CO_3)_6(OH)_{12}^{2-}$ polynuclear species, which can only form under the conditions of high-metal-ion concentration or high ionic strength (Clark, Hobart and Neu 1995). At uranyl concentrations above 10^{-3} M, the trimeric cluster $(UO_2)_3(CO_3)_6^{6-}$ can also be present in significant concentrations. When the uranyl ion concentration begins to exceed the carbonate concentration, hydrolysis will play an increasingly important role (Clark, Hobart and Neu 1995).

It is generally accepted that the major complex in solution at high carbonate concentrations is $UO_2(CO_3)_3^{4-}$ (Kramer-Schnabel et al. 1992; Peper et al. 2004). However, at I = 0.5 M and I = 3 M, the polynuclear $(UO_2)_3(CO_3)_6^{6-}$ species becomes an important competitor of $UO_2(CO_3)_3^{4-}$. Grenthe et al. (1984 indicated) that the formation of $(UO_2)_3(CO_3)_6^{6-}$ is favored at high ionic strengths as a result of possible stabilization of the complex by ions of the background electrolyte.

At high pH, Yamamura et al. (1998) demonstrated that hydrolysis overwhelms carbonate complexation. The solubility of U(VI) was measured in highly basic solutions ($11 \leq pH \leq 14$) at an ionic strength of I = 0.5 – 2 M over a wide range of carbonate concentrations (10^{-3} – 0.5 M) using both oversaturation and undersaturation approaches. In the oversaturation experiments, the solubility of U(VI) decreased with increasing equilibration time from one week to one year and was explained as an increase in the crystallinity of the solid phase with aging. The solid phase was identified as $Na_2U_2O_7 \cdot xH_2O$ by XRD. The undersaturation experiments conducted for one month with the solid phase indicated a rapid equilibrium. These data were interpreted by considering the formation of $UO_2(OH)_3^-$, $UO_2(OH)_4^{2-}$, and $UO_2(CO_3)_3^{4-}$ (Yamamura et al. 1998).

A few experimental investigations were reported on the influence of carbonate on U(VI) solubility in highly saline solutions (Yamazaki et al. 1992; Reed and Wygmans 1997; Lin et al. 1998; Fanghänel and Neck 2002). Lin et al. (1998) evaluated U(VI) solubilities with up to 5M NaCl in a range of carbonate concentrations. At carbonate-ion concentrations greater than 10^{-7} M, $UO_2(CO_3)_3^{4-}$ was the dominant U(VI) complex in solution. At higher CO_2 partial pressures,

the solubility-controlling solid phase was found to be UO_2CO_3(s), whereas at lower partial pressures, sodium uranate was identified as the solid phase in NaCl-saturated solutions.

Yamazaki et al. (1992) measured the solubility of U(VI) in synthetic brine and an air atmosphere. The results obtained at pC_{H+} = 8.4 using both oversaturation and undersaturation approaches are listed in Table SOTERM-16. At this pC_{H+} value, millimole concentrations of uranium were measured in solution. Solids obtained at pC_{H+} = 8.4 were identified as poorly crystalline metaschoepite ($UO_3 \cdot xH_2O$) by XRD. Yamazaki carried out some calculations to model the competition between calcium and magnesium for carbonate complexation in order to interpret his experimental solubility data. He concluded that the uranium solubility decrease above pC_{H+} = 8.4 was related to a shift from the triscarbonato uranyl complex $UO_2(CO_3)_3^{4-}$ to the uranyl hydroxide complexes $UO_2(OH)_n^{2-n}$, as precipitation of calcium carbonate ($CaCO_3$) occurred, and to the conversion of schoepite to potassium di-uranate.

Prior to the CCA, the only U(VI) solubility values available in the literature that were obtained in the presence of carbonate under WIPP-relevant conditions were featured in the fiscal year 1997 year-end report by Reed and Wygmans (1997). The experiments were carried out in ERDA-6 brine at pH 8 and 10, and in G-Seep brine at pH 5 and 7. U(VI), Np(VI), and Pu(VI) were added to the brine samples. Carbonate (10^{-4} M) was also added to some of the samples. The experiments were conducted under a hydrogen atmosphere at 25 ± 5 °C. Concentrations and oxidation states of the actinides were monitored over time. The U(VI) concentration was stable at approximately 1×10^{-4} M when measured as a function of time in ERDA-6 brine at pH 10 in the presence of carbonate (Reed and Wygmans 1997).

The solubility of U(VI) in the absence and the presence of carbonate has since been more extensively studied in simulated GWB and ERDA-6 brine (Lucchini et al. 2010a, 2010b, 2013a and 2013b). A summary of these results is shown in Figure SOTERM-18 and a comparison of these results with other solubility data in the literature is given in Table SOTERM-15. No U(IV) solubility studies were conducted since Th(IV) is the analog for the IV actinides.

In the absence of carbonate, the measured U(VI) solubilities were about 10^{-6} M in GWB brine at $pC_{H+} \geq 7$ and about 10^{-8} - 10^{-7} M in ERDA-6 at $pC_{H+} \geq 8$ (Lucchini et al. 2007, 2010a and 2010b). These results put an upper bound of ~10^{-6} M for the solubility of uranyl in the carbonate-free WIPP brines for the investigated range of experimental conditions. At the expected pC_{H+} in the WIPP (~9.5), the measured uranium solubility was between 10^{-7} M and 10^{-6} M. In the presence of carbonate, the highest uranium solubility obtained experimentally was ~ 10^{-4} M, under WIPP-relevant conditions (pC_{H+} ~ 9.5). It is important to note that this uranium solubility, in the absence of carbonate, was 10-100 times lower than published results. The uranium (VI) solubility experiments reported in two other relevant publications (Yamazaki et al.1992; Diaz-Arocas and Grambow 1998) were performed in brines close to the WIPP brine composition, but possibly with a less rigorous control of a carbon dioxide-free environment. The impact of carbonate concentration on the solubility of uranium (VI) in the two simulated WIPP brines can be explained in terms of three distinctive pC_{H+} regions.

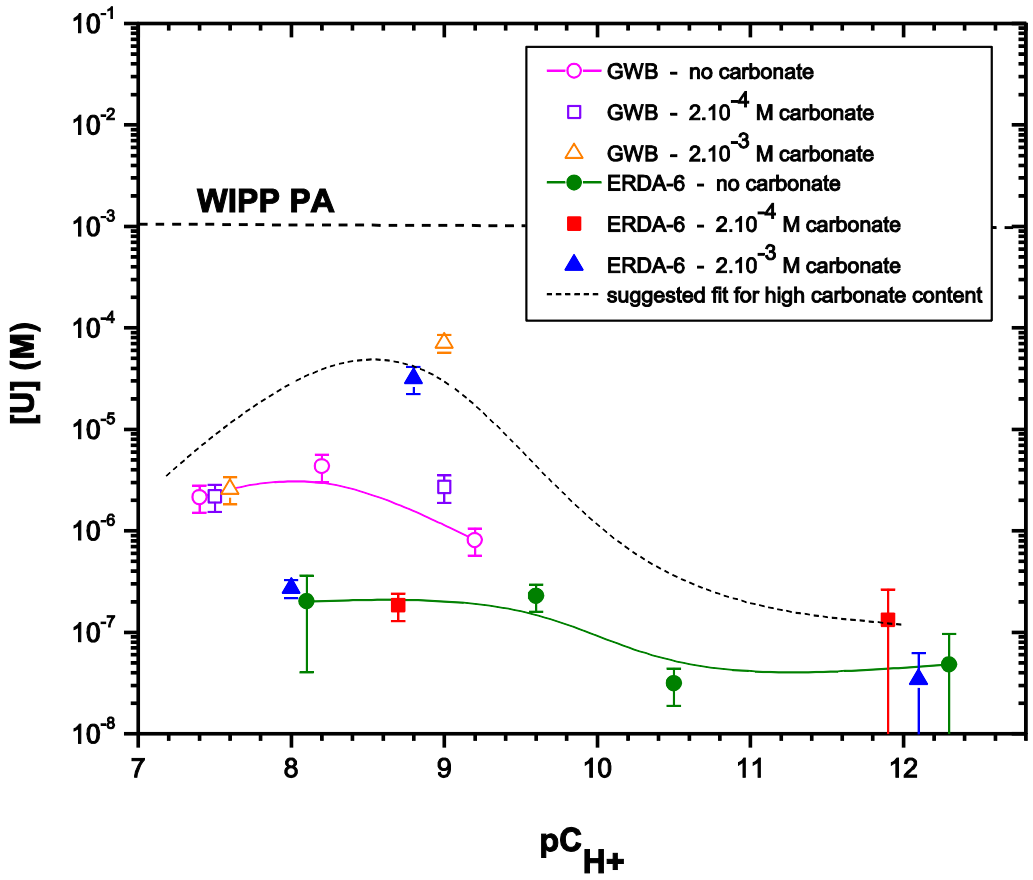

Figure SOTERM-18. Uranium Concentration in ERDA-6 (Open Symbols) and GWB (filled symbols) Versus pC_{H+}. in Nitrogen Controlled Atmosphere, in the Absence of Carbonate or in the Presence of Two Concentrations of Carbonate (2×10^{-4} M and 2×10^{-3} M) at the Beginning of the Experiments. The Carbonate Systems Data Correspond to 17 Samplings Performed Over 994 Days.

The first pC_{H+} region is $7.5 \leq pC_{H+} \leq 8$. In this pC_{H+} region, the uranium concentration was stable in both brines and independent of the carbonate concentration. However, there were small differences in the uranium solubility due to differences in the composition of the brine: ~ 10^{-6} M in GWB, and ~ 10^{-7} M in ERDA-6. These data indicated that there was no impact of carbonate in this pC_{H+} region ($7.5 \leq pC_{H+} \leq 8$), but there was certainly an effect due to one or more components of the brines that were present in higher amounts in GWB than in ERDA-6. Based on our investigation of neodymium solubility (Borkowski et al. 2009), we postulated that borate may also play a role in defining the uranium (VI) solubility in this pC_{H+} region (see also Borkowski et al. 2010). This possibility was confirmed experimentally (Lucchini, Borkowski and Richmann 2013a).

The second pC_{H+} region of interest, $8 \leq pC_{H+} \leq 10$, is directly relevant to the WIPP. In this pC_{H+} region, not only was there a compositional effect between the two brines studied (higher uranium concentrations in GWB than in ERDA-6 for identical carbonate content), but there was also an

impact of carbonate on the observed uranium solubility in each brine. At high carbonate content (2×10^{-3} M in our experiments), the uranium concentrations reached 10^{-4} M, which was two or more orders of magnitude higher than in the absence of carbonate. The low carbonate content data (2×10^{-4} M) did not reflect a strong influence of carbonate on uranium solubility, since the measured solubility was similar to the ones obtained in carbonate-free systems.

Lastly, the third pC_{H+} region of interest is at $10 \leq pC_{H+}$. In that pC_{H+} region, the uranium concentrations were stable around 10^{-7}-10^{-8} M. It is likely that hydrolysis overwhelmed any other possible effects on uranium solubility.

These newly obtained solubility data for uranium (VI) in the WIPP brine accomplished the following:

- Provided the first WIPP-relevant data for the VI actinide oxidation state that established the solubility of uranium (VI) over an extended pCH+ range for GWB and ERDA-6 brines in the absence or presence of carbonate;
- Established an upper limit of ~ 10-6 M uranyl concentration at the reference pCH+ WIPP case in the absence of carbonate, and an upper limit of ~ 10-4 M uranyl concentration at the reference pCH+ WIPP case in the presence of 2 mM carbonate;
- Confirmed a lack of significant amphotericity in the WIPP simulated brines at high pH values;
- Demonstrated a small effect of borate complexation in the pCH+ range of 7.5 to 10; and
- Supported the current assumption in PA that the solubility of U(VI), under the expected range of conditions in the WIPP, will not exceed 1 mM.

SOTERM-5.5.2 Literature review since CRA-2014

Recently, a number of studies have been dedicated to U reduction and uptake processes with nanoscale zero-valent iron (nZVI) for environmental purposes. Various modification methods were applied, i.e., the presence of Na-bentonite (Sheng et al. 2014), reduced grapheneoxide (Sun et al. 2014), Fe(II) and Fe(III) (Yan et al. 2014), montmorillonite (Xu et al. 2014), dissolved oxygen (Crane and Scott 2014), sodium, calcium and bicarbonate (Crane et al. 2015, Tsarev et al. 2016, Hua et al. 2018), graphene composite (Li et al. 2015), U(VI)-CO_3 and Ca-U(VI)-CO_3 (Zhang et al. 2015). Under oxic conditions, the removal mechanism was defined as adsorption of UO_2^{2+}, whereas under anoxic conditions, U was removed from the solution by reduction, sorption and co-precipitation processes. The presence of the Fe(II)/Fe(III) couple facilitates the reduction of U(VI) to U(IV), while associated ions have an effect on the removal processes.

Paradis et al. (2016) investigated U redox behavior in the presence of nitrate following sulfate reducing conditions. The authors concluded that sulfate reduced species are not enough to immobilize uranium when oxidizing solids or aqueous species are present.

Cevirim-Papaioannou et al. (2018) performed a redox study on U(VI/IV) in the presence of different reducing conditions where redox kinetics and presence of surface effects were discussed. The presence of Fe(0) and magnetite were also evaluated. The reduction of U(VI) to

U(IV) was observed in most of the cases when strongly reducing conditions (pe+pH ~ 2) were maintained and these observations were confirmed by X-Ray Absorption Near Edge Structure (XANES) analysis. The results show that the reduction kinetics are dependent on the initial uranium concentration, pH, Eh and concentration and the form of the reducing chemical. The reduction was not completed in the time frame of the experiments in only 5.0 M NaCl systems due to the fast precipitation of $Na_2U_2O_7 \cdot H_2O$(cr) and the slow transformation to UO_2(am, hyd).

Cachoir et al. (2016) performed solubility experiments with depleted UO_2 powders in alkaline tetramethylammonium solutions. The leaching experiments showed an increase of solubility of up to 10^{-5} M due to the oxidation to U(VI) controlled by U(VI) hydrolysis species at a pH range of 12.5-13.5. Latta et al. 2016 investigated the effect of Ca and PO_4 on the U(IV) oxidation rate. Although, the addition of Ca and PO_4 decreased the oxidation rate and the oxidation products passivate the surface of the UO_2 phase, oxidation can still be completed within days under oxic conditions.

U(VI) solubility with phosphate was investigated by Mehta et al. 2014 in the presence of Na^+ and Ca^{2+}. The results show an incorporation of these cations into the solid phase, forming sodium autunite $Na_2(UO_2)_2(PO_4)_2$ and autunite $Ca(UO_2)_2(PO_4)_2$ depending on the pH investigated. Addition of Na causes a decrease in U solubility, on the other hand, Ca promoted U adsorption onto the surfaces of the precipitated phases which were a less effective immobilization process in the longer term.

Recently, Altmaier et al. (2017a), Cevirim-Papaioannou et al. (2018) and Yalcintas et al. (2019) published the series of experimental solubility data of U(VI) in NaCl, KCl and $MgCl_2$ solutions. These studies also included chemical, thermodynamic and activity (SIT/Pitzer) models based on extensive solid and aqueous phase characterization as well as an extensive evaluation of other existing data and models in the literature. The authors investigated the chemical thermodynamics of U(VI) hydrolysis species and oxide/hydroxide solid phases forming in carbonate-free dilute to concentrated NaCl, KCl and $MgCl_2$ solutions. The solid phase controlling the solubility from near-neutral to hyperalkaline pH range was characterized as $UO_3 \cdot 2H_2O$(cr), $Na_2U_2O_7 \cdot H_2O$(cr) or $K_2U_2O_7 \cdot H_2O$(cr) depending on the salt type and concentration by XRD, SEM-EDS, quantitative chemical analysis and thermogravimetry/differential thermal analyzer (TG/DTA). The chemical and thermodynamic models reported in the literature were extensively compared and discussed with the new solubility data. The solubility products for $UO_3 \cdot 2H_2O$(cr), $Na_2U_2O_7 \cdot H_2O$(cr) and $K_2U_2O_7 \cdot H_2O$(cr) as well as an activity model for the solubility of U(VI) in NaCl, KCl and $MgCl_2$ systems by SIT and Pitzer models were developed based on literature data and newly generated experiments. Uranium concentrations obtained in 5 M NaCl are presented in Table SOTERM-18. The experimental data in 5.0 M NaCl and $MgCl_2$ solutions are shown in Figure SOTERM 19. These studies provide the missing chemical, thermodynamic and Pitzer model for the An(VI).

The solubility of U(VI) in 0.5 M NaCl solutions from 25 to 80 ^oC was investigated by Endrizzi et al. (2016). The solubility of $UO_3 \cdot 2H_2O$(cr) decreased at pH_m 4-5 due to solid phase transformation to $Na_2U_2O_7.H_2O$(cr) and an increase of solubility was observed from neutral to alkaline pH region with increasing temperature up to 80 ^oC. This was explained by the increase in acidity and the associated thermodynamic data that was derived.

Table SOTERM-18. Pitzer Interaction Parameters for U(VI) Hydrolysis Species Determined in Yalcintas et al. 2019.

U(VI) species			Pitzer binary parameters				
i	**j**		**$\beta^{(0)}$**	**$\beta^{(1)}$**	**$\beta^{(2)}$**	**C^{φ}**	**References**
UO_2^{2+}	Cl^-		0.4274	1.644	0	–0.0368	Pitzer 1991
UO_2OH^+	Cl^-		0.15	0.3	0	0	Yalcintas et al. 2019
$(UO_2)_2(OH)_2^{2+}$	Cl^-		0.389	2.259	0	0	Yalcintas et al. 2019
$(UO_2)_3(OH)_4^{2+}$	Cl^-		0.08	1.4	0	0	Yalcintas et al. 2019
$(UO_2)_3(OH)_5^+$	Cl^-		0.146	0.6	0	0	Yalcintas et al. 2019
$(UO_2)_4(OH)_7^+$	Cl^-		0.23	0.3	0	0	Yalcintas et al. 2019
$UO_2(OH)_3^-$	Na^+		–0.26	0.34	0	0	Yalcintas et al. 2019
	K^+		–0.26	0.34	0	0	Yalcintas et al. 2019
	Mg^{2+}		0.20	1.6	0	0	Yalcintas et al. 2019
$UO_2(OH)_4^{2-}$	Na^+		0.06	1.98	0	0	Yalcintas et al. 2019
	K^+		0.13	2.05	0	0	Yalcintas et al. 2019
$(UO_2)_3(OH)_7^-$	Na^+		–0.26	0.34	0	0	Yalcintas et al. 2019
	K^+		–0.26	0.34	0	0	Yalcintas et al. 2019
	Mg^{2+}		0.20	1.6	0	0	Yalcintas et al. 2019
$UO_2(OH)_2(aq)$	Na^+, K^+, Mg^{2+},Cl^-		0	0	0	0	Yalcintas et al. 2019
i	**j**	**i′**	**Pitzer ternary parameters**				
UO_2^{2+}	Cl^-	Na^+	$\theta_{ii'}$ = 0.03		$\Psi_{iji'}$ = –0.01		Yalcintas et al. 2019
	Cl^-	Mg^{2+}	$\theta_{ii'}$ = 0.08		$\Psi_{iji'}$ = –0.072		Yalcintas et al. 2019
$(UO_2)_3(OH)_4^{2+}$	Cl^-	Na^+			$\Psi_{iji'}$ = 0.02		Yalcintas et al. 2019

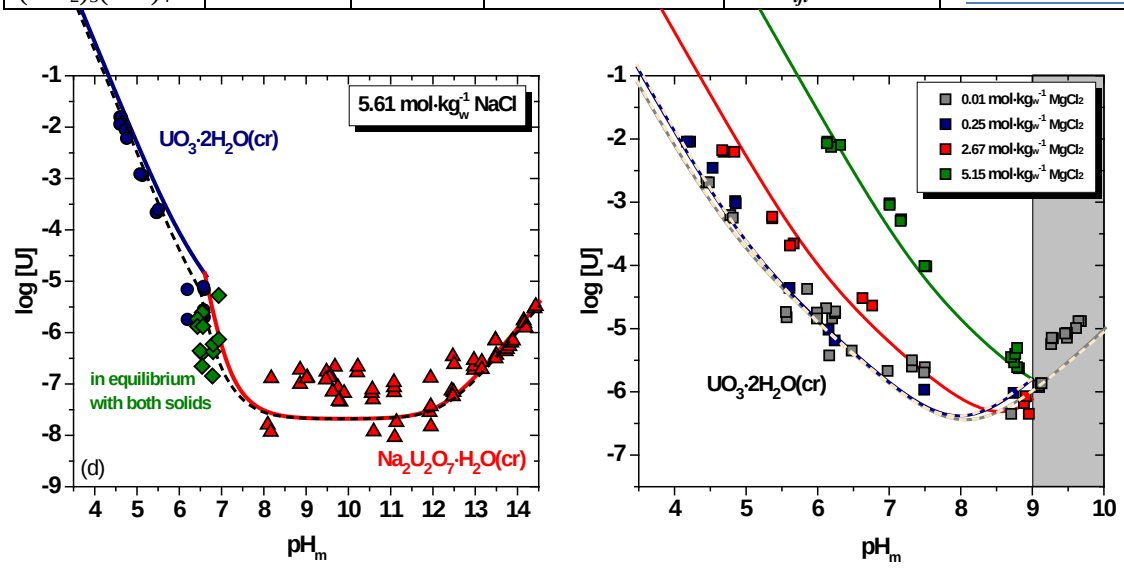

Figure SOTERM 19. Experimental Solubility Data of U(VI) in 5.61 mol·kgw $^{-1}$ NaCl (left) and in $MgCl_2$ (right) Solutions. Solid and Dashed Lines are the Calculated Solubility with the Thermodynamic and Pitzer Activity Models Derived in Yalcintas et al. 2019 and Altmaier et al. 2017a, respectively. The Graphs are Taken from Yalcintas et al. 2019.

Baik et al. 2015 determined the U(VI) species in granitic groundwater at Kaeri Underground Research Tunnel in Korea by TRLFS. The dominant species was found as $Ca_2(UO_2)(CO_3)_3(aq)$ in the presence of 11-20 mg/L Ca^{2+} among other ions in the groundwater. The chemical speciation of U(VI) in seawater and solubility products of forming solid phases are recently reviewed (Endrizzi et al. 2016). The solubility products of the solid phases forming under given saline conditions, i.e., liebigite, $Ca_2(UO_2)(CO_3)_3 \cdot 10H_2O(cr)$, swartzite $CaMg(UO_2)(CO_3)_3 \cdot 12H_2O(cr)$, bayleyite $Mg_2(UO_2)(CO_3)_3 \cdot 18H_2O(cr)$ and andersonite $Na_2Ca(UO_2)(CO_3)_3 \cdot 6H_2O(cr)$ are re-evaluated. According to the reviewed data, more than 50% of the total uranium concentration was dominated by the $M_m(UO_2)(CO_3)_3^{2(m-2)}$ complexes at $pH_m = 8.2$ in seawater where the concentration of Ca^{2+} and Mg^{2+} are 10×10^{-3} and 53×10^{-3} M, respectively. The $Ca_2(UO_2)(CO_3)_3(aq)$ complex is predicted to be predominant in solution, in contrast to commonly accepted $(UO_2)(CO_3)_3^{4-}$ species.

U(VI) sorption mechanism and kinetics were developed by a number of authors with the repository relevant minerals, i.e., maghemite (Foerstendorf et al. 2014), Fe-Mn binary oxide (Du et al. 2011), Ca-bentonite (Philipp and Schemeide 2016; Philipp et al. 2019), montmorillonite (Tournassat et al. 2018).

The complexation behavior of U with organic ligands is mostly based on the acidic pH region, not representative for WIPP relevant conditions. The most relevant solubility studies by Felipe-Sotelo et al. (2015 and 2017) were performed with U(VI) in 95%-saturated $Ca(OH)_2$ (pH 12.3) in the presence of organic ligands and CDP (cellulose degradation products). U(VI) solubility increases up to 3 orders of magnitude in the presence of citrate and an order of magnitude in the presence of CDP. The solid phase characterization showed that the solubility controlling solid phases are not transformed in the presence of organic ligands.

SOTERM-5.5.3 WIPP-Specific Results since the CRA-2014

There are no new quality (QL1) WIPP-relevant results on the chemistry and speciation of U since CRA-2014. Developmental experiments were completed to establish the effects of EDTA on U(IV) solubility (Yalcintas et al. 2019; also see discussion in SOTERM-3.3)

SOTERM-5.6 Neptunium Chemistry

Neptunium is a TRU component in the WIPP, but is not expected to be a primary contributor to potential release at this time. The WIPP repository is expected to contain ~50 Kilogram (kg) of Np as of closure in 2033 according to PAIR 2018. Neptunium is primarily present as the ^{237}Np isotope ($t_{½} = 2.144 \times 10^6$ yr) and its inventory is expected to increase with time, from the decay of ^{241}Am and possible ^{238}U (n, 2n) reactions, to 331 kg at 1000 y after closure (See Table SOTERM-13). At these masses, ^{237}Np is expected to be the 31st most predominant actinide isotope within the WIPP at closure and to rise to the 7th most abundant within just a few hundred years (by 2383). Further, ^{237}Np is expected to reach the level of 5th most abundant actinide isotope by 12033 based on current inventory information. Other isotopes of neptunium will be present at only relatively trace levels, ~ 2 mg of ^{239}Np is expected at closure, and will not be associated with analogous increases in mass.

In the WIPP PA, Np is assumed to be present in the IV and V oxidation states. Np speciates as Np(IV) in 50% of the PA vectors and as Np(V) in the other 50% of the PA vectors. The contribution of Np to actinide release from the WIPP was included in the CRA-2014 PA calculation, though its effect on release was found to be negligible at that time.

SOTERM-5.6.1 Neptunium Environmental Chemistry

Np can exist in up to five oxidation states (III – VII) within aqueous media. Of these, Np(IV) is expected to dominate in relatively reducing, natural groundwater conditions and Np(V) is expected to be the most common state in more oxidizing waters. The neighboring oxidation states, Np(III) and Np(VI), are not expected to occur to any appreciable extent in the WIPP as the former has not been shown to occur environmentally and the latter is readily reduced to Np(V) with re-oxidation being disfavored by measured potentials (Hobart 1990). Np redox potentials under WIPP-relevant, basic conditions include (Martinot and Fuger 1985; Silva and Nitsche 1995):

$$\underset{}{} \quad \overset{+0.6\ V}{} \quad \overset{+0.6\ V}{} \quad \overset{+0.3V}{} \quad \overset{-2.1V\ 2.2V}{}$$

$$NpO_5^{3-} \rightarrow NpO_2(OH)_2 \rightarrow NpO_2OH \rightarrow NpO_2 \rightarrow Np(OH)_3 \rightarrow Np \quad \text{(SOTERM.8)}$$

The environmental chemistry of Np is somewhat unique in the actinide series as a result of the relatively high stability of the NpO_2^+ species, in the V oxidation state, under a wide range of conditions typically found in the subsurface. This species is mobile as a result of relatively high solubility and is not strongly sorbed or complexed. Further, NpO_2^+ does not hydrolyze strongly, with little or no measurable hydrolysis until pH >9 (Neck, Kim, and Kanellakopulos 1992; Itagaki et al. 1992, Neck 2003). Much of the available complexation data for inorganic and organic complexes for Np pertains to the V oxidation state for this reason (Lemire et al. 2001).

Np(IV) and Np(VI) oxidation states can occur in groundwaters, as Np^{4+} and NpO_2^{2+} complexes, under certain conditions (Hobart 1990; Keller 1971 [pp. 195–215]; Clark, Hobart and Neu 1995). Unlike in the V state, Np(VI) is strongly hydrolyzed at near-neutral pH and is readily reduced by many constituents typically found in groundwater (e.g., organics and most reduced metals). For these reasons, it does not tend to persist in groundwater under most conditions.

Under reducing, anoxic conditions, the Np^{4+} species can predominate in groundwaters. These Np^{4+} species readily undergo hydrolysis and are comparable to Pu^{4+} in this regard. This system is highly irreversible and possibly polymeric in nature, as is observed for Pu^{4+}. The measured solubility of Np^{4+} is $10^{-8.5}$ to $10^{-8.1}$ M, with $Np(OH)_4$ as the predominant aqueous species (Rai and Ryan 1985; Eriksen et al. 1993). The importance and predominance of the Np(IV) oxidation state in reducing conditions is even more pronounced when anaerobic bacteria are present. Np(V) was readily reduced by sulfate-reducing bacteria (Banaszak, Reed, and Rittmann 1998a) and methanogenic consortia (Banaszak et al. 1999), and precipitated as Np(IV) solids. Np complex and oxidation state information relevant to WIPP conditions is summarized in Figure SOTERM-20.

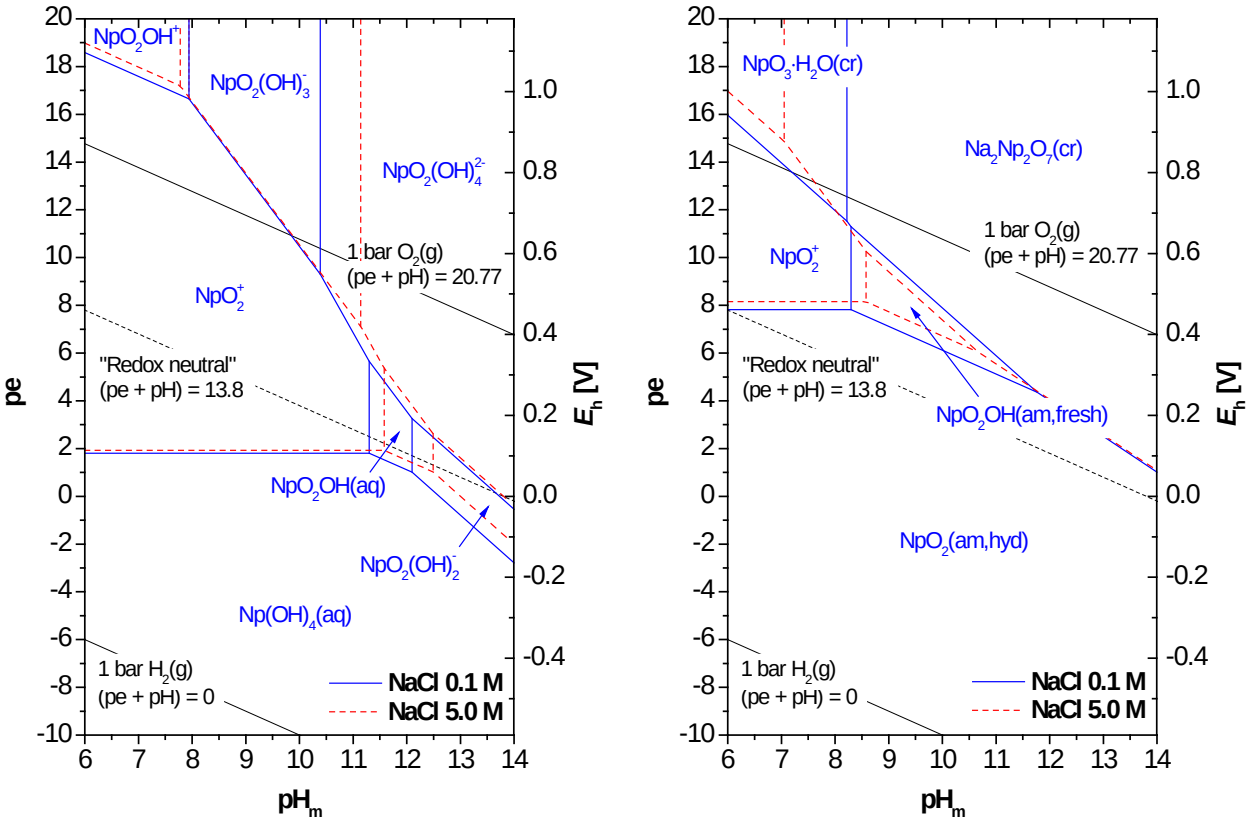

Figure SOTERM-20. E_h/pH Diagrams Illustrating the Current View for Np Oxidation State Distribution in the WIPP; Left: Aqueous Phase, Right: Solid Phase. (Provided by Institute of Nuclear Waste Disposal - INE, Karlsruhe.)

Several WIPP-specific studies exist to support the current assignment of PA vectors between the IV and V oxidation states. For example, spectroscopic evidence for the reduction of Np(VI) to Np(V) in ERDA-6 (Castile) brine at pH 10 was observed along with complete reduction of Np(VI) to Np(V) in G-Seep (Salado) brine at pH 7 when no iron or microbial activity were present (Reed and Wygmans 1997). In the presence of oxalate, citrate, and EDTA, rapid and complete reduction of Np(VI) to Np(V) coupled with a slower formation of Np(IV) species was observed. The stability of Np(V) under these conditions was further confirmed by Neck, Runde, and Kim (1995), who showed that Np(V) carbonate complexes are stable in 5M NaCl. In the expected WIPP environment, however, where anoxic and reducing conditions with microbial activity and reduced iron are expected to be present, Np(IV) is expected to be the predominant oxidation state (Rai and Ryan 1985; Rai, Strickert, and McVay 1982; Kim et al. 1985; Pryke and Rees 1986). This is based on studies of the solubility of NpO_2OH in 1 M and 5 M NaCl solutions at pH 6.5, where the reduction of Np(V) to Np(IV) was observed (Kim et al. 1985; Neck, Kim, and Kanellakopulos 1992). Related thermodynamic data for the above discussions is provided in Table SOTERM-19.

Table SOTERM-19. Thermodynamic Data Relevant to Np Redox, Solubility and Reaction Chemistries.

Reaction	$Log_{10}K°$	Reference
Redox processes		
Np3+ ↔ Np4+ + e–	– (3.695 ± 0.169)	NEA–TDB, 2003
Np4+ + 2H2O(l) ↔ NpO2+ + 4H+ + e–	–(10.21 ± 0.12)	NEA–TDB, 2001
NpO2+ ↔ NpO22+ + e–	–(19.59 ± 0.07)	NEA–TDB, 2001
Solubility and hydrolysis of Np (IV)		
NpO_2 (am,hyd) ↔ Np^{4+} + $4OH^-$	–(56.7 ± 0.5)	NEA–TDB, 2003
Np^{4+} + H_2O(l) ↔ $Np(OH)^{3+}$ + H^+	(0.55 ± 0.2)	NEA–TDB, 2003
Np^{4+} + $2H_2O$(l) ↔ $Np(OH)_2^{2+}$ + $2H^+$	(0.35 ± 0.3)	NEA–TDB, 2003
Np^{4+} + $4H_2O$(l) ↔ $Np(OH)_4$(aq) + $4H^+$	-(8.3 ± 1.1)	NEA–TDB, 2003
Solubility and hydrolysis of Np(V)		
NpO_2OH (am,aged) + H^+ ↔ NpO_2^+ + H_2O(l)	(4.7 ± 0.5)	NEA–TDB, 2003
NpO_2OH (am,fresh) + H^+ ↔ NpO_2^+ + H_2O(l)	(5.3 ± 0.2)	NEA–TDB, 2003
NpO_2^+ + H_2O(l) ↔ NpO_2OH (aq) + H^+	-(11.3 ± 0.7)	NEA–TDB, 2003
NpO_2^+ + $2H_2O$(l) ↔ $NpO_2(OH)_2^-$ + $2H^+$	-(23.6 ± 0.5)	NEA–TDB, 2003
Carbonate Reactions		
NpO_2 (am,hyd) + $4CO_3^{2-}$ + $2H_2O$ ↔ $Np(CO_3)_4^{4-}$ + $4OH^-$	-(17.79 ± 0.22)	NEA–TDB, 2003
$Np(CO_3)_4^{4-}$+ CO_3^{2-} ↔ $Np(CO_3)_5^{6-}$	-(1.07 ± 0.30)	NEA–TDB, 2003
NpO_2^+ + CO_3^{2-} ↔ $NpO_2CO_3^-$	(4.96 ± 0.06)	NEA–TDB, 2003
$NpO_2CO_3^-$ + CO_3^{2-} ↔ $NpO_2(CO_3)_2^{3-}$	(1.57 ± 0.08)	NEA–TDB, 2003
$NpO_2(CO_3)_2^{3-}$ + CO_3^{2-} ↔ $NpO_2(CO_3)_3^{5-}$	-(1.03 ± 0.11)	NEA–TDB, 2003

$Log_{10}K°$ = the standard equilibrium constant of the reaction, logarithmic

SOTERM-5.6.2 New Literature Results Since the CRA-2014

Gaona (2013) demonstrated that Np(V) can be incorporated into calcium rich phases within cementitious materials, leading to decreased mobility. In experimental efforts conducted under anoxic conditions, pH ~10-13.5, and employing XANES and EXAFS techniques, this incorporation was shown to yield no Np(VI) in the absence of NaOCl. The potential presence of Np(IV) could not be ruled out and the degree of Np(V) incorporation was not fully determined. These efforts align with current PA vector assignments for Np, which are distributed evenly between the IV and V states, and support reduced Np transport in scenarios potentially involving cements.

Graser et al. (2015) explored the analytical applications of capillary electrophoresis mated to inductively coupled plasma sector field mass spectrometry (CE-ICP-SF-MS) for sensitive redox speciation of iron, neptunium and plutonium in repository related investigations. This effort established the analytical basis for use of CE-ICP-SF-MS in the measurement of trace neptunium species following solution preparation and sorption experiments with mineral surfaces as illustrated in Figure SOTERM-21.

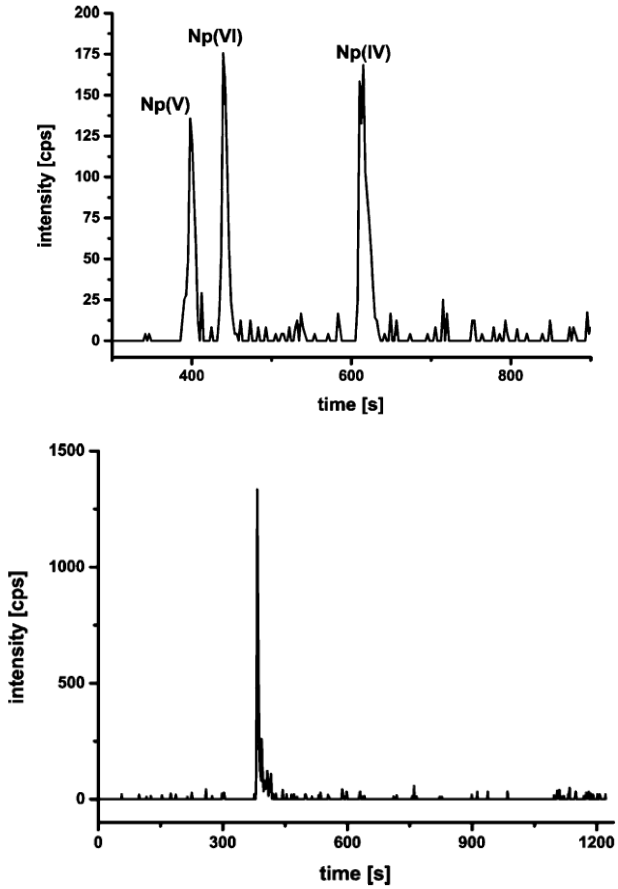

Figure SOTERM-21. Top: CE-ICP-SF-MS Results Reflecting Redox State Distribution of Freshly Prepared Np in 1 M $HClO_4$. Bottom: Np Fraction, Reflecting 100% Np(V) Distribution, Measured in the Supernatant of a Suspension with Illite. From Graser et al. (2015).

Fellhauer et al. (2016a and 2016b) have examined the solubility, speciation and solid phase formation behavior of Np(V) in carbonate-free, $CaCl_2$ solutions of varying concentration between pH_m 8 and 12. While the authors openly highlighted distinct chemical behaviors relative to NaCl systems, several points of WIPP relevance were noted. Three CaNp hydroxide solids ($CaNpO_2(OH)_{2.6}Cl_{0.4}\cdot 2H_2O$(s), $Ca_{0.5}NpO_2(OH)_2\cdot 1.3H_2O$(s), and $Ca_{0.5}NpO_2(OH)_2$(s)) were identified and found to have solubilities three orders of magnitude less than the characteristic NpO_2OH(am). In general, Np(V) solubility was found to decrease as pH_m increased, up to approximately 11, then increased again. Even in the highest concentration $CaCl_2$ solutions (4.5 M) at pH_m ~12, the ultimate Np solubility was still below that of the pure NaCl brine case for any $pH_m > 8$. As a cementitious system would not produce pure calcium chloride brine in most repository systems, these results could be considered bounding. Fellhauer does indicate a solubility enhancing effect for the ternary aqueous Np(V) species, mainly by formation of $Ca_3[NpO_2(OH)_5]^{2+}$, occurring at medium and high calcium concentrations. However, calcium levels (0.25 – 4.5 M) and pH (>11) associated with formation of this species exceed those expected within the WIPP.

Petrov et al. (2017) examined the solubility and hydrolysis of Np(V) in NaCl solutions between 0.1 and 5 M and pH_m ranging 9 to 14, in contrast to the $CaCl_2$ solutions used by Fellhauer et al. (2016a and 2016b). Their findings support the validity of the NEA-TDB hydrolysis scheme for Np(V), and amorphous NpO_2OH as the solubility controlling phase under WIPP relevant conditions. Further, Petrov et al. (2017) were unable to confirm the existence of an aged $NpO_2OH(am)$ phase or observe the impact of such a phase on resulting Np solubility in NaCl solutions. As a result, the authors recommended use of data associated with the fresh solid to avoid underestimation of Np(V) concentrations during thermodynamic calculations.

Yang et al. (2017) examined the reductive precipitation of Np onto iron surfaces under anoxic conditions. Iron surfaces used were either pristine Fe(0) or pre-corroded in oxygen-free water, to produce a magnetite corrosion layer. All systems were determined to be reducing, with E_h ~ -260 millivolt (mV). In all cases, a highly disordered Np(IV) phase was found associated with the iron samples, after having started with a Np(V) phase.

Zhang et al. (2017) examined the effect of temperature on the hydrolysis of actinides in solution. These efforts employed potentiometric and calorimetric titration experiments to evaluate changes in the hydrolysis constants for Np(V) between 283 and 358 K. It was noted that first and second order hydrolysis of NpO_2^+, yielding $NpO_2OH(aq)$ and $NpO_2(OH)_2^-$, became less endothermic at higher temperatures but that such reactions did not become exothermic under any tested conditions. Such efforts, however, represent a disagreement with selected database values for NpO_2^+ hydrolysis, and would benefit from further confirmation within the community (Neck et al. 2006) before use in thermodynamic calculations.

The works discussed above are consistent with expectations on Np chemistry and do not significantly impact the current view in the WIPP. There is however a growing role for Np(IV) as an analog for An(IV) and the redox controls needed to perform long term studies were developed (Altmaier et al. 2017b). There are clearly potential applications of this development to the WIPP-specific case.

SOTERM-5.6.3 WIPP-Specific Results since the CRA-2014

As neptunium is not a key contributor to release from the WIPP, there are no new WIPP-relevant results on the chemistry and speciation of Np since CRA-2014.

SOTERM-5.7 Plutonium Chemistry

Plutonium is a key TRU component that contributes significantly to the potential for TRU release from the WIPP under all release mechanisms considered by PA. Pu isotopes, estimated to now be approaching ~16 metric tons (~ 30% higher than in CRA-2014) at the time of closure, represent approximately 77% of the Ci content for actinides in TRU waste (see Table SOTERM-11) at emplacement. This changes with time to 62%, 83% and >99% at 100, 1000 and 10,000 years after emplacement due to radioactive decay and the relatively long half-life of ^{239}Pu. There are five isotopes of Pu that make a significant contribution to the Pu inventory, but ^{239}Pu, ^{238}Pu, and ^{241}Pu are the major contributors to the Ci content. Under the conditions expected in the WIPP, Pu(IV) has long been expected to be the predominant oxidation state (Weiner 1996). An

additional assessment of Pu subsurface speciation issues as they pertain to the WIPP case was completed (Reed 2018).

In WIPP PA, all of the Pu is assumed to be reduced and present in the III or IV oxidation state. Half of the PA vectors contain 100% Pu(III), with the other half of the vectors containing 100% Pu(IV) species. The two higher-valent Pu oxidation states, Pu(V) and Pu(VI), are not considered in PA because they have been shown to not persist under the expected reducing and anoxic conditions in the WIPP (see following discussion in SOTERM 5.7.1 and 5.7.3). For CRA-2019, the solubility of Pu(III) is approximately 3 times higher when directly compared to Pu(IV) under similar conditions and can be lower that the concentration of Pu(IV) in PA realizations for the mobile actinide source term that account for the higher uncertainty associated with the solubility of Pu(IV) – see SOTERM Section 6.6.4 What is most important is that Pu(III/IV) rather than Pu(V/VI) predominates and there are no new project-specific data that contradict this result. These altogether continue to support the current actinide oxidation-state distribution model and its PA implementation in CRA-2019.

SOTERM-5.7.1 Plutonium Environmental Chemistry

Generally, Pu can exist in oxidation states III, IV, V, VI, and VII (Katz, Seaborg, and Morss 1986, p. 781), with each state exhibiting unique solubilities, redox behavior, sorption characteristics, etc. Of the available states, only Pu(V), Pu(IV), and Pu(III) are expected to be important under environmentally relevant oxidizing and reducing conditions. Pu(VII) is very unstable and exists only in extremely basic solutions (for example, 7 M NaOH) that are not expected in the WIPP. Pu(VI) and Pu(V) can persist in the WIPP in the absence of reductants, but they are readily reduced in the presence of Fe(II/0) species, reduced by many organic chelators (Reed et al. 1998), and possibly reduced in anaerobic, biologically active systems (Reed et al. 2007; Icopini, Boukhalfa, and Neu 2007). The reduction of Pu(VI/V), under WIPP-relevant conditions, was shown by Clark and Tait (1996), Reed and Wygmans (1997), and Reed et al. (2007). In this context, only Pu(III) and Pu(IV) oxidation state species are expected to be present under WIPP-relevant conditions, as explained below, with Pu(IV) being predominant.

SOTERM-5.7.1.1 Importance of Redox for Plutonium Speciation

The role and importance of redox reactions in determining actinide mobility and solubility are beyond question (Van Luik et al. 1987; Allard 1982; Choppin and Rao 1992). The redox potentials for the various oxidation states at pH 7 are (Cleveland 1979, pp. 11–46)

$$\underset{+0.94\ V}{\underbrace{PuO_2(OH)_2\,(aq) \xrightarrow{+0.77\ V} PuO_2^{+} \xrightarrow{+1.11\ V} PuO_2{\cdot}H_2O\,(s)}} \xrightarrow{-0.63\ V} Pu^{3+} \qquad \text{(SOTERM.9)}$$

A phase diagram for Pu in groundwater that illustrates the importance of redox is shown in Figure SOTERM-22. This continues to show that the DOE expects Pu(IV) as the predominant oxidation state with Pu(III) likely at the low E_h range of the repository conditions.

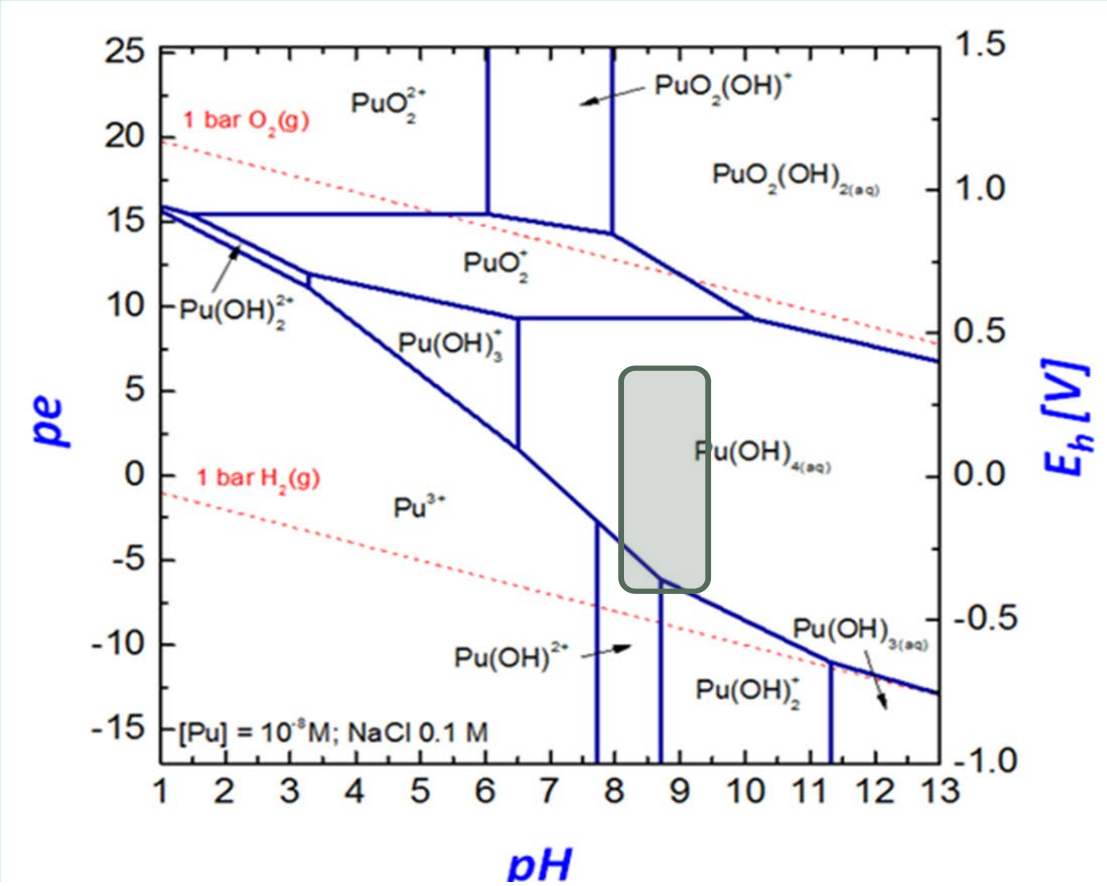

Figure SOTERM-22. Pourbaix Diagram for Aqueous Plutonium Hydrolysis Species that Qualitatively Illustrates the Current WIPP Concept for Pu Oxidation State Distribution in the WIPP (Altmaier 2017b). Shaded Area was Added to Illustrate the Approximate Range of WIPP-relevant Conditions.

Higher-valent Pu, specifically Pu(V) and Pu(VI), can be present in near-surface oxidizing groundwaters (Orlandini, Penrose, and Nelson 1986). The association of Pu(V) with organic colloidal material was proposed as the mechanism by which subsurface migration occurred. Pu(VI), in near-neutral systems, is strongly and irreversibly hydrolyzed (Okajima and Reed 1993). It is also readily reduced by organics and reduced metal species even when oxygen is present to form Pu(V), and is not generally stable under most groundwater-relevant conditions.

Pu(V), by analogy with Np(V), does not undergo hydrolysis until pH >7 and tends to form weak complexes. It readily disproportionates to form Pu(IV) and Pu(VI) at high concentrations and is relatively easy to reduce in the environment under anoxic conditions. Fe^{2+}(aq), Fe(II) minerals, and metallic iron reduce Pu(V) to Pu(IV).

In geochemical systems, redox control is often interpreted in terms of the iron, and in a broader sense, reduced metal, mineralogy, and associated aqueous chemistry (Sanchez, Murray, and Sibley 1985; White, Yee, and Flexser 1985). In the WIPP case, iron will undergo anoxic corrosion, producing Fe^{2+}. Both metallic iron (Fe^0) and Fe^{2+} have been shown to quantitatively reduce Pu(VI) in the WIPP brines to either Pu(IV) or Pu(III). Clark and Tait (1996) and Felmy et

al. (1996) have experimentally observed the reduction of Pu(VI) carbonates by either Fe^0 or Fe^{2+} to Pu(IV). In the absence of carbonates, a quantitative reduction of Pu(VI) is also observed, but the oxidation state of the resulting species cannot be definitively determined because its concentration is below the lower detection limit of the oxidation state analytical process (about 10^{-9} M). However, since this concentration is well below the expected solubility of Pu(V) species, it was reasonably assumed that the Pu must have been reduced to either the IV or III oxidation state. Neretnieks (1982) has shown that when dissolved actinides in moving groundwater came in contact with Fe(II), the actinides were reduced to a much-less-soluble oxidation state and precipitated.

General studies of Pu in brine have been done by a number of investigators (Büppelmann et al. 1986; Büppelmann, Kim, and Lierse 1988; Clark, Hobart, and Neu 1995; Nitsche et al. 1992; Nitsche et al. 1994; Pashalidis et al. 1993; Villareal, Bergquist, and Leonard 2001; Reed et al. 1993; Reed, Okajima, and Richmann 1994; Reed and Wygmans 1997). There has also been an assessment of the actinide chemistry in the WIPP CCA (Oversby 2000; Brush, Moore, and Wall 2001; U.S. EPA 2006). These studies confirm reduction of higher-valent Pu under the expected WIPP conditions and establish the key speciation trends for Pu in the WIPP (see Figure SOTERM-23). These trends are captured in the WIPP PA through analogy with Am(III) for Pu(III) and with Th(IV) for Pu(IV).

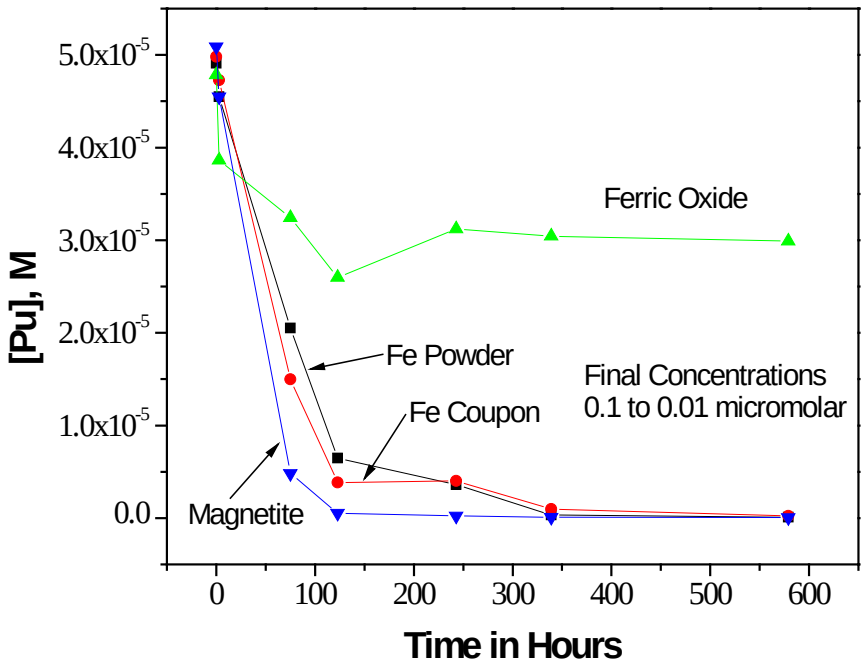

Figure SOTERM-23. The Concentration of Pu as a Function of Time in the Presence of Iron Powder, Iron Coupon, Ferric Oxide, and Magnetite (Mixed Iron Oxide). These Data Show the Reduction of Pu(VI) to Pu(IV) Species when there is Available Fe(0,II) that Effectively Lowers the Concentration of Pu in the Timeframe of 100 Hours Under the Conditions of the Experiments (Reed et al. 2010).

SOTERM-5.7.2 Thermodynamic Stability of Higher-Valent Plutonium: PuO_{2+x}

It has long been held that Pu oxide, as PuO_2, is the thermodynamically favored form of Pu oxide. This oxide is likely the predominant form of Pu in TRU waste and is believed to be the most important phase under WIPP-relevant conditions. There are, however, a number of studies that question this key and fundamental assumption.

Haschke, Allen, and Morales (2000) reported that near-stoichiometric plutonium dioxide reacts with water vapor at temperatures between 25 °C and 350 °C (77 °F and 662 °F) according to the following reaction:

$$PuO_2(s) + xH_2O(g) \rightarrow PuO_{2+x}(s) + xH_2(g) \qquad \text{(SOTERM.10)}$$

Here, water vapor is reduced by polycrystalline PuO_2 to produce hydrogen (H) and a previously unknown higher-oxide PuO_{2+x} with *x* as large as 0.27. If only Pu(IV) and Pu(V) are present in $PuO_{2.27}$, this oxide has 46% Pu(IV) and 54% Pu(V). Once formed, the PuO_{2+x} may dissolve in contact with groundwater to form aqueous PuO_2^+ or PuO_2^{2+} species (Haschke and Ricketts 1995).

There remains some controversy about the mechanisms that led to the observation of higher-valent Pu in the PuO_{2+x}. This process only occurs under unsaturated conditions at high relative humidities. Haschke, Allen, and Morales (2000) argue that this conversion is due to a chemical reaction (that is, the above reaction has a Gibbs energy less than zero) rather than a radiolysis-induced reaction because the reaction rate is temperature dependent. However, there seems to be some contribution from radiolysis in this process and this may be the dominant mechanism (LaVerne and Tandon 2002). Neither of these mechanisms are expected to impact WIPP repository performance. Furthermore, no further updates regarding this topic/consideration have been identified in the open literature from recent years.

The behavior of PuO_2 in contact with water was studied as a function of time by means of the short-lived isotope ^{238}Pu, as well as the longer-lived ^{239}Pu (Rai and Ryan 1982). This study concluded that crystalline PuO_2, amorphous PuO_2, and amorphous $PuO_3 \cdot xH_2O$ all convert to a material intermediate between crystalline PuO_2 and a hydrated amorphous material that contains both Pu(IV) and Pu(VI). These authors hypothesized that alpha particles generated by ^{238}Pu or ^{239}Pu irradiated water to generate OH radicals that reacted to form Pu(V) and/or Pu(VI) on the oxide surface. These observations are why the formation of localized oxidizing zones, where some higher-valent Pu can exist, is recognized by the WIPP. Reduction of these species, however, leads to a reformation of Pu(IV) hydrous oxide precipitates.

The overall issue of a thermodynamic driver for higher-valent Pu oxides, although it has received much attention in the literature, is not yet resolved, but has a relatively insignificant impact on the WIPP regardless of the mechanisms at work. A prolonged unsaturated phase in the WIPP could lead to the formation of some PuO_{2+x}, but this will be quickly overwhelmed in an aqueous environment and the higher-valent Pu will be reduced to Pu(III/IV) species, as described in SOTERM Section 5.7.1.1. Both DBR and transport-release scenarios assume brine inundation and, correspondingly, the rapid introduction of reducing conditions.

SOTERM-5.7.3 New Literature Results Since the CRA-2014

The long-term stability and relative importance of Pu(IV) and Pu(III) under environmental conditions that are WIPP-relevant continues to be an active area of research within the actinide community.

Cho et al. (2016) examined the hydrolysis behavior of trivalent Pu and solubility of $Pu(OH)_3$ (am) under reducing conditions in 0.1 M $NaClO_4$. Coulometric and spectroscopic data from 20 different samples were used to determine solution speciation and equilibrium constants for the hydrolysis:

$$Pu^{3+} + H_2O\ (l) \leftrightarrows Pu(OH)^{2+} + H^+ \qquad \text{(SOTERM.11)}$$

And solubilization of the obtained solid:

$$Pu(OH)_3\ (am) + nH^+ \leftrightarrows Pu^{3+} + 3H_2O\ (l) \qquad \text{(SOTERM.12)}$$

The equilibrium constant associated with the hydrolysis reaction shown above was calculated as $\log_{10} {}^{*}K^{0}_{1,1} = -(6.18 \pm 0.25)$ and the conditional solubility product for $Pu(OH)_3$ (am) was calculated $\log_{10} {}^{*}K^{0}_{s,0} = (14.58 \pm 0.50)$. The authors noted that these values are lower than previous NEA-TDB recommended values. These ongoing discrepancies consistently point to the need for additional research to refine associated modelling predictions. From a WIPP PA perspective, the possible role of Pu(III) is conservatively taken into account by assuming that Pu is speciated as Pu(III) in 50% of the PA vectors.

Two new investigations are also reported on higher-valent Pu oxidation states. Neither of these are directly relevant to the WIPP but are briefly described for the sake of completeness. The chemistry of Pu(V), as well as the analogy with Np(V), was recently examined by Topin and Aupiais (2016). This work discussed the use of capillary electrophoresis methods in recent years (e.g., Graser et al. 2015) to advance current knowledge of actinide redox chemistry in solution and to confirm the applicability of Np(V) as a Pu(V) surrogate. Additionally, Huang et al. (2015) explored the possible existence of the Pu(VIII) state for highly oxidizing conditions that are not relevant to the environment. Ultimately, even under these extreme Eh conditions, the authors were not able to positively identify Pu(VIII) species.

SOTERM-5.7.4 WIPP-Specific Results since the CRA-2014

Since the CRA-2014, the WIPP-specific Pu-Fe interaction studies (Reed et al. 2010) were extended in time to approximately 10 years to establish the long-term oxidation state distribution of plutonium in these iron-dominated brine systems. These investigations are described in more detail elsewhere (CRA-2014 Appendix SOTERM, Section 3.6.2) and the latest XANES data are shown in Figure 24 (Bone et al. 2019). These data continue to support previously reported work in that a mixture of Pu oxidation states are observed depending on the conditions of the experiment. A summary of all WIPP relevant work is given in Table SOTERM-20.

The plutonium (III/IV) solids data show a qualitative correlation with the Fe(II)/Fe(III) ratio and measured redox potential (E_h). Experiments with less negative E_h also had a greater amount of Fe(III) and Pu(IV) species present in the system. This adds to the linkages seen by others between the iron and plutonium chemistry in subsurface conditions. Although these specific experiments were performed in brine, they are consistent with the correlation between iron chemistry and other metals observed in low ionic strength groundwater (Masue-Slowey et al. 2011; Holm and Curtiss 1989; Christensen et al. 2000). The overall reaction sequence is given by:

$$\mathrm{Pu(V/VI)} \xrightarrow{\text{Rapid}} \mathrm{Pu(IV)} \xrightarrow{\text{Slow}} \mathrm{Pu(III/IV)} \qquad \text{(SOTERM.13)}$$

Here rapid reduction, on the scale of days to weeks, of Pu(V/VI) to Pu(IV) was always noted in the presence of Fe(0, II) phases. Full equilibration to a mixture of Pu(III) and Pu(IV) species occurred on a much slower timescale (months to years) when anoxic conditions were strictly maintained. The predominance of Pu(III) at long times (multiple years) provides a strong data point on the reducing conditions that iron creates under WIPP-relevant conditions, but does not account for radiolytic impacts on E_h, and the effects of organic complexation which will stabilize Pu(IV) relative to Pu(III). These data, taken in context, strongly support the current WIPP PA assumption that Pu(III) and Pu(IV) will be prevalent in the WIPP and both oxidation states will contribute to the actinide source term.

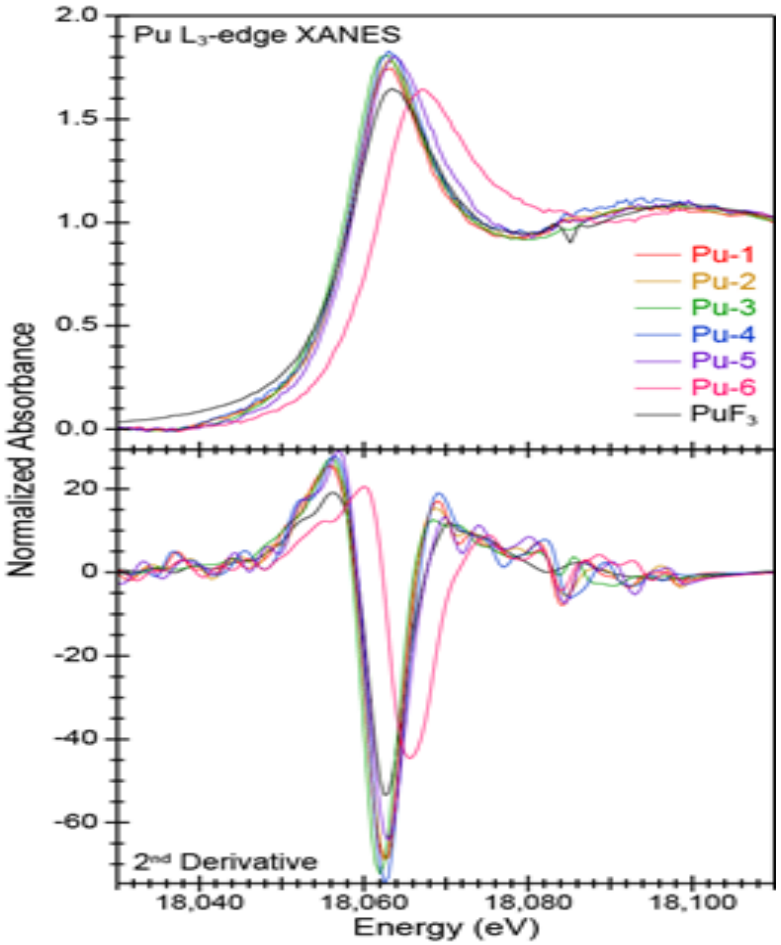

Figure SOTERM-24. XANES Analysis of Plutonium Precipitates in the Magnetite and Iron Reduction Experiments at ~ 10 year in the Pu-242-Fe Experiments (Bone et al. 2019). Pu(III) Phases were Predominantly Noted When Only Fe(0,II) was Present and are Denoted by the Inflection Points that Agree with the PuF_3 Standard Used. Pu(V) was Noted in the Presence of Fe(III) Only, Denoted by the One Shifted Edge Position Above, and Pu(III/IV) Mixtures are Observed for Mixed Valent Fe(II/III) Phases when a Slight Shift is Noted.

An assessment of the plutonium literature was also completed to support CRA-2019. The redox and solubility chemistry of Pu have been investigated for decades to define the redox borders and the solubility limits of respective Pu oxidation states. The solubility study of $Pu(OH)_3$(am) performed by Felmy et al. (1989) is still considered to be the most reliable Pu(III) data. This study, however, has some limitations: the experiments were relatively short-term (up to 20 days); the authors did not consider Pu(III) hydrolysis species in their model calculations; and sufficient solid phase characterization was not performed. In the 2000s, a number of studies were dedicated to reductive dissolution of PuO_2 (am, hyd) according to reaction SOTERM.14:

$$PuO_2 \cdot xH_2O(s) + e^- + 4H^+ \Leftrightarrow Pu^{3+} + (2+x)H_2O \qquad \text{SOTERM.14}$$

Table SOTERM-20. Under Expected WIPP Conditions (ANL Work Highlighted in Green) a Predominance of Pu(IV) is Observed. Pu(III) is Predominantly Noted in the Low Radiolysis Case When No Fe(III) is Present. When Both Fe (II) and Fe(III) are Present, a Mixture of Pu(III) and Pu(IV) Occurs. (ANL work: Reed et al. 2006; LANL/ACRSP work: Reed et al. 2010; Reed et al. 2018; Bone et al. 2019)

Summary of all WIPP project-specific data for the Pu-Fe systems since the inception of the WIPP project			
Conditions	**Experiments**	**Result/Observation**	**Reference**
"oxidizing" no reducing agent present	Pu(VI), as Pu-239, was added to WIPP-specific brine - > 4 year experiments	Pu(VI) as an aquo complex and carbonate complex was mostly stable with some Pu(V) formation noted no reduction to Pu(IV/III) was observed.	ANL work
	Pu(VI), as Pu-242, was added to Fe(III) solids	Pu(VI)/Pu(V) mixture observed – no reduction to Pu(IV/III)	LANL/ACRSP post CRA-2014 data
WIPP (expected conditions)	Pu(VI), as Pu-239, was equilibrated for ~ 4 years in brine and then Fe(O) was added	Pu(V/VI) in solution was rapidly reduced to Pu(IV) in all cases, XANES confirmed that only Pu(IV) was formed	ANL work
Mixed reducing conditions	Pu(VI), as Pu-242, was added to Magnetite (Fe(II/III) in WIPP-specific brine	Rapid reduction to Pu(IV) was noted and confirmed in the solid phase by XANES. In the longer term, ~6 years results, a ~ 10-75% Pu(IV) with the rest Pu(III). Full reduction to Pu(III) was never noted.	CRA-2014 Appendix SOTERM
Reducing conditions	Pu(VI), as Pu-242, was added to zero-valent Fe (powder and coupon) in WIPP-specific brine	Rapid reduction to Pu(IV) and confirmed in the solid phase by XANES. In time, this was further reduced to ~ 100% Pu(III). The nature of the Pu(III) solid phase was not established.	CRA-2014 appendix SOTERM and Post-CRA-2014 cutoff data.

The pe + pH conditions can be varied and set by various reducing agents such as Fe(II), Fe(0), hydroquinone, tin, and $Na_2S_2O_4$ (Fujiwara et al. 2002; Rai et al. 2002; Altmaier et al. 2009) and these various approaches are fully discussed elsewhere (Altmaier et al. 2017b). PuO_2(am, hyd) was predicted to control the solubility of Pu in equilibrium with Pu(III)(aq)+Pu(IV)(aq), although none of these studies provide sufficient solid phase characterization. Cho et al. (2016) updated the thermodynamic data for the solubility of $Pu(OH)_3$(am) by combining spectroscopy with solubility experiments under well-controlled reducing conditions and reported a lower solubility product ($\log {}^{*}K^{o}_{s,0} = 14.58$) than the currently accepted value ($\log {}^{*}K^{o}_{s,0} = 15.8$) in the

NEA-TDB, 2003. A recent study by Tasi et al. 2018 also investigated the solid phase controlling the Pu solubility at pH_m = 9 and 12 at low ionic strength in the presence of Sn(II) (pe + pH = 2) by EXAFS measurements after 146 days of contact time. The authors reported the presence of Pu(III)(s) together with Pu(IV)(s) in both cases, although the aqueous Pu concentration remained in the 10^{-11} M range, which implied that the concentration was being defined by the solubility limit of PuO_2(am,hyd) in equilibrium with $Pu(OH)_4$(aq) (Tasi et al. 2018). The experimental data from these studies in comparison with current solubility model calculations are shown in Figure SOTERM-25. All of these studies and current thermodynamic data confirm the complexity of the Pu(III)/Pu(IV) redox chemistry at neutral to the alkaline pH range and thus, pH, reducing conditions and the ionic strength are most critical in geologic repository applications.

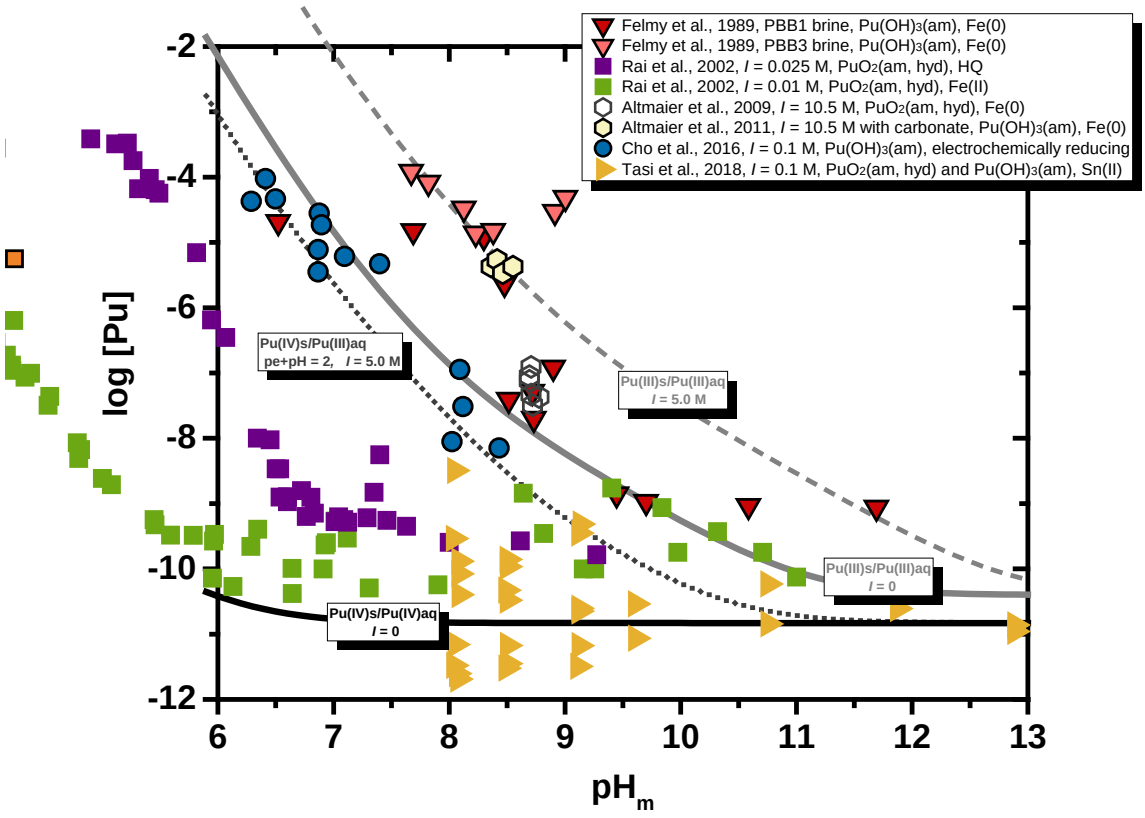

Figure SOTERM-25. The Experimental Solubility Data Reported in the Literature. The Solubility Models are Calculated with Selected Thermodynamic Data for the Analogs of Pu Used in the WIPP Model. Solid Lines are the Solubility of PuO_2(am,hyd)(black) and $Pu(OH)_3$(am)(grey) Calculated at I = 0. Dotted Line is the Solubility of PuO_2(am,hyd) at I = 5.0 M NaCl in Equilibrium with $[Pu]_{tot}$ = Pu(III)(aq) + Pu(IV)(aq) at pe + pH = 2. Dashed Line is the Solubility of $Pu(OH)_3$(am) in Equilibrium with $[Pu]_{tot}$ = Pu(III)(aq) at I = 5.0 M NaCl.

The role of EDTA as a reducing/oxidizing agent was also assessed in the literature (Table SOTERM-21 and 22). EDTA is a strong complexant of Pu(III) and Pu(IV) and has a strong solubilizing effect on both oxidation states. It is clear that Pu(V) and Pu(VI) are reduced by EDTA, as is the case with other organic complexants such as citrate. This was confirmed in WIPP-specific experiments (Reed et al. 1997). There are however mixed results in the literature

on the reduction of Pu(IV) and/or the oxidation of Pu(III) and this process is clearly pH dependent and impacted by ionic strength. These data are best interpreted as inconclusive as they may impact the long-term stability or formation of Pu(III) under WIPP-relevant conditions.

Table SOTERM-21. Results of Literature Search on the Impacts of EDTA on the Reduction and Oxidation of Pu in Abiotic Systems.

Abiotic Studies of Pu-EDTA Systems		
Study	**What was done**	**Result**
WIPP-specific Studies Reed (ANL-1990s study) Reed et al., 1998	Pu(VI) added to acetate, oxalate, citrate, EDTA in WIPP-specific brines (multiyear study) all was under anoxic conditions	An(IV) complexes formed. With EDTA, Pu(V) formation was the fastest, Pu(IV) formation the slowest – no Pu(III) noted in any studies
Rai et al., 2012	Complexation of Pu(III) with EDTA. pH 1-13	Reductant was added to suppress Pu(III) oxidation, no evidence for reduction of EDTA
Thakur et al., 2009	Pu(IV)-EDTA study, mostly under acidic conditions	Marginal relevance to WIPP, no evidence for EDTA reduction
Meyer et al., 2010	Pu(IV)-EDTA study, under acidic conditions.	Marginal relevance to WIPP, no evidence for EDTA reduction
Rai et al., 2007	EDTA complexation of Pu(IV) in the presence of metal competition.	Metal competition marginalized the effect of EDTA on Pu. Reduction to Pu(III) not noted.
Boukhalfa et al., 2003a	Reduction of Pu(IV)-EDTA complex to Pu(III)-EDTA complex was investigated.	EDTA does shift the redox potential, but reduction to Pu(III) only occurred with applied potential.
Boukhalfa et al., 2003b	Explored relative stability of Pu(III/IV) EDTA complexes	Pu(IV)-EDTA complexes are stabilized over Pu(III) complexes
Bolton et al., 2006	Pu(III)-EDTA study	Pu(III) stabilized by addition of reductants

Table SOTERM-22. Results of Literature Search on the Impacts of EDTA on the Reduction and Oxidation of Pu in Biotic Systems.

Biotic Pu-EDTA Studies		
Study	**What was done**	**Result**
Icopini et al., 2009	Bioreduction of Pu(V/VI) by Geobacter	Reduction noted, Pu(IV)O2 is stable product
Boukhalfa et al., 2007	Pu(IV) reduction by Geobacter and shewanella	Bioreduction from Pu(IV) to Pu(III) noted. Pu(IV) introduced as an EDTA complex was reduced to Pu(III) EDTA
Plymale et al., 2012	Reductive solubilization of Pu(IV) through abiotic and biotic pathways. Metal-reducing bacteria.	Pu(III) solid phase noted in biotic experiments indicating bioreduction. EDTA accelerated this process. Proposed that Pu(III)-EDTA is more important process.
Kimber et al., 2012	Bioreduction of Pu(IV) to Pu(III) by anoxic biostimulation	Pu(III) formed microbially.

SOTERM-5.8 Americium and Curium Chemistry

There are relatively small quantities of Am in TRU waste (see Table SOTERM-11), and this is anticipated to be ~ 338 Kg at emplacement (up from 151 Kg in CRA-2014). The high activity of ^{241}Am ($t_{½}$ = 432 years, 3.443 Ci/g) makes Am a key contributor to potential actinide release from the WIPP at earlier times in repository history (~26% initially, decreasing to 17% and ~0% at 1000 and 10,000 years after emplacement). In the WIPP PA, Am is in the trivalent state in all vectors and the aqueous concentration consists of Am^{3+} complexes and colloidal species.

Cm is also present in very small quantities in the WIPP (Table SOTERM-11) and exists primarily as the ^{244}Cm isotope (0.0.122 Kg in CRA-2014, up to 2.13 Kg in 2016). The high activity of this isotope ($t_{½}$ = 18.11 years) makes Cm an important species in the WIPP at the very early stages of repository history. It is essentially unimportant for the PA because it has decayed away by the end of the 100-year period for active institutional controls. However, other Cm isotopes with longer half-lives are present in the inventory and are considered by the WIPP PA. The environmental chemistry of Am and Cm are very similar, and most of what is said in this section about the environmental chemistry of Am also applies to Cm.

A more detailed review of the literature for Am can be found as part of a WIPP report (Borkowski et al. 2009). The solubility of An(III) was measured in the WIPP brine over a wide range of conditions using Nd(III) as a redox-invariant analog. These data support current WIPP PA calculations for the solubility of Pu(III) and Am(III) in the WIPP brine and are also summarized in Borkowski et al. (2009).

SOTERM-5.8.1 Americium and Curium Environmental Chemistry

Am is a 5f electron element and, like other elements of the actinide group, can exist in aqueous solution in several oxidation states. The electrode potentials for some Am couples are presented in Figure SOTERM-26. The trivalent state of Am is the most stable aqueous oxidation state (Katz, Seaborg, and Morss 1986, p. 912), and it is quite difficult to oxidize in aqueous solution (Hobart, Samhoun, and Peterson 1982). The trivalent Am ion has an ionic radius of 97.5 picometers (pm) (coordination number [CN]=6) and its chemical properties can be used as an analog for Pu(III), which has a similar ionic radius (100 pm at CN=6) and charge density, as well as for Cm(III) (97 pm at CN=6).

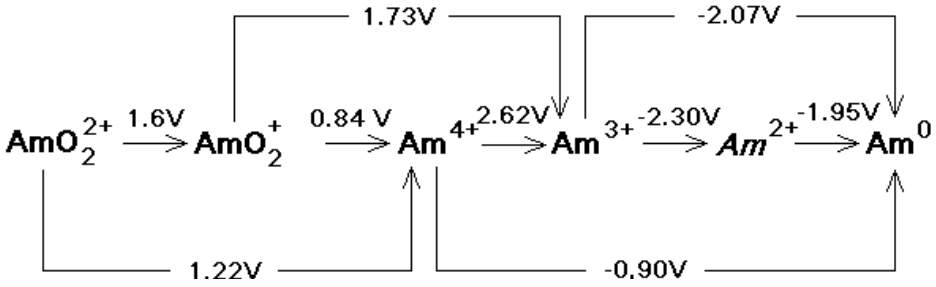

Figure SOTERM-26. Redox Potential for Some Am Redox Couples (Silva et al. 1995, p. 74)

The *Am(II)* species is italicized to stress that it is only a transient species. As discussed by Martinot and Fuger (1985), there is evidence for the formation of *Am(II)* in aqueous perchlorate solution in the pulse radiolysis experiment. The half-life of this species was estimated to be approximately 5 μs. This species is not observed during the electroreduction of Am(III) to the metal in non-complexing media (David, Maslennikov, and Peretrukhin 1990).

Cm is also distinguished by the relatively great stability of the III oxidation state with respect to oxidation or reduction (Katz, Seaborg, and Morss 1986, p. 970). The stability of Cm(III) may be attributed to the half-filled f-shell electronic configuration ($5f^7$). The oxidation of Cm(III) is achieved only with the strongest oxidizing agents, and only one report claims evidence for an oxidation state higher than IV (Korpusov, Patrusheva, and Dolidze 1975). The Cm(III) to Cm(IV) transition has not been successfully induced by ozone or electrochemically, and the Cm(IV) phosphotungstate produced by oxidizing with peroxysulfate is considerably less stable than the Am(IV) analog (Katz, Seaborg, and Morss 1986, p. 971). In the reducing environment of the WIPP repository, any higher-valent Cm produced radiolytically would be unstable. For all these reasons, the predominant oxidation state for Cm in the WIPP environment is Cm(III).

Higher-valent Am species have also been noted. Am(IV) species, with an ionic radius estimated by Shannon (1976) to be 85 pm when six coordinate, is only stable in the presence of strongly complexing anions such as carbonate, fluoride, phosphate, or phosphotungstate, and was never found in any appreciable amount in trivalent Am solutions.

The pentavalent and hexavalent dioxoamericium ions AmO_2^+ and AmO_2^{2+} can be generated under strongly oxidizing conditions. Free radicals produced from α particles in water readily reduce these dioxoamericium ions back to Am^{3+}. In concentrated NaCl solution, in which the

radiolysis products are strong oxidants, pentavalent and hexavalent Am are the predominant species (Büppelmann et al. 1986). Without an oxidant, the pentavalent dioxoamericium ion slowly disproportionates to AmO_2^{2+} and Am^{3+}. These higher oxidation states are not stable in natural waters and can be readily reduced by action of reductants naturally present in those waters.

The speciation of Am in groundwater under mildly alkaline conditions is primarily defined by hydrolysis and carbonate complexation. Hydrolysis is generally represented by the following reaction:

$$Am^{3+} + nH_2O \leftrightarrows Am(OH)_n^{(3-n)} + nH^+ \qquad \text{(SOTERM.18)}$$

Silva measured the $^{243}Am(OH)_3$(crystalline [cr]) and $Nd(OH)_3$(cr) solubilities in 0.1 M $NaClO_4$ solution at 25±1 ºC within the pH range 6 to 10 (Silva et al. 1995, p. 79-97). This is the only study with Am hydroxide using an x-ray-characterized crystalline solid. The solid phase was prepared by rigorously controlled, high-temperature transformation of $Am(OH)_3$(am). Optical viewing by scanning electron microscope (SEM) of the solid samples at the end of the solubility experiments showed no changes in the crystal. The use of the ^{243}Am isotope diminished α-particle damage of the crystal as a result of the 17-times-lower specific activity compared to ^{241}Am. The weakness of this experiment was the relatively short equilibration time of only 48 days. A log (K_{sp}) of 16.6 ± 0.4 was obtained for the $Am(OH)_3$ phase. The corresponding hydrolysis constants are listed in Table SOTERM-23. Similar values for Nd(III) hydrolysis were derived from the $Nd(OH)_3$(cr) solubility measurements.

Stadler and Kim (1988) investigate the pH dependence of $Am(OH)_3$(s) solubility in 0.1 M $NaClO_4$ and more concentrated Na chloride and perchlorate solutions at 25 ± 0.5 ºC. The effect of α-induced radiolysis on solubility was also studied using different total concentrations of ^{241}Am. The solid phase was not characterized in this work. Although the solid used in this work was different than that used by Silva et al. (1995, pp. 275-76), the reported solubility products are in agreement. It is unclear, however, if the same phase controls the Am solubility in these two cases, because of markedly different preparation conditions of the starting solids.

Kim et al. (1984) measured the solubility of $Am(OH)_3$(s) at I = 0.1 and 0.3 M $NaClO_4$, in the absence of CO_2 and at $pCO_2 = 10^{-3.5}$ atm, and attributed the solubility measured in terms of contributions from the hydroxy, carbonato- and mixed Am hydroxy-carbonato complexes. No characterization of the solid was reported in this work, so it was proposed to be $AmCO_3OH$(s). Several investigators found that changes in the solid phase in aqueous suspensions of Am(III) hydroxide due to aging conditions became evident in hours and continued for weeks. Similar results were reported by Felmy, Rai, and Fulton (1990). These authors measured the solubility of $AmCO_3OH$(cr) at $pCO_2 = 10^{-3}$ atm. The change in total Am concentration measured in this work as a function of pH was similar to that reported by Kim et al. (1984). Similar plots for the solubility of Nd in 5 M NaCl were measured by Borkowski et al. (2009); however, the Nd concentrations obtained for the comparable pC_{H+} values were two to three orders of magnitude greater as a result of the higher ionic strength present.

Table SOTERM-23. Hydrolysis Constants of Am(III) (in Logarithmic Units) Corresponding to Equation SOTERM.18.

$AmOH^{2+}$	$Am(OH)_2^+$	$Am(OH)_3(aq)$	Medium	Reference
-7.93 ± 0.35	-14.77 ± 0.25	-24.71 ± 0.11	0.1 M $NaClO_4$	Kim et al. 1984
-7.5 ± 0.3	-15.4 ± 0.4	-26.9 ± 0.5	0.1 M $NaClO_4$	Stadler and Kim 1988
-7.8 ± 0.4	-15.4 ± 0.5	-26.9 ± 0.5	0.1 M NaCl	Stadler and Kim 1988
-8.1 ± 0.3	-15.8 ± 0.4	-27.0 ± 0.5	0.6 M NaCl	Stadler and Kim 1988
-7.7 ± 0.3	-16.7 ± 0.7	-25.0 ± 0.3	0.1 M $NaClO_4$	Silva et al. 1995, p. 81
-6.9 ± 0.2		-23.8 ± 0.9	0.1 M $NaClO_4$	Rösch et al. 1989
<-8.2	-17.1 ± 0.7	<-27.0	I → 0	Rai et al. 1983
-6.40 ± 0.11	-13.40 ± 0.16	-20.31 ± 0.17	3 M $NaClO_4$	Pazukhin and Kochergin 1989
-7.0 ± 0.4	-15.1 ± 0.4	-26.4 ± 0.5	0.1 M $NaClO_4$	Silva et al. 1995, p. 294
-7.2 ± 0.5	-15.1 ± 0.7	-26.2 ± 0.5	I = 0.1 M	Neck et al. 2009, p. 1557

Am complexation by carbonate was extensively investigated by solvent extraction, spectrophotometry, electromigration, and solubility (Kim et al. 1984; Rösch et al. 1989; Felmy, Rai, and Fulton 1990; Meinrath and Kim 1991; Nitsche et al. 1995; Torretto et al. 1995). Many different soluble species have been proposed for the Am-water-carbonate system: pure carbonate, bicarbonate, and/or mixed hydroxy-carbonate complexes. Silva et al. (1995) carefully studied and reinterpreted the literature data. It is the consensus in these studies that $Am(CO_3)_n^{(3-2n)}$, with n = 1, 2 and 3, are the predominant carbonate complexes. According to Silva et al. (1995), there is no experimental evidence for the existence of a complex with n = 4 even at the highest carbonate concentrations. The report also suggests that there is no evidence for the formation of Am(III)-bicarbonate or hydroxy-carbonate complexes in solution. These data are, however, in disagreement with the more recent work done by Fanghänel and Kim (1998), which reports spectroscopic evidence for the formation of the n = 4 species. In the WIPP model implementation, n=1-4 carbonate species are used (see SOTERM Section 6.5.1).

Data reported by Kim et al. (1984) indicate that up to pC_{H+} = ~8.0, the carbonate complexation does not affect the solubility of Am(III). Analysis of Yuci groundwaters by Chen et al. (2010), with a composition and E_h intermediate to the Yucca Mountain J-13 and UE-25 well compositions, demonstrates an americium carbonate solubility of 1.8×10^{-9} M at pH = 7.0 and 1.2×10^{-9} M at pH = 8.5 when equilibrated against solid $AmOH(CO)_3$. The presence of 10^{-4}– 10^{-2} M carbonate was shown not to influence americium solubility in the pH range of 8-10. For the higher pC_{H+}, the presence of carbonate in 0.1-0.3 M $NaClO_4$ increases solubility of Am(III) in relation to carbonate-free systems, and at pC_{H+} = 10 this difference is almost 4 orders of

magnitude. The predominance of carbonate complexation is observed in the pC_{H+} range from 7.5 to 10. At higher pC_{H+}, hydrolysis predominates over carbonate complexation.

Neck et al. (2009) used known data on the solubility of $Am(OH)_3$, the hydrolysis of Am(III) and Cm(III), additional data from an extensive solubility study of $Nd(OH)_3(s)$ in NaCl, $MgCl_2$ and $CaCl_2$ media of various ionic strength media and time-resolved laser fluorescence spectroscopy (TRLFS) data for Cm(III) in alkaline $CaCl_2$ to evaluate a comprehensive set of standard-state equilibrium constants and ion interaction parameters for the specific ion interaction theory SIT and Pitzer equations at 25 °C in the M(III) - H^+ - Na^+ - Mg^{2+} - Ca^{2+} - Cl^- - OH^- - H_2O system. The solubility and hydrolysis behavior of Am(III), Cm(III) and Nd(III) in both calcium-free and calcium-containing solutions is consistently described using a model that includes the ternary Ca-M(III)-OH complexes $Ca[M(OH)_3]^{2+}$, $Ca_2[M(OH)_4]^{3+}$ and $Ca_3[M(OH)_6]^{3+}$. Data are presented in Neck Tables 1, 2 and 3 (Neck et al. 2009) for the SIT and Pitzer parameters for this system. Solubility studies in NaCl – NaOH, $NaClO_4$ – NaOH, pure NaOH and KOH solutions up to pH = 14 showed no evidence for the formation of $Am(OH)_4^-$, which would increase the americium solubility at high pH. Study of the TRLFS behavior of curium in alkaline solutions of various media at pH > 10 showed that $Cm(OH)_3(aq)$, which would be expected to dominate the speciation at pH = 11-14, nor the complex $Cm(OH)_4^-$, could be detected, primarily due to low curium solubility. Almost all of the curium is present as $Cm_m(OH)_{3m}$ polymers or colloidal $Cm(OH)_3(am)$. In alkaline $CaCl_2$ solutions at I = 0.1 – 3M and pH ~ 10.5, as opposed to the sodium-based media above, the behavior of curium is strikingly different. Cm(III) emission bands were observed caused by complexes with three, four and six OH^- ligands. These complexes, not found in NaCl – NaOH media, are stabilized by the association of Ca^{2+} ions, e.g., the ternary complexes $Ca_p[Cm(OH)_n]^{3+2p-n}$. Stability constants for the complexation reaction:

$$pCa^{2+} + Cm^{3+} + nH_2O = Ca_p[Cm(OH)_n]^{3+2p-n} + nH^+ \qquad \text{(SOTERM.15)}$$

are log ${}^*\beta^o_{1,1,3}$ = -26.3 ± 0.5, log ${}^*\beta^o_{2,1,4}$ = -37.2 ± 0.6 and log ${}^*\beta^o_{3,1,6}$ = -60.7 ± 0.5. These reactions do not affect the WIPP case under current conditions.

An extensive series of experiments, reported for CRA-2009, were performed to determine the solubility of Nd(III) as an analog for Pu(III) and Am(III) solubility in the brine (Borkowski et al. 2009). In this study, the solubility was determined in GWB and ERDA-6 brine, over a pH range of 6-12, and as a function of carbonate concentration. These solubility data extended earlier studies in simplified brines to simulated WIPP brine compositions and cover a broader range of experimental conditions. A composite of literature and WIPP-specific data is shown in Figure SOTERM-27.

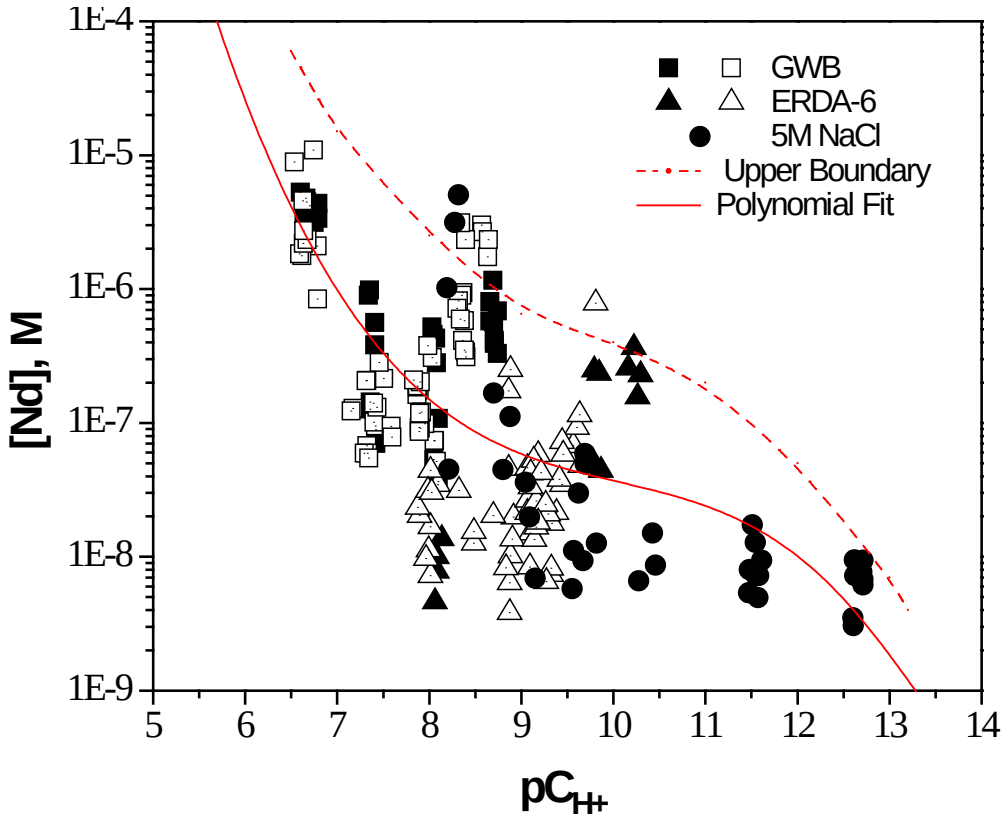

Figure SOTERM-27. Composite of Nd Solubility Trends Under All Conditions Investigated (Borkowski et al. 2009). Open Symbols Correspond to Undersaturation Experiments and Closed Symbols Correspond to Oversaturation Experiments.

SOTERM-5.8.2 New Literature Results Since CRA-2014

Hinz et al. (2015) studied the complexation behavior of borate with neodymium and curium in NaCl, $MgCl_2$ and $CaCl_2$ solutions. Borate was demonstrated to decrease neodymium solubility in dilute NaCl and $MgCl_2$ solutions at $pH_c \leq 9$ with $[B] \geq 40$ mM as well as in concentrated NaCl and $MgCl_2$ solutions with $[B] \geq 160$ mM. Experimentation with curium, known for its use in time-resolved laser-induced fluorescence experimentation and a suitable analog for neodymium, indicates that two-different borate species are likely responsible for the solubility behaviors observed.

SOTERM-5.8.3 WIPP-Specific Results since the CRA-2014 PA

There are no new WIPP-specific data since CRA-2014 that are centered on the solubility of An(III) in brine. An(III) data that pertains to biocolloid and intrinsic colloid formation were re-assessed CRA-2019 PA (see discussion in SOTERM Sections 3.5 and 4.2).

SOTERM-6.0 Calculation of the WIPP Actinide Source Term

A general description of the conceptual model used to define the actinide mobile concentration (e.g., actinide source term), an overview of the changes implemented in CRA-2019, and the current description and assessment of the oxidation-state-specific actinide models used in this process are given in this section. The calculated WIPP mobile actinide source term is a critical input into the overall assessment of the release of TRU from the WIPP through the DBR and transport scenarios.

The detailed calculational approach for the actinide source term used for CRA-2019 is described in Appendix PA (U.S. DOE 2019, Appendix PA Section 4.4). This was done using the computer code EQ3/6 (Wolery 1992; Wolery and Daveler 1992; Wolery 2008; Wolery et al. 2010) version 8.0a and the database DATA0.FM4 (Domski 2019b), the actinide solubilities modeled (Domski and Sisk-Scott 2019), the associated actinide uncertainties determined (Domski 2019a) and the element-specific colloid parameters (Reed et al. 2019a).

SOTERM-6.1 Overview of WIPP Approach to Calculate Mobile Actinide Concentrations

The overall approach used to establish the key actinides, and correspondingly their mobile concentration, important in WIPP release calculations is summarized in this section (See CRA-2019 Appendix PA Section 4.4 for a more detailed discussion). This approach consists of the following:

- Assess the WIPP inventory and regulations that govern the recertification of the WIPP to determine the likely actinides of interest and, correspondingly, the key waste components that may affect their solubility.
- Establish a conceptual model for the key subsurface interactions and release mechanisms. This is done using a combination of literature review and WIPP-specific experimental results to establish the likely oxidation state distribution, the species that affect actinide solubility, and the parameters required to model the system at high ionic strength. This approach features the following:
    - Conservative assumptions (i.e., those that lead to defensibly higher predicted concentrations), within the bounds of the conditions expected, for the oxidation state distributions.
    - Use of redox-invariant analogs for multivalent actinides to determine formation constants for complexants and establish oxidation-state-specific solubilities and interactions.
    - Use of the Pitzer activity-coefficient model and associated parameters to model solubilities at the high ionic strengths present. The Pitzer approach is recognized as the best approach for I > 3 M in brine systems (NEA 1997).
    - Calculate the solubility of the key actinides in the WIPP using the EQ3/6 code and the associated WIPP Pitzer database (Domski 2019b; Domski and Sisk-Scott 2019). The solubilities are modeled in reacted GWB and ERDA-6 brines and reflect the

effects of selected organic complexation (see SOTERM Section 3.3 for the organics modeled in PA). This is expected to bracket the range in the composition of the brine after repository closure.

- Establish the colloidal contributions to the solubilities calculated (See Reed et al. 2013; SOTERM Section 3.5; and CRA-2019 Appendix GEOCHEM Section 5 for a detailed description and assessment of the WIPP colloid model).
- Tabulate and assign uncertainty distributions in the range of expected conditions and brine compositions to these mobile actinide concentration data. The details of this method are in CRA-2019 Appendix GEOCHEM Section 5 and the distribution used is given in Domski (2019a).

This range of possible mobile concentrations for the range of possible conditions expected defines the actinide source term that is used in WIPP PA for the calculation of TRU release from the WIPP.

SOTERM-6.1.1 WIPP Mobile Actinide Source Term

The principles of actinide/brine chemistry model development and implementation, established in the CCA times (ASTP), have not changed and continue to be followed. The host rock (halite and interbeds) is also critical in that it provides self-sealing and isolation, helps define the range in composition in high ionic-strength brines, and potentially makes available interbed materials that interact with the emplaced waste and materials. That being said, it is also clear that many, if not most, of the key chemical parameters are established by the introduced waste/materials and the associated chemistry in the salt repository concept. This feature is somewhat unique in repository concepts as it is realistically expected that the waste/material components and engineered barrier chemistry will predominate throughout the 10,000 year performance lifetime.

Within this framework, the development of an actinide/chemistry model involved the following critical steps:

1) Establish the relevant chemistry and scope of the model. This was done by a combination of site characterization and careful tracking and understanding of the chemistry associated with the emplaced waste and engineering materials. What is relevant to the WIPP is what is emplaced in the repository and their interactions with the host rock components and introduced brines. These interactions are well understood (see discussion in SOTERM Section 3.2), and form the basis of benchmarking and challenging the predictions of the WIPP model. This predictive challenge using site-relevant experiments was established as a core approach in the ASTP that supported the CCA (U.S. DOE 1996). Track inventory as a key input to the overall PA process. The projected inventory is tracked annually for WIPP project planning activities. The PAIR 2018 TRU waste inventory, and its evolution as a function of time, are key inputs used in the implementation of PA for WIPP recertification.

2) Account for the key contributions made by the reactive properties of the emplaced Fe(0) and the MgO engineered barrier.

    a. The reactivity of MgO defines the repository pH and carbon dioxide fugacity. This sets a reasonably well-defined foundation for the brine chemistry that will establish the solubility of the actinides. From the point of view of actinide immobilization, it is important that this brine chemistry is mildly alkaline pH (~ 9.5) and relatively low in carbonate (typically < 10 mM). The presence of MgO also greatly improves the predictability of the expected chemistry in the repository and this predictability improves the defensibility of the calculated solubilities because it lessens the uncertainty.

    b. The reactivity of Fe(0), mainly introduced as container material for the emplaced waste, defines the reducing environment and redox conditions that are expected within the WIPP concept. The presence of a redox controlling material, such as iron, is critical to the overall performance of the WIPP. Iron not only effectively scavenges oxygen (via corrosion) to very quickly drive the repository towards anoxic conditions, its corrosion essentially pumps Fe^{2+} species into the brine which is an effective reductant of multivalent actinides. In this context, the iron chemistry has the key role in defining the actinide oxidation state distribution in the WIPP model. Magnetite, which is a stable Fe(II/III) iron oxide phase, likely establishes the upper redox boundary under WIPP-relevant conditions. The Fe(0), Fe(II), and to a lesser extent, Fe(III) iron chemistry all contribute to defining the range of redox conditions predicted in the WIPP.

3) Establish the range in redox conditions for the mobile actinide source term. The E_h under the expected repository conditions cannot be directly measured or calculated in a meaningful way that translates to the prediction of actinide oxidation-state distributions. This is done qualitatively and used to assign a range in the redox conditions. In this case, the actinide oxidation-state distribution can be determined by a combination of expert opinion (U.S. DOE 1996), available site-specific data, and calculations using the bounding conditions for the redox conditions expected. The boundary conditions on the most reducing side of the redox range are set by hydrogen fugacity and Fe(0) to be at or near the water stability field for the expected range in pH. These strongly reducing conditions correspond to the most reduced oxidation state of the relevant multivalent actinides. The upper boundary cannot be defined in a straightforward way and includes the Fe(0)-impacted limit combined with residual WIPP-relevant processes that could lead to slightly more oxidized conditions (but still reducing overall). In the WIPP, the most important of these processes are radiolysis, residual oxidants (e.g., nitrates, oxidized metals) emplaced in the WIPP, produced and emplaced Fe(III) phases that span the redox stability field expected, and organics that may preferentially solubilize higher-valent actinides. This is not explicitly set by the conceptual model, but project-specific data points toward the stability field of magnetite as an upper E_h boundary. Less reducing conditions have always been acknowledged as possible but do not persist in the WIPP when there are available Fe(0/II) phases (Reed et al. 2007; 2010).

4) Define defensible (e.g., conservative) oxidation-state-specific actinide solubility models based on expert opinion, site-relevant data, and the best available literature/data. This will

be used to calculate the source term for each key actinide and associated oxidation state. This was not trivial and was based on a combination of the availability of data, Nuclear Energy Agency (NEA) guidelines for data selection (NEA 1997), and a general understanding of the range and importance of the relevant chemistry. Critical phases predicted in the mildly alkaline pH range are hydroxo, carbonato, oxide and various ternary salts for some oxidation states. In the high magnesium and complex brine systems predicted, amorphous phases will dominate experimental results over the typical timeframe of experiments performed (<10 years) although specific crystalline phases may be obtained in simplified brine systems. The prevalence of crystallinity in the 10,000 period of repository evaluation for complex brine systems is not certain although predicted by the Ostwald step rule (Santen 1984). Crystalline phases are almost always lower in solubility and in some cases much lower in solubility. For this reason, the WIPP has always utilized well-defined amorphous phases in its PA implementation. This use would define defensible upper limits to actinide concentrations. In the implementation of solubility studies, it is often difficult to define the phase that is controlling solubility, particularly when multiple phases are present/expected. Additionally, the equilibration and transformation time between crystalline and amorphous forms of the same phase can vary with pH and brine composition. The many conservatisms in the WIPP model (see discussion in the following section) continue to support WIPPs certification in CRA-2019.

SOTERM-6.1.2 Conservatisms and Assumptions in the WIPP Source-Term Modeling Approach

The WIPP solubility model, although strategically simple in design, remains defensible because it includes a number of conservatisms and simplifications that lead to an overprediction of actinide solubility. This subsequently leads to an overprediction of potential releases in PA calculations. The most important of these are given in this section:

Assumptions that simplify PA calculations:

1) Well-mixed repository: The emplaced waste (TRU, iron/lead, cement, oxyanions and organics), engineered barrier (MgO), and introduced brine are well mixed and equilibrated at all times. In this view, there are no sustained micro-environments and the actinide source term can be estimated based on the overall chemistry predicted by this homogenized mixture.
2) No-sorption assumption: Since the CCA, no credit is taken for sorption in defining the mobile actinide source term. This is a large conservatism built into the model that has a large impact on inventory-limited actinides (essentially Am, Cm, Ac, and Np). The conceptual model recognizes that there will be many phases within the WIPP that will be sorptive and in some cases highly sorptive. Iron minerals are the most important example of this. Lead oxides, phases of other metals, and microbes/biomass provide highly sorptive surfaces that in reality enhance immobilization.
3) No-incorporation assumption: The current model (also since the CCA), does not recognize phase incorporation, co-precipitation and solid solutions, all of which would lower the effective solubilities of the actinides.

4) Minimal-competition assumption: This has two aspects. First, metal cations, frequently present in WIPP at much higher concentrations than the actinides, will compete with the actinides for anionic complexants (most importantly, borate, carbonate and organic chelators). There are many metals that will be soluble in WIPP – most importantly, Ca^{2+}, Mg^{2+}, Fe^{2+}, Fe^{3+}, Pb^{2+}, Ni^{2+}, and likely others. All of these form well known and strong complexes with most of the organic ligands (see discussion in SOTERM Section 3.3) that are not fully accounted for in current PA calculations. Second, since element-specific oxidation states are calculated separately, the availability of organic chelators is exaggerated in that they are made fully available for each oxidation state and actinide. These two calculational simplifications have order-of-magnitude effects that increase the effective solubility of many of the key actinides (most importantly Pu(III), Am(III) and U(VI)).

Actinide Solubility and Mobile Concentration Assumptions:

1) Modeling of high ionic-strength brine systems using the Pitzer approach: The high ionic strength chemistry that is predicted in the WIPP is modeled using the standard Pitzer equation approach with limited coefficients to empirically describe the effects of high ionic-strength on actinide solubility. This approach, although empirical, works very well for the expected WIPP brine systems (see additional discussion in SOTERM Section 6.5).
2) Use of oxidation-state-invariant analogs for multivalent actinides: Lanthanides and actinides that have high redox stability are used as analogs for multivalent actinides (e.g., U, Np and Pu) to avoid the experimental complexity of having to define the oxidation state distribution accurately — something that is often very difficult to do. In the WIPP model, Th(IV) is used for all An(IV) actinides and Am/Nd are used for all An(III) actinides. This introduced a relatively small error (less than a factor of two) for the An(III) case, as Am and Nd are relatively good analogs. It, however, overpredicts the An(IV) solubility by 1-2 orders of magnitude since Th(IV) is used. It is important to note that the nature of the analogy matters, and this assumption is primarily used for modeling solubility. It does not extend well for other analogies used to define the source term, for example colloidal tendencies, and is not generally used in this way.
3) Amorphous and crystalline phases: Experimentally, when site-specific complex brines are used, most actinides will form amorphous phases and perhaps assemblages of more than one phase (even after ~ 10-year experiments). In many simplified brines (e.g., binary systems of NaCl, $CaCl_2$ or $MgCl_2$) crystalline phases can often form, although this is not always the case. The repository lifetime of 10,000 years is short from the perspective of geologic time, and disequilibria are known to persist in nature for millions of years. For all these reasons the selection of the solubility-controlling phase is not straightforward. The Ostwald step rule predicts that the tendency in nature is toward more highly crystalline phases and lower solubility; however, the timeframe of this process is not well defined and can be different for different phases of the same element. For these reasons, higher solubility amorphous phases are used to conservatively estimate solubility when there is a good case for their stability or metastability under WIPP-relevant conditions. When available, and expected, crystalline phases are used. Using amorphous phases introduces a 1-4 order of magnitude conservatism in the PA calculations.

4) Colloid model assumptions: In the WIPP, due to the high ionic-strength nature of the brine systems, which both suppress microbial growth and destabilizes classical colloid formation, little/no colloid formation is predicted. Humic and fulvic acids are unstable, microbial growth is not likely, classical colloidal associations are not stable and most mineral colloidal species are highly transient and should lead to precipitated immobilization processes rather than mobilization. The conservative assumptions currently employed in defining the enhancement parameters (see Reed et al. 2013) can lead to a significant increase in the calculated mobile actinide concentrations (see also tables in SOTERM Section 6.6.3) for some oxidation states (40-45% for An(III); factors of 2.5 to 27 for An(IV)) with little or no effect on others (~10% for An(V) and ~ 1% for An(VI)).

EPA-Directed Assumptions:

1) Complexation assumption (Cotsworth 2004): This required the project to account for the impacts of organic complexants, specifically acetate, oxalate, citrate and EDTA, on actinide speciation and solubility. These complexants, although likely unstable in the WIPP environment, are assumed to be non-degradable. Additionally, there are no measured inventory data for these complexants, especially in legacy waste that pre-dates 1970. For this reason, the inventory estimates are conservatively high. This assumption increases An(III) solubility by 1-2 orders of magnitude in currently implemented calculations and would increase the other oxidation state solubilities, as well if there were a more complete speciation description in the WIPP actinide model.
2) Microbial Assumption (Cotsworth 2005): This required the project to assume that there is an infinite availability of anhydrite from the interbeds that will provide excess calcium and sulfate into the brine chemistry. This was introduced to suppress methanogenic processes that would alter/reduce the carbonate generation equation (see SOTERM equations 3-5) and require biodegradation to proceed along the path of sulfate reduction. It has since been shown by the project (Swanson et al. 2016; also discussion in SOTERM Section 4.2.2) that methanogenesis is not a likely process within the WIPP.
3) Uranium (VI) Concentration Assumption (U.S. EPA 2005): The uranium (VI) concentration was set to 1 mM to account for the lack of data on the effects of carbonate on An(VI) solubility and the absence of an An(VI) model in the WIPP. Site specific data (Lucchini et al. 2007; 2010a; 2010b) show this to be approximately 3-4 orders of magnitude high (See also discussion in SOTERM Section 5.5.2). This remains a conservatism in CRA-2019 PA that overpredicts the concentration of U(VI) in the repository.

This list leads to a high degree of conservatism (defined here as overpredicting actinide concentrations) in the calculated mobile concentrations in the actinide source term and add to the overall defensibility of current PA calculations.

SOTERM-6.1.3 Overview of Changes Implemented in CRA-2019 PA

There was essentially no significant change in the overall WIPP modeling approach for the mobile actinide source term used in CRA-2019. There were, however, some key parameter

changes in the application of the chemistry and actinide chemistry models. The continuing key features and CRA-2019 changes are summarized below, but are described more extensively in CRA-2019 Appendix GEOCHEM:

- Primary reliance on the Pitzer approach using EQ3/6 for the actinide solubility calculations (Domski 2019a) was continued. Some SIT parameters were introduced for modeling lead and iron (see CRA-2019 Appendix GEOCHEM Section 4 for a more detailed discussion).
- The colloid enhancement parameters for the actinides were updated based on new WIPP-specific data, reanalysis to address comments received from the EPA, and published literature (see Reed et al. 2019a; CRA-2019 Appendix GOECHEM Section 5). These changes, overall, do not have a large impact on the mobile actinide concentrations although there are changes in the relative contributions (see additional discussion in SOTERM Section 6.6).
- Calcium and magnesium interactions with EDTA were added to the WIPP model. These have a large (~order of magnitude) effect on the calculated actinide solubilities as these effectively compete with EDTA and lower its effect on An(III) solubilities.
- The issue of radiolytic effects on actinide speciation is now screened in (as well as gas generation) and was considered in the evaluation of redox arguments for the actinide oxidation-state distributions. This is driven by the continuing/significant increase in the TRU content within the projected WIPP inventory and changes in the screening argument.
- The key changes in inventory (see SOTERM Section 3.1 and 5.2) are addressed. The 1700-fold increase in the lead inventory increases its relative importance and this is the justification for the addition of the lead model in CRA-2019. Although significant increases in the plutonium inventory are reported, plutonium is solubility limited and, other than the small increase in radiolysis, there are no changes in the modeling approach being used.

SOTERM-6.1.4 Critical Assessment of the Current WIPP Modeling Approach

The WIPP model remains a defensible model that overpredicts potential releases (see discussion in SOTERM Section 6.1.2). The overall modeling approach being used by the WIPP continues to support its certification. The modeling of high ionic-strength brine systems, however, remains an active area of research (see the many summaries within SOTERM Section 5). These collectively continue to affirm the path chosen by the WIPP project in the CCA and continue to establish the WIPP actinide/brine modeling as conservative from the point of view of overestimating the mobile actinide concentration and subsequently potential releases in WIPP PA.

SOTERM-6.2 Role, Importance and Impacts of the Actinide Inventory Data

The actinide inventory used in the CRA-2019 PA was the 2018 inventory (Van Soest 2018) that was summarized in SOTERM Section 5.2 (see Table SOTERM-11) for the key radioisotopes and SOTERM Section 3.1 (see Tables SOTERM-3 and SOTERM-4) for the emplaced materials. These inventory data lead to the following key implications on the calculation of the mobile actinide source term:

- MgO will be present in sufficient quantity to achieve its design goal of buffering the pH and carbonate levels should brine inundation occur. Additionally, there is a sufficient MgO to cement ratio (>5) to mitigate the effects of cement on pH (Kienzler et al. 2016).
- The WIPP remains an iron-dominated system and this will drive the system anoxic, and establish reducing conditions for the actinides. The projected low-valent iron inventory is 1.54×10^7 Kg (2.8×10^8 moles), which is well over a 1000 times the total TRU inventory projected.
- For the key transuranics (see Table SOTERM-24), only plutonium and neptunium have a high enough inventory to sustain solubility-controlled concentrations throughout the repository lifetime. The combination of relatively low activity and solubility for neptunium make it a small contributor to overall release. Thorium and uranium are present in excess and will also not be inventory limited.
- The inventories of curium and actinium (see Table SOTERM-24) are all too low to sustain solubility limits. Their concentration will be defined by the available inventory present.
- Americium is initially solubility limited. At 5000 years after emplacement, it is slightly below this limit and is well below this limit by 10,000 years after emplacement.

In the current model implementation, this prioritization established Am/Pu as the most important actinides in the early part of repository history, shows that only plutonium is solubility-limited throughout repository history, justifies the lower priority given to Ac, Cm, and supports a continued assessment of Np, Th, and U.

Table SOTERM-24. Comparison of Inventory-limited Concentration and Projected Solubility for the Actinides.

Actinide	Inventory at 2033 y (Kg)	Inventory-Defined Concentration (M)	[1]Calculated Mobile Concentration (M)	Ratio of Inventory to Calculated Concentration
Ac	3.6×10^{-4}	9.1×10^{-11}	5.12×10^{-7}	1.8×10^{-4}
Th	1.08×10^{3}	2.7×10^{-4}	1.22×10^{-7}	2213
U	1.28×10^{5}	3.1×10^{-2}	1.0×10^{-3}	31
[2]Np	48.5	1.2×10^{-5}	1.32×10^{-6}	9.1
Pu	1.56×10^{4}	3.8×10^{-3}	5.12×10^{-7}	7422
[3]Am	338	8.1×10^{-5}	5.12×10^{-7}	158
Cm	2.13	5.0×10^{-7}	5.12×10^{-7}	1.02

[1]Calculated based on the higher baseline solubility of the two brines (GWB or ERDA-6). (Domski and Sisk-Scott 2019).

[2]Np increases in inventory and has a concentration ratio of 73.3 at 5000y.

[3]Am is below inventory limit at 5000 y after emplacement.

SOTERM-6.3 Role and Use of Oxidation-State-Invariant Analogs

The solubility and speciation of multivalent actinides are often investigated with lanthanide and actinide analogs that mimic the property of interest but, for various reasons, provide an advantage to the experimenter (see specific examples in the critical review later in this section). The best example of this, used extensively in the WIPP modeling approach, is the use of redox-invariant analogs for the multivalent actinides, most notably Pu, to determine oxidation-state-specific properties (e.g., solubility or complexation). The advantage of these types of analogs is that they remove the uncertainty of oxidation-state change from the experiment, which is a complexity that can often lead to uncertain or incorrect interpretations of the results obtained.

For the TRU actinides, the redox-invariant analogs used are lanthanides or other actinides. Lanthanides, as 4f-electron elements, possess physical and chemical characteristics that make them good analogs for the actinides when they are redox-invariant under the conditions of the experiment. Correspondingly, actinides with their 5f-electron character also have good physical and chemical properties to be analogs for other actinides if they also have redox stability under WIPP-relevant conditions. This analog approach considerably simplifies experimental design and consequently improves the reliability of the experimental data (Choppin 1999).

A key argument for the use of analogs in WIPP-relevant experiments is that key complexants that define actinide solubility in the WIPP are hard-donor complexants (e.g., hydroxide, carbonate, borate, chloride, and/or sulfate). The use of lanthanides as analogs for actinides is based on observations in many extraction systems, along with the associated crystallographic data (Siekierski 1988) that show they are good analogs for compounds containing hard donor ligands (oxygen) where the cation-anion interactions are primarily electrostatic in nature. In this

context, Nd(III) is a good analog for the chemical behavior of Am(III) and Pu(III) under most circumstances in the WIPP. Not only do these species have the same 3+ charge, they also have similar ionic radii for coordination number 6 (CN=6): 97.5 pm for Am^{3+}, 98.3 pm for Nd^{3+}, and 100 pm for Pu^{3+} (Shannon 1976). In this context, the magnitudes of electrostatic attractions between these metal ions and corresponding ligands will be similar, yielding comparable thermodynamic stabilities.

Th is used by the WIPP as a redox-invariant analog for Pu(IV), U(IV), and Np(IV). The use of the Th^{4+} stability constants to represent the other An(IV) species is conservative. Th^{4+} is the largest of the tetravalent actinide ions. It therefore has the lowest charge density and, correspondingly, relatively weaker ionic interactions when compared to the other tetravalent actinides. This is best exhibited by its lower tendency towards hydrolysis and intrinsic polymer formation relative to the other actinides (see SOTERM Section 3.5). For these reasons, the use of Th^{4+} as an analog is conservative, as Th will likely be the most soluble of the actinides in the tetravalent state under comparable WIPP-relevant conditions.

To a lesser extent, actinides are used as analogs for each other, depending on the oxidation state. Np(V), which has much greater redox stability than Pu(V) and much more favorable spectroscopy, is often used as an analog for Pu(V). U(VI), which has much higher redox stability than Pu(VI) and Np(VI), is also used as an analog for these TRU actinides, although U(VI) is in fact a poor analog for Pu(VI) solubility. Am(III) and Cm(III) are also excellent analogs for Pu(III) as a result of their much greater redox stability and comparable ionic radii.

Critical Review of the Use of Analogs in the WIPP Model

The current implementation of the analog approach continues to support the overall goals of WIPP PA to provide a defensible safety case for DBR and transport scenarios.

The An(III) analog approach uses both Am^{3+} and Nd^{3+} data to model An(III) behavior. Pu, Nd and Am all are good analogs for each other and this approach does not lead to much calculational uncertainty in the model implementation. In this context, experimental advantages determine which is used (e.g., Am/Cm for spectroscopy; Nd for convenience and non-rad applications).

The An(IV) analog, in contrast, is less straightforward. Thorium is widely used in nuclear safety case applications because it is mildly radioactive (so easy to use) and is redox-invariant. This continues to provide a conservatively high estimate of the An(IV) solubility but the tendencies towards metastable and nano-colloidal species makes experimental evaluation somewhat difficult at the moderately high pH that is most relevant to the WIPP. From an actinide perspective, the most important An(IV) actinide is Pu(IV). This is most accurately modeled by Np(IV) or U(IV), rather than Th(IV), which had a distinctly different tendency towards hydrolysis than the other three actinides (see Figure SOTERM-28). This is particularly important in the evaluation of colloidal species associated with An(IV) and in fact it cannot be done in a straightforward manner. With the improvement of oxidation-state control and redox buffers (see Altmaier et al. 2017b), the options of using U(IV) and Np(IV) have greatly improved and can be utilized and matched to experimental considerations (Np for spectroscopy, U for low-rad applications).

There are really no good analogs for Np(V), which is the most important An(V) considered in PA. This should continue to be modeled with Np(V) data. Although we do not model An(VI) in PA, there are no good analogs for this chemistry. U(VI), Np(VI) and Pu(VI) have distinctly different solution properties and redox tendencies/stabilities. Of these, U(VI) is the most important and should continue to be modeled as U(VI).

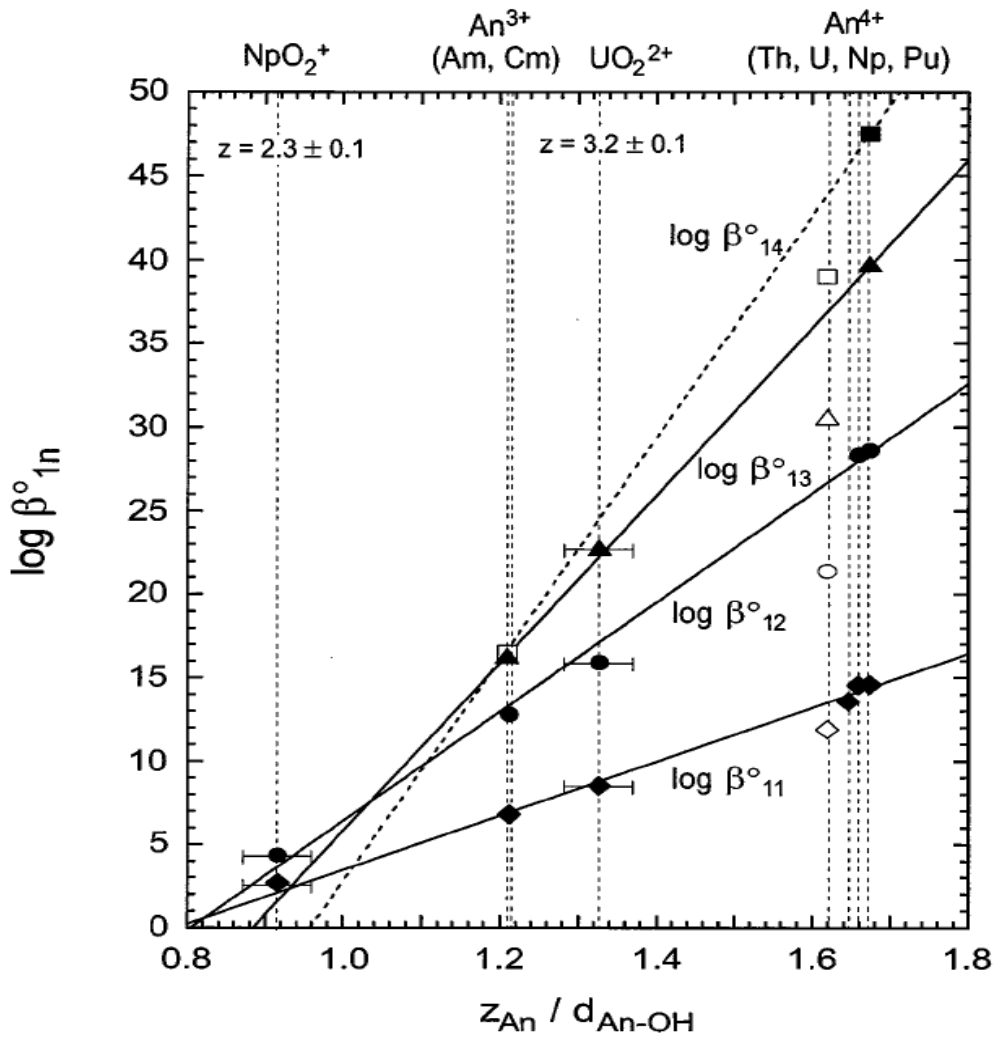

Figure SOTERM-28. Systematic Trends in An(IV) Hydrolysis Constants. Here the hydrolysis constants (log β^0_{1n}) are plotted against the ratio of the charge of the metal ion (Z_m) and the distance between the centers of the metal and the hydroxide (d_{An-OH}). Note that there is a Very Wide (Over 30 Orders of Magnitude) Range of Hydrolysis Constants for the An(IV) Actinides. The First Hydrolysis Constant for a Given Actinide (the Mono-Hydroxo-Complex) State is Given as log β_{11}, the Second as Log β_{12}, etc…, and Shown as Identical Symbols. The Data for Th(IV), Indicated as Open Symbols, Do Not Strictly Follow the General Trend Established by the Other Actinides (Altmaier et al. 2017b).

SOTERM-6.4 Redox and Oxidation State Distribution in the WIPP

The oxidation states used by the WIPP PA to model actinide solubility are tabulated in Table SOTERM-25. There are no changes to this distribution proposed and implemented in the CRA-2019 PA. Also included in this Table are the assumed abundance percent of each oxidation state and the speciation data set used in EQ3/6 for each oxidation state. This table is based on the general understanding of the corresponding actinide chemistry summarized in SOTERM Section 5.0.

Table SOTERM-25. Oxidation State Distribution of the Actinides in the WIPP Used in the CRA-2019 PA.

Actinide Element	Oxidation States, Abundance (%), and Analog Used (If Any)				
	Oxidation State[a,b]				
	III	IV	V	VI	EQ3/6 Speciation Data Used
Thorium	—	100 %	—	—	Thorium
Uranium	—	50 %	—	50 %	1 mM assumed for VI, Th for IV
Neptunium	—	50%	50 %	—	Np for V Th for IV
Plutonium	50 %	50 %	—	—	Am for III Th for IV
Americium	100 %	—	—	—	Americium
Curium	100 %	—	—	—	Americium

a Oxidation state distributions (percentages) refer to the percent of PA vectors that have 100% of the specified oxidation state.

b In PA calculations, the distribution of oxidation states is correlated for U, Np, and Pu such that the states for all three elements are simultaneously either in the lower oxidation state (U(IV), Np(IV), and Pu(III)) or in the higher oxidation state (U(VI), Np(V), and Pu(IV)).

There are a number of assumptions and simplifications reflected in this table:

1) Use of 1 mM concentration for the solubility of U(VI) as directed by the EPA. The actual solubility of U(VI) in the WIPP under the expected range of conditions is estimated to be <<0.1 mM.
2) Use of Th as an analog for the IV actinides (see discussion in SOTERM Section 6.3 and SOTERM Section 5.4).
3) The assumption that 50% of the vectors have Pu(III) and 50% of the vectors have Pu(IV) was implemented in the CCA to increase the degree of conservatism in that it was thought to exaggerate the amount of Pu(III) present.
4) The assumption of a probability that 50% of the vectors have U(IV) and 50% of the vectors have U(VI). The predominant uranium species expected is U(IV), which is approximately four orders of magnitude less soluble than U(VI), based on current assumptions.

Critical Assessment of WIPP Oxidation Distribution Model

The WIPP oxidation-state distribution model continues to be the subject of much discussion due to new short and long-term data within and outside of the WIPP project, and the inclusion in CRA-2019 of 6 metric tons of surplus plutonium. The core issue in this discussion is centered on the conservatism of the 50/50 assumption for Pu(III)/Pu(IV) distribution in the WIPP model but in fact affects all the oxidation assumptions within the model (see Reed 2018) if a consistent redox model is applied.

The project continues to confirm that only Pu(III) and Pu(IV) phases are observed under WIPP relevant conditions. The predominant Pu solid phase, based on currently available data (Reed 2018; Tasi et al. 2018) expected at pH > ~ 8 is Pu(IV). There are in fact no known Pu(III) high-pH crystalline phases although metastable amorphous phases can be formed. From a repository perspective, it is now clear that some Pu(III) is likely given these recent data. The project continues to confirm that strongly reducing conditions are established and sustained in WIPP-relevant systems (see full discussion in SOTERM Section 5.7). The extent that this remains a conservatism (meaning overpredicts [Pu] in the source term) is not straightforward as the solubility of Pu(III) in CRA-2019 is now less than a factor of three higher than the solubility of Pu(IV) phases. This places them in agreement (see discussion of conservatisms in SOTERM Section 6.1.2). This view is complicated by the much higher uncertainty associated with the An(IV) solubilities that makes the total concentration of Pu(IV) actually higher in many of the PA realizations evaluated.

That the WIPP is being shown to be more reducing than previously thought strengthens the WIPP safety case for plutonium containment. This overall issue is illustrated by Figure SOTERM-29. The more strongly reduced system puts greater distance between the redox conditions predicted and that needed to promote the formation of Pu(V) and Pu(VI) which have much higher solubilities. As the project moves toward a more realistic description of the Pu(III) and Pu(IV) chemistry, the baseline solubilities of these two oxidation states have approached each other, and in CRA-2019, only differ by a factor of approximately 3 (see Table SOTERM-26). These ratios can be quite different once the uncertainty distribution, which vary quite significantly between An(III) and An(IV) are included. This, in environmental systems, makes them within reasonable uncertainty of each other and approximately equivalent. As discussed in SOTERM Sections 5.5 and 5.7, there are also known An(IV) ternary species that may be important at high pH that are currently not in the WIPP model. These would increase the An(IV) solubility relative to An(III) and bring their concentration ratio even closer. The addition of more Pu, which in the brine will lead to slightly more oxidizing conditions, will in this context improve the overall safety case by poising the E_h more towards the Pu(IV) E_h/pH regime. The impacts of radiolysis on the actinide solution chemistry will push the redox in a positive direction (see discussion in SOTERM Section 3.4). So there is no question about directional impact on E_h of increased radiolysis, only a question of magnitude and correspondingly the extent that the iron chemistry will suppress/counter this effect.

A second issue is that it is not the relative solubility of the An(III) and An(IV) actinides that determines the overall effect on the mobile actinide source term. What directly impacts this is the PA implementation which, although based on solubility, also includes colloidal enhancements and the assigned uncertainty distributions. The associated uncertainties are significantly higher

for An(IV) than An(III). If conservatism alone is the argument for change, the oxidation state distributions should be assessed within the full implementation of PA and not simply based on solubility comparisons. In this context, it is possible that a shift to more Pu(III) would lead to a lower overall release. These solubilities, mobile concentrations, and associated PA implementation make these two oxidation states fairly close to each other and it makes the best sense to describe what is most credible rather than from the perspective of higher/lower apparent solubility.

Lastly, the WIPP conceptual model has always implied an effective E_h range by the actinide distributions used for the most and least reducing limits. It is important that this conceptualization be implemented consistently for all the actinides and not just for plutonium.

Table SOTERM-26. Ratio of the Baseline Solubility of Pu(III) and Pu(IV) Phases for each CRA Showing how this has Evolved with Time and PA Implementation.

Brine Formulation	Certification Application Year				
	CCA-PAVT	2004	*2009	2014	#2019
GWB	9.2	6.9	29.4	42.8	3
ERDA-6	3.2	4.2	21.6	21.1	3.3

*Organic complexation assumption implemented -main contributor to the observed solubility is the EDTA complex.

#Ca/Mg competition with EDTA introduced which mitigates the An(III) -EDTA enhancement.

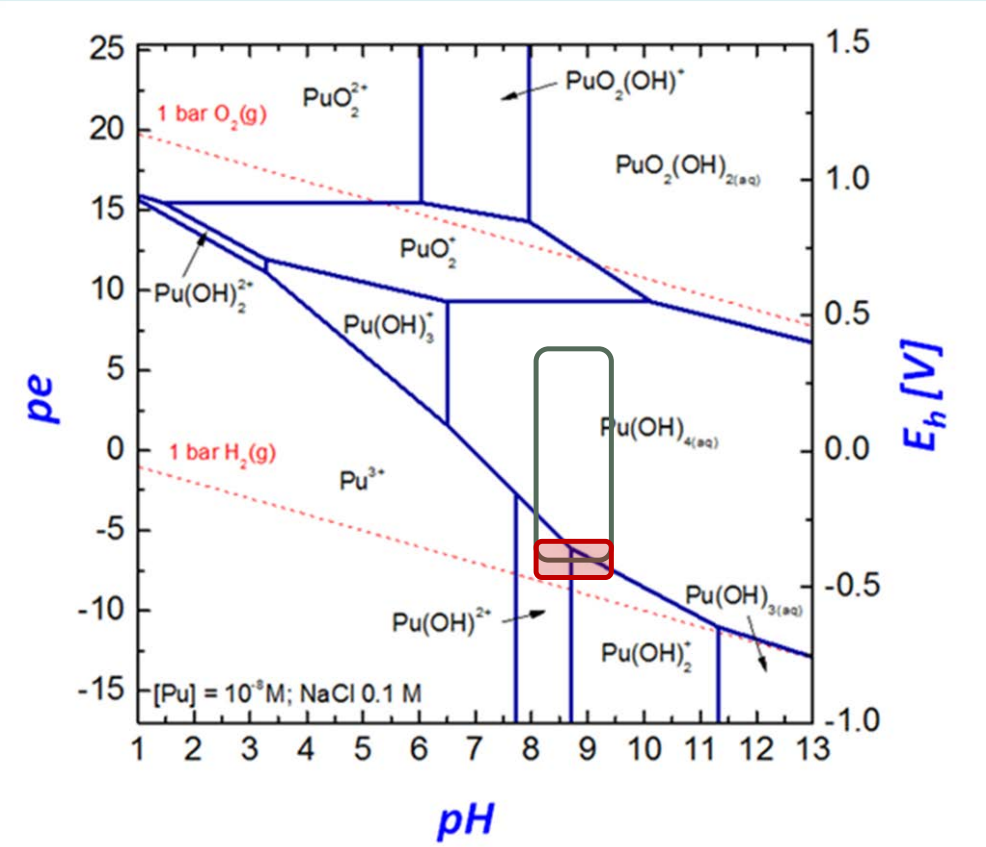

Figure SOTERM-29. Potential Shift in Redox View to Reflect a Lower E_h Range for WIPP (From the Larger Open Area, to the Lower Shaded Area)

SOTERM-6.5 Actinide Speciation Reactions Used in EQ3/6

The version of the database used with the EQ3/6 code for the CRA-2019 PA was DATA0.FM4 (Domski 2019b). This is a significant change from the DATA0.FM1 used in the CRA-2014 (see CRA 2019, Appendix GEOCHEM for explanations of the changes made). The actinide model that is the basis of current solubility calculations is summarized and assessed in this Section.

SOTERM-6.5.1 The III Actinides: Ac(III), Pu(III), Am(III), Cm(III)

The thermodynamic database for the III actinides currently used in EQ3/6 was described by Giambalvo (2002a) and updated by Wolery, Xiong and Long (2010). Nd, Am, and Cm are generally used to establish solubility of An(III) because, unlike plutonium, they have redox-stable trivalent oxidation states. Speciation and solubility data for the III actinides were parameterized for use in the Pitzer activity-coefficient model by Felmy et al. (1989) for the Na^+-Pu^{3+}-Cl^--H_2O system; by Felmy, Rai, and Fulton (1990) for the Na^+-Am^{3+}-OH^--HCO_3^--H_2O system; by Rai, Felmy, and Fulton (1995) for the Na^+-Am^{3+}-PO_4^{3-}-SO_4^{2-}-H_2O system; and by Rao et al. (1996) for the Na^+-Nd^{3+}-CO_3^{2-}-HCO_3^--H_2O system. EQ3/6 uses the Am(III) data to calculate the solubility for all the III actinides.

The aqueous and solubility-limiting species (See also Appendix GEOCHEM Table GEOCHEM-46) for Am(III) that represent An(III) in the WIPP model are:

Am(III) Reactions	log K	
Solid Formation Reactions		
$Am^{3+} + 3OH^- = Am(OH)_3(s)$	27.5	(SOTERM.17)
$Am^{3+} + OH^- + CO_3^{2-} \leftrightarrows AmOHCO_3(s)$	22.7	(SOTERM.18)
$Am^{3+} + Na^+ + 2CO_3^{2-} + 6H_2O \leftrightarrows NaAm(CO_3)_2 \cdot 6H_2O(s)$	21.4	(SOTERM.19)
$Am^{3+} + PO_4^{3-} \leftrightarrows AmPO_4(cr)$	24.8	(SOTERM.20)
Inorganic Aqueous Formation Reactions		
$Am^{3+} + CO_3^{2-} \leftrightarrows AmCO_3^+$	8.1	(SOTERM.21)
$Am^{3+} + 2CO_3^{2-} \leftrightarrows Am(CO_3)_2^-$	13.0	(SOTERM.22)
$Am^{3+} + 3CO_3^{2-} \leftrightarrows Am(CO_3)_3^{3-}$	15.2	(SOTERM.23)
$Am^{3+} + 4CO_3^{2-} \leftrightarrows Am(CO_3)_4^{5-}$	13.0	(SOTERM.24)
$Am^{3+} + OH^- \leftrightarrows AmOH^{2+}$	6.4	(SOTERM.25)
$Am^{3+} + 2OH^- \leftrightarrows Am(OH)_2^+$	12.3	(SOTERM.26)
$Am^{3+} + 3OH^- \leftrightarrows Am(OH)_3(aq)$	16.3	(SOTERM.27)
$Am^{3+} + Cl^- \leftrightarrows AmCl^{2+}$	0.24	(SOTERM.28)
$Am^{3+} + 2Cl^- \leftrightarrows AmCl_2^+$	-0.74	(SOTERM.29)
$Am^{3+} + SO_4^{2-} \leftrightarrows Am(SO_4)^+$	3.25	(SOTERM.30)
$Am^{3+} + 2SO_4^{2-} \leftrightarrows Am(SO_4)_2^-$	3.7	(SOTERM.31)
Organic Aqueous Formation Reactions		
$Am^{3+} + Acetate^- \leftrightarrows AmAcetate^{2+}$	2.74	(SOTERM.32)
$Am^{3+} + Citrate^{3-} \leftrightarrows AmCitrate(aq)$	8.80	(SOTERM.33)
$Am^{3+} + EDTA^{4-} \leftrightarrows AmEDTA^-$	18.97	(SOTERM.34)
$Am^{3+} + Lactate^- \leftrightarrows AmLactate^{2+}$	3.71	(SOTERM.35)
$Am^{3+} + Oxalate^{2-} \leftrightarrows AmOxalate^+$	6.16	(SOTERM.36)

In these reactions, “aq,” “cr,” and “s” are the abbreviations for aqueous, crystalline, and solid, respectively. The An(III) database was extended to mixed Na^+-CO_3^{2-}-Cl^-- media, and was shown to reproduce the independently measured solubility of $NaAm(CO_3)_2(s)$ in 5.6 M NaCl (Runde and Kim 1994) and the measured Nd(III) solubility in the WIPP brine (Borkowski et al. 2009).

The dominant speciation for the An(III) actinides is shown in Table SOTERM-27. The 1:2 hydroxide complex ($An(OH)_2^+$) accounts for 88% and 67% of the speciation for GWB and

ERDA-6, respectively. The 1:1 organic species for EDTA, citrate and acetate are also present as well, and these species with the hydrolysis complex account for approximately 99% of the An(III) speciation. The contributions of carbonate, sulfate, borate, and chloride, based on the current modeling assumptions, are negligible.

Table SOTERM-27. Predominant Species for the An(III) Actinides

Species	% Contribution to GWB	% Contribution to ERDA-6
$An(OH)_2^+$	88.17	66.79
$AnEDTA^-$	6.55	21.00
AnCit	2.06	6.10
$AnAc^{2+}$	1.71	4.79
Total % of Species Present	98.49	98.68

SOTERM-6.5.2 The IV Actinides: Th(IV), U(IV), Pu(IV), Np(IV)

The IV actinides addressed by the WIPP PA are Th(IV), U(IV), Pu(IV), and Np(IV). The variation in charge-to-radius ratio for the tetravalent actinides is greater than for actinides in other oxidation states (Cotton and Wilkinson 1988, pp. 11–46). This was also illustrated by Figure SOTERM-28. For this reason, larger differences in the chemical behavior among the IV actinides is expected. The application of the Th(IV) model to the other IV species (U(IV), Np(IV), and Pu(IV)) is more uncertain, yet still conservative because Th(IV) is the most soluble of these elements under WIPP conditions. The model was evaluated against data for Pu(IV) and Np(IV) solubility and demonstrated to predict the chemical behavior of these actinides conservatively (Altmaier et al. 2017b).

The thermodynamic database for the IV actinides currently used in EQ3/6 was described by Giambalvo (2002b). Speciation and solubility data for Th(IV) were parameterized for the Pitzer activity-coefficient model for the Na^+-K^+ -Mg^{2+}-Cl^-- SO_4^{2-}-CO_3^{2-}-HCO_3^- -OH^--H_2O system. This model requires the species Th^{4+}, $Th(OH)_2SO_4$ (s), $Th(SO_4)_3^{2-}$, $Th(SO_4)_2$ (aq), ThO_2, $Th(OH)_4$(aq), $Th(OH)_3CO_3^-$, and $Th(CO_3)_5^{6-}$ to describe the data pertinent to the WIPP (Felmy, Mason, and Rai 1991; Rabindra et al. 1992; Felmy et al. 1996).

The aqueous and solubility-limiting species (see also Appendix GEOCHEM, Table GEOCHEM-50) for Th(IV) that represent An(IV) in the WIPP model are:

Th(IV) Reactions	log K	
Solid Formation Reactions		
$Th^{4+} + 4OH^- \leftrightarrows ThO_2(am) + 2H_2O$	45.5	(SOTERM.37)
$Th^{4+} + 2SO_4^{2-} + 9H_2O \leftrightarrows Th(SO_4)_2{\cdot}9H_2O(s)$;	13.0	(SOTERM.38)
$Th^{4+} + 2SO_4^{2-} + 8H_2O \leftrightarrows Th(SO_4)_2{\cdot}8H_2O(s)$	12.9	(SOTERM.39)
$Th^{4+} + 2Na^+ + 3SO_4^{2-} + 6H_2O \leftrightarrows Th(SO_4)_2{\cdot}Na_2SO_4{\cdot}6H_2O(s)$	17.6	(SOTERM.40)

Th(IV) Reactions	**log K**	
$Th^{4+} + 2K^{+} + 3SO_4^{2-} + 4H_2O \leftrightarrows Th(SO_4)_2{\cdot}K_2SO_4{\cdot}4H_2O(s)$	18.1	(SOTERM.41)
$Th^{4+} + 4K^{+} + 4SO_4^{2-} + 2H_2O \leftrightarrows Th(SO_4)_2{\cdot}2K_2SO_4{\cdot}2H_2O\ (s)$	21.2	(SOTERM.42)
$Th^{4+} + 7K^{+} + 5.5SO_4^{2-} \leftrightarrows Th(SO_4)_2{\cdot}3.5K_2SO_4(s)$	24.7	(SOTERM.43)
Inorganic Aqueous Formation Reactions		
$Th^{4+} + 4OH^{-} \leftrightarrows Th(OH)_4(aq)$	38.5	(SOTERM.44)
$Th^{4+} + 3OH^{-} + CO_3^{2-} \leftrightarrows Th(OH)_3CO_3^{-}$	38.3	(SOTERM.45)
$Th^{4+} + 5CO_3^{2-} \leftrightarrows Th(CO_3)_5^{6-}$	27.1	(SOTERM.46)
$Th^{4+} + 2SO_4^{2-} \leftrightarrows Th(SO_4)_2(aq)$	11.6	(SOTERM.47)
$Th^{4+} + 3SO_4^{2-} \leftrightarrows Th(SO_4)_3^{2-}$	12.4	(SOTERM.48)
Organic Aqueous Formation Reactions		
$Th^{4+} + Acetate^{-} \leftrightarrows ThAcetate^{3+}$	7.36	(SOTERM.49)
$Th^{4+} + 2Acetate^{-} \leftrightarrows Th(Acetate)_2^{2+}$	11.2	(SOTERM.50)
$Th^{4+} + Citrate^{3-} \leftrightarrows ThCitrate^{+}$	15.2	(SOTERM.51)
$Th^{4+} + EDTA^{4-} \leftrightarrows ThEDTA(aq)$	23.6	(SOTERM.52)
$Th^{4+} + Lactate^{-} \leftrightarrows ThLactate^{3+}$	6.83	(SOTERM.53)
$Th^{4+} + 2Lactate^{-} \leftrightarrows Th(Lactate)_2^{2+}$	11.2	(SOTERM.54)
$Th^{4+} + Oxalate^{2-} \leftrightarrows ThOxalate^{2+}$	11.4	(SOTERM.55)

The predominant speciation for the An(IV) actinides is given in Table SOTERM-28. This is dominated by two species: the 1:4 neutral hydroxide complex and the 1:3:1 ternary hydroxy-carbonate complex. These two species account for ~ 100% of the speciation calculated based on current modeling assumptions.

Table SOTERM-28. Predominant Species for the An(IV) Actinides

Species	% Contribution to GWB	% Contribution to ERDA-6
$Th(OH)_4$ (aq)	82.33	82.44
$Th(OH)_3CO_3^{-}$	17.67	17.56
Total % of Species Present	100	100

SOTERM-6.5.3 The V Actinides: Np(V)

The only V actinide of interest to the WIPP is Np(V), which exists as the neptunyl ion, NpO_2^+. Pu(V), which can be formed under some conditions, is transitory and not expected to persist in significant quantities in the WIPP. The base model for Np(V) comes from Fanghänel, Neck, and Kim (1995), constructed for the German repository program.

The thermodynamic database for the V actinides currently used in EQ3/6 is described by (Giambalvo 2002c). Np(V) speciation and solubility were parameterized in the Pitzer activity-coefficient model for the Na^+-K^+ -Mg^{2+}-Cl^-- SO_4^{2-}-CO_3^{2-}-HCO_3^- -OH^--H_2O system. The model requires the aqueous species NpO_2^+, $NpO_2OH(aq)$, $NpO_2(OH)_2^-$, $NpO_2CO_3^-$, $NpO_2(CO_3)_2^{3-}$, and $NpO_2(CO_3)_3^{5-}$, and the solid species $NpO_2OH(am)$, $NpO_2OH(aged)$, $Na_3NpO_2(CO_3)_2(s)$, $KNpO_2CO_3{\cdot}2H_2O(s)$, $K_3NpO_2(CO_3)_2{\cdot}0.5H_2O(s)$, and $NaNpO_2CO_3{\cdot}3.5H_2O(s)$ to explain the available data.

The aqueous and solubility-limiting species (See Appendix GEOCHEM, Table GEOCHEM-55) for Np(V) that are used for the An(V) WIPP model are:

Np(V) Reactions	log K	
Solid formation Reactions		
$NpO_2^+ + OH^- \leftrightarrows NpO_2OH(s, aged)$	9.5	(SOTERM.56)
$NpO_2^+ + OH^- \leftrightarrows NpO_2OH(s, am)$	8.8	(SOTERM.57)
$Na^+ + NpO_2^+ + CO_3^{2-} + 3.5H_2O \leftrightarrows NaNpO_2(CO_3){\cdot}3.5H_2O(s)$	11.1	(SOTERM.58)
$3Na^+ + NpO_2^+ + 2CO_3^{2-} \leftrightarrows Na_3NpO_2(CO_3)_2(s)$	14.2	(SOTERM.59)
$K^+ + NpO_2^+ + CO_3^{2-} \leftrightarrows KNpO_2(CO_3)(s)$	13.6	(SOTERM.60)
$3K^+ + NpO_2^+ + 2CO_3^{2-} + 0.5H_2O \leftrightarrows K_3NpO_2(CO_3)_2{\cdot}0.5H_2O(s)$	-4.8	(SOTERM.61)
Inorganic Aqueous Formation Reactions		
$NpO_2^+ + OH^- \leftrightarrows NpO_2OH(aq)$	2.7	(SOTERM.62)
$NpO_2^+ + 2OH^- \leftrightarrows NpO_2(OH)_2^-$	4.5	(SOTERM.63)
$NpO_2^+ + CO_3^{2-} \leftrightarrows NpO_2CO_3^-$	5.0	(SOTERM.64)
$NpO_2^+ + 2CO_3^{2-} \leftrightarrows NpO_2(CO_3)_2^{3-}$	6.4	(SOTERM.65)
$NpO_2^+ + 3CO_3^{2-} \leftrightarrows NpO_2(CO_3)_3^{5-}$	5.3	(SOTERM.66)
Organic Aqueous Formation Reactions		
$NpO_2^+ + Acetate^- \leftrightarrows NpO_2Acetate(aq)$	1.37	(SOTERM.67)
$NpO_2^+ + Citrate^{3-} \leftrightarrows NpO_2Citrate^{2-}$	3.50	(SOTERM.68)
$NpO_2^+ + EDTA^{4-} + 2H_2O \leftrightarrows NpO_2H_2EDTA^- + 2OH^-$	-7.1	(SOTERM.69)

$NpO_2^+ + EDTA^{4-} + H_2O \leftrightarrows NpO_2HEDTA^{2-} + OH^-$	1.5	(SOTERM.70)
$NpO_2^+ + EDTA^{4-} \leftrightarrows NpO_2EDTA^{3-}$	8.54	(SOTERM.71)
$NpO_2^+ + Lactate^- \leftrightarrows NpO_2Lactate(aq)$	1.97	(SOTERM.72)
$NpO_2^+ + Oxalate^{2-} \leftrightarrows NpO_2Oxalate^-$	4.24	(SOTERM.73)

The predominant speciation of the An(V) actinides in WIPP is given in Table SOTERM-29. The dominant species, based on current modeling assumptions, is the acetate complex followed by the aquo species, the carbonato complex and organic complexes. The EDTA complex is a minor contributor.

Table SOTERM-29. Predominant Speciation for the An(V) Actinides in the WIPP

Species	% Contribution to GWB	% Contribution to ERDA-6
$NpO_2(Ac)$ (aq)	58.34	81.50
NpO_2^+ (aquo)	17.52	8.02
$NpO_2CO_3^-$	16.12	6.67
NpO_2Ox^-	6.66	2.79
NpO_2Cit^{2-}	0.85	0.61
$NpO_2(OH)$ (aq)	0.35	0.34
Total % of Species Present	99.84	99.93

SOTERM-6.5.4 The VI Actinides: U(VI)

The An(VI) EQ3/6 model has not been developed sufficiently for reliable use in predicting concentrations of this oxidation state in the WIPP brines under various solution conditions. Although uranyl carbonate can be successfully modeled, the hydrolysis behavior of U(VI) is quite complicated and no satisfactory predictive models applicable to WIPP-like conditions are yet available. Because the implementation of an MgO backfill limits the pmH and f_{CO_2} to discrete ranges, empirical measurement of the solubility of U(VI) in WIPP and/or WIPP–like brines became practical. As documented in Hobart and Moore (1996) and used in prior PA calculations, the solubility of U(VI) at pH 10, in the absence of carbonate, was determined to be 8.8×10^{-6} m. This is augmented by additional data from U(VI) solubility studies in WIPP-relevant carbonate-free brines reported in SOTERM Section 3.3.2 (Lucchini et al. 2010a, 2013a and 2013b). Here, the measured U(VI) solubility was 10^{-7} M to 10^{-6} M for GWB and ERDA-6 brine, respectively. The solubility of U(VI) currently used in the WIPP PA was directed by the EPA to be 1 mM (U.S. EPA 2005) to account for the potential effects of carbonate.

SOTERM-6.6 Calculations of Actinide Solubility Using the EQ3/6 Computer Code

Details of the implementation of EQ3/6 and the Pitzer approach for the WIPP are described in more detail elsewhere (Wolery 2008; Wolery and Jarek 2003; Wolery, Xiong and Long 2010;

Brush and Domski 2013, and NEA 1997. There is also some discussion in Appendix GEOCHEM Sections 4 and 5. EQ3/6 calculates chemical equilibrium for user-specified total element amounts in aqueous or aqueous/mineral geochemical systems. The EQ3/6 calculations of actinide solubility in the WIPP system performed for the WIPP PA included pre-equilibration with halite, anhydrite, brucite, and hydromagnesite (Domski and Sisk-Scott 2019), which are the minerals present in large quantities in the repository. The effects of the MgO backfill are realized by equilibrating brine with brucite, magnesite, and hydromagnesite.

SOTERM-6.6.1 Pitzer Approach for High-Ionic-Strength Brines

The Pitzer activity-coefficient model is substantially different in approach from the classic Debye-Hückel (D-H) theory of the behavior of ionic solutions. The latter is a theoretical approach to describing the behavior of dilute solutions. Because many ionic solutes do not behave ideally even at very low concentrations, D-H provides a means to calculate the activity, a_i, of a desired species. The Gibbs free energies of the various species in solution can be used to calculate solution equilibria if one knows the effective concentration of those species, i.e., their "activity" in solution. The activity of a given species i is tied to the molality of that species as $a_i = \gamma_i m_i$. Since the molality of species i is known, the unknown that must be calculated to determine a_i is, therefore, γ_i. The simplest form relating activity to molality from the D-H law is:

$$\log \gamma_i = -A_\gamma z_i^2 \left(\frac{\sqrt{I}}{1+\sqrt{I}} \right) \qquad \text{(SOTERM.74)}$$

where $A\gamma$ is the Debye-Hückel parameter, z_i is the charge of the ith species and I is the overall solution ionic strength. The fundamental difficulty with the D-H formalism is that even with extensions (Davies equation, B-dot equation) (Wolery 2008), the D-H law begins to deviate significantly from real solution behavior somewhere in the general region of I = 0.3 molal. As the WIPP brines (and many other highly concentrated ionic species of interest) are well above this level of ionic strength, many times with $I > 5$, another description is required to properly describe the activities of the ionic species.

In 1973, Pitzer proposed a set of semi-empirical equations to describe a_i. Pitzer (1973) wrote the Gibbs excess energy of a solution as a virial expansion, where a portion of the overall expansion can be expressed as a formalism similar to the D-H law and the majority of the remaining constants are empirically determined from measurements of the desired ions. The most general form of the equation is:

$$\ln \gamma_i = \left(\frac{z_i^2}{2} \right) f'(I) + 2\sum_i \lambda_{ij}(I) m_j + \sum_{ik} \left(\left(\frac{z_i^2}{2} \right) \lambda'_{jk}(I) + 3\mu_{ijk} \right) m_j m_k , \qquad \text{(SOTERM.75)}$$

where $f(I)$ is a Debye-Hückel function, $f'(I)$ is its derivative df/dI, the λ_{ij} are second-order interaction coefficients, $\lambda'_{ij}(I)$ is the derivative $d\lambda_{ij}/dI$, and the μ_{ijk} are third-order interaction coefficients. The experimentally observable values $\beta^{(0)}$, $\beta^{(1)}$, $\beta^{(2)}$, α_1, α_2, C^φ, and so forth are used to calculate the λ_{ij} and μ_{ijk} values needed to calculate γ_i (for more detail, see Wolery and Daveler 1992).

This approach has proven effective and has successfully described the behavior of solutions at high ionic strength. The disadvantage of this technique is that binary and ternary coefficients for the expansion are normally needed to completely describe all the activities of the different species; in addition, if the number of species in solution grows, the number of calculations grows that much faster, i.e., on the order of the cube of the number of species. Many of the terms describing neutral species can be legitimately neglected in geochemical systems.

This parameter-determination problem is of particular interest in the description of actinide behavior in the WIPP, since the GWB and ERDA-6 brines of interest contain a wide variety of ions in and of themselves, in addition to the actinides introduced into the repository. As a result of this, it was necessary to constrain the total number of possible species in solution, aqueous, solid or gas, and in addition, to determine Pitzer parameters for many species by analogy to others rather than by experimental measurement. This is the basis of the parameter and species selection in the current database, DATA0.FM4, which contains the parameters for those species incorporated into the limited species set description. In practice, this has worked well to describe solution behavior in the WIPP within a limited set of pH values at 25 ºC.

SOTERM-6.6.2 Calculated Actinide Solubilities

The oxidation-state-specific actinide solubilities calculated through the CRA-2019 are summarized in Table SOTERM-30. For historical perspective, the calculated solubilities from prior PA analyses are also tabulated. In the CRA-2019 PA, the data are shown for two brines in the presence of organics, and as a function of equilibration with hydromagnesite. The hydromagnesite case is recognized by the project as the most relevant to the WIPP. It is important to note that, overall, the calculated solubilities have not changed much over time except for the effects of increased and/or decreased complexation of the An(III) actinides with organics as the organic inventory and complexation model has changed.

As shown in Table SOTERM-30, the calculated solubility of the III actinides was 1.63×10^{-7} M to 1.78×10^{-7} M in the CRA-2019 PA. These solubilities have decreased by a factor of 8-16 relative to CRA-2014. The expected solubility of the IV actinides ranges between 5.45×10^{-8} M and 5.44×10^{-8} M and is essentially unchanged from CRA-2014 and independent of the brine composition. Overall the solubility of the IV actinides is around 3 times lower than that predicted for the III actinides. The main reason for decreases in An(III) concentrations noted in CRA-2019 PA was the addition of the Mg and Ca competition for the organics in the brines in the WIPP model.

Four organic ligands are included in EQ3/6 calculations of actinide solubilities. These are acetate ($CH_3CO_2^-$), citrate [$(CH_2CO_2)_2C(OH)(CO_2)^{3-}$], EDTA [$(CH_2CO_2)_2N(CH_2)_2N(CH_2CO_2)_2^{4-}$], and oxalate ($C_2O_4^{2-}$). The PAIR inventory of these complexing agents and their concentrations (used in solubility calculations) were summarized in Tables SOTERM-4 and SOTERM-6. These ligands are included in the solubility calculations because (1) approximately 60 organic compounds were identified among the nonradioactive constituents of the TRU waste to be emplaced in the WIPP (Brush 1990; Drez 1991; U.S. DOE 1996); (2) 10 of these 60 organic compounds could, if present in the WIPP, increase actinide solubilities because they are soluble in aqueous solutions such as the WIPP brines, and because they form complexes with dissolved actinides (Choppin 1988); and (3) of these 10 water-soluble organic ligands that form complexes

with actinides, 4 (acetate, citrate, EDTA, and oxalate) are included in PA and tracked in the WIPP inventory (see the CCA, Appendix SOTERM, p. 96).

Uncertainties in the solubility data are also accounted for in PA. This is discussed more completely in CRA-2019, Appendix PA Section 4.4, Appendix GEOCHEM Section 4, and Domski 2019a.

Table SOTERM-30. Historical Actinide Baseline Solubilities Calculated for the CRA-2004 PABC, the CRA-2009 PABC, CRA-2014 PA (Brush and Domski 2013, Table SOTERM-13), and CRA-2019 (Domski and Sisk-Scott 2019).

Actinide Oxidation State, and Brine	CRA-2004 PABC (M)	CRA-2009 PABC (M)	CRA-2014 PA (M)	CRA-2019 PA (M)
III, GWB	3.87×10^{-7}	1.66×10^{-6}	2.59×10^{-6}	1.63×10^{-7}
III, ERDA-6	2.88×10^{-7}	1.51×10^{-6}	1.48×10^{-6}	1.78×10^{-7}
IV, GWB	5.64×10^{-8}	5.63×10^{-8}	6.05×10^{-8}	5.45×10^{-8}
IV, ERDA-6	6.79×10^{-8}	6.98×10^{-8}	7.02×10^{-8}	5.44×10^{-8}
V, GWB	3.55×10^{-7}	3.90×10^{-7}	2.77×10^{-7}	4.02×10^{-7}
V, ERDA-6	8.24×10^{-7}	8.75×10^{-7}	8.76×10^{-7}	1.20×10^{-6}

SOTERM-6.6.3 Calculation of Colloidal Contribution to Actinide Solution Concentrations

The importance and role of colloids in defining the concentration of actinides in the WIPP was discussed in SOTERM Section 3.5, and more extensive discussions of WIPP-relevant results are available (Reed et al. 2013; CCA Appendix SOTERM, Section 6; Appendix GEOCHEM, Section 5). The PA conceptual approach used to account for colloidal enhancement of actinide concentrations was developed as part of the CCA and has not changed since this initial implementation. The four types of colloids identified as relevant to the WIPP are listed and described in Table SOTERM-31. For CRA-2019, although there is no change in the model, there were significant changes in how the parameters were determined (See discussion in SOTERM Section 3.5) as well as PA implementation (Sarathi 2019). The oxidation-state and brine-specific base solubility, colloidal contributions, and total mobile actinide concentrations are shown in Table SOTERM-32 for the median uncertainty case. These colloidal contributions, in the way the modeling is currently being implemented, make a significant contribution (factors of 2 to 27) to the source term for the An(III) and An(IV) actinides, which are the most important oxidation states in the WIPP safety case.

Table SOTERM-31. Classification of Four Colloid Types Considered by the WIPP PA

Mineral Fragment Colloids	Hydrophobic, hard-sphere particles that are kinetically stabilized or destabilized by electrostatic forces and may consist of crystalline or amorphous solids. Mineral fragments may be made kinetically stable by coatings with steric stabilizers that prevent close contact. Mineral fragments may act as substrates for sorption of actinides, or they may consist of precipitated or co-precipitated actinide solids.
Intrinsic Actinide Colloids	Intrinsic actinide colloids (also known as true colloids, real colloids, Type I colloids, and Eigenkolloide) are macromolecules of actinides that, at least in some cases, may mature into a mineral-fragment type of colloidal particle. When immature, they are hydrophilic; when mature, they become hydrophobic.
Humic Colloids	Humic substances are hydrophilic, soft-sphere particles that are stabilized by solvation forces. They are often powerful substrates for uptake of metal cations and are relatively small (less than 100,000 atomic mass units).
Microbial Colloids	Microbes are relatively large colloidal particles stabilized by hydrophilic coatings on their surfaces, which behave as steric stabilizing compounds. They may act as substrates for extracellular actinide sorption or actively bioaccumulate actinides intracellularly.

SOTERM-6.6.4 WIPP Actinide Source Term (Total Mobile Actinide Concentration)

A historical comparison of the dissolved, colloidal and total mobile actinide concentrations relative to past recertifications is given in Table SOTERM-33. Overall trends for An(III) and An(IV) are lower for all three concentrations relative to CRA-2014. The results for An(VI) are essentially unchanged.

Table SOTERM-32. Actinide Solubility and Colloidal Contributions for CRA-2019 (U.S. DOE 2019, Appendix PA Section 4.4)

An	Brine	Baseline Solubility	Uncertainty Exponent	Dissolved	Mineral	Intrinsic	Humic	Microbial (Corrected)	Sum Colloidal	Total Mobile
		mol/L	log10()	mol/L	mol/L	mol/L	mol/L	mol/L	mol/L	mol/L
Am(III)	**Castile(ERDA-6)**	**1.78E-07**	3.46E-01	3.95E-07	2.60E-08	9.50E-09	7.90E-08	2.30E-09	1.17E-07	**5.12E-07**
Am(III)	**Salado(GWB)**	**1.63E-07**	3.46E-01	3.62E-07	2.60E-08	9.50E-09	7.24E-08	2.30E-09	1.10E-07	**4.72E-07**
Np(IV)	**Castile(ERDA-6)**	**5.44E-08**	-9.96E-02	4.33E-08	2.60E-08	4.30E-08	4.33E-10	9.08E-09	7.85E-08	**1.22E-07**
Np(IV)	**Salado(GWB)**	**5.45E-08**	-9.96E-02	4.33E-08	2.60E-08	4.30E-08	4.33E-10	9.10E-09	7.85E-08	**1.22E-07**
Np(V)	**Castile(ERDA-6)**	**1.20E-06**	0.00E+00	1.20E-06	2.60E-08	4.30E-08	8.88E-09	3.80E-08	1.16E-07	**1.32E-06**
Np(V)	**Salado(GWB)**	**4.02E-07**	0.00E+00	4.02E-07	2.60E-08	4.30E-08	3.66E-10	3.80E-08	1.07E-07	**5.09E-07**
Pu(III)	**Castile(ERDA-6)**	**1.78E-07**	3.46E-01	3.95E-07	2.60E-08	4.30E-08	7.90E-08	3.80E-08	1.86E-07	**5.81E-07**
Pu(III)	**Salado(GWB)**	**1.63E-07**	3.46E-01	3.62E-07	2.60E-08	4.30E-08	7.24E-08	3.80E-08	1.79E-07	**5.41E-07**
Pu(IV)	**Castile(ERDA-6)**	**5.44E-08**	-9.96E-02	4.33E-08	2.60E-08	4.30E-08	4.33E-10	9.08E-09	7.85E-08	**1.22E-07**
Pu(IV)	**Salado(GWB)**	**5.45E-08**	-9.96E-02	4.33E-08	2.60E-08	4.30E-08	4.33E-10	9.10E-09	7.85E-08	**1.22E-07**
Th(IV)	**Castile(ERDA-6)**	**5.44E-08**	-9.96E-02	4.33E-08	2.60E-08	4.30E-08	4.33E-10	9.08E-09	7.85E-08	**1.22E-07**
Th(IV)	**Salado(GWB)**	**5.45E-08**	-9.96E-02	4.33E-08	2.60E-08	4.30E-08	4.33E-10	9.10E-09	7.85E-08	**1.22E-07**
U(IV)	**Castile(ERDA-6)**	**5.44E-08**	-9.96E-02	4.33E-08	2.60E-08	1.40E-06	4.33E-10	9.08E-09	1.44E-06	**1.48E-06**
U(IV)	**Salado(GWB)**	**5.45E-08**	-9.96E-02	4.33E-08	2.60E-08	1.40E-06	4.33E-10	9.10E-09	1.44E-06	**1.48E-06**
U(VI)	**Castile(ERDA-6)**	**1.00E-03**	0.00E+00	1.00E-03	2.60E-08	1.40E-06	1.10E-05	3.80E-08	1.25E-05	**1.01E-03**
U(VI)	**Salado(GWB)**	**1.00E-03**	0.00E+00	1.00E-03	2.60E-08	1.40E-06	1.10E-05	3.80E-08	1.25E-05	**1.01E-03**

Table SOTERM-33. Concentrations (M) of Dissolved, Colloidal, and Total Mobile Actinides Obtained Using Median Parameter Values for the CCA PAVT, CRA-2004 PABC, CRA-2009 PABC, CRA-2014 PA, and CRA-2019 PA.

Actinide Oxidation State and Brine	PAVT	CRA-2004 PABC	CRA-2009 PABC	CRA-2014 PA	CRA-2019 PA
Pu(III), dissolved, Salado brine	9.75 × 10-8	3.61 × 10-7	1.96 × 10-6	3.46 × 10-7	3.62 × 10-7
Pu(III), colloidal, Salado brine	7.48 × 10-8	2.04 × 10-7	9.87 × 10-7	7.21 × 10-7	1.79 × 10-7
Pu(III), total mobile, Salado brine	1.72 × 10-7	5.64 × 10-7	2.95 × 10-6	1.07 × 10-6	5.41 × 10-7
Pu(III), dissolved, Castile brine	1.06 × 10-8	2.68 × 10-7	1.78 × 10-6	1.98 × 10-7	3.95 × 10-7
Pu(III), colloidal, Castile brine	4.46 × 10-8	4.75 × 10-7	3.00 × 10-6	6.65 × 10-7	1.86 × 10-7
Pu(III), total mobile, Castile brine	5.52 × 10-8	7.44 × 10-7	4.79 × 10-6	8.62 × 10-7	5.81 × 10-7
Am(III), dissolved, Salado brine	9.75 × 10-8	3.61 × 10-7	1.96 × 10-6	3.46 × 10-7	3.62 × 10-7
Am(III), colloidal, Salado brine	3.96 × 10-7	1.39 × 10-6	7.45 × 10-6	9.57 × 10-8	1.10 × 10-7
Am(III), total mobile, Salado brine	4.93 × 10-7	1.75 × 10-6	9.41 × 10-6	4.42 × 10-7	4.72 × 10-7
Am(III), dissolved, Castile brine	1.06 × 10-8	2.68 × 10-7	1.78 × 10-6	1.98 × 10-7	3.95 × 10-7
Am(III), colloidal, Castile brine	7.78 × 10-8	1.34 × 10-6	8.88 × 10-6	3.01 × 10-7	1.17 × 10-7
Am(III), total mobile, Castile brine	8.83 × 10-8	1.61 × 10-6	1.07 × 10-5	4.98 × 10-7	5.12 × 10-7
Th(IV), dissolved, Salado brine	1.06 × 10-8	6.70 × 10-8	1.70 × 10-8	6.46 × 10-7	4.33 × 10-8
Th(IV), colloidal, Salado brine	1.25 × 10-7	6.56 × 10-7	1.86 × 10-7	4.12 × 10-6	7.85 × 10-8
Th(IV), total mobile, Salado brine	1.36 × 10-7	7.23 × 10-7	2.03 × 10-7	4.76 × 10-6	1.22 × 10-7
Th(IV), dissolved, Castile brine	3.33 × 10-8	8.07 × 10-8	2.11 × 10-8	7.50 × 10-7	4.33 × 10-8
Th(IV), colloidal, Castile brine	3.39 × 10-7	7.85 × 10-7	2.24 × 10-7	4.77 × 10-6	7.85 × 10-8
Th(IV), total mobile, Castile brine	3.73 × 10-7	8.65 × 10-7	2.45 × 10-7	5.52 × 10-6	1.22 × 10-7
U(IV), dissolved, Salado brine	1.06 × 10-8	6.70 × 10-8	1.70 × 10-8	6.46 × 10-7	4.33 × 10-8
U(IV), colloidal, Salado brine	9.26 × 10-8	4.48 × 10-7	1.33 × 10-7	4.13 × 10-6	1.44 × 10-6
U(IV), total mobile, Salado brine	1.03 × 10-7	5.15 × 10-7	1.50 × 10-7	4.77 × 10-6	1.48 × 10-6
U(IV), dissolved, Castile brine	3.33 × 10-8	8.07 × 10-8	2.11 × 10-8	7.50 × 10-7	4.33 × 10-8
U(IV), colloidal, Castile brine	2.36 × 10-7	5.35 × 10-7	1.59 × 10-7	4.78 × 10-6	1.44 × 10-6

Table SOTERM-33. Concentrations (M) of Dissolved, Colloidal, and Total Mobile Actinides Obtained Using Median Parameter Values for the CCA PAVT, CRA-2004 PABC, CRA-2009 PABC, CRA-2014 PA, and CRA-2019 PA (Continued).

Actinide Oxidation State and Brine	PAVT	CRA-2004 PABC	CRA-2009 PABC	CRA-2014 PAa	CRA-2019 PA
U(IV), total mobile, Castile brine	2.69×10^{-7}	6.15×10^{-7}	1.80×10^{-7}	5.53×10^{-6}	1.48×10^{-6}
Pu(IV), dissolved, Salado brine	**1.06×10^{-8}**	**6.70×10^{-8}**	**1.70×10^{-8}**	**6.46×10^{-7}**	**4.33×10^{-8}**
Pu(IV), colloidal, Salado brine	**9.67×10^{-8}**	**4.69×10^{-7}**	**1.39×10^{-7}**	**4.12×10^{-6}**	**7.85×10^{-8}**
Pu(IV), total mobile, Salado brine	**1.07×10^{-7}**	**5.36×10^{-7}**	**1.56×10^{-7}**	**4.76×10^{-6}**	**1.22×10^{-7}**
Pu(IV), dissolved, Castile brine	**3.33×10^{-8}**	**8.07×10^{-8}**	**2.11×10^{-8}**	**7.50×10^{-7}**	**4.33×10^{-8}**
Pu(IV), colloidal, Castile brine	**2.47×10^{-7}**	**5.60×10^{-7}**	**1.66×10^{-7}**	**4.77×10^{-6}**	**7.85×10^{-8}**
Pu(IV), total mobile, Castile brine	**2.80×10^{-7}**	**6.40×10^{-7}**	**1.87×10^{-7}**	**5.52×10^{-6}**	**1.22×10^{-7}**
U(VI), dissolved, Salado brine	7.07×10^{-6}	1.00×10^{-3}	1.00×10^{-3}	1.00×10^{-3}	1.00×10^{-3}
U(VI), colloidal, Salado brine	8.89×10^{-7}	1.31×10^{-5}	1.31×10^{-5}	1.11×10^{-5}	1.25×10^{-5}
U(VI), total mobile, Salado brine	7.96×10^{-6}	1.01×10^{-3}	1.01×10^{-3}	1.01×10^{-3}	1.01×10^{-3}
U(VI), dissolved, Castile brine	7.15×10^{-6}	1.00×10^{-3}	1.00×10^{-3}	1.00×10^{-3}	1.00×10^{-3}
U(VI), colloidal, Castile brine	3.69×10^{-6}	1.31×10^{-5}	1.31×10^{-5}	1.11×10^{-5}	1.25×10^{-5}
U(VI), total mobile, Castile brine	1.08×10^{-5}	1.01×10^{-3}	1.01×10^{-3}	1.01×10^{-3}	1.01×10^{-3}

SOTERM-7.0 References

(*Indicates a reference that has not been previously submitted.)

Allard, B. 1982. Solubilities of Actinides in Neutral or Basic Solutions. Actinides in Perspective. N. Edelstein, ed. New York: Pergamon Press. pp. 553–80. ISBN 978-0-08-029193-2

Allard, S., and C. Ekberg. 2006a. Complexing Properties of α-Isosaccharinate: Thorium. Radiochimica Acta 94: 537–540.

Allard, S., and C. Ekberg. 2006b. Complexing Properties of α-Isosaccharinate: Stability Constants, Enthalpies and Entropies of Th-Complexation with Uncertainty Analysis. Journal of Solution Chemistry 35: 1173–1186.

Altmaier, M., V. Neck and T. Fanghänel. 2004. Solubility and Colloid Formation of Th(IV) in Concentrated NaCl and $MgCl_2$ Solutions. Radiochimica Acta 92: 537–543.

Altmaier, M., V. Neck, R. Müller and T. Fanghänel, 2005. Solubility of ThO_2 xH_2O(am) in Carbonate Solution and the Formation of Ternary Th(IV) Hydroxide-Carbonate Complexes. Radiochimica Acta 93: 83–92.

Altmaier, M., V. Neck,, M. Denecke, R. Yinand T. Fanghänel. 2006. Solubility of ThO_2 $\cdot xH_2O$(am) and the Formation of Ternary Th(IV) Hydroxide-Carbonate Complexes in $NaHCO_3$-Na_2CO_3 Solutions Containing 0–4M NaCl. Radiochimica Acta 94: 495–500.

Altmaier, M., V. Neckand T. Fanghänel. 2008. Solubility of Zr(IV), Th(IV) and Pu(IV) Hydrous Oxides in $CaCl_2$ Solutions and the Formation of Ternary Ca-M(IV)-OH Complexes. Radiochimica Acta 96: 541-550.

Altmaier, M., V. Neck, J. Lützenkirchenand Th. Fanghänel. 2009. Solubility of Plutonium in $MgCl_2$ and $CaCl_2$ Solutions in Contact with Metallic Iron. Radiochimica Acta, **97**(4-5): p. 187-192. *

Altmaier, M., X. Gaona and T. Fanghänel, T. 2013. Recent Advances in Aqueous Aquatic Chemistry and Thermodynamics. Chemistry Reviews 113: 901-943. *

Altmaier, M., E. Yalçıntas, X. Gaona, V. Neck, R. Müller, M. Schlieker and T. Fanghänel. 2017a. Solubility of U(VI) in Chloride Solutions I: the Stable Oxides/Hydroxides in NaCl Systems, Solubility Products, Hydrolysis Constants and SIT Coefficients. The Journal of Chemical Thermodynamics 114: 2-13. *

Altmaier, M., D. Fellhauer, X. Gaona and E. Yalcintas. 2017b. Assessment of Np(IV) and U(IV) as Improved Analogs for Pu(IV) in High Ionic-Strength Brine Systems. KIT/INE Report, Karlsruhe, Germany. *

Ams, D.A., J.S. Swanson, J. Szymanowski, J.B. Fein, M. Richmann and D.T. Reed. 2013. The Effect of High Ionic Strength on Neptunium(V) Adsorption to a Halophilic Bacterium. Geochimica et Comoschimica Acta 110: 45-57.

Baik, M.H., E.C. Jung and J. Jeong. 2015. Determination of Uranium Concentration and Speciation in Natural Granitic Groundwater Using TRLFS. Journal of Radioanalytical and Nuclear Chemistry 305: 589-598. *

Banaszak, J.E., D.T. Reed, and B.E. Rittmann. 1998a. Speciation-Dependent Toxicity of Neptunium(V) Towards Chelatobacter heintzii. Environmental Science and Technology 32: 1085–1091.

Banaszak, J., B.E. Rittmann and D.T. Reed. 1998b. Subsurface Interactions of Actinide Species and Microorganisms: Implications for the Bioremediation of Actinide-Organic Mixtures. Argonne, IL: Argonne National Laboratory. ANL-98/26.

Banaszak, J.E., S.M. Webb, B.E. Rittmann, J.-F. Gaillard, and D.T. Reed. 1999. Fate of Neptunium in an Anaerobic, Methanogenic Microcosm. Materials Research Society Symposium Proceedings 556: 1141-1149.

Barkatt, A., A. Barkatt and W. Sousanpour. 1983. Gamma Radiolysis of Aqueous Media and Its Effects on the Leaching Processes of Nuclear Waste Disposal Materials. Nuclear Technology 60: 218-227. *

Barnhart, B.J., E.W. Campbell, E. Martinez, D.E. Caldwell and R. Hallett. 1980. Potential Microbial Impact on Transuranic Wastes under Conditions Expected in the Waste Isolation Pilot Plant (WIPP). Los Alamos National Laboratory. Los Alamos, NM. LA-8297-PR

Begemann, M.B., M.R. Mormile, O.C. Sitton, J.D. Wall and D.A. Elias. 2012. A Streamlined Strategy for Biohydrogen Production with Halanaerobium hydrogeniformans, an Alkaliphilic Bacterium. Frontiers in Microbiology 3: article 93. *

Bone, S., S. Kozimor and D.T. Reed. 2019. WIPP Pu Data: SSRL Beamline 11-2; March 2016. Los Alamos National Laboratory. Carlsbad NM. Los Alamos Report LA-UR-19-27778,*

Bonin, L., G. Cote, and P. Moisy. 2008. Speciation of An(IV) (Pu, Np, U and Th) in Citrate Media, Radiochimica Acta 96: 145–152. *

Booker, A.E., M.A. Borton, R.A. Daly, S.A. Welch, C.D. Nicora, D.W. Hoyt, T. Wilson, S.O. Purvine, R.A. Wolfe, S. Sharma, P. Mouser, D.R. Cole, M.S. Lipton, K.C. Wrighton, and M.J. Wilkins. 2017. Sulfide Generation by Dominant Halanaerobium Microorganisms in Hydraulically Fractured Shales. mSphere 2: e00257-17. *

Borkowski, M., J.-F. Lucchini, M.K. Richmann, and D.T. Reed. 2009. Actinide (III) Solubility in WIPP Brine: Data Summary and Recommendations. Los Alamos National Laboratory; Carlsbad, NM. LA-UR-10-14360.

Borkowski, M., M.K. Richmann, D.T Reed, and Y.-L. Xiong. 2010. Complexation of Nd(III) with Tetraborate Ion and its Effect on Actinide(III) Solubility in WIPP Brine. Radiochimica Acta 98: 577–582.

Borkowski, M., M.K. Richmann, and J.-F. Lucchini. 2012. Solubility of An(IV) in WIPP Brine: Thorium Analog Studies in WIPP Simulated Brine.. Los Alamos National Laboratory; Carlsbad, NM. LCO-ACP-17. LA-UR-12-24417.

Boukhalfa, H., S.D. Reilly, W.H. Smith, and M.P. Neu. 2004. EDTA and Mixed-Ligand Complexes of Tetravalent and Trivalent Plutonium. Inorg Chem**,** 43, 5816-5823. *

Brandt, K.K., F. Vester, A.N. Jensen, and K. Ingvorsen. 2001. Sulfate Reduction Dynamics and Enumeration of Sulfate-Reducing Bacteria in Hypersaline Sediments of the Great Salt Lake (Utah, USA). Microbial Ecology 41: 1-11. *

Brendebach, B., M. Altmaier, J. Rothe, V. Neck, and M. Denecke. 2007. EXAFS Study of Aqueous Zr(IV) and Th(IV) Complexes in Alkaline $CaCl_2$ Solutions: $Ca_3[Zr(OH)_6]^{4+}$ and $Ca_4[Th(OH)_8]^{4+}$. Inorganic Chemistry 46: 6804–6810.

Brown, M.A., A.J. Kropf, A. Paulenova, and A.V. Gelis. 2014. Aqueous Complexation of Citrate with Neodymium(III) and Americium(III): a Study by Potentiometry, Absorption Spectrophotometry, Microcalorimetry, and XAFS. Dalton Transactions 43: 6446-6454. *

Brunel B., V. Philippini, M. Mendes, and J. Aupiais. 2015. Actinide Oxalate Complexes Formation as a Function of Temperature by Capillary Electrophoresis Coupled with Inductively Coupled Plasma Mass Spectrometry. Radiochimica Acta 103: 27–37. *

Brush, L.H. 1990. Test Plan for Laboratory and Modeling Studies of Repository and Radionuclide Chemistry for the Waste Isolation Pilot Plant. SAND90-0266. Sandia National Laboratories; Albuquerque, NM. ERMS 226015.

Brush, L.H., D. Grbic-Galic, D.T. Reed, X. Tong, R.H. Vreeland, and R.E.Westerman. 1990. Preliminary Results of Laboratory Studies of Repository Chemistry for the Waste Isolation Pilot Plant. Materials Research Society Symposium Proceedings 212: 893-900. *

Brush, L.H. 1985. Position Paper on Gas Generation in the Waste Isolation Pilot Plant. Sandia National Laboratories: Albuquerque, NM. CONF-941244-1. *

Brush, L.H. 1995. Systems Prioritization Method—Iteration 2 Baseline Position Paper: Gas Generation in the Waste Isolation Pilot Plant (March 17). Albuquerque, NM: Sandia National Laboratories. ERMS 228740.

Brush, L. H., R.C. Moore, and N.A. Wall. 2001. Response to EEG-77, Plutonium Chemistry under Conditions Relevant for WIPP Performance Assessment: Review of Experimental Results and Recommendations for Future Work, by V. Oversby. Sandia National Laboratories; Carlsbad, NM. ERMS 517373.

Brush, L.H., and P.S. Domski. 2013. Prediction of Baseline Actinide Solubilities for the WIPP CRA-2014 PA. Analysis Report, January 21, 2013. Carlsbad, NM: Sandia National Laboratories. ERMS 559138.

Bundschuh, T., R. Knopp, R. Müller, J.I. Kim, V. Neck, and T. Fanghänel. 2000. Application of LIBD to the Determination of the Solubility Product of Thorium(IV)-Colloids. Radiochimica Acta 88: 625–629.

Büppelmann, K., S. Magirius, Ch. Liersem and J.I Kim. 1986. Radiolytic Oxidation of Am (III) to Am (V) and PU (IV) to Pu (VI) in Saline Solution. Journal of Less-Common Metals. Vol 122: 29-36.

Büppelmann, K., J.I. Kim, and C. Lierse. 1988. The Redox Behavior of Pu in Saline Solutions under Radiolysis Effects. Radiochimica Acta 44/45: 65–70.

Cabello, P., M.D. Roldán, and C. Moreno-Vivián. 2004. Nitrate Reduction and the Nitrogen Cycle in Archaea. Microbiology 150: 3527-3546. *

Cachoir, C., S. Salah, T. Mennecart, and K Lemmens. 2016. Uranium Dissolution in Hyperalkaline TMA-OH Solutions: Preliminary Results. Procedia Chemistry 21: 306-313. *

Caldwell, D.E., M.A. Molecke, E. Martinez, and B.J. Barnhart. 1987. Rates of CO_2 Production from the Microbial Degradation of Transuranic Wastes under Simulated Geologic Isolation Conditions. Sandia National Laboratories: Albuquerque, NM. SAND87-7170. *

Camphouse, R., D. Kicker, S. Kim, T. Kirchner, J. Long, B. Malama, and T. Zeitler. 2013. Summary Report for the 2014 WIPP Compliance Recertification Application Performance Assessment. Sandia National Laboratories; Carlsbad, NM. ERMS 560252.

Casas, I., J. De Pablo, J. Gimenez, M.E. Torrero, J. Bruno, E. Cera, R.J. Finch, and R.C. Ewing. 1998. The Role of pe, pH, and Carbonate on the Solubility of UO_2 and Uraninite under Nominally Reducing Conditions. Geochimica et Cosmochimica Acta 62: 2223–2231.

Cevirim-Papaioannou, N., E. Yalcintas, X. Gaona, K. Dardenne, M. Altmaier, and M.H. Geckeis. 2018. Redox chemistry of uranium in reducing, dilute to concentrated NaCl solutions. Applied Geochemistry, 98: 286-300. *

Chen, T., X. Wang, W. Tian, M. Sun, C. Li, X. Liu, L. Wang, and C. Liu. 2010. Solubility Analysis of Americium in Yuci Groundwater. Acta Physico-Chimica Sinica 26: 811-816.

Cho, H.-R., Y.-S. Youn, E.C. Jung, and W. Cha. 2016. Hydrolysis of Trivalent Plutonium and Solubility of Pu(OH)3 (am) under Electrolytic Reducing Conditions. Dalton Transactions 45: 19449-19457. *

Choppin, G.R. 1988. Letter to L.H. Brush. 29 December 1988. WIPP Central Files, Tallahassee, FL.

Choppin, G.R., and L.F. Rao. 1992. Reduction of Neptunium(VI) by Organic Compounds. Transuranium Elements: A Half Century (pp. 262–75). L.R. Morss and J. Fuger, eds. Washington, DC: American Chemical Society. INIS RN:24025811

Choppin, G.R. 1999. Utility of Oxidation State Analogs in the Study of Plutonium Behavior. Radiochimica Acta 85: 89–95.

Choppin, G.R., A.H. Bond, M. Borkowski, M.G. Bronikowski, J.G. Chen, S. Lis, J. Mizera, O. Pokrovski, N.A. Wall, Y.X. Xia, and R.C Moore. 1999. WIPP Actinide Source Term Test Program: Solubility Studies and Development of Modeling Parameters. Sandia National Laboratories; Albuquerque, NM. SAND 99-0943.

Choppin, G.R., J. Liljenzin, and J.O. Rydberg. 2004. Radiochemistry and Nuclear Chemistry. 3rd ed. Woburn, MA: Butterworth-Heinenmann.

Christensen, T.H., P.L. Bjerg, S.A. Banwart, R. Jakobsen, G. Heron, and H.-J. Albrechtsen. 2000. Characterization of Redox Conditions in Groundwater Contaminant Plumes. Journal of Contaminant Hydrology 45: 165-241.

Clark, D.L., D.E. Hobart, and M.P. Neu. 1995. Actinide Carbonate Complexes and their Importance in Actinide Environmental Chemistry. Chemical Reviews 95: 25-48.

Clark, D.L., and C.D. Tait. 1996. Monthly reports under Sandia National Laboratories Contract AP2274. Sandia WIPP Central File A: WBS 1.1.10.1.1. WPO 31106.

Cleveland, J.M. 1979. The Chemistry of Plutonium. La Grange Park, IL: American Nuclear Society.

Cotsworth, E. 2004. Letter from E. Cotsworth to P. Detwiler, EPA 3rd completeness letter. September 2, 2004. EPA Comment C-23-13.

Cotsworth, E. 2005. Letter to I. Triay. Subject: EPA Letter on Conducting the Performance Assessment Baseline Change (PABC) Verification Test. 4 March 2005. U.S. Environmental Protection Agency, Office of Air and Radiation, Washington, DC. ERMS 538858.

Cotton, F.A., and G. Wilkinson. 1988. Advanced Inorganic Chemistry. 5th ed. New York: Wiley.

Crane R. A. and T. B. Scott. 2014. The Removal of Uranium onto Nanoscale Zero-Valent Iron Particles in Anoxic Batch Systems. Journal of Nanomaterials 2014: Article ID 956360. *

Crane R.A., H. Pullin, and T.B. Scott. 2015. The Influence of Calcium, Sodium and Bicarbonate on the Uptake of Uranium onto Nanoscale Zero-Valent Iron Particles. Chemical Engineering Journal 277: 252–259. *

Cui, D., and K. Spahiu. 2002. The Reduction of U(VI) on Corroded Iron under Anoxic Conditions. Radiochimica Acta 90: 623–28.

David, F., A.G. Maslennikov, V.P. Peretrukhin. 1990. Electrochemical Reduction of Actinides Ions in Aqueous Solution: Application to Separations and Some Intermetallic Compound Synthesis. Journal of Radioanalytical Nuclear Chemistry 143: 415–426.

Day, B. 2019a. Reassessment of Need and Parameter Justification for Modeling Gas Generation due to Radiolysis of Brine and Cellulose/Plastic/Rubber in WIPP for CRA-2019. Sandia National Laboratories, Carlsbad, NM. ERMS 570873. *

Day, B. 2019b. Analysis Package for Salado Flow in the 2019 Compliance Recertification Application Performance Assessment (CRA-2019 PA). Sandia National Laboratories, Carlsbad, NM. ERMS 571368. *

Degueldre, C., and A. Kline. 2007. Study of Thorium Association and Surface Precipitation on Colloids. Earth and Planetary Science Letters 264: 104–113.

DeVeaux, L.C., J.A. Müller, J. Smith, J. Petrisko, D.P. Wells, and S. DasSarma. 2007. Extremely Radiation-Resistant Mutants of a Halophilic Archaeon with Increased Single-Stranded DNA-Binding Protein (RPA) Gene Expression. Radiation Research 168: 507-514. *

Diaz-Arocas, P., and B. Grambow. 1998. Solid-Liquid Phase Equilibria of U(VI) in NaCl Solutions. Geochimica et Cosmochimica Acta 62: 245–263.

Dodge, C.J., A.J. Francis, J.B. Gillow, G.P. Halada, C. Eng,and C.R. Clayton. 2002. Association of Uranium with Iron Oxides Typically Formed on Corroding Steel Surfaces. Environmental Science and Technology 36: 3504–3511.

Domski, P.S. 2019. An Update to the EQ3/6 Pitzer Thermodynamic Database DATA0.FM1 with the Creation of DATA0.FM4. Sandia National Laboratories, Carlsbad, New Mexico. ERMS# 571052. *

Domski, P.S. 2019a. Uncertainty Analysis of Actinide Solubilities for CRA 2019. Sandia National Laboratories, Carlsbad, New Mexico. ERMS# 571179. *

Domski, P.S., and C. Sisk-Scott. 2019. Prediction of Baseline Actinide Solubilities for CRA-2019 with an Updated EQ3/6 Pitzer Thermodynamic Database, DATA0.FM4. Sandia National Laboratories Report. ERMS 571178. *

Draganic, I.G., and Z.D. Draganic. 1971. Primary Products of Water Radiolysis: Oxidizing Species–the Hydroxyl Radical and Hydrogen Peroxide. In: The Radiation Chemistry of Water (pp. 91–121). New York: Academic.

Drez, P.E. 1991. Preliminary Nonradionuclide Inventory of CH-TRU Waste, Preliminary Comparison with 40 CFR Part 191, Subpart B for the Waste Isolation Pilot Plant, December 1991. Volume 3: Reference Data (pp. A-43 through A-53). Eds. R. Rechard, A. Peterson, J. Schreiber, H. Iuzzolino, M. Tierney, and J. Sandha. Albuquerque, NM: Sandia National Laboratories. SAND91-0893/3.

Du, X., B. Boonchayaanant, W.-M. Wu, S. Fendorf, J. Bargar, and C.S. Criddle. 2011. Reduction of Uranium(VI) by Soluble Iron(II) Conforms with Thermodynamic Predictions. Environmental Science & Technology 45: 4718-4725.

Duro, L., S. El Aamrani, M. Rovira, and J. de Pablo. 2008. Study of the Interaction Between U(VI) and the Anoxic Corrosion Products of Carbon Steel. Applied Geochemistry 23: 1094-1100. *

Ekberg, C., Y. Albinsson, M. Comarmond, and P. Brown. 2000. Studies on the Behavior of Thorium(IV). Journal of Solution Chemistry 29: 63–86.

Emmerich, M., A. Bhansali, T. Losekann-Behrens, C. Schroder, A. Kappler, and S. Behrens. 2012. Abundance, Distribution, and Activity of Fe(II)-Oxidizing and Fe(III)-Reducing Microorganisms in Hypersaline Sediments of Lake Kasin, Southern Russia. Applied and Environmental Microbiology 78: 4386-4399.

Endrizzi F., C.J. Leggett, L. Rao. 2016. Scientific Basis for Efficient Extraction of Uranium from Seawater. I: Understanding the Chemical Speciation of Uranium under Seawater Conditions. Industrial Engineering and Chemistry Research 55: 4249−4256. *

Eriksen, T.E., P. Ndamamba, D. Cui, J. Bruno, M. Caceci. and K. Spahiu. 1993. Stockholm: Svensk Kärnbränsleforsorjning AB. SKB Technical Report 93-18.

Ershov, B.G., M. Kelm, E. Janata, A.V. Gordeev, E. Bohnert. 2002. Radiation-Chemical Effects in the Near-Field of a Final Disposal Site: Role of Bromine on the Radiolytic Processes in NaCl-Solutions. Radiochimica Acta 90: 617-622.

Fanghänel, Th., V. Neck, and J.I. Kim. 1995. Thermodynamics of Neptunium(V) in Concentrated Salt Solutions: II. Ion Interaction (Pitzer) Parameters for Np(V) Hydrolysis Species and Carbonate Complexes. Radiochimica Acta, vol. 69: 169–76.

Fanghänel, T., and J.I. Kim. 1998. Spectoscopic Evaluation of Thermodynamics of Trivalent Actinides in Brines. Journal of Alloys and Compounds 271–273: 728–737.

Fanghänel, T., and V. Neck. 2002. Aquatic Chemistry and Solubility Phenomena of Actinide Oxides/hydroxides. Pure Applied Chemistry 74: 1895–1907.

Farrell, J., W.D. Bostick, R.J. Jarabeck, and J.N. Fiedor. 1999. Uranium Removal from Ground Water Using Zero Valent Iron Media. Ground Water 37: 618–624.

Felipe-Sotelo, M., M. Edgar, T. Beattie, P. Warwick, N.D.M. Evans, and D. Read. 2015. Effect of Anthropogenic Organic Complexants on the Solubility of Ni, Th, U(IV) and U(VI). Journal of Hazardous Materials 300: 553–560. *

Felipe-Sotelo, M., J. Hinchliff, L.P. Field, A.E. Milodowski, O. Preedy, and D. Read. 2017. Retardation of Uranium and Thorium by a Cementitious Backfill Developed for Radioactive Waste Disposal. Chemosphere 179: 127-138. *

Fellhauer, D., J. Rothe, M. Altmaier, V. Neck, J. Runke, T. Wiss, and T. Fanghänel. 2016a. Np(V) Solubility, Speciation and Solid Phase Formation in Alkaline $CaCl_2$ Solutions. Part I: Experimental Results. Radiochimica Acta 104: 355-379. *

Fellhauer, D., M. Altmaier, X. Gaona, J. Lützenkirchen, and T. Fanghanel. 2016b. Np(V) Solubility, Speciation and Solid Phase Formation in Alkaline $CaCl_2$ Solutions. Part II: Thermodynamics and Implications for Source Term Estimations of Nuclear Waste Disposal. Radiochimica Acta 104: 381-397. *

Felmy, A.R., D. Rai, J.A.S. Schramke, and J.L. Ryan. 1989. The Solubility of Plutonium Hydroxide in Dilute Solution and in High-Ionic Strength Chloride Brines. Radiochimica Acta 48: 29–35.

Felmy, A.R., D. Rai, and R.W. Fulton. 1990. The Solubility of $AmOHCO_3$(cr) and the Aqueous Thermodynamics of the System Na^+-Am^{3+}-HCO_3^--CO_3^{2-}-OH^-—H_2O. Radiochimica Acta 50: 193–204.

Felmy, A.R., M.J. Mason, and D. Rai. 1991. The Solubility of Hydrous Thorium(IV) Oxide in Chloride Media: Development of an Aqueous Ion-Interaction Model. Radiochimica Acta, vol. 55: 177–85.

Felmy, A.R., D. Rai, S.M. Sterner, M.J. Mason, N.J. Hess, and S.D. Conradson. 1996. Thermodynamic Models for Highly Charged Aqueous Species: The Solubility of Th(IV) Hydrous Oxide in Concentrated $NaHCO_3$ and Na_2CO_3 Solutions (August 14). ERMS 240226. Sandia National Laboratories; Carlsbad, NM.

Felmy, A., H. Cho, D.A. Dixon, Y. Xia, N.J. Hess, and Z. Wang. 2006. The Aqueous Complexation of Thorium with Citrate under Neutral to Basic Conditions. Radiochimic Acta 94: 205–212. *

Fiedor, J., W.D. Bostick, R.J. Jarabek, and J. Farrell. 1998. Understanding the Mechanism of Uranium Removal from Groundwater by Zero-Valent Iron Using X-Ray Photoelectron Spectroscopy. Environmental Science and Technology 32: 1466–1473.

Foerstendorf, H., N. Jordan, and K. Heim. 2014. Probing the Surface Speciation of Uranium(VI) on Iron (Hydr)oxides by In Situ ATR FT-IR Spectroscopy. Journal of Colloid and Interface Science 416: 133-138. *

Francis, A.J. and J.B. Gillow. 1994. Effects of Microbial Processes on Gas Generation under Expected Waste Isolation Pilot Plant Repository Conditions. Sandia National Laboratories: Albuquerque, NM. SAND93-7036.

Francis, A.J., J.B. Gillow, and M.R. Giles. 1997. Microbial Gas Generation under Expected Waste Isolation Pilot Plant Repository Conditions. Sandia National Laboratories: Albuquerque, NM. SAND96-2582.

Francis, A.J., J.B. Gillow, C.J. Dodge, M.K. Dunn, K. Mantione, B.A. Strietelmeier, M.E. Pansoy-Hjelvik, and H.W. Papenguth. 1998. Role of Bacteria as Biocolloids in the Transport of Actinides from a Deep Underground Radioactive Waste Repository. Radiochimica Acta 82: 347-354. *

Francis A.J., J. Gillow, C. Dodge, R. Harris, T. Beveridge, H. Papenguth. 2004. Uranium association with halophilic and non-halophilic Bacteria and Archaea. Radiochimica Acta 92: 481-488.

Fredrickson, J.K., J.K. Zachara, D.L. Balkwill, D. Kennedy, S.W. Li, H.M. Kostandarithes, M.J. Daly, M.F. Romine, F.J. Brockman. 2004. Geomicrobiology of High-Level Nuclear Waste-Contaminated Vadose Sediments at the Hanford Site, Washington State. Applied and Environmental Microbiology 70: 4230-4241. *

Fröhlich, D.R., A. Skerencak-Frech, N. Bauer, A. Rossberg, and P.J. Panak. 2015. "The pH Dependence of Am(III) Complexation with Acetate: An EXAFS Study". J. Synchrotron Radiation, 22(1), pp 99-104.

Fujiwara, K., H. Yamana, T. Fujii, and H. Moriyama. 2002. Solubility Product of Plutonium Hydrous Oxide and its Ionic Strength Dependence. Radiochimica Acta 90: 857-861. *

Fujiwara, K., H. Yamana, T. Fujii, K. Kawamoto, T. Sasaki, and H. Moriyama. 2005. Solubility Product of Hexavalent Uranium Hydrous Oxide. Journal of Nuclear Science and Technology 42: 289-294.*

Gallegos, T. J., C.C. Fuller, S. M. Webb, and W. Betterton. 2013. Uranium(VI) Interactions with Mackinawite in the Presence and Absence of Bicarbonate and Oxygen. Env. Sci and Tech., vol 47(13), pp. 7357-7364.

Gaona, X. 2013. Np(V/VI) Redox Chemistry in Cementitious Systems: XAFS Investigations on the Speciation Under Anoxic and Oxidizing Conditions. Applied Geochemistry 28: 109-118. *

Gayer, K.H., and H. Leider. 1957. The Solubility of Uranium (IV) Hydroxide in Solutions of Sodium Hydroxide and Perchloric Acid at 25°C. Canadian Journal of Chemistry 35: 5–7.

Giambalvo, E.R. 2002a. Memorandum to L.H. Brush (Subject: Recommended Parameter Values for Modeling An(III) Solubility in WIPP Brines). 25 July 2002. Carlsbad, NM: Sandia National Laboratories. ERMS 522982.

Giambalvo, E.R. 2002b. Memorandum to L.H. Brush. Subject: Recommended Parameter Values for Modeling An(IV) Solubility in WIPP Brines. 26 July 2002. Carlsbad, NM: Sandia National Laboratories. ERMS 522986.

Giambalvo, E.R. 2002c. Memorandum to L.H. Brush. Subject: Recommended Parameter Values for Modeling An(V) Solubility in WIPP Brines. 26 July 2002. Carlsbad, NM: Sandia National Laboratories. ERMS 522990.

Gillow, J.B. and A.J. Francis. 2006. Microbial Gas Generation under Expected Waste Isolation Pilot Plant Repository Conditions: Final Report. Sandia National Laboratories; Albuquerque, NM. BNL-96148-2011-IR.

Grambow, B., E. Smailos, H. Geckeis, R. Müller, and H. Hentschel. 1996. Sorption and Reduction of Uranium (VI) on Iron Corrosion Products under Reducing Saline Conditions. Radiochimica Acta 74: 149–154.

Graser, C.-H., N. lal Banik, K.A. Bender, M. Lagos, C.M. Marquardt, R. Marsac, V. Montoya, and H. Geckeis. 2015. Sensitive Redox Speciation of Iron, Neptunium, and Plutonium by Capillary Electrophoresis Hyphenated to Inductively Coupled Plasma Sector Field Mass Spectrometry. Analytical Chemistry 87: 9786-9794. *

Grenthe, I., D. Ferri, F. Salvatore, and G. Riccio. 1984. Studies on Metal Carbonate Equilibria. Part 10. A Solubility Study of the Complex Formation in the Uranium (VI)-Water-Carbon Dioxide (g) System at 25ºC. Journal of the Chemical Society, Dalton Transactions 11: 2439–2443.

Gu, B., L. Liang, M.J. Dickey, X. Yin, and S. Dai. 1998. Reductive Precipitation of Uranium (VI) by Zero-Valent Iron. Environmental Science and Technology 32: 3366–3373.

Guillaumont, R., T. Fanghänel, J. Fuger, I. Grenthe, V. Neck, D.A. Palmer, and M.H. Rand. 2003. Update on the Chemical Thermodynamics of Uranium, Neptunium, Plutonium, Americium and Technetium. F.I. Mompean, M. Illemassene, C. Domenech-Orti, and K. Ben Said, eds. Amsterdam: Elsevier. Chemical Thermodynamics. Vol. 5.

Hallsworth, J.E., M.M. Yakimov, P.N. Golyshin, J.L.M. Gillion, G. D'Auria, F. de Lima Alves, V. La Cono, M. Genovese, B.A. McKew, S.L. Hayes, G. Harris, L. Giuliano, K.N. Timmis, and T.J. McGenity. 2007. Limits of Life in $MgCl_2$-Containing Environments: Chaotropicity Defines the Window. Environmental Microbiology 9: 801-813. *

Haschke, J.M., and T.E. Ricketts. 1995. Plutonium Dioxide Storage: Conditions for Preparing and Handling. Los Alamos National Laboratory; Los Alamos, NM. LA-12999.

Haschke, J.M., T.H. Allen, and L.A. Morales. 2000. Reaction of Plutonium Dioxide with Water: Formation and Properties of PuO_{2+x}. Science 287: 285–287.

Hinz, K., M. Altmaier, X. Gaona, T. Rabung, D. Schild, M. Richmann, D. Reed, E. Alekseev, and H. Geckeis. 2015. Interaction of Nd(III) and Cm(III) with Borate in Dilute to Concentrated Alkaline NaCl, $MgCl_2$, and $CaCl_2$ Solutions: Solubility and TRLFS Studies. New journal of Chemistry 39:2, 1-30. *

Hobart, D.E., K. Samhoun, and J.R. Peterson. 1982. Spectroelectrochemical Studies of the Actinides: Stabilization of Americium (IV) in Aqueous Carbonate Solution. Radiochimica Acta 31: 139–145.

Hobart, D.E. 1990. Actinides in the Environment. Proceedings of the Robert A. Welch Foundation Conference on Chemical Research, No. XXXIV: 50 Years With Transuranium Elements (pp. 378–436). Houston, TX: Robert A. Welch Foundation.

Hobart, D.E. and R.C. Moore. 1996. Analysis of Uranium (VI) Solubility Data for WIPP Performance Assessment. (May 28, 1996). Unpublished report. Albuquerque, NM: Sandia National Laboratories. AP-028.

Holm, T.R. and C.D. Curtiss. 1989. A Comparison of Oxidation-Reduction Potentials Calculated from the As(V)/As(III) and Fe(III)/Fe(II) Couples with Measured Platinum-Electrode Potentials in Groundwater. Journal of Contaminant Hydrology 5: 67-81.

Hua, Y., W. Wand, X. Huang, T. Gu, D. Ding, L. Ling and W Zhang. 2018. "Effect of Bicarbonate on Aging and Reactivity of Nanoscale Zerovalent iron (nZVI) toward Uranium Removal," Chemosphere, vol. 201, pp. 603-611.

Huang, W., P. Pyykko, and J. Li. 2015. Is Octavalent Pu(VIII) Possible? Mapping the Plutonium Oxyfluoride Series PuO_nF_{8-2n} (n=0-4). Inorganic Chemistry 54: 8825-8831.*

Huber, F., D. Schild, T. Vitova, J. Rothe, R. Kirsch, and T. Schäfer. 2012. "U(VI) Removal Kinetics in Presence of Synthetic Magnetite Nanoparticles." Geochimica et Cosmochimica Acta, vol 96, pp. 154-173.

Icopini, G.A., H. Boukhalfa, and M.P. Neu. 2007. Biological Reduction of Np(V) and Np(V) Citrate by Metal-Reducing Bacteria. Environmental Science and Technology 41: 2764–2769.

Ilton, E.S., J.S. Lezama Pacheco, J.R. Bargar, Z. Shi, J. Liu, L. Kovarik, M.H. Engelhard, and A.R. Felmy. 2012. Reduction of U(VI) Incorporated in the Structure of Hematite. Environmental Science and Technology 46: 9428-9436.

Itagaki, H., S. Nakayama, S. Tanaka, and M. Yamawaki. 1992. Effect of Ionic Strength on the Solubility of Neptunium(V) Hydroxide. Radiochimica Acta 58/59: 61–66.

Katz, J.J., G.T. Seaborg, and L.R. Morss. 1986. The Chemistry of the Actinide Elements. 2nd ed. New York: Chapman and Hall.

Keller, C. 1971. The Chemistry of Transuranium Elements. Weinheim, Germany: Verlag Chemie.

Kelm, M., I. Pashalidis, and J.I. Kim. 1999. Spectroscopic Investigation on the Formation of Hypochlorite by Alpha Radiolysis in Concentrated NaCl Solutions. Applied Radiation and Isotopes 51: 637–642.

Kerisit, S., A.R. Felmy, and E.S. Ilton. 2011. Influence of Magnetite Stoichiometry on U(VI) Reduction. Environmental Science and Technology 45: 2770-2776.

Khasanova, A.B., N.S. Shcherbina, S.N. Kalmykov, Yu A. Teterin, and A.P. Novikov. 2007. Sorption of Np(V), Pu(V), and Pu(VI) on Colloids of Fe(III) Oxides and Hydrous Oxides and MnO_2. Radiochemistry 49: 419–425.

Kienzler, B., C. Borkel, V. Metz, and M. Schlieker. 2016. Lon-Term Interactions of Full-Scale Cemented Waste Simulates with Salt Brines. Karlsruhe Institute of Technology, Karlsruhe, Germany. KIT Scientific Reports #7721. *

Kim, J.I., M. Bernkopf, C. Lierse, and F. Koppold. 1984. Hydrolysis Reactions of Am(III) and Pu(VI) Ions in Near-Neutral Solutions. In: Geochemical Behavior of Disposed Radioactive Waste (pp. 115–34). G.S. Barney, J.D. Navratill, and W.W. Schultz, eds. Washington, DC: American Chemical Society. ACS Symposium Series No. 246.

Kim, J.I., C. Apostolidis, G. Buckau, K. Büppelmann, B. Kanellakopulos, C. Lierse, S. Magirius, R. Stumpe, I. Hedler, C. Rahner, and W. Stoewer. 1985. Chemisches Verhalten von Np, Pu und Am in Verschiedenen Konzentrierten Salzloesunger = Chemical Behaviour of Np, Pu, and Am in Various Brine Solutions. RCM 01085. Munich, Germany: Institut für Radiochemie der Technische Universitaet Muenchen. (Available from National Technical Information Service, 555 Port Royal Road, Springfield, VA 22161, 703/487-4650 as DE857 2334.)

Kim, W.H., K.C. Choi, K.K. Park, and T.Y. Eom. 1994. Effects of Hypochlorite Ion on the Solubility of Amorphous Schoepite at 25°C in Neutral to Alkaline Aqueous Solutions. Radiochimica Acta 66/67: 45–49.

Kim, S.S., M.H. Baik, J.W. Choi, H.S. Shin, and J.I. Yun. 2010. The Dissolution of ThO_2(cr) in Carbonate Solutions and a Granitic Groundwater. Journal of Radioanalytical Nuclear Chemistry 286: 91-97.

Kish, A., G. Kirkall, C. Robinson, R. Rosenblatt, P. Jaruga, M. Dizdaroglu, and J. DiRuggiero 2009. Salt Shield: Intracellular Salts Provide Cellular Protection Against Ionizing Radiation in the Halophilc Archaeon, Halobacterium salinarum NRC-1. Environmental Microbiology 11: 1066-1078. *

Kjeldsen, K.U., A. Loy, T.F. Jakobsen, T.R. Thomsen, M. Wagner, K. Ingvorsen. 2007. Diversity of Sulfate-Reducing Bacteria from an Extreme Hypersaline Sediment, Great Salt Lake (Utah). FEMS Microbiology Ecology 60: 287-298. *

Kjeldsen, K.U., T.F. Jakobsen, J. Glastrup, and K. Ingvorsen. 2010. Desulfosalsimonas propionicica gen. nov., sp. nov., a Halophilic, Sulfate-Reducing Member of the Family Desulfobacteriaceae Isolated from a Salt-Lake Sediment. International Journal of Systematic and Evolutionary Microbiology 60: 1060-1065. *

Korpusov, G.V., E.N. Patrusheva, and M.S. Dolidze. 1975. The Study of Extraction Systems and the Method of Separation of Trivalent Transuranium Elements Cm, Bk, and Cf. Soviet Radiochemistry 17: 230–236.

Kramer-Schnabel, U., H. Bischoff, R.H. Xi, and G. Marx. 1992. Solubility Products and Complex Formation Equilibria in the Systems Uranyl Hydroxide and Uranyl Carbonate at 25°C and I=0.1M. Radiochimica Acta 56: 183–188.

Kulp, T.R., S. Han, C.W. Saltikov, B.D. Lanoil, Z. Zargar, and R.S. Oremland. 2007. Effects of Imposed Salinity Gradients on Dissimilatory Arsenate Reduction, Sulfate Reduction, and Other

Microbial Processes in Sediments from Two California Soda Lakes. Applied and Environmental Microbiology 73: 5130-5137. *

Langmuir, D. and J.S. Herman. 1980. Mobility of Thorium in Natural Waters at Low Temperatures. Geochimica et Cosmochimica Acta 44: 1753–1766.

Latta, D.E., C.A. Gorski, M.I. Boyanov, E.J. O'Loughlin, K.M. Kemner, and M.M. Scherer. 2012. Influence of Magnetite Stoichiometry on U(VI) Reduction. Environmental Science and Technology 46: 778-786.

Latta, D.E., K.M. Kemner, B. Mishra, M.I. Boyanov. 2016. Effects of Calcium and Phosphate on Uranium(IV) Oxidation: Comparison between Nanoparticulate Uraninite and Amorphous U-IV-Phosphate. Geochimica et Cosmochimica Acta 174: 122-142. *

LaVerne, J.A. and L. Tandon. 2002. H_2 Production in the Radiolysis of Water on CeO_2 and ZrO_2. Journal of Physical Chemistry B 106: 380–386.

Lee, S.Y., M.H. Baik, H. Cho, E.C. Jung, J.T. Jeong, J.W. Choi, Y.B. Lee, and Y.J. Lee. 2013. Abiotic Reduction of Uranium by Mackinawite (FeS) Biogenerated under Sulfate-Reducing Conditions. Journal of Radioanalytical and Nuclear Chemistry 296: 1311–1319. *

Lemire, R.J., J. Fuger, H. Nitsche, P. Potter, M.H. Rand, J. Rydberg, K. Spahiu, J.C. Sullivan, W.J. Ullman, P. Vitorge, and H. Wanner. 2001. Chemical Thermodynamics of Neptunium and Plutonium. Elsevier. Amsterdam. Chemical Thermodynamics vol. 4.

Li Z., L. Wang, L. Yuan, C. Xiao, L. Mei, L. Zheng, J. Zhang, J. Yang, Y. Zhao, Z. Zhu, Z. Chai, and W. Shi. 2015. Efficient removal of uranium from aqueous solution by zero-valent iron nanoparticle and its graphene composite. Journal of Hazardous Materials 290: 26–33. *

Liang, R., I.A. Davidova, C.R. Marks, B.W. Stamps, B.H. Harriman, B.S. Stevenson, K.E. Duncan, and J.M. Suflita. 2016. Metabolic Capability of a Predominant Halanaerobium sp. in Hydraulically Fractured Gas Wells and its Implication in Pipeline Corrosion. Frontiers in Microbiology 7: article 988. *

Lin, M.R., P. Paviet-Hartmann, Y. Xi, and W.H. Runde. 1998. Uranyl Compounds in NaCl Solutions: Structure, Solubility and Thermodynamics. Abstract for the National Meeting of the American Chemical Society, Division of Environmental Chemistry, Boston: 23-27 August. 216th ACS National Meeting: Preprints of Extended Abstracts, vol. 38: 208.

Lipus, D., A. Vikram, D. Ross, D. Bain, D. Gulliver, R. Hammack, and K. Bibby. 2017. Predominance and Metabolic Potential of Halanaerobium in Produced Water from Hydraulically Fractured Marcellus Shale Wells. Applied and Environmental Microbiology 83: e02659-16. *

Lloyd, J.R. and L.E. Macaskie. 2002. Biochemical Basis of Microbe-Radionuclide Interactions. In Interactions of Microorganisms with Radionuclides. M.J. Keith-Roach and F.R. Livens , editors. London: Elsevier Science Ltd. pp. 313-342.

Lucchini, J.-F., M. Borkowski, M.K. Richmann, S. Ballard, and D.T. Reed. 2007. Solubility of Nd^{3+} and UO_2^{2+} in WIPP Brine as Oxidation-State Invariant Analogs for Plutonium. Journal of Alloys and Compounds 444/445: 506–511.

Lucchini, J.-F., H. Khaing, M. Borkowski, M.K. Richmann, and D.T. Reed. 2010a. Actinide (VI) Solubility in Carbonate-free WIPP Brine: Data Summary and Recommendations. Los Alamos National Laboratory; Carlsbad, NM. LCO-ACP-10. LA-UR-10-00497.

Lucchini, J.-F., H. Khaing, and D.T. Reed. 2010b. Uranium (VI) Solubility in Carbonate-free ERDA-6 Brine. Scientific Basis for Nuclear Waste Management XXXIV, edited by K.L. Smith, S. Kroeker, B. Uberuaga, K.R. Whittle, Material Research Society Symposium Proceedings, vol.1265: 21-26.

Lucchini, J.-F., M.K. Richmann, M. Borkowski. 2013a. Uranium (VI) Solubility in WIPP Brine. Los Alamos National Laboratory; Carlsbad, NM. LCO-ACP-14. LA-UR-13-20786.

Lucchini, J.-F., M. Borkowski, M.K. Richmann, and D.T. Reed. 2013b. Uranium(VI) Solubility in Carbonate-Free WIPP Brine. Radiochimica Acta 101: 391-398.

Lucchini, J.-F., M. Borkowski, H. Khaing, M.K. Richmann, J. Swanson, K. Simmons, and D.T. Reed. 2013c. WIPP Actinide-Relevant Brine Chemistry. Los Alamos National Laboratory; Carlsbad, NM. LCO-ACP-15. LA-UR-13-20620.

Magirius, S., W.T. Carnall, and J.I. Kim. 1985. Radiolytic Oxidation of Am(III) to Am(V) in NaCl Solution. Radiochimical Acta 38: 29–32.

Mancinelli, R.L. and L.I. Hochstein. 1986. The Occurrence of Denitrification in Extremely Halophilic Bacteria. FEMS Microbiology Letters 35: 55-58. *

Martinot, L. and J. Fuger. 1985. Standard Potentials in Aqueous Solution. A.J. Bard, R. Parsons, and J. Jordan, eds. New York: Dekker. The Actinides (pp. 631–674).

Masue-Slowey, Y., B.D. Kocar, S.A.B. Jofré, K.U. Mayer, and S. Fendorf. 2011. Transport Implications Resulting from Internal Redistribution of Arsenic and Iron within Constructed Soil Aggregates. Environmental Science and Technology 45: 582-588.

McCabe, A. 1990. The Potential Significance of Microbial Activity in Radioactive Waste Disposal. Experientia 46: 779-787.

McGenity, T.J., R.T. Gemmell, W.D. Grant, and H. Stan-Lotter. 2000. Origins of Halophilic Microorganisms in Ancient Salt Deposits. Environmental Microbiology 2: 243-250. *

Mehta, V.S., F. Maillot, Z. Wang, J.G. Catalano, and D.E. Giammar. 2014. Effect of Co-Solutes on the Products and Solubility of Uranium(VI) Precipitated with Phosphate. Chemical Geology 364: 66-75. *

Meinrath, G. and J.I. Kim. 1991. The Carbonate Complexation of the Am(III) Ion. Radiochimica Acta 52/53: 29–34.

Meyer, D., S. Fouchard, E. Simoni, and C. DenAuwer. 2002. Selective Dissolution of Am in Basic Media in the Presence of Ferricyanide Ions: a Mechanistic and Structural Study on Am(V) and Am(VI) Compounds. Radiochimica Acta 90: 253–258.

Moriyama, H., T. Sasaki, T. Kobayashi, and I. Takagi. 2005. Systematics of Hydrolysis Constants of Tetravalent Actinide Ions. Journal of Nuclear Science and Technology 42: 626–635.

Moore, R. C., M. Borkowski, M. G. Bronikowski, J. Chen, O. S. Pokrovsky, Y. Xia, and G. R. Choppin, 1999. Thermodynamic modeling of actinide complexation with acetate and lactate at high ionic strength. Journal of Solution Chemistry, Vol. 28: 521-53

Morss, L.R., N. Edelstein, and J. Fuger. 2006. The Chemistry of the Actinide and Transactinide Elements. 3rd ed. New York: Springer.

Moulin, C., B. Amekraza, S. Hubert, and V. Moulin. 2001. Study of Thorium Hydrolysis Species by Electrospray-Ionization Mass Spectrometry. Analytica Chimica Acta 441: 269–279.

Moutte, A. and R. Guillaumont. 1969. Complexes Citriques d'Actinium et de Curium. Revue de Chimie Minérale 6: 603-610. *

Müller, J.A. and S. DasSarma. 2005. Genomic Analysis of Anaerobic Respiration in the Archaeon Halobacterium sp. Strain NRC-1: Dimethyl Sulfoxide and Trimethylamine N-Oxide as Terminal Electron Acceptors. Journal of Bacteriology 187: 1659-1667. *

Myllykylä, E. and K. Ollila. 2011. Reduction of Uranyl Carbonate and Hydroxide Complexes by Ferrous Ions in Aqueous Solution under Anaerobic Conditions., 13th International Conference on the Chemistry and Migration Behaviour of Actinides and Fission Products in the Geosphere Migration, Beijing, China, September 18-23, 2011. Abstract PA4-3

Neck, V., J.I. Kim, and B. Kanellakopulos. 1992. Solubility and Hydrolysis Behavior of Neptunium (V). Radiochimica Acta 56: 25–30.

Neck, V., W. Runde, and J.I. Kim. 1995. Solid-Liquid Equilibria of Np(V) in Carbonate Solutions at Different Ionic Strengths: II. Journal of Alloys and Compounds 225: 295–302.

Neck, V. and J.I. Kim. 2001. Solubility and Hydrolysis of Tetravalent Actinides. Radiochimica Acta 89: 1–16.

Neck, V., R. Müller. M. Bouby, M. Altmaier, J. Rothe, M.A. Denecke, and J.I. Kim. 2002. Solubility of Amorphous Th(IV) Hydroxide: Application of LIBD to Determine the Solubility Product and EXAFS for Aqueous Speciation Radiochimica Acta 90: 485–494.

Neck, V., M. Altmaier, R. Müller, A. Bauer, T. Fanghänel, and J.I. Kim. 2003. Solubility of Crystalline Thorium Dioxide. Radiochimica Acta 91: 253–62.

Neck, V. 2003. Comments on 'Hydrolysis of Neptunium(V) at Variable Temperatures (10-85 ˚C)' by L. Rao, T.G. Srinivasan, A. Yu. Garnov, P. Zanonato, P. Di Bernardo, and A. Bismondo. Geochimica et Cosmochimica Acta 70: 4551-4555. *

Neck, V., M. Altmaier, and T. Fanghänel. 2006. Ion Interaction (SIT) Coefficients for the Th^{4+} Ion and Trace Activity Coefficients in $NaClO_4$, $NaNO_3$ and NaCl Solution Determined by Solvent Extraction with TBP. Radiochimica Acta 94: 501–507.

Neck, V., M. Altmaier, T. Rabung, J. Lützenkirchen, and T. Fanghänel. 2009. Thermodynamics of Trivalent Actinides and Neodymium in NaCl, $MgCl_2$, and $CaCl_2$ Solutions: Solubility, Hydrolysis and Ternary Ca-M(III)-OH Complexes. Pure and Applied Chemistry 81: 1555-1568.

Nemer, M. and J. Stein. 2005. Analysis Package for BRAGFLO: 2004 Compliance Recertification Application Performance Assessment Baseline Calculation. Sandia National Laboratories, Albuquerque, NM. ERMS 540527. *

Neretnieks, I. 1982. The Movement of a Redox Front Downstream From a Repository for Nuclear Waste. Stockholm: Svensk Kärnbränsleforsorjning AB. KBS Report TR 82-16.

Nitsche, H., K. Roberts, R.C. Gatti, T. Prussin, K. Becraft, S.C. Leung, S.A. Carpenter, and C.F. Novak 1992. Plutonium Solubility and Speciation Studies in a Simulant of Air Intake Shaft Water from the Culebra Dolomite at the Waste Isolation Pilot Plant. Sandia National Laboratories; Albuquerque, NM. WPO 23480. SAND92-0659.

Nitsche, H., K. Roberts, R. Xi, T. Prussin, K. Becraft, I. Al Mahamid, H.B. Silber, S.A. Carpenter, R.C. Gatti, and C.F. Novak. 1994. Long-Term Plutonium Solubility and Speciation Studies in a Synthetic Brine. Radiochimica Acta 66/67: 3-8.

Nitsche, H., K. Roberts, K. Becraft, T. Prussin, D. Keeney, S. Carpenter, and D. Hobart. 1995. Solubility and Speciation Results from Over- and Under-Saturation Experiments on Neptunium, Plutonium and Americium in Water from Yucca Mountain Region Well UE-25p#1. Los Alamos National Laboratory; Los Alamos, NM. Report LA-13017-MS.

Noronha, D.M., I.C. Pius, and S. Chaudhury. 2017. Co-precipitation of Plutonium(IV) and Americium(III) from Nitric Acid–Oxalic Acid Solutions with Bismuth Oxalate. Journal of Radioanalytical and Nuclear Chemistry 313: 523–529. *

Nuclear Energy Agency, Themodynamic Database Project. 1997. Modeling in Aquatic Chemistry. OECD, NEA-TDB Publications. *

Nuclear Energy Agency, Thermochemical Database (TDB), 2001, Ooransation for Economic Cooperation and Development. Accessed at: https://www.oecd-nea.org/dbtdb/.

Nuclear Energy Agency, Thermochemical Database (TDB), 2003, Organization for Economic Cooperation and Development. Accessed at: https://www.oecd-nea.org/dbtdb/.

O'Loughlin, E.J., S.E. Kelly, R.E. Cook, R. Csencsits, and K.M. Kemner. 2003. Reduction of Uranium (VI) by Mixed Iron (II)/ Iron (III) Hydroxide (Green Rust): Formation of UO_2 Nanoparticles. Environmental Science and Technology 37: 721–727.

Offner, D. 2019. Private communication, response to inquiry about MgO content in the WIPP. Los Alamos National Laboratory, Carlsbad, NM 88220. Los Alamos Report LA-UR-19-28471. *

Okajima, S. and D.T. Reed. 1993. Initial Hydrolysis of Pu(VI). Radiochimica Acta 60: 173–84.

Okamoto, Y., Y. Mochizuki, and S. Tsushima. 2003. Theoretical Study of Hydrolysis Reactions of Tetravalent Thorium Ion. Chemical Physics Letters 373: 213–217.

Oren, A. and H.G. Trüper. 1990. Anaerobic Growth of Halophilic Archaeobacteria by Reduction of Dimethylsulfoxide and Trimethylamine N-Oxide. FEMS Microbiology Letters 70: 33-36. *

Oren, A. 1991. Anaerobic Growth of Halophilic Archaeobacteria by Reduction of Fumarate. Journal of General Microbiology 137: 1387-1390. *

Oren, A. 1999. Bioenergetic Aspects of Halophilism. Microbiology and Molecular Biology Reviews 63: 334-348.

Oren, A. 2006. The Order Halobacteriales. In: The Prokaryotes. Falkow, S., Rosenberg, E., Schleifer, K.-H., Stackebrandt, E., Dworkin, M., editors. New York: Springer. pp. 113-164.

Oren, A. 2011. Thermodynamic Limits to Microbial Life at High Salt Concentrations. Environmental Microbiology 13: 1908-1923.

Orlandini, J.A., W.R. Penrose, and D.M. Nelson. 1986. Pu(V) as the Stable form of Oxidized Plutonium in Natural Waters. Marine Chemistry 18: 49–57.

Östhols, E., J. Bruno, and I. Grenthe. 1994. On the Influence of Carbonate on Mineral Dissolution: III: The Solubility of Microcrystalline ThO_2 in CO_2-H_2O Media. Geochimica et. Cosmochimica Acta 58: 613–623.

Oversby, V.M. 2000. Plutonium Chemistry under Conditions Relevant for WIPP Performance Assessment: Review of Experimental Results and Recommendations for Future Work (September). Environmental Evaluation Group. Albuquerque, NM. EEG-77.

Papenguth, H.W. 1996. Letter to Christine T. Stockman (Subject: Parameter Record Package for Colloidal Actinide Source Term Parameters, Attachment A: Rationale for Definition of Parameter Values for Microbes). 7 May 1996. Sandia National Laboratories; Carlsbad, NM. ERMS 416348

Paradis, C.J., S. Jagadamma, D.B. Watson, L.D. McKay, T.C. Hazen, M. Park, and J.D. Istok. 2016. In Situ Mobility of Uranium in the Presence of Nitrate Following Sulfate-Reducing Conditions. Journal of Contaminant Hydrology 187: 55-64. *

Pashalidis, I., J.I. Kim, C. Lierse, and J. Sullivan. 1993. The Chemistry of Pu in Concentrated Aqueous NaCl Solution: Effects of Alpha Self-Radiolysis and the Interaction between Hypochlorite and Dioxo Plutonium (VI). Radiochimica Acta 60: 99-101.

Pazukhin, E.M. and S.M. Kochergin. 1989. Stability Constants of Hydrolyzed Forms of Americium(III) and Solubility Product of its Hydroxide. Soviet Radiochemistry 31: 430–436.

Pedersen, K. 2005. Microorganisms and Their Influence on Radionuclide Migration in Igneous Rock Environments. Journal of Nuclear and Radiochemical Sciences 6: 11-15. *

Peper, S.M., L.F. Brodnax, S.E. Field, R.A. Zehnder, and S.N. Valdez, and W.H. Runde. 2004. "Kinetic Study of the Oxidative Dissolution of UO2 in Aqueous Carbonate Media." Industrial Engineering Chemical Research, vol. 43: 8188–93.

Petrov, V.G., D. Fellhauer, X. Gaona, K. Dardenne, J. Rothe, S.N. Kalmykov, and M. Altmaier. 2017. Solubility and Hydrolysis of Np(V) in Dilute to Concentrated Alkaline NaCl Solutions: Formation of Na-Np(V)-OH Solid Phases at 22 ˚C. Radiochimica Acta 105: 1-20. *

Philipp, T. and K. Schmeide. 2016. Uranium(VI) Retention by Ca-Bentonite Under (Hyper)alkaline Conditions. Annual Report. Helmholtz-Zentrum Dresden-Rossendorf Institute of Resource Ecology. Rossendorf; Germany. *

Philipp, T., A.A.S. Shams, A. Rossberg, N. Huittinen, K. Schmeide, and T. Stumpf. 2019. U(VI) Sorption on Ca-Bentonite at (Hyper)alkaline Conditions – Spectroscopic Investigations of Retention Mechanisms. The Science of the Total Environment 676: 469-481. *

Pitzer, K.S. 1973. Thermodynamics of Electrolytes. I. Theoretical Basis and General Equations. The Journal of Physical Chemistry, vol. 77(2): 268-277.

Pitzer, K. S. 1991. Ion interaction approach: theory and data correlation, in Pitzer, K.S., ed. Activity Coefficients in Electrolyte Solutions, 2nd edition, Ch. 3, 75-153, CRC Press, Boca Raton, Florida. TIC: 251799. *

Porter, D., A.N. Roychoudhury, D. Cowan. 2007. Dissimilatory Sulfate Reduction in Hypersaline Coastal Pans: Activity across a Salinity Gradient. Geochimica et Cosmochimica Acta 71: 5102-5116.

Pryke, D.C. and J.H. Rees. 1986. Understanding the Behaviour of the Actinides Under Disposal Conditions: A Comparison between Calculated and Experimental Solubilities. Radiochimica Acta 40: 27–32.

Rabindra, N.R., K.M. Vogel, C.E. Good, W.B. Davis, L.N. Roy, D.A. Johnson, A.R. Felmy, and K.S. Pitzer. 1992. Activity Coefficients in Electrolyte Mixtures: HCl + $ThCl_4$ + H_2O for 5–55 °C. Journal of Physical Chemistry, vol. 96: 11,065–072.

Rai, D., R.G. Strickert, and G.L. McVay. 1982. Neptunium Concentrations in Solutions Contacting Actinide-Doped Glass. Nuclear Technology 58: 69–76.

Rai, D. and J.L. Ryan. 1982. Crystallinity and Solubility of Pu(IV) Oxide and Hydrous Oxide in Aged Aqueous Suspensions. Radiochimica Acta 30: 213–216.

Rai, D., J.L. Ryan, D.A. Moore, and R.G. Strickert. 1983. Am(III) Hydrolysis Constants and Solubility of Am(III) Hydroxide. Radiochimica Acta 33: 201–206.

Rai, D. and J.L. Ryan. 1985. Neptunium (IV) Hydrous Oxide Solubility under Reducing and Carbonate Conditions. Inorganic Chemistry 24: 247–251.

Rai, D., A.R. Felmy, and J.L. Ryan. 1990. Uranium (VI) Hydrolysis Constants and Solubility Products of $UO_2.xH_2O$ (am). Inorganic Chemistry 29: 260–264.

Rai, D., A.R. Felmy, and R.W. Fulton. 1995. Nd^{3+} and Am^{3+} Ion Interaction with Sulfate Ion and Their Influence on $NdPO_4$(c) Solubility. Journal of Solution Chemistry, vol. 24: 879–95.

Rai, D., A.R. Felmy, S.M. Sterner, D.A. Moore, M.J. Mason, and C.F. Novak. 1997. The Solubility of Th(IV) and U(IV) Hydrous Oxides in Concentrated NaCl and $MgCl_2$ Solutions. Radiochimica Acta 79: 239–247.

Rai, D., A.R. Felmy, N.J. Hess, and D.A. Moore. 1998. A Thermodynamic Model for the Solubility of UO_2(am) in the Aqueous K^+-Na^+-HCO_3^--CO_3^{2-}-OH^--H2O System. Radiochimica Acta 82: 17–25.

Rai, D., D.A. Moore, C.S. Oakes, and M. Yui. 2000. Thermodynamic Model for the Solubility of Thorium Dioxide in the Na^+-Cl^--OH^--H_2O System at 23 °C and 90°C. Radiochimica Acta 88: 297–306.

Rai, D., Y. Gorby, J. Fredrickson, D. Moore, and M. Yui. 2002. Reductive Dissolution of PuO_2(am): The Effect of Fe(II) and Hydroquinone. Journal of Solution Chemistry: **32**: p. 6. *

Rao, L., D. Rai, A.R. Felmy, R.W. Fulton, and C.F. Novak. 1996. Solubility of $NaNd(CO_3)_3 \cdot 6H_2O$(c) in Concentrated Na_2CO_3 and $NaHCO_3$ Solutions. Radiochimica Acta, Vol. 75, 141–147.

Reed, D.T., S. Okajima, L.H. Brush, and M.A. Molecke. 1993. Radiolytically Induced Gas Production in Plutonium-Spiked WIPP Brine. Materials Research Society Symposium Proceedings (pp. 431–38). Vol. 294. Warrendale, PA: Materials Research Society.

Reed, D.T., S. Okajima, and M.K. Richmann, M.K. 1994. Stability and Speciation of Plutonium(VI) in WIPP Brine. Radiochimica Acta 66/67: 95–101.

Reed, D.T. and D.R. Wygmans. 1997. Actinide Stability/Solubility in Simulated WIPP Brines (March 21). WPO44625. Argonne, IL: Argonne National Laboratory, Actinide Speciation and Chemistry Group, Chemical Technology Group.

Reed, D.T., S.B. Aase, D. Wygmans, and J.E. Banaszak, J.E. 1998. The Reduction of Np(VI) and Pu(VI) by Organic Chelating Agents. Radiochimica Acta 82: 109-114.

Reed, D.T., Y. Vojta, J.W. Quinn, and M.K. Richmann. 1999. Radiotoxicity of Plutonium in NTA-Degrading Chelatobacter heintzii Cell Suspensions. Biodegradation 10: 251-260. *

Reed, D.T., J.-F. Lucchini, S.B. Aase, and A.J. Kropf. 2006. Reduction of Plutonium (VI) in Brine under Subsurface Conditions. Radiochimica Acta 94: 591–597.

Reed, D.T., S.E. Pepper, M.K. Richmann, G. Smith, R. Deo, and B.E. Rittmann, 2007. Subsurface Bio-Mediated Reduction of Higher-Valent Uranium and Plutonium. Journal of Alloys and Compounds 444/445: 376–382.

Reed, D.T., J.-F. Lucchini, M. Borkowski, and M.K. Richmann. 2010. Reduction of Higher Valent Plutonium by Iron under Waste Isolation Pilot Plant (WIPP) Relevant Conditions: Data Summary and Recommendations.. Los Alamos National Laboratory; Carlsbad, NM. LANL\ACRSP Report. LCO-ACP-09.

Reed, D.T., R. Deo, and B.E. Rittmann. 2010. Subsurface Interactions of Actinide Species and Microorganisms. In: The Chemistry of the Actinide and Transactinide Elements. L.R. Morss, N.M. Edelstein and J. Fuger eds., Chapter 33. Netherlands: Springer Press, 2010.

Reed, D.T., J.S. Swanson, J.-F. Lucchini, and M.K. Richmann. 2013. Intrinsic, Mineral, and Microbial Colloid Enhancement Parameters for the WIPP Actinide Source Term. Los Alamos National Laboratory; Carlsbad, NM. LCO-ACP-18, LA-UR-13-20858.

Reed, D. 2018. Plutonium Oxidation State Distribution in the WIPP: Conceptual Model, Project-Specific Data, and Current/Ongoing Issues. Los Alamos National Laboratory; Carlsbad, NM. LA-UR-18-25748. *

Reed, D., J. Swanson, and F. Stanley. 2019a. LANL/ACRSP Parameter Recommendations for the CRA-2019 Deferred Performance Assessment. Los Alamos National Laboratory: Carlsbad, NM. LCO-ACP-24. LA-UR-19-22787. *

Reed, D.T., M. Altmaier, and X. Gaona. 2019b. “Plutonium-Microbial Interactions in the Environment.” Elsevier publications. Plutonium Handbook, Chapter 26. *

Robinson, C.K., K. Webb, A. Kaur, P. Jaruga, M. Dizdaroglu, N.S. Baliga, A. Place, and J. DiRuggiero. 2011. A Major Role for Nonenzymatic Antioxidant Processes in the Radioresistance of Halobacterium salinarum. Journal of Bacteriology 193: 1653-1662. *

Rösch, F., T. Reimann, G.V. Buklanov, M. Milanov, V.A. Khalkin, and R. Dreyer. 1989. Electromigration of Carrier-Free Radionuclides 13. Ion Mobilities and Hydrolysis of 241Am-Am(III) in Aqueous Inert Electrolytes. Journal of Radioanalytical and Nuclear Chemistry 134: 109-128. *

Ruggiero, C.E., H. Boukhalfa, J.H. Forsythe, J.G. Lack, L.E. Hersman, and M.P. Neu. 2005. Actinide and Metal Toxicity to Prospective Bioremediation Bacteria. Environmental Microbiology 7: 88-97. *

Runde, W., and J.I. Kim. 1994. Untersuchungen der Übertragbarkeit von Labordaten natürliche Verhältnisse. Chemisches Verhalten von drei- und fünfwertigem Americium in salinen NaCl-Lösungen. Report RCM-01094, Munich: Institut für Radiochemie, Technische Universität München. (Available from National Technical Information Service, 555 Port Royal Road, Springfield, VA, 22161, 703/487-4650 as DE 95752244.)

Runde, W. 2000. The Chemical Interactions of Actinides in the Environment. Los Alamos Science 26: 330-411.

Runde, W. and M. Neu. 2010. Actinide Environmental Chemistry. In The Chemistry of the Actinide and Transactinide Elements. L.R. Morss, N.M. Edelstein, J. Fuger, eds. Springer Press; Netherlands.

Ryan, J.L and D. Rai. 1983. The Solubility of Uranium (IV) Hydrous Oxide in Sodium Hydroxide Solutions under Reducing Conditions. Polyhedron 2: 947–952.

Sanchez, A.L., J.W. Murray, T.H. Sibley, T.H. 1985. The Adsorption of Plutonium IV and V on Geothite. Geochimica Cosmochimica Acta 49: 2297-2307.

Santen, R.A. 1984. The Ostwald Step Rule. J. Phys. Chem., 88(24) 5768-5769. *

Sarathi, R., 2019. Memo to R. Camphouse. Subject: Explanations of CAPMIC definition and usage in PA calculations. January 14, 2019. Sandia National Laboratories. ERMS 570685. *

Shannon, R.D. 1976. Revised Effective Ionic Radii and Systematic Studies of Interatomic Distances in Halides and Chalcogenides. Acta Crystallographica A32: 751–67.

Sheng, G., X. Shao, Y. Li, J. Li, H. Dong, W. Cheng, X. Gao, and Y. Huang. 2014. Enhanced Removal of Uranium(VI) by Nanoscale Zerovalent Iron Supported on Na−Bentonite and an Investigation of Mechanism. Journal of Physical Chemistry 118: 2952−2958. *

Siekierski, S. 1988. Comparison of Yttrium, Lanthanides and Actinides in Respect to Unit Cell Volumes of Isostructural Compounds and Thermodynamic Functions of Complex Formation. Journal of Radioanalytical Nuclear Chemistry, vol. 122: 279–84.

Silva, R.J., G. Bidoglio, M.H. Rand, P.B. Robouch, H. Wanner, and I. Puigdomenech, I. 1995. Chemical Thermodynamics of Americium. New York Elsevier. In Chemical Thermodynamics Series 2.

Silva, R.J. and H. Nitsche. 1995. Actinide Environmental Chemistry. Radiochimica Acta 70/71: 377-396. *

Simonnet, M., N. Barré, R. Drot, C. Le Naour, V. Sladkov, and S. Delpech. 2016. Multiparametric study of thorium oxide dissolution in aqueous media. Radiochimica Acta 104(10): 691–700. *

Singer, D.M., S.M. Chatman, E.S. Ilton, K.M. Rosso, J.F. Banfield, and G.A. Waychunas. 2012a. Identification of Simultaneous U(VI) Sorption Complexes and U(VI) Nanoprecipitates on the Magnetite (111) Surface. Environmental Science and Technology 46: 3811-3820.

Singer, D.M., S.M. Chatman, E.S. Ilton, K.M. Rosso, J.F. Banfield, and G.A. Waychunas. 2012b. U(VI) Sorption and Reduction Kinetics on the Magnetite (111) Surface. Environmental Science and Technology 46: 3821-3830.

Skerencak-Frech A., M. Maiwald, M. Trumm, D.R. Froehlich, and P.J. Panak. 2015. The Complexation of Cm(III) with Oxalate in Aqueous Solution at T = 20−90 °C: A Combined TRLFS and Quantum Chemical Study. Inorganic Chemistry 54: 1860−1868. *

Sorokin, D.Y. and G. Muyzer. 2010. Bacterial Dissimilatory MnO_2 Reduction at Extremely Haloalkaline Conditions. Extremophiles 14: 41-46.

Sorokin, D.Y., S.V. Toshchakov, T.V. Kolganova, I.V. Kublanov. 2015. Halo(natrono)archaea Isolated from Hypersaline Lakes Utilize Cellulose and Chitin as Growth Substrates. Frontiers in Microbiology 6: article 942. *

Sorokin, D.Y., I.V. Kublanov, S.N. Gavrilov, D. Rojo, P. Roman, P.N. Golyshin, V.Z. Slepak, F. Smedile, M. Ferrer, E. Messina, V. LaCono, and M.M. Yakimov. 2016. Elemental Sulfur and Acetate Can Support Life of a Novel Strictly Anaerobic Haloarchaeon. The ISME Journal 10: 240-252. *

Sorokin, D.Y., E. Messina, F. Smedile, P. Roman, J.S. Sinninghe Damsté, S. Ciordia, M.C. Mena, M. Ferrer, P.N. Golyshin, I.V. Kublanov, N.I. Samarov, S.V. Toshchakov, V. LaCono, and M.M. Yakimov. 2017. Discovery of Anaerobic Lithoheterotrophic Haloarchaea, Ubiquitous in Hypersaline Habitats. The ISME Journal 11: 1245-1260. *

Spinks, J.W.T. and R.J. Woods. 1990. Radiation Sources: The Interaction of Radiation with Matter. In: Wiley; New York. Introduction to Radiation Chemistry (pp. 243–313).Wiley.

Stadler, S. and J.I. Kim. 1988. Hydrolysis reactions of Am(III) and Am(V). Radiochimica Acta 44/45: 39–44.

Sun Y., C. Ding, W. Cheng, and X. Wang. 2014. Simultaneous adsorption and reduction of U(VI) on reduced grapheneoxide-supported nanoscale zerovalent iron. Journal of Hazardous Materials 280: 399–408. *

Swanson, J.S., D.M. Norden, H.M. Khaing, and D.T. Reed. 2013b. Degradation of Organic Complexing Agents by Halophilic Microorganisms in Brines. Geomicrobiology Journal 30: 189-198.

Swanson, J.S., K.A. Simmons, D.A. Ams, J-F. Lucchini, M.K. Richmann, and D.T. Reed. 2013c. Update on Microbiology Research in the Waste Isolation Pilot Plant (WIPP). Los Alamos National Laboratory, Carlsbad NM. Los Alamos report LA-UR-13-22647. *

Swanson, J.S. and K.A. Simmons. 2013. Update on Microbial Characterization of WIPP Groundwaters. Los Alamos National Laboratory; Carlsbad, NM. LCO-ACP-20. LA-UR-13-20623.

Swanson, J., D. Reed, M. Richmann, and D. Cleveland. 2015. Investigation into the Post-Excavation Sources of Methane from INL TRU Waste Drums. Los Alamos National Laboratory: Carlsbad, NM. LA-UR-15-26657.*

Swanson, J.S., A. Cherkouk, T. Arnold, A. Meleshyn, and D.T. Reed. 2016. The Microbiology of Subsurface, Salt-Based Nuclear Waste Repositories: Using Microbial Ecology, Bioenergetics, and Projected Conditions to Help Predict Microbial Effects on Repository Performance. Los Alamos National Laboratory: Carlsbad, NM. LA-UR-16-28895. *

Swanson, J.S. and D.T. Reed. 2018a. Update on Microbiology Research for the Waste Isolation Pilot Plant. Los Alamos National Laboratory: Carlsbad, NM. LA-UR-18-31313. *

Swanson, J. and D. Reed. 2018b. Biomass-Based Approach to Determine the CAPMIC Biocolloid Parameter for the WIPP. Los Alamos National Laboratory; Carlsbad, NM. LA-UR-18-22808.*

Swanson, J.S., F.E. Stanley, and D.T. Reed. 2019. Review of the Microbial Colloid Contribution to the WIPP Actinide Source Term. Los Alamos National Laboratory: Carlsbad, NM. LCO-ACP-23, Rev. 0. LA-UR-19-22310. *

Tasi, A., X. Gaona, D. Fellhauer, M. Böttle, J. Rothe, K. Dardenne, D. Schild, M. Grivé, E. Colàs, J. Bruno, K. Källström, M. Altmaier, and H. Geckeis. 2018. Redox Behavior and Solubility of Plutonium under Alkaline, Reducing Conditions. Radiochimica Acta 106: 259-279.*

Tits, J., E. Wieland, and M.H. Bradbury. 2005. The Effect of Isosaccharinic Acid and Gluconic Acid on the Retention of Eu(III), Am(III) and Th(IV) by Calcite. Applied Geochemistry 20: 2082-2096. *

Topin, S. and J. Aupiais. 2016. The Pentavalent Actinide Solution Chemistry in the Environment. Journal of Environmental Radioactivity 153: 237-244. *

Torrero, M.E., I. Casas, J. de Pablo, M.C.A. Sandino, and B.A. Grambow. 1994. Comparison Between Unirradiated UO_2(s) and Schoepite Solubilities in 1 M NaCl Medium. Radiochimica Acta 66/67: 29–35.

Torretto, P., K. Becraft, T. Prussin, K. Roberts, S. Carpenter, D. Hobart, and H. Nitsche. 1995. Solubility and Speciation Results from Oversaturation Experiments on Neptunium, Plutonium and Americium in a Neutral Electrolyte with a Total Carbonate Similar to Water from Yucca Mountain Region Well UE-25p#1. Los Alamos, NM: Los Alamos National Laboratory. Report LA-13018-MS.

Tournassat, C., R.M. Tinnacher, S. Grangeon, and J.A. Davis. 2018. Modeling Uranium (VI) Adsorption onto Montmorillonite under Varying Carbonate Concentrations: A Surface

Complexation Model Accounting for the Spillover Effect on Surface Potential. Geochimica et Cosmochimica Acta 220: 291-308. *

Tremaine, P.R., J.D. Chen, G.J. Wallace, and W.A. Boivin. 1981. “Solubility of Uranium (IV) Oxide in Alkaline Aqueous Solutions to 300 C.” Journal of Solution. Chemistry, vol. 10: 221–30.

Trolard, F., J.M.R. Genin, M. Abdelmoula, G. Bourrie, B. Humbert, and A. Herbillon. 1997. Identification of a Green Rust mineral in a Reductomorphic Soil by Mossbauer and Raman Spectroscopies. Geochimica et Cosmochimica Acta 63: 1107–1111.

Tsarev, S., T.D. Waite, R.N. Collins. 2016. Uranium Reduction by Fe(II) in the Presence of Montmorillonite and Nontronite. Environmental Science and Technology 50: 8223-8230. *

U.S. Department of Energy (DOE). 1996. Title 40 CFR Part 191 Compliance Certification Application for the Waste Isolation Pilot Plant (October). 21 vols. Carlsbad, NM: Carlsbad Field Office. DOE/CAO-1996-2184.

U.S. Department of Energy (DOE). 1996. Title 40 CFR Part 191 Compliance Certification Application for the Waste Isolation Pilot Plant, Appendix SOTERM. Title 40 CFR Part 191, Subparts B and C. Actinide Chemistry Source Term. 1996. United States Department of Energy/Waste Isolation Pilot Plant. Carlsbad Field Office; Carlsbad, NM.

U.S. Department of Energy (DOE). 2004. Title 40 CFR Part 191 Compliance Recertification Application for the Waste Isolation Pilot Plant (March). 10 vols. Carlsbad, NM: Carlsbad Field Office. DOE/WIPP 2004-3231.

U.S. Department of Energy (DOE). 2009. Title 40 CFR Part 191 Subparts B and C Compliance Recertification Application 2009, Appendix PA, Attachment SOTERM. Carlsbad Field Office, Carlsbad, NM. DOE/WIPP 2009-3424

U.S. Department of Energy (DOE). 2014. Title 40 CFR Part 191 Subparts B and C. Compliance Recertification Application for the Waste Isolation Pilot Plant (March). Carlsbad Field Office, Carlsbad, NM. DOE/WIPP 2014-3503. *

U.S. Department of Energy (DOE). 2019. Title 40 CFR Part 191 Subparts B and C. Compliance Recertification Application for the Waste Isolation Pilot Plant (March 26, 2019and December 18, 2019). Carlsbad Field Office, Carlsbad, NM. DOE/WIPP 2019-3609. *

U.S. Environmental Protection Agency (EPA). 1993. 40 CFR Part 191: Environmental Radiation Protection Standards for the Management and Disposal of Spent Nuclear Fuel, High-Level and Transuranic Radioactive Wastes; Final Rule. Federal Register, vol. 58 (December 20, 1993): 66398–416.

U.S. Environmental Protection Agency (EPA). 2005. Teleconference with U.S. Department of Energy (DOE), Sandia National Laboratories (SNL), and Los Alamos National Laboratory (LANL). Subject: Change in U(VI) Solubility Assumption to a Concentration to 1 mM. 2 March 2005.

U.S. Environmental Protection Agency (EPA). 2006. Technical Support Document for Section 194.24: Evaluation of the Compliance Recertification Actinide Source Term and Culebra Dolomite Distribution Coefficient Values (March). Washington, DC: Office of Radiation and Indoor Air.

Van Loon, L.R., M.A. Glaus, S. Stallone, and A. Laube. 1997. Alkaline Degradation of Cellulose: Estimation of the Concentration of Isosaccharinic Acid in Cement Pore Water. Materials Research Society Symposium Proceedings 506: 1009-1010.

Van Luik, A.E., M.J. Apted, W.J. Bailey, J.H. Haberman, J.S. Shade, R.E. Guenther, R.J. Serne, E.R. Gilbert, R. Peters, and R.E. Williford. 1987. Spent Nuclear Fuel as a Waste Form for Geologic Disposal: Assessment and Recommendations on Data and Modeling Needs. Richland, WA: Pacific Northwest Laboratories. PNL-6329.

Van Soest, G. 2012. Performance Assessment Inventory Report – 2012 (PAIR 2012). Los Alamos National Laboratory; Carlsbad, NM. INV-PA-12. LA-UR-12-26643.

Van Soest, G. 2018. Performance Assessment Inventory Report – 2018 (PAIR 2018). Los Alamos National Laboratory; Carlsbad, NM. INV-PA-18. LA-UR-18-31882. *

Vandenborre, J., B. Grambow, and A. Abdelouas. 2010. Discrepancies in Thorium Oxide Solubility Values: Study of Attachment/Detachment Processes at the Solid/Solution Interface. Inorganic Chemistry 49: 8736-8748.

Villareal, R., J.M. Bergquist, and S.L. Leonard. 2001. The Actinide Source-Term Waste Test Program (STTP): Final Report. 3 vols. Los Alamos National Laboratory; Los Alamos, NM. LA-UR-01-6822, LA-UR-01-6912, and LA-UR 01-6913.

Vreeland, R.H., A. F. Piselli Jr, S. McDonnough, S.S. Meyers. 1998. Distribution and Diversity of Halophilic Bacteria in a Subsurface Salt Formation. Extremophiles 2: 321-331.

Walther, C. 2003. Comparison of Colloid Investigations by Single Particle Analytical Techniques: A Case Study on Thorium-Oxyhydroxides. Colloids and Surfaces A: Physicochemical Engineering Aspects 217: 81–92.

Wang, Z., R.C. Moore, A.R. Felmy, M.J. Mason, and R.K. Kukkadapu. 2001. A Study of the Corrosion Oroducts of Mild Steel in High Ionic Strength Brines. Waste Management 21:335-341.

Wang Y. and A.J. Francis. 2005. Evaluation of Microbial Activity for Long-Term Performance Assessments of Deep Geologic Nuclear Waste Repositories. Journal of Nuclear and Radiochemical Science 6: 43-50.

Wang, Y., and L. Brush. 1996. Memorandum to M.S. Tierney.Subject: Estimates of Gas-Generation Parameters for the Long-Term WIPP Performance Assessment. 26 January 1996. Sandia National Laboratories; Carlsbad, NM. ERMS 231943.

Warwick, P., N. Evans, and S. Vines. 2006. Studies on Some Divalent Metal α-Isosaccharinic Acid Complexes. Radiochimica Acta 94: 363-368.

Weiner, R. 1996. Technical memorandum to SWCF-A: Records Center.Subject: Documentation Package For: Oxidation State Distribution of Actinides in the Repository. 27 March 1996. Sandia National Laboratories; Albuquerque, NM. ERMS 25194.

White, A.F., A. Yee, S. Flexer. 1985. Surface Oxidation-Reduction Kinetics Associated with Experimental Basalt-Water Reactions at 25 °C. Chemical Geology 49: 73-86.

Wolery, T.J. 1992. EQ3/6, A Software Package for Geochemical Modeling of Aqueous Systems: Package Overview and Installation Guide (Version 7.0). Livermore, CA: Lawrence Livermore National Laboratory. UCRL-MA-110662 PT 1

Wolery, T.J., and S.A. Daveler. 1992. EQ3/6, A Computer Program for Reaction Path Modeling of Aqueous Geochemical Systems: Theoretical Manual, User's Guide, and Related Documentation (Version 7.0). Livermore, CA: Lawrence Livermore National Laboratory. UCRL-MA-110662-Pt. 4.

Wolery, T.J. and R.L. Jarek. 2003. Software User's Manual: EQ3/6, Version 8.0. Albuquerque, NM: Sandia National Laboratories. Software Document No. 10813-UM-8.0-00.

Wolery, T.J. 2008. Analysis Plan for EQ3/6 Analytical Studies. AP-140, Rev. 0., 15 May 2008. Carlsbad, NM: Sandia National Laboratories. ERMS 548930

Wolery, T.J., Y.-L. Xiong, and J.J. Long. 2010. Verification and Validation Plan/Validation Document for EQ3/6 Version 8.0a for Actinide Chemistry, Document Version 8.10. Carlsbad, NM: Sandia National Laboratories. ERMS 550239.

Xia, Y.X., A.R. Felmy, L.F. Rao, N.J. Hess, Z. Wang. 2003. Thermodynamic Model for the Solubility of ThO_2(am) in the Aqueous Na^+-H^+-OH^--NO_3^--H_2O-EDTA System. Radiochimica Acta 91: 751-760. *

Xu, J., Y. Li, C. Jing, H. Zhang, and Y. Ning. 2014. Removal of uranium from aqueous solution using montmorillonite-supported nanoscale zero-valent iron. Journal of Radioanalytical and Nuclear Chemistry 299: 329–336. *

Yajima, T., Y. Kawamura, and S. Ueta. 1995. Uranium(IV) Solubility and Hydrolysis Constants Under Reduced Conditions. Materials Research Society; Warrendale, PA.Materials Research Society Symposium Proceedings 353: 1137–1142.

Yalcintas E., X. Gaona, M.K. Richmann, K. Dardenne, M. Altmaier, and D.T. Reed. 2019. Spectroscopy and Solubility of U(IV) in Dilute to Concentrated NaCl Solutions in the Presence of EDTA at pH_m 1-11. Los Alamos National Laboratory, Carlsbad NM, 88220. LA-UR-19-28330. *

Yamamura, T., A. Kitamura, A. Fukui, S. Nishikawa, T. Yamamoto, and H. Moriyama 1998. Solubility of U(VI) in Highly Basic Solutions. Radiochimica Acta 83: 139–146.

Yamazaki, H., B. Lagerman, V. Symeopoulos, and G.R. Choppin. 1992. Solubility of Uranyl in Brine. Radioactive Waste Management 1992: 1607–1611.

Yan S., Y. Chen, W. Xiang, Z. Bao, C. Liu, and B. Deng. 2014. Uranium(VI) Reduction by Nanoscale Zero-Valent Iron in Anoxic Batch Systems: The Role of Fe(II) and Fe(III). Chemosphere 117: 625–630. *

Yang, H., D. Cui, D. Grolimund, V.V. Rondinella, R. Brutsch, M. Amme, C. Kutahyali, A.T. Wiss, A. Puranen, and K. Spahiu. 2017. Reductive Precipitation of Neptunium on Iron Surfaces Under Anaerobic Conditions. Journal of Nuclear Materials 496: 109-116. *

Zhang Z., J. Liu, X. Cao, X. Luo, R. Hua, Y. Liu, X. Yu, L. He, and Y. Liu. 2015. Comparison of U(VI) Adsorption onto Nanoscale Zero-Valent Iron and Red Soil in the Presence of U(VI)–CO_3/Ca–U(VI)–CO_3 Complexes. Journal of Hazardous Materials 300: 633–642.*

Zhang, Z., Y. Gao, P. Di Bernardo, P. Zanonato, and L. Rao. 2017. Effect of Temperature on the Hydrolysis of Actinide Elements in Solution. Journal of Chemical Thermodynamics 114: 55-65.*